

The University of Nottingham
School of Civil Engineering



**NUMERICAL MODELLING OF
RAPIDLY VARIED RIVER FLOW**

SANG-HEON LEE, BSc.

GEORGE GREEN LIBRARY OF
SCIENCE AND ENGINEERING

Thesis submitted to the University of Nottingham
for the degree of Doctor of Philosophy

NOVEMBER 2010

Abstract

A new approach to solve shallow water flow problems over highly irregular geometry both correctly and efficiently is presented in this thesis. Godunov-type schemes which are widely used with the finite volume technique cannot solve the shallow water equations correctly unless the source terms related to the bed slope and channel width variation are discretized properly, because Godunov-type schemes were developed on the basis of homogeneous governing equations which is not compatible with an inhomogeneous system.

The main concept of the new approach is to avoid a fractional step method and transform the shallow water equations into homogeneous form equations. New definitions for the source terms which can be incorporated into the homogeneous form equations are also proposed in this thesis. The modification to the homogeneous form equations combines the source terms with the flux term and solves them by the same solution structure of the numerical scheme. As a result the source terms are automatically discretized to achieve perfect balance with the flux terms without any special treatment and the method does not introduce numerical errors.

Another point considered to achieve well-balanced numerical schemes is that the channel geometry should be reconstructed in order to be compatible with the numerical flux term which is computed with piecewise constant initial data. In this thesis, the channel geometry has been changed to have constant state inside each cell and, consequently, each cell interface is considered as a discontinuity. The definition of the new flux related to the source terms has been obtained on the basis of the modified channel geometry.

A simple and accurate algorithm to solve the moving boundary problem in two-dimensional modelling case has also been presented in this thesis. To solve the moving boundary condition, the locations of all the cell interfaces between the wet and dry cells have been detected first and the integrated numerical fluxes through the interfaces have been controlled according to the water surface level of the wet cells.

The proposed techniques were applied to several well-known conservative schemes including Riemann solver based and verified against benchmark tests and natural river flow problems in the one and two dimensions. The numerical results shows good agreement with the analytical solutions, if available, and recorded data from other literature. The proposed approach features several advantages: 1) it can solve steady problems as well as highly unsteady ones over irregular channel geometry, 2) the numerical discretization of the source terms is always performed as the same way that the flux term is treated, 3) as a result, it shows strong applicability to various conservative numerical schemes, 4) it can solve the moving (wetting/drying) boundary problem correctly. The author believes that this new method can be a good option to simulate natural river flows over highly irregular geometries.

Publication

A part of the research conducted for this thesis has resulted in the following publication:

Lee S and Wright N : Simple and efficient solution of the shallow water equations with source terms. *International Journal for Numerical Methods in Fluids*, volume 63, Issue 3 : 313-340, 30/5/2010

Acknowledgements

I would like to thank my supervisor Dr. Nigel Wright for his support and assistance throughout this Ph.D..

I would also like to thank Dr. Ignacio Villanueva for his advice about numerical methods and Riemann solver based techniques.

I am grateful for the financial support received from the Korean Government including the Ministry of Land, Transport and Maritime Affairs which made the study possible.

Finally, a special thank should go to my wife Woon-Jung and two lovely daughters Kyoung-Eun and Young-Eun who supported and encouraged me during my study.

Contents

Chapter 1 Introduction	1
Chapter 2 Hydraulic River Modelling	5
2.1 Steady Flow Model	5
2.1.1 Uniform Flow Model	5
2.1.2 Non-uniform Flow Model	6
2.2 Hydrodynamic Model	8
2.2.1 Shallow Water Model	10
2.2.2 Further Simplification of the Shallow Water Model	19
Chapter 3 Literature Review	21
3.1 Governing Equations	21
3.2 Hyperbolic Conservation Law	22
3.3 Numerical Discretization	24
3.3.1 Finite Difference Method	24
3.3.2 Finite Volume Method	29
3.4 Roe's Approximate Solution	35
3.4.1 The Shallow Water Equations and Roe's Riemann Solver	36
3.4.2 Second-order Schemes and High Resolution Method	42
3.4.3 Discretization of the Source Terms	53
3.4.4 Two-dimensional Modelling	64
3.4.5 Wetting/Drying Boundary Condition	73

3.5 Application of Riemann Solver Based Scheme to Natural River Flows	78
3.6 Conclusion	83
Chapter 4 Homogeneous Form of the Shallow Water Equations ..	85
4.1 Introduction	85
4.2 Homogeneous Form of the Shallow Water Equations	87
4.3 Conservative Schemes	93
4.3.1 Roe's Approximate Riemann Solver	93
4.3.2 HLL Approximate Riemann Solver	97
4.3.3 Lax-Friedrichs Scheme	100
4.3.4 Lax-Wendroff Scheme	103
4.3.5 MacCormack Scheme	107
4.4 Numerical Tests and Results	109
4.4.1 Test Problems	111
4.4.2 Results and Discussion	116
4.5 Conclusion	120
Chapter 5 Extension of the Homogeneous Approach to Two-dimensions and Wetting/Drying Problem	140
5.1 The Two-dimensional Shallow Water Equations	140
5.2 Homogeneous Form of the Shallow Water Equations	141
5.2.1 Numerical Discretization	142
5.2.2 Definition of Source Flux Vector	144

5.3	Conservative Schemes	146
5.4	The Wetting/Drying Problem	151
5.5	Numerical Tests and Results	155
5.6	Conclusion	172
Chapter 6 Application : flood modelling over natural geometry		174
6.1	One-dimensional Modelling of the Im-jin River Flood.....	174
6.1.1	Introduction	174
6.1.2	Overview of the Study Site and Input Data	176
6.1.3	Numerical Results	178
6.2	Two-dimensional Modelling of Floodplain Inundation	187
6.2.1	Introduction	187
6.2.2	Numerical Results	189
6.3	Numerical Modelling of Urban Flooding	192
6.3.1	Introduction	192
6.3.2	Overview of the Study Site and Input Data	192
6.3.3	Numerical Results	194
6.3	Summary	200
Chapter 7 Conclusions		201
7.1	Summary	201
7.2	Conclusions	202
7.3	Recommended Future Work	205
References		207

List of Figures

Figure 2.1 Definition sketch for the derivation of unsteady flow equations: (a)Control volume, section view, (b)cross seciton and (c) plan view [28]	12
Figure 2.2 Flow in a channel with free surface under gravity [63]	16
Figure 2.3 Discretization elements in the quasi two-dimensional model [4]	20
Figure 3.1 Numerical domain of the finite volume method at time $n\Delta t$	30
Figure 3.2 Initial data of the Riemann problem	31
Figure 3.3 Piecewise constant distribution of initial data	32
Figure 3.4 The solution structureof a Riemann problem	33
Figure 3.5 (a) The Sweby digram of several flux limiters and (b) Second order TVD region	44
Figure 3.6 The concept of the upwind approach [80]	56
Figure 3.7 Details of the two-dimensional cells [11]	66
Figure 3.8 1D-2D hybrid discretization of channel junction [71]	81
Figure 4.1 Reconstruction of geometry: (a) section view and (b) plan view	89
Figure 4.2 Ideal dam-break problem with Roe's solver	97
Figure 4.3 The structure of HLL Riemann solver	98

Figure 4.4	Ideal dam-break problem with HLL solver	99
Figure 4.5	Ideal dam-break problem with Lax-Friedrichs (LF) scheme	103
Figure 4.6	Ideal dam-break problem with Lax-Wendroff (LW) scheme	106
Figure 4.7	Ideal dam-break problem with TVD Lax-Wendroff (TVD-LW) scheme	106
Figure 4.8	Ideal dam-break problem with MacCormack and TVD MacCormack scheme	108
Figure 4.9	Cross section used for test problems	110
Figure 4.10	Bed elevation and width variation for Problems 1 and 2	114
Figure 4.11	Water surface and bed elevation for Problem 3-1	114
Figure 4.12	Water surface and bed elevation for Problem 3-2	115
Figure 4.13	Bed level and widthvariation for Problem 4	115
Figure 4.14	Water surface level and discharge profile at $t = 10000s$ in Problem 1: (a) Roe, (b) HLL, (c) LF, (d) TVD-LW and (e) TVD-MC.....	123
Figure 4.15	Water surface level and discharge profile at $t = 10,800s$ in Problem 2 with rectangular channel: (a) Roe, (b) HLL, (c) LF, (d) TVD-LW and (e) TVD- MC	125

Figure 4.16	Water surface level and discharge profile at $t = 10,800s$ in Problem 2 with trapezoidal channel: (a) Roe, (b) HLL, (c) LF, (d) TVD-LW and (e) TVD-MC	127
Figure 4.17	Water depth and discharge profile in Problem 3-1: (a) Roe, (b) HLL, (c) LF, (d) TVD-LW and (e) TVD-MC	129
Figure 4.18	Water depth and discharge profile in Problem 3-2: (a) Roe, (b) HLL, (c) LF, (d) TVD-LW and (e) TVD-MC	131
Figure 4.19	Convergence history for Problem 3-1	132
Figure 4.20	Convergence history for Problem 3-2	132
Figure 4.21	Water depth and discharge profile in Problem 4 with subcritical flow: (a) Roe, (b) HLL, (c) LF, (d) TVD-LW and (e) TVD-MC	134
Figure 4.22	Water depth and discharge profile in Problem 4 with transcritical flow: (a) Roe, (b) HLL, (c) LF, (d) TVD-LW and (e) TVD-MC	136
Figure 4.23	Convergence history for Problem 4 (subcritical flow)	137
Figure 4.24	Convergence history for Problem 4 (transcritical flow)	137
Figure 4.25	Water surface profile in Problem 5: (a) Roe, (b) HLL and (c) LF, (d) TVD-LW and (e) TVD-MC	139
Figure 4.26	Graph of l_2 error against number of cells (N) in Problem 5	139
Figure 5.1	Finite volume grid in two-dimensional domain	142

Figure 5.2	Water surface profiles at $t = 0.69s$ after the breaking of a circular dam: (a)Roe, (b)HLL, (c)LF and (d)TVD-LW	150
Figure 5.3	Comparison of depth profiles at $t = 0.69s$ for the circular dam-break	151
Figure 5.4	Two categories of wetting/drying boundary	153
Figure 5.5	Decrease of water depth after a time step Δt	154
Figure 5.6	Recalculation of numerical fluxes on a quadrilateral grid	155
Figure 5.7	Geometry and initial condition for Problem 1	156
Figure 5.8	Water surface profiles for Problem 1: (a)Roe, (b)HLL, (c)LF and (d)TVD-LW	157
Figure 5.9	Water surface contours for Problem 1: (a)Roe, (b)HLL, (c)LF and (d)TVD-LW	158
Figure 5.10	Water surface profiles at $y = 0.5m$	159
Figure 5.11	Water surface profiles at $x = 0.8m$	159
Figure 5.12	Initial condition for Problem 3: (a)surface profile and (b)depth contour	161
Figure 5.13	Comparison of the water surface level at $t = 1T$ for Problem 2: (a)Roe, (b)HLL, (c)LF and (d)TVD-LW	162
Figure 5.14	Comparison of the velocity components at $t = 1T$ for Problem 2: (a)Roe, (b)HLL, (c)LF and (d)TVD-LW	163

Figure 5.15 Water depth contours at $t = 1T$ for Problem 2: (a)Roe, (b)HLL, (c)LF and (d)TVD-LW	164
Figure 5.16 Geometry and initial condition for Problem 3	165
Figure 5.17 Water depth profiles for Problem 3: (a)Roe, (b)HLL, (c)LF and (d)TVD-LW	166
Figure 5.18 Mass conservation error histories for Problem 3: (a)Roe, (b)HLL, (c) LF and (d)TVD-LW	167
Figure 5.19 Channel geometry and initial water depth for Problem 4	168
Figure 5.20 Water surface profiles for Problem 4: (a)Roe, (b)HLL, (c)LF and (d)TVD-LW	169
Figure 5.21 Water surface contours for Problem 4: (a)Roe, (b)HLL, (c)LF and (d)TVD-LW	170
Figure 5.22 Water surface profiles at $y = 15m$	171
Figure 5.23 Water surface profiles at $y = 5m$	171
Figure 5.24 Mass conservation error histories for Problem 4: (a)Roe, (b)HLL, (c)LF and (d)TVD-LW	172
Figure 6.1 1999 flood event : (a) Downstream area of the Im-jin River, (b) An inundated village near the Im-jin River	175
Figure 6.2 Diagram of the Im-jin River network: (a) planview and (b) simplified view of the river network [88]	177

Figure 6.3 Cross-sectional profiles at different locations: (a) 3.2km, (b) 4.8km, (c) 5.9km, (d) 26.2km, (e) 35.8km and (f) 53.8km from the upstream boundary ..	180
Figure 6.4 Boundary conditions for 1996 flood event	181
Figure 6.5 Boundary conditions for 1999 flood event	181
Figure 6.6 Tributary inflow data for 1996 flood event	182
Figure 6.7 Boundary conditions for 1999 flood event	182
Figure 6.8 Numerical results for 1996 flood event: (a) water level and (b) discharge history at the Juk-seong station	183
Figure 6.9 Numerical results for 1996 flood event: (a) water level and (b) discharge history at the Tong-il bridge station	184
Figure 6.10 Numerical results for 1999 flood event: (a) water level and (b) discharge history at the Juk-seong station	185
Figure 6.11 Numerical results for 1999 flood event: (a) water level and (b) discharge history at the Tong-il bridge station	186
Figure 6.12 Planview of the Sung-seo district and the Nak-dong River	188
Figure 6.13 Inundation extent predicted by Roe's scheme at 5 hours into the event	190
Figure 6.14 Inundation extent predicted by HLL scheme at 5 hours into the event	190
Figure 6.15 Inundation extent predicted by LF scheme at 5 hours into the event ..	191

Figure 6.16 Inundation extent predicted by TVD-LW scheme at 5 hours into the event	191
Figure 6.17 Map of the study site and some relevant locations	193
Figure 6.18 (a) Inflow hydrograph and (b) total mass volume introduced to the domain	194
Figure 6.19 Water depth histories at the gauge points: (a) G1, (b) G2, (c) G3 and (d) G4	195
Figure 6.20 Predicted inundation extents at $t = 15$ min: (a) Roe and (b) TVD-LW	196
Figure 6.21 Predicted inundation extents at $t = 30$ min: (a) Roe and (b) TVD-LW	197
Figure 6.22 Predicted inundation extents at $t = 45$ min: (a) Roe and (b) TVD-LW	198
Figure 6.23 Predicted inundation extents at $t = 60$ min: (a) Roe and (b) TVD-LW	199

List of Tables

Table 4.1 The root mean square errors of water surface level at $t = 10,800s$ with rectangular channel in Problem 2.....	119
Table 4.2 The root mean square errors of water surface level in Problem 3-1 and 5	120
Table 6.1 The recorded rainfalls and losses in 1996 and 1999 flood events	176
Table 6.2 The variation of the inundated area during the flood simulation ($T = 5hours$)	189

Chapter 1

Introduction

Computational fluid dynamics (CFD) has become an indispensable tool for hydraulic engineering after the development of numerical techniques in computer science. Especially, CFD is playing a very important role in the design of flood defence systems by predicting the dynamic behaviour of flood waves with relatively less cost and time than physical models which need vast amount of space and resources. Most modern flood warning systems include hydraulic modules developed on the basis of CFD techniques as a key module and many important decisions in environmental engineering are being made by the central or local authorities with the results obtained from CFD-based hydraulic models. For example, the predicted arrival time of a flood wave and its magnitude can be crucial information for local governments to decide when to evacuate residents and the calculated inundation extents of floodplain or urban catchments can be very useful data for developers and urban planners. Due to the importance of CFD in hydraulic and environmental engineering, a lot of research has been carried out in this area and, subsequently, a large number of new techniques have been developed.

The development of CFD in river flow modelling is based on the shallow water equations which describe the dynamic behaviour of flood waves. The shallow water equations form a hyperbolic system of partial differential equations and, as a result, it is very difficult to find accurate analytical solutions except ideal problems. However, the development of mathematical analysis and computer engineering enable one to solve the partial differential equations by approximating the solutions with various numerical techniques such as finite difference and finite volume methods. Until relatively recently the most popular approach to solve the shallow water equations has been the implicit finite difference method and many hydraulic software packages such as HEC-RAS, MIKE 11 and ISIS developed on the basis of this approach have been

widely used to simulate flood events. While the implicit finite difference models have in general demonstrated reasonable and numerically stable results, the main defect of using this approach is its inability to solve highly transient flows such as dam-break problems. To tackle this problem, Godunov-type finite volume schemes which were initially proposed in aeronautics have been introduced in fluvial hydraulics. Godunov-type schemes has become particularly popular since the introduction of approximate Riemann solvers which shows almost similar results to exact solutions with much less computing resources. The advantage of using Godunov-type finite volume schemes is its conservative property and strong shock capturing ability which can solve highly unsteady and transcritical solutions. These significant merits have made many researchers focus on the development of Riemann solver based numerical schemes and, subsequently, many technical advances have been made in this area.

While lots of new Godunov-type schemes have been developed and applied to many hydraulic engineering problems, their application to real flow problems over natural geometry has been relatively limited due to the difficulty of dealing with irregular geometry. The irregularity of the geometry such as the bottom slope and the variation of channel width is incorporated into the source terms in the shallow water equations and these source terms cause numerical errors if they are not treated properly. The main cause of this difficulty is that most of numerical techniques used for Godunov-type numerical schemes were initially developed on the basis of homogeneous governing equations without source terms. As a result, very careful and accurate treatment is needed for the numerical discretisation of the source terms in order to obtain correct solutions of the shallow water equations. To solve this problem, many researchers have proposed new source term discretisation techniques such as the upwind treatment and the surface gradient method (SGM). However, these methods are specialised for a certain category of numerical schemes and cannot be generalised for the shallow water equations with source terms. For example, the upwind source term treatment is an effective method for Roe's Riemann solver based schemes and the SGM can be used for MUSCL-type TVD schemes.

The main objective of the research presented here is to develop a novel and general method to solve the shallow water flows over highly irregular geometry and its

application to real flow problems. To achieve this goal, a new approach in which the original shallow water equations with source terms are modified into a homogeneous form equations will be proposed in this thesis. By adopting this new approach, many aspects of numerical difficulties related to the treatment of source terms can be solved efficiently and accurately. In the one-dimensional case, new definitions of geometric source terms will be presented in order to achieve well-balanced numerical solutions in an arbitrary non-prismatic channel, while, in case of two-dimensional problems, a simple and efficient wetting/drying boundary problem solver and a method to reduce mass conservation error will be developed on the basis of the homogeneous form shallow water equations. For the successful implementation of the research, the author followed three steps. At first, the one-dimensional shallow water equations will be modified into a homogeneous form and solved by using well-known conservative numerical schemes. Secondly, the proposed methods were extended to the two-dimensional case and a new algorithm to solve wetting/drying boundary condition was developed. Finally, all the newly developed methods were applied to flood modelling cases over natural geometries.

In Chapter 2, various hydraulic modelling methods are introduced and the governing equations for this thesis, the one- and two-dimensional shallow water equations, are derived.

Chapter 3 gives basic information about numerical methods to solve the shallow water equations. Subsequently, recent research about numerical methods for the shallow water equations, source term treatment techniques and the application of Godunov-type numerical schemes to real flow problems are reviewed to analyse what has been done so far.

In Chapter 4, the modification of the one-dimensional shallow water equations (or, the St. Venant equations) into a homogeneous form is presented. To achieve numerically well-balanced conservative schemes, new definitions for the geometric source terms are proposed. The modified shallow water equations are solved by using well-known Godunov-type conservative numerical schemes including approximate Riemann solvers. The proposed numerical methods are applied to several steady and unsteady

benchmark test cases and the results are compared with analytical solutions to demonstrate their robustness and accuracy.

In Chapter 5, the numerical methods developed in Chapter 4 are expanded to the two-dimensional case. The two-dimensional shallow water equations are modified into a homogeneous form and solved by several conservative schemes. Moreover, the numerical algorithm to solve wetting/drying boundary condition and the flux correction method to reduce mass conservation error in two-dimensional modelling are developed on the basis of the homogeneous form governing equations. The presented numerical techniques are applied to several well-known benchmark tests to verify their ability.

Chapter 6 focuses on the application of the numerical schemes developed in Chapter 4 and 5 to the modelling of flood events. 1996 and 1999 flood events in the Im-jin River, Korea are used for the validation of the one-dimensional schemes. The numerical results of the proposed schemes are compared with those obtained from HEC-RAS as well as some observed data. The two-dimensional schemes are applied to inundation modelling over a floodplain on the Nak-dong River, Korea and an urban area within the city of Glasgow, U.K..

Finally, Chapter 7 contains the summary of the study and the conclusions obtained from the results presented in the previous chapters. In addition, some ideas to expand the proposed methods in this area are also recommended.

Chapter 2

Hydraulic River Modelling

Hydraulic river modelling is the simulation of flow conditions based on the formulation and solution of the mathematical relationships expressing known hydraulic principles [28]. Hydraulic principles such as the mass conservation law lead to mathematical equations describing water flows. The dynamic motion of unsteady flow in river channels or floodplains can be described by the shallow water equations while other simplified form of equations are available for different types of flows. The hydraulic river modelling methods can be classified by the governing equations and the properties of the flow. In this chapter, the basic information of hydraulic river modelling methods and the shallow water equations are introduced.

2.1 Steady Flow Model

Open channel flows can be split to steady and unsteady state. A flow is steady if the parameters describing that flow do not vary with time [21]. Strictly speaking, the flow in a natural river is not steady but unsteady. Especially, in case of a flood wave, the discharge and water level at one point vary rapidly as time goes by. So, the steady state flow modelling methods are not a good tool to simulate natural river flows. However, in some special cases, the state of the flow can be considered as steady, i.e. flow in an artificial channel, irrigational channel and so on. Steady flow modelling methods are generally used in designing new artificial channels or evaluating the effects caused by some new river engineering works: e.g. calculation of the backwater profile due to a new dam construction.

2.1.1 Uniform Flow Model

Open channel flow is said to be uniform if the parameter describing that flow is the same at every section of the channel [21]. Uniform flow can be steady or unsteady.

However, unsteady uniform flow is practically impossible, so uniform flow generally means steady uniform flow. In case of uniform flow, the discharges and the velocities at any point in a river channel can be computed by using uniform flow equations with the given cross-sectional properties and bottom slope. This method is the simplest technique to model river flow. However, uniform flow is very rare in natural river so this method is generally not used to model river flow by itself.

This model is governed by uniform flow equations such as Manning's equation. In Manning's equation, the velocity V and the discharge Q at the point i can be written as

$$V_i = \frac{1}{n} R_i^{2/3} S_o^{1/2},$$

$$Q_i = \frac{1}{n} A_i R_i^{2/3} S_o^{1/2}$$

where n is the Manning's roughness coefficient, R is the hydraulic radius, A is the wetted cross-sectional area and S_o is the bottom slope which is same as the friction slope S_f in uniform flows. This method is generally used for the design of new river cross-sections or artificial channels to pass the design peak discharge, and the calculation of the friction term in unsteady flow models.

2.1.2 Non-uniform Flow Model - Gradually varied flow equation

River flows can be considered as gradually varied flows unless there are rapid changes of flow parameters as time goes by. This method can produce a water surface profile at a given uniform discharge by using the gradually varied flow equation which can be derived from the energy conservation equations.

The gradually varied flow equation for a river channel can be derived from the energy equation. The total energy H at a cross section is

$$H = z_b + h + \alpha \frac{V^2}{2g} = z_s + \alpha \frac{V^2}{2g}$$

where, z_s is the water surface level which is the sum of the bottom level (z_b) and water depth (h), α is the energy correction factor. The change of total energy head with respect to location along a channel is

$$\frac{dH}{dx} = \frac{dz_s}{dx} + \frac{d}{dx} \left(\alpha \frac{V^2}{2g} \right). \quad (2.1)$$

The total energy loss H in a river channel is mainly due to friction losses (S_f) and contraction-expansion losses (S_e):

$$\frac{dH}{dx} = -S_f - S_e. \quad (2.2)$$

Substituting (2.1) into (2.2) results in

$$-S_f - S_e = \frac{dz_s}{dx} + \frac{d}{dx} \left(\alpha \frac{V^2}{2g} \right). \quad (2.3)$$

The ordinary differential equation (2.3) can be replaced by the following difference equation

$$z_{si} + \alpha_i \frac{V_i^2}{2g} = z_{s(i+1)} + \alpha_{i+1} \frac{V_{i+1}^2}{2g} + S_f \Delta x + S_e \Delta x \quad (2.4)$$

where the subscripts i and $i+1$ represent the upstream and downstream cross section, respectively. The friction slope S_f can be calculated by using Manning's equation:

$$S_f = \frac{n^2 Q^2}{A^2 R^{4/3}} = \frac{Q^2}{K^2} = \frac{Q^2}{2} \left(\frac{1}{K_1^2} + \frac{1}{K_2^2} \right)$$

where K_1 and K_2 are the conveyances of the cross section 1 and 2, respectively. The contraction/expansion loss term S_e can be expressed for a contraction loss as

$$S_e = \frac{C_c}{dx} \left[\alpha_2 \frac{V_2^2}{2g} - \alpha_1 \frac{V_1^2}{2g} \right] \text{ for } d \left(\alpha \frac{V^2}{2g} \right) = \left[\alpha_2 \frac{V_2^2}{2g} - \alpha_1 \frac{V_1^2}{2g} \right] > 0$$

and for an expansion loss as

$$S_e = \frac{C_e}{dx} \left[\alpha_2 \frac{V_2^2}{2g} - \alpha_1 \frac{V_1^2}{2g} \right] \text{ for } d \left(\alpha \frac{V^2}{2g} \right) < 0$$

where C_c and C_e are the energy loss coefficients for contraction and expansion, respectively.

Given the cross-sectional properties, the water level at each point of a river channel can be calculated by the gradually varied flow equation with uniform discharge. The general procedure to get water surface profile is as follows [66]:

- 1) Start at a point in the channel where the water surface is known or can be approximated: the downstream boundary for a subcritical flow and the upstream boundary for a supercritical flow. Computation proceeds upstream for a subcritical flow and downstream for a supercritical flow.
- 2) Choose a water surface elevation z'_{si} at the upstream end of the reach for a subcritical flow or z'_{si+1} at the downstream end of the reach for a supercritical flow. This water surface elevation will be slightly lower or higher depending upon the type of the water surface profile.
- 3) Next compute the friction loss and the expansion/contraction loss using the assumed water surface elevation. Solve equation (2.4) for z_{si} (subcritical flow) or z_{si+1} (supercritical flow).
- 4) Compare the calculated water surface elevation z_s with the assumed water surface elevation z'_s . If the calculated and assumed elevations do not agree within an acceptable tolerance, then set $z'_{si} = z_{si}$ (for subcritical flow) and $z'_{si+1} = z_{si+1}$ (for supercritical flow) and repeat the previous procedure.

This method can determine water surface profile along the river channel and generally be used to get backwater curve caused by river works such as construction of a new bridge, weir, dam, etc.. This technique is applied in the steady state simulation module of HEC-RAS model developed by the U.S. Army Corps of Engineers (USACE) [14]. However, this method cannot simulate time dependent flows like unsteady flood waves due to the assumption of uniform discharge.

2.2 Hydrodynamic Model – Unsteady Flow

Hydrodynamic models can simulate unsteady flows by using the equations derived from the principles of mass and momentum conservation. This type of model is

widely used for hydraulic modelling of river flows because it can calculate time dependent flow problems such as the flood wave propagation simulation. The most widely used two flood propagation modelling methods are the Navier-Stokes model and the Shallow Water model [3].

The Navier-Stokes model uses the Navier-Stokes equations derived on the basis of the principles of mass and momentum conservation as the governing equations. The Navier-Stokes equations can reasonably describe the dynamic properties of flood propagation problems because these equations can express the flow of fluid in three dimensions and include the effects of turbulence and various external forces. However the Navier-Stokes modelling methods are considered to be unsuitable for the simulation of flood propagation problems in natural river channels except for some special cases because these are too complicated and require vast amounts of data and computing power. Although the Reynolds-Averaged Navier-Stokes (RANS) modelling methods have been developed to ease these problems, there are still many difficulties in using the Navier-Stokes equations to model real flood propagation problems.

The shallow water equations can be derived either through depth averaging of the Navier-Stokes equations or the mass and momentum conservation principles. By using the shallow water equations, the three-dimensional Navier-Stokes equations can be reduced to two-dimensional or one-dimensional problems. However, the Shallow Water model has some potential for errors due to the assumptions used in deriving the equations: 1) neglecting vertical velocity profile 2) hydrostatic pressure 3) small bottom slope 4) uniform horizontal velocity field in one-dimensional cases 5) friction formulae. Despite these shortcomings, the SW modelling method is believed to be the most reasonable method to simulate flood propagation problems at present. Especially, in case of the macroscopic modelling of a large river basin, the Navier Stokes model needs much larger amount of computing resources than the Shallow Water model. On the other hand, the Navier Stokes equations are suitable for modelling the effect of the turbulence in a small area of a river system. As a result, in this thesis, the main focus will be on the shallow water models.

2.2.1 Shallow Water Model

This type of models are governed by the shallow water equations (or, the St. Venant equations in one-dimensional case) which describes the motion of shallow water in a channel or floodplain. The shallow water model is widely used for river flow modelling because it generally produces reasonable solutions with limited computing resources and has a simpler form than the Navier-Stokes equations. The shallow water equations can be expressed by various forms according to spatial dimension and the choice of conserved variables. The flow in a long channel can be assumed to be one-dimensional problem which is governed by the one-dimensional shallow water equations while flood wave propagation over floodplain can be described by the two-dimensional shallow water equations.

The One-dimensional Shallow Water Equations

The one-dimensional shallow water equations are called the St. Venant equations due to being based on the St. Venant hypothesis [28]. The St. Venant hypothesis is the basic supposition for the one-dimensional unsteady flow problem and can be expressed as the following series of assumptions:

- (i) The flow is one-dimensional i.e. the velocity is uniform over the cross section and the water level across the section is horizontal.
- (ii) The streamline curvature is small and vertical accelerations are negligible, hence the pressure is hydrostatic.
- (iii) The effect of boundary friction and turbulence can be accounted for by using resistance laws analogous to those used for steady state flow.
- (iv) The average channel bed slope is small so that the cosine of the angle it makes with the horizontal may be replaced by unity.

The detailed derivation of the St. Venant equations was given by Cunge et al. [28]

At first, the equations are derived by considering conservation of mass and momentum for a control volume for which all the St. Venant hypotheses are valid. A control volume in the (x,t) plane between two cross sections x_1 and x_2 and between

the times t_1 and t_2 as shown in Figure 2.1 can be considered. A and u represent the area of the wetted cross section and the average cross-sectional velocity, respectively.

The net inflow of mass into the control volume can be defined by the time integral of the difference between the entering and leaving mass flowrates:

$$\int_{t_1}^{t_2} [(\rho u A)_{x_1} - (\rho u A)_{x_2}] dt,$$

and must be equal to the change of the mass stored in the control volume during the time interval $[t_1, t_2]$:

$$\int_{x_1}^{x_2} [(\rho A)_{t_1} - (\rho A)_{t_2}] dx$$

where ρ is water density. Consequently, the mass conservation relation for constant density is

$$\int_{x_1}^{x_2} [(A)_{t_1} - (A)_{t_2}] dx + \int_{t_1}^{t_2} [(Q)_{x_1} - (Q)_{x_2}] dt = 0 \quad (2.5)$$

where $Q = uA$ represents the discharge.

Momentum is the product of mass and velocity and momentum flux is the product of the mass flow rate and velocity:

$$\text{Momentum flux} = \rho u A \times u = \rho u^2 A.$$

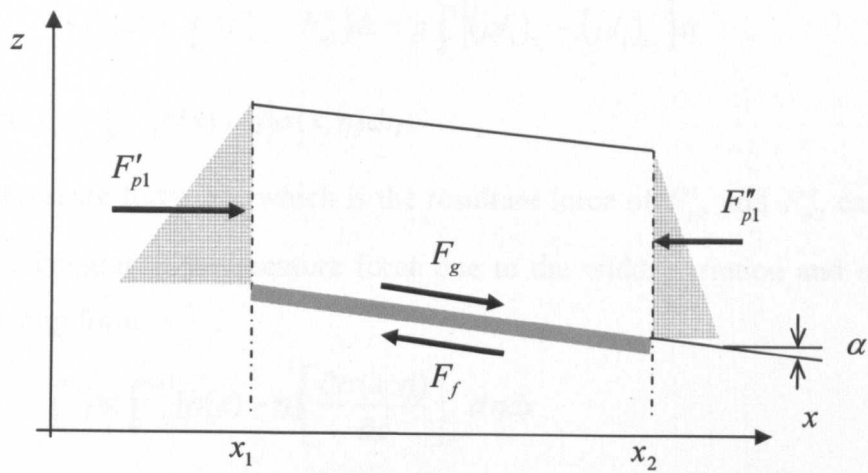
The net momentum flux into the control volume over the time interval $[t_1, t_2]$ can be obtained by integrating the difference between momentum fluxes entering and leaving the control volume :

$$M_f = \int_{t_1}^{t_2} [(\rho u^2 A)_{x_1} - (\rho u^2 A)_{x_2}] dt.$$

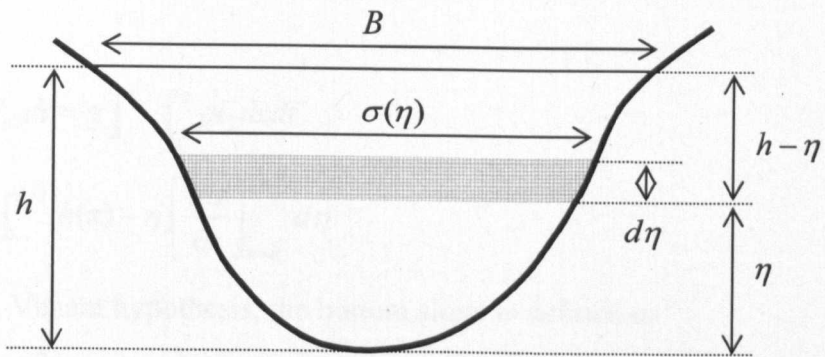
The net increase of the momentum over the time interval within the control volume is

$$\Delta M = \int_{x_1}^{x_2} [(\rho u A)_{t_2} - (\rho u A)_{t_1}] dx.$$

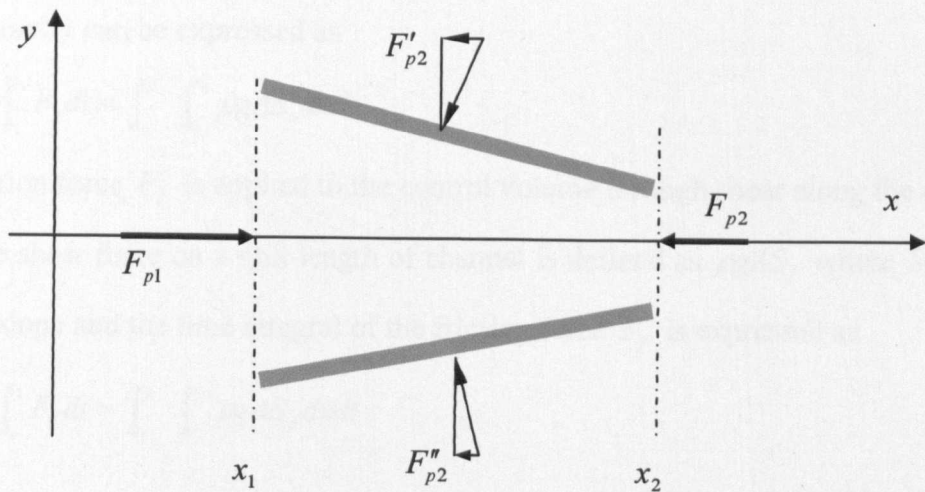
From the St. Venant hypothesis, only the following external forces are considered: pressure, gravity and friction resistance. The hydrostatic pressure force F'_{p1} and F''_{p1} are applied at boundaries x_1 and x_2 , respectively. The time integral of the net hydrostatic pressure force, $F_{p1} = F'_{p1} - F''_{p1}$, is defined as



(a)



(b)



(c)

Figure 2.1 Definition sketch for the derivation of unsteady flow equations:
 (a) Control volume, section view, (b) cross section and (c) plan view [28]

$$\int_1^2 F_{p1} dt = \int_1^2 (F'_{p1} - F''_{p1}) dt = g \int_1^2 [(\rho I_1)_{x_1} - (\rho I_1)_{x_2}] dt$$

where $I_1 = \int_0^{h(x)} [h(x) - \eta] \sigma(x, \eta) d\eta$.

The pressure force F_{p2} which is the resultant force of F'_{p2} and F''_{p2} can be considered as the integral of the pressure force due to the width variation and expressed in the following form

$$\int_{x_1}^{x_2} \rho g \int_0^{h(x)} [h(x) - \eta] \left[\frac{\partial \sigma(x, \eta)}{\partial x} \right]_{h_0} d\eta dx$$

where h_0 is constant water depth. The time integral of the pressure force F_{p2} is

$$\int_1^2 F_{p2} dt = \int_1^2 \int_{x_1}^{x_2} \rho g \int_0^{h(x)} [h(x) - \eta] \left[\frac{\partial \sigma(x, \eta)}{\partial x} \right]_{h_0} d\eta dx dt$$

or

$$\int_1^2 F_{p2} dt = g \int_1^2 \int_{x_1}^{x_2} \rho I_2 dx dt$$

where $I_2 = \int_0^{h(x)} [h(x) - \eta] \left[\frac{\partial \sigma}{\partial x} \right]_{h=h_0} d\eta$

From the St. Venant hypothesis, the bottom slope is defined as

$$S_o = -\frac{\partial z_b}{\partial x}$$

for very small bottom slope and $\tan \alpha \approx \sin \alpha$, while the time integral of the force F_g due to gravity can be expressed as

$$\int_1^2 F_g dt = \int_1^2 \int_{x_1}^{x_2} \rho g A S_o dx dt.$$

The friction force F_f is applied to the control volume through shear along the channel bed. The shear force on a unit length of channel is defined as $\rho g A S_f$ where S_f is the friction slope and the time integral of the friction force F_f is expressed as

$$\int_1^2 F_f dt = \int_1^2 \int_{x_1}^{x_2} \rho g A S_f dx dt.$$

Finally, the conservation of momentum leads to

$$\Delta M = M_f + \int_1^2 F_{p1} dt + \int_1^2 F_{p2} dt + \int_1^2 F_g dt - \int_1^2 F_f dt$$

and, for constant density, the integral form of the momentum equation can be given by

$$\begin{aligned}
\int_{x_1}^{x_2} [(uA)_{t_2} - (uA)_{t_1}] dx &= \int_1^2 [(u^2 A)_{x_1} - (u^2 A)_{x_2}] dt \\
&+ \int_1^2 [(I_1)_{x_1} - (I_1)_{x_2}] dt - g \int_1^2 I_2 dx dt \\
&+ \int_1^2 \int_{x_1}^{x_2} A(S_o - S_f) dx dt.
\end{aligned} \tag{2.6}$$

Equations (2.5) and (2.6) compose the integral form of the St. Venant equations for modelling of unsteady one-dimensional flows in natural channels.

The one-dimensional shallow water equations can be expressed as the differential form which is more widely used by researchers. From the assumption that the dependent variables are continuous and differentiable function, the integral equations can be changed to the differential equations. According to the Taylor series expansion,

$$\begin{aligned}
(A)_{t_2} &= (A)_{t_1} + \frac{\partial A}{\partial t} \Delta t + \frac{\partial^2 A}{\partial t^2} \frac{\Delta t^2}{2} + \dots \\
(Q)_{t_2} &= (Q)_{t_1} + \frac{\partial Q}{\partial t} \Delta t + \frac{\partial^2 Q}{\partial t^2} \frac{\Delta t^2}{2} + \dots
\end{aligned}$$

By neglecting second or higher order terms and assuming that Δx and Δt approach zero, the following relation holds

$$\begin{aligned}
\lim_{t_2 \rightarrow t_1} \int_{x_1}^{x_2} [(A)_{t_2} - (A)_{t_1}] dx &= \int_{x_1}^{x_2} \int_{t_1}^{t_2} \frac{\partial A}{\partial t} dt dx \\
\lim_{t_2 \rightarrow t_1} \int_{x_1}^{x_2} [(Q)_{t_2} - (Q)_{t_1}] dx &= \int_{x_1}^{x_2} \int_{t_1}^{t_2} \frac{\partial Q}{\partial t} dt dx.
\end{aligned}$$

As a result, the mass conservation equation (2.5) becomes

$$\int_{x_1}^{x_2} \int_{t_1}^{t_2} \left[\frac{\partial A}{\partial t} + \frac{\partial Q}{\partial x} \right] dt dx = 0. \tag{2.7}$$

In a similar way,

$$\begin{aligned}
(u^2 A)_{x_2} - (u^2 A)_{x_1} &= \frac{\partial (u^2 A)}{\partial x} \Delta x + \frac{\partial^2 (u^2 A)}{\partial x^2} \frac{\Delta x^2}{2} + \dots \\
(uA)_{t_2} - (uA)_{t_1} &= \frac{\partial Q}{\partial t} \Delta t + \frac{\partial^2 Q}{\partial t^2} \frac{\Delta t^2}{2} + \dots
\end{aligned}$$

$$(I_1)_{x_2} - (I_1)_{x_1} = \frac{\partial I_1}{\partial x} \Delta x + \frac{\partial^2 I_1}{\partial x^2} \frac{\Delta x^2}{2} + \dots$$

and the momentum conservation equations becomes

$$\int_{x_1}^{x_2} \int_{t_1}^{t_2} \left[\frac{\partial Q}{\partial t} + \frac{\partial(u^2 A)}{\partial x} \right] dt dx = -g \int_{x_1}^{x_2} \int_{t_1}^{t_2} \left[\frac{\partial I_1}{\partial x} - I_2 - A(S_o - S_f) \right] dt dx. \quad (2.8)$$

If the equations (2.7) and (2.8) are to hold everywhere in the (x,t) plane, they can be expressed as the following two differential equations consisting the differential form of the St. Venant equations

$$\frac{\partial A}{\partial t} + \frac{\partial Q}{\partial x} = 0 \quad (2.9)$$

$$\frac{\partial Q}{\partial t} + \frac{\partial}{\partial x} \left(\frac{Q^2}{A} + I_1 \right) = gA(S_o - S_f) + gI_2. \quad (2.10)$$

The one-dimensional shallow water equations can be written in different forms according to the choice of dependent variables. The commonly used alternative forms of the equations are presented in [28].

Two-Dimensional Shallow Water Equations

The two-dimensional shallow water equations describe the flow in shallow water bodies in a two-dimensional domain and can be derived by depth averaging the three-dimensional mass and momentum conservation equations. In a two-dimensional domain the vertical acceleration within the fluid is negligible and pressure is assumed hydrostatic. The following derivation is taken from Toro [77].

At first, the three-dimensional mass and momentum conservation equations in free surface gravity flow were considered. In the three-dimensional domain depicted in Figure 2.2, the horizontal plane is given by the coordinates x and y , and the vertical direction is given by z . The water in the channel is considered to be incompressible, non-viscous, non-heat conducting. The velocity vector has three components like $V = (u, v, w)$.

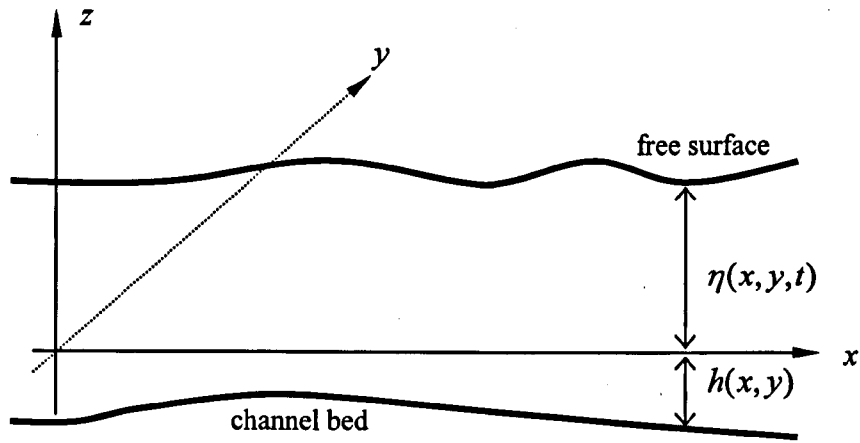


Figure 2.2 Flow in a channel with free surface under gravity [63]

The mass and momentum conservation equations for incompressible fluid are expressed as

$$u_x + v_y + \omega_z = 0 \quad (2.11)$$

$$u_t + uu_x + vv_y + \omega\omega_z = -\frac{1}{\rho} p_x \quad (2.12)$$

$$v_t + uv_x + vv_y + \omega v_z = -\frac{1}{\rho} p_y \quad (2.13)$$

$$\omega_t + u\omega_x + v\omega_y + \omega\omega_z = -\frac{1}{\rho} p_z - g \quad (2.14)$$

where ρ is density. The equations can be simplified by using the substantial derivative

$$\frac{D\phi}{Dt} = \frac{\partial\phi}{\partial t} + V \cdot \text{grad}(\phi) \quad \text{with} \quad \text{grad}(\phi) = \left(\frac{\partial\phi}{\partial x}, \frac{\partial\phi}{\partial y}, \frac{\partial\phi}{\partial z} \right),$$

which represents the time rate of change of variable ϕ as registered by an observer moving with the fluid velocity $V = (u, v, \omega)$. Then, the equations (2.11~2.14) can be rewritten as

$$\frac{D\rho}{Dt} = \rho_t + V \cdot \text{grad}(\rho) = 0 \quad (2.15)$$

$$\frac{Du}{Dt} = u_t + V \cdot \text{grad}(u) = -\frac{1}{\rho} p_x \quad (2.16)$$

$$\frac{Dv}{Dt} = v_t + V \cdot \text{grad}(v) = -\frac{1}{\rho} p_y \quad (2.17)$$

$$\frac{D\omega}{Dt} = \omega_t + V \cdot \text{grad}(\omega) = -\frac{1}{\rho} p_z - g. \quad (2.18)$$

To solve these equations, boundary conditions should be given: two boundary conditions are given for the free surface

$$\frac{D}{Dt}(\eta - z) = 0 \quad \text{and} \quad p = p_{atm} \approx 0 \quad \text{at} \quad z = \eta(x, y, t), \quad (2.19)$$

and one for the bottom boundary

$$\frac{D}{Dt}(h + z) = 0 \quad \text{at} \quad z = -h(x, y). \quad (2.20)$$

The two-dimensional shallow water equations are an approximation to the full three dimensional equations (2.11~2.14) based on the assumption that the vertical component of the acceleration is negligible, i.e. $D\omega/Dt \approx 0$. Inserting $D\omega/Dt = 0$, equation (2.18) gives

$$p = \rho g(\eta - y)$$

and this represents the hydrostatic pressure. From this, the momentum equations in x and y directions can be rewritten as

$$u_t + uu_x + vv_y = -g\eta_x \quad (2.21)$$

$$v_t + uv_x + vv_y = -g\eta_y. \quad (2.22)$$

The meaningful expression for the shallow water equations can be obtained by integrating mass conservation equations (2.11) with respect to z :

$$\int_h^\eta u_x dz + \int_h^\eta v_y dz + \omega|_{-h}^\eta = 0. \quad (2.23)$$

According to the definition of substantial derivative, the boundary conditions (2.19) and (2.20) can be expressed as

$$(\eta_t + u\eta_x + v\eta_y - \omega)|_{z=\eta} = 0 \quad (2.24)$$

$$(uh_x + vh_y + \omega)|_{z=-h} = 0. \quad (2.25)$$

By substituting (2.24) and (2.25), equations (2.23) can be rewritten as

$$\int_h^\eta u_x dz + \int_h^\eta v_y dz + \eta_t + (u|_{z=\eta})\eta_x + (v|_{z=\eta})\eta_y + (u|_{z=-h})h_x + (v|_{z=-h})h_y = 0,$$

and by using the partial integral,

$$\eta_t + \frac{\partial}{\partial x} \int_h^\eta u dz + \frac{\partial}{\partial y} \int_h^\eta v dz = 0. \quad (2.26)$$

The velocity components u and v are independent of z and the equation (2.26) becomes

$$(\eta + h)_t + [u(\eta + h)]_x + [v(\eta + h)]_y = 0 \quad (2.27)$$

where $h_t = 0$ because $h(x, y)$ is independent of t .

The momentum equations (2.21) and (2.22) can be expressed as similar form. The addition of (2.27) multiplied by u and (2.21) multiplied by $(\eta + h)$ gives,

$$[u(\eta + h)]_t + [u^2(\eta + h)]_x + [uv(\eta + h)]_y = -g(\eta + h)\eta_x. \quad (2.28)$$

Similarly, (2.28) and (2.22) gives,

$$[v(\eta + h)]_t + [uv(\eta + h)]_x + [v^2(\eta + h)]_y = -g(\eta + h)\eta_y. \quad (2.29)$$

The right hand side terms of the equations (2.28) and (2.29) represent the surface gradients in x and y directions, respectively, and can be decomposed as

$$-g(\eta + h)\eta_x = g(\eta + h)h_x - \frac{1}{2}g[(\eta + h)^2]_x$$

$$-g(\eta + h)\eta_y = g(\eta + h)h_y - \frac{1}{2}g[(\eta + h)^2]_y.$$

Finally, the two-dimensional shallow water equations can be given by

$$\phi_t + (\phi u)_x + (\phi v)_y = 0$$

$$(\phi u)_t + (\phi u^2 + \frac{1}{2}\phi^2)_x + (\phi uv)_y = g\phi S_{ox}$$

$$(\phi v)_t + (\phi uv)_x + (\phi v^2 + \frac{1}{2}\phi^2)_y = g\phi S_{oy}$$

where the geopotential $\phi = gH$ with the surface elevation $H = \eta + h$ and the bottom slope $S_{ox} = h_x$. The effect of bottom friction can be considered using friction slope S_f and combined to bottom slope term.

The equations can be written using variable h , hu and $h\nu$, which gives the most well known form of the shallow water equations:

$$h_t + (hu)_x + (h\nu)_y = 0 \quad (2.30)$$

$$(hu)_t + (hu^2 + \frac{1}{2}gh^2)_x + (huv)_y = gh(S_{ox} - S_{fx}) \quad (2.31)$$

$$(h\nu)_t + (huv)_x + (h\nu^2 + \frac{1}{2}gh^2)_y = gh(S_{oy} - S_{fy}). \quad (2.32)$$

2.2.2 Further Simplification of the Shallow Water Model

The shallow water equations (or St. Venant equations) is the hyperbolic partial differential equation system and it needs lots of computing resources and time to solve the full equations. To avoid this difficulties, several simplified form of hydrodynamic modelling methods have been developed. These methods are based on the simplified form of the shallow water equations.

Kinematic Wave Model

This model is based on the one-dimensional kinematic wave equations which is the simplest form of the St. Venant equations. The kinematic wave equations has the following form and can be obtained by neglecting the local acceleration terms, convective acceleration term and pressure term of the momentum equation

- Mass equation:
$$\frac{\partial A}{\partial t} + \frac{\partial Q}{\partial x} = 0$$

- Momentum equation:
$$S_o - S_f = 0$$

The friction slope S_f can be computed by using the Manning's friction coefficient, n , and the momentum equation can be rewritten as

$$S_o - \frac{n^2 P^{4/3} Q^2}{A^{10/3}} = 0$$

where P is the wetted perimeter of the channel. This method can be used when the inertia terms (or the acceleration terms) are small compared to the bottom slope. This method has been widely used in various river models because of its simple structure: LISFLOOD-FP model [5] and HEC-1 model developed by the U.S. Army Corps of Engineers (USACE) [14] use the kinematic wave equation to simulate open channel

flows. This model has the potential to cause errors in case of large spatial velocity changes, because it neglects the inertia terms in the momentum equation.

Quasi Two-dimensional Model

Flow over floodplain is different from channel flow and can be simulated by two-dimensional modelling methods. However, there are many crisscrossing structures such as dykes and roads in real floodplains, so it is convenient to consider the floodplain as a series of linked cells in the two-dimensional domain [28]. In this method, river channel flow is modelled by the one-dimensional shallow water equations where the water depth of each flood plain cell is calculated by using the following continuity equation

$$\frac{dh_i}{dt} = \frac{\sum_k Q(h_i, h_k)}{A_i}$$

where h_i and A_i is the water surface level and the corresponding surface area of the cell under consideration, k denotes the neighbouring cells and $Q(h_i, h_k)$ means discharge between cell i and k . The discharge between two cells is only due to the difference of water surface levels and usually calculated by hydraulic equations like the weir equation. An example of the quasi two-dimensional model is depicted in *Figure 2.3*. In *Figure 2.3 (a)*, the floodplain is composed of several storage cells, and the whole river system is considered as a network of the one-dimensional cells in the river channel and storage cells in the floodplain as shown in *Figure 2.3 (b)*.

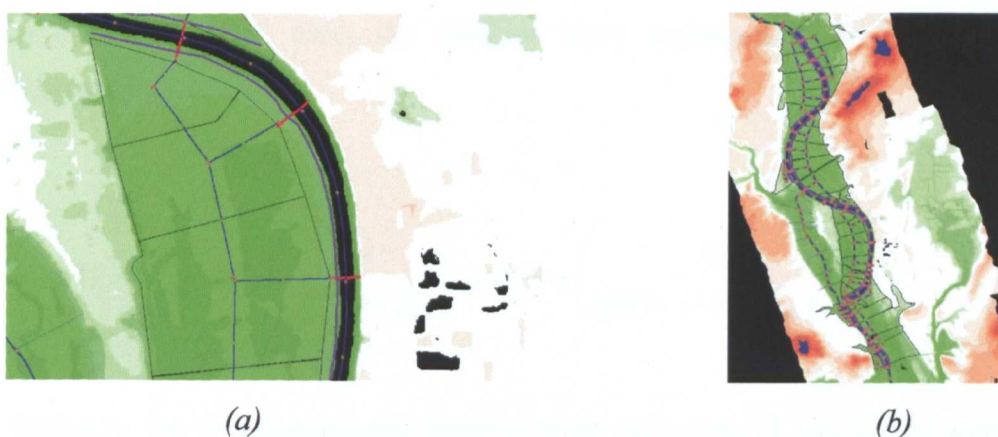


Figure 2.3 Discretization elements in the quasi two-dimensional model [4]

Chapter 3

Literature Review

The main objective of this thesis is to demonstrate how to solve the shallow water equations accurately and efficiently in the case of highly unsteady flows over irregular geometries. It is almost impossible to solve the shallow water equations which is a system of partial differential equations by analytical methods. However, lots of numerical techniques such as the finite difference or finite volume methods have been developed and the solutions can be approximated by using these numerical methods. In this chapter, basic information and knowledge which is essential for finding numerical solutions of the shallow water equations was studied and recently developed techniques by other researchers were reviewed.

3.1 Governing Equations

Unsteady flows are considered to be governed by the shallow water equations. As presented in Chapter 2, the shallow water equations are a hyperbolic partial differential equation system derived from the principles of mass and momentum conservation. The equations have a simpler form and give more useful information when expressed in a vector form as shown below.

In one-dimensional case, the shallow water equations (2.9) and (2.10) can be expressed as

$$\frac{\partial \mathbf{U}}{\partial t} + \frac{\partial \mathbf{F}}{\partial x} = \mathbf{S}$$

$$\text{with } \mathbf{U} = \begin{pmatrix} A \\ Q \end{pmatrix}, \mathbf{F} = \begin{pmatrix} Q \\ Q^2/A + gI_1 \end{pmatrix} \text{ and } \mathbf{S} = \begin{pmatrix} 0 \\ gA(S_o - S_f) + gI_2 \end{pmatrix}. \quad (3.1)$$

Similarly, the two-dimensional shallow water equations (2.30), (2.31) and (2.32) can be rewritten as

$$\frac{\partial \mathbf{U}}{\partial t} + \frac{\partial \mathbf{F}}{\partial x} + \frac{\partial \mathbf{G}}{\partial y} = \mathbf{S} \quad (3.2)$$

$$\text{with } \mathbf{U} = \begin{pmatrix} h \\ hu \\ h\nu \end{pmatrix}, \mathbf{F} = \begin{pmatrix} hu \\ hu^2 + \frac{1}{2}gh^2 \\ hu\nu \end{pmatrix}, \mathbf{G} = \begin{pmatrix} h\nu \\ hu\nu \\ h\nu^2 + \frac{1}{2}gh^2 \end{pmatrix} \text{ and } \mathbf{S} = \begin{pmatrix} 0 \\ gh(S_{ax} - S_{fx}) \\ gh(S_{ay} - S_{fy}) \end{pmatrix}.$$

These are called “conservation form” or “conservation law” because the vector \mathbf{U} is considered as the vector of conserved variables and $\mathbf{F}(\mathbf{U})$ (or $\mathbf{G}(\mathbf{U})$) is the flux vector. As a result, it is very important to understand the properties of conservation laws to solve the governing equation accurately and efficiently.

3.2 Hyperbolic Conservation Law

The motion of fluids such as water and gas can be described by the principles of mass and momentum (and energy) conservation. The governing equations of fluid motion derived from the conservation principles such as the shallow water equations have the following form of the time dependent partial differential equation system and this form is called “conservation law”:

$$\frac{\partial}{\partial t} u(x,t) + \frac{\partial}{\partial x} f(u(x,t)) = 0 \quad (3.3)$$

u is an m dimensional vector of conserved variables and $f(u)$ is a flux function. By applying the chain rule to the second term of the left hand side, equations (3.3) can be rewritten as

$$\frac{\partial u}{\partial t} + \frac{\partial f(u)}{\partial u} \frac{\partial u}{\partial x} = 0 \quad \text{or} \quad \frac{\partial u}{\partial t} + A \frac{\partial u}{\partial x} = 0 \quad (3.4)$$

where $A = \partial f / \partial u$ is the Jacobian matrix. The system (3.4) is “hyperbolic”, if the $m \times m$ Jacobian matrix A has m real eigenvalues and the matrix is diagonalizable, i.e. there is a complete set of m linearly independent eigenvectors. However, these partial differential equation systems have difficulties in dealing with discontinuous solution because partial differential equations do not hold at discontinuities. In order to avoid this problem, the integral form of “conservation law” is generally used and it has the form

$$\int_{x_1}^{x_2} u(x, t_2) dx = \int_{x_1}^{x_2} u(x, t_1) dx + \int_{t_1}^{t_2} f(u(x_1, t)) dt - \int_{t_1}^{t_2} f(u(x_2, t)) dt$$

for any rectangular control volume $[x_1, x_2] \times [t_1, t_2]$.

Decomposition of Linear Systems

A linear hyperbolic conservation law system has the form

$$U_t + AU_x = 0. \quad (3.5)$$

The $m \times m$ Jacobian matrix A has m real eigenvalues ($\lambda_1 \leq \lambda_2 \leq \dots \leq \lambda_m$). From the assumption of hyperbolicity,

$$Ae_k = \lambda_k e_k \quad \text{for } k = 1, 2, \dots, m$$

where e_k is the k th right eigenvector. Then, the Jacobian matrix A can be diagonalised as

$$R^{-1}AR = \Lambda \quad \text{and} \quad A = R\Lambda R^{-1}$$

where R is the matrix whose columns are the right eigenvectors of A and Λ is the diagonal matrix of eigenvalues:

$$\Lambda = \begin{bmatrix} \lambda_1 & & & \\ & \lambda_2 & & \\ & & \dots & \\ & & & \lambda_m \end{bmatrix}.$$

Hyperbolic equation systems can be decomposed by using the above properties.

Equation (3.5) can be rewritten by multiplying R^{-1} on both sides:

$$R^{-1}U_t + R^{-1}ARR^{-1}U_x = 0,,$$

or by setting $W = R^{-1}U$:

$$W_t + \Lambda W_x = 0.$$

Since Λ is a diagonal matrix, the hyperbolic system (3.5) can be changed to m independent advection equations and the k th equation is

$$\frac{\partial w_k}{\partial t} + \lambda_k \frac{\partial w_k}{\partial x} = 0 \quad \text{for } k = 1, 2, \dots, m \quad (3.6)$$

where w_k is the k th component of the vector W . The solution of variable w_k can be easily calculated by solving the decomposed equation (3.6). Finally, the solution U can be obtained by the following relation

$$U = RW,$$

then the solution is regarded as a combination of m “waves” propagating at the characteristic speeds $\lambda_1, \lambda_2, \dots, \lambda_m$, respectively. These values define the characteristic curves along which information propagates in each equation. The decomposition technique of a linear hyperbolic equation system can be applied to non-linear hyperbolic equation systems like the shallow water equations, which makes it easier to find approximate solutions of the equations.

3.3 Numerical Discretization

The shallow water equations are a hyperbolic system which is composed of several partial differential equations. By using numerical methods, continuous values of the partial differential equation systems can be replaced with a finite set of discrete values. To obtain discrete values, the domain of the partial differential equations has to be discretized into a finite set of points or volumes (cells) on a grid. The solutions of the partial differential equations can be approximated as discretized values by solving the discretized form of the equations with data stored in the finite set of points or volumes. The most well known and widely used numerical methods to solve hyperbolic conservation laws are the Finite Difference Method and the Finite Volume Method. In the Finite Difference Method, discretized values are considered as point values at grid points while the Finite Volume Method regards these values as averages (piecewise constants) over finite volumes (cells).

3.3.1 Finite Difference Method

The Finite Difference Method is based on the differential form of a conservation law. This technique has been widely used in real river flow modelling because it is straightforward and simple to develop new numerical scheme. In the Finite Difference Method, values of variables are stored on grid points and the derivatives of partial differential equations are replaced by the truncated approximations which are based on Taylor series expansion. For example, the first derivative of the smooth function $u(x)$ at x can be defined as

$$u_x \equiv \frac{\partial u}{\partial x} = \lim_{\Delta x \rightarrow 0} \frac{u(x + \Delta x) - u(x)}{\Delta x}. \quad (3.7)$$

By using Taylor series expansion, $u(x + \Delta x)$, $u(x - \Delta x)$ can be expressed as

$$u(x + \Delta x) = u(x) + (\Delta x)u_x(x) + \frac{(\Delta x)^2}{2}u_{xx}(x) + \dots = u(x) + \sum_k \frac{(\Delta x)^k}{k!}u^{(k)}(x) \quad (3.8)$$

$$u(x - \Delta x) = u(x) - (\Delta x)u_x(x) + \frac{(\Delta x)^2}{2}u_{xx}(x) + \dots = u(x) + \sum_k \frac{(-\Delta x)^k}{k!}u^{(k)}(x). \quad (3.9)$$

The first derivative u_x can be obtained by substituting (3.8) into (3.7):

$$\frac{u(x + \Delta x) - u(x)}{\Delta x} = u_x + \frac{\Delta x}{2}u_{xx} + \dots.$$

By neglecting second- and higher-order terms, u_x can be expressed as

$$u_x(x) = \frac{u(x + \Delta x) - u(x)}{\Delta x} + o(\Delta x).$$

This is a first-order forward approximation of $u_x(x)$ because the leading term of the error is of order of (Δx) . If Δx is sufficiently small, this formula can be regarded as an approximation of the first derivative u_x . Similarly, the backward and central approximations can be defined as

$$\text{Backward : } u_x(x) = \frac{u(x) - u(x - \Delta x)}{\Delta x} + o(\Delta x)$$

$$\text{Central : } u_x(x) = \frac{u(x + \Delta x) - u(x - \Delta x)}{2\Delta x} + o(\Delta x)^2.$$

The second derivative $u_{xx}(x)$ can be obtained by adding (3.8) and (3.9):

$$u_{xx}(x) = \frac{u(x + \Delta x) - 2u(x) + u(x - \Delta x)}{(\Delta x)^2} + o(\Delta x)^2.$$

To apply this technique to the governing equation, the numerical domain should be discretized as a uniform grid of dimensions of Δx (spacing in the x direction) by Δt (time step). The discrete values of the function $u(x, t)$ at the grid point $(i\Delta x, n\Delta t)$, where $i = 1, 2, \dots$ and $n = 1, 2, \dots$, can be denoted as u_i^n . By using this notation, partial differential equations can be changed to finite difference equations. For example, the linear advection equation

$$u_t + au_x = 0 \quad (3.10)$$

with a constant speed a can be considered. The time derivative u_t at the grid point $(i\Delta x, n\Delta t)$ can be discretized by using the first-order forward approximation

$$u_t = \frac{u_i^{n+1} - u_i^n}{\Delta t}, \quad (3.11)$$

while the spatial derivative u_x is discretized by the second-order central approximation

$$u_x = \frac{u_{i+1}^n - u_{i-1}^n}{2\Delta x}. \quad (3.12)$$

By substituting equation (3.11) and (3.12) into the partial differential equation (3.10), the following finite difference equation can be obtained:

$$\frac{u_i^{n+1} - u_i^n}{\Delta t} + a \frac{u_{i+1}^n - u_{i-1}^n}{2\Delta x} = 0.$$

The ultimate purpose of numerical analysis in time dependent problems is to get the solution u_i^{n+1} at next time level which can be updated by the following form

$$u_i^{n+1} = u_i^n - \frac{\nu}{2}(u_{i+1}^n - u_{i-1}^n) \quad (3.13)$$

where $\nu = a \frac{\Delta t}{\Delta x}$ is the dimensionless quantity known as the Courant-Friedrichs-Lewy number or CFL number which is closely related to the stability of the numerical scheme. The Courant-Friedrichs-Lewy (CFL) number can be regarded as the ratio of two speeds, namely the wave propagation speed a and the grid speed $\frac{\Delta x}{\Delta t}$ [28].

Explicit/Implicit Scheme

The temporal discretization of the finite difference method can be classified into the two following approaches: explicit and implicit. In the finite difference equation (3.13), the spatial derivative u_x is approximated in terms of values at time level $n\Delta t$. As a result, the solution u_i^{n+1} at new time level $(n+1)\Delta t$ can be easily computed with the known values $u_{i-1}^n, u_i^n, u_{i+1}^n$ at time level $n\Delta t$. This is an explicit method because the way to find the solutions is very clear and direct. On the contrary, if the spatial derivative u_x is approximated with the values at time level $(n+1)\Delta t$, the finite difference equation (3.13) can be rewritten as

$$\frac{u_i^{n+1} - u_i^n}{\Delta t} + v \frac{u_{i+1}^{n+1} - u_{i-1}^{n+1}}{2\Delta x} = 0 \quad \text{or} \quad u_i^{n+1} + \frac{v}{2}(u_{i+1}^{n+1} - u_{i-1}^{n+1}) = u_i^n.$$

This is an implicit method in which the solutions cannot be obtained directly. In an implicit scheme, the solution u_i^{n+1} cannot be calculated explicitly because it is coupled with u_{i+1}^{n+1} and u_{i-1}^{n+1} . Generally, implicit schemes can be solved by using special numerical techniques like the iterative method. Both explicit and implicit methods have merits and demerits. The explicit method is conceptually simple and easy to program, but explicit schemes are liable to be numerically unstable if large time step Δt (or CFL number larger than 1) is chosen. On the contrary, the implicit method is more stable than the explicit method and generally not restricted by numerical stability, i.e. a large time step is allowed, while it is more complicated and difficult to program.

The Upwind Scheme

The finite difference method can produce correct solutions with less numerical errors when it uses certain spatial discretization techniques like the upwind method. The numerical scheme (3.13) uses the central approximation for the spatial derivative. Alternatively, the one-sided approximation for the spatial derivative can be used and the advection equation (3.10) can be rewritten using the backward approximation:

$$u_i^{n+1} = u_i^n - v(u_i^n - u_{i-1}^n). \quad (3.14)$$

If the wave propagation speed $a > 0$, this scheme can produce very correct solutions because it is discretized in the same direction that the wave, or the characteristic information, of the problem propagates. This technique is the upwind method and known to offer discrete solutions which are closer to the physical process than the central approximation [61]. The upwind method is well adapted to advection dominated problems and has first-order accuracy in space and time. Similarly, the upwind technique can be applied to the case of $a < 0$:

$$u_i^{n+1} = u_i^n - v(u_{i+1}^n - u_i^n). \quad (3.15)$$

Equation (3.14) and (3.15) can be combined into one equation which can be used for both positive and negative wave speed a by using the notations

$$a^+ = \max(a,0) = \frac{1}{2}(a + |a|), \quad a^- = \min(-a,0) = \frac{1}{2}(a - |a|)$$

and

$$v^+ = a^+ \frac{\Delta t}{\Delta x}, \quad v^- = a^- \frac{\Delta t}{\Delta x}.$$

Then the general form of the first-order upwind scheme can be expressed as

$$u_i^{n+1} = u_i^n - v^+(u_i^n - u_{i-1}^n) - v^-(u_{i+1}^n - u_i^n).$$

This technique can be used to solve a systems of conservation law by defining Jacobian A^+ and A^- as

$$A = A^+ + A^-, \quad A^+ = \frac{1}{2}(A + |A|), \quad A^- = \frac{1}{2}(A - |A|),$$

and, the first-order upwind scheme for a system of conservation law can be expressed as

$$U_i^{n+1} = U_i^n - A^+ \frac{\Delta t}{\Delta x} (U_i^n - U_{i-1}^n) - A^- \frac{\Delta t}{\Delta x} (U_{i+1}^n - U_i^n).$$

Other Well-known Schemes

Conservation laws can be numerically discretized and solved by using the finite difference method. The following numerical schemes are well-known methods which have been widely used to solve the shallow water equations. Each scheme has different form because it uses different temporal and spatial discretization techniques.

Explicit Schemes

Lax-Friedrichs scheme : u_i^n in the finite difference equation (3.13) is replaced by the average $(u_{i+1}^n + u_{i-1}^n)/2$, first-order accurate in space and time:

$$u_i^{n+1} = \frac{1}{2}(u_{i+1}^n + u_{i-1}^n) - \frac{1}{2}v(u_{i+1}^n - u_{i-1}^n).$$

Leap-Frog scheme : one of the earliest schemes used for numerical method, first-order accurate in space and time:

$$u_i^{n+1} = u_i^{n-1} - v(u_{i+1}^n - u_{i-1}^n).$$

Lax-Wendroff scheme : second derivative u_{xx} term is added to (3.13), second-order accurate in space and time, shows oscillatory behaviour in the upstream areas of discontinuities:

$$u_i^{n+1} = u_i^n - \frac{1}{2}v(u_{i+1}^n - u_{i-1}^n) + \frac{1}{2}v^2(u_{i+1}^n - 2u_i^n + u_{i-1}^n).$$

Warming & Beam : one-sided approximation is used in spatial derivative term, second-order accurate in space and time, shows oscillatory behaviour after discontinuous solutions:

$$u_i^{n+1} = u_i^n - \frac{1}{2}v(3u_i^n - 4u_{i-1}^n + u_{i-2}^n) + \frac{1}{2}v^2(u_i^n - 2u_{i-1}^n + u_{i-2}^n).$$

Implicit Schemes

Backward Euler scheme : the simplest implicit scheme, second-order accurate in space and first-order in time:

$$u_i^{n+1} = u_i^n - \frac{1}{2}v(u_{i+1}^{n+1} - u_{i-1}^{n+1}).$$

Box scheme : second-order accurate in space and time, used in the ISIS modelling package:

$$\left(\frac{u_{i+1}^{n+1} - u_{i+1}^n}{2\Delta t} + \frac{u_i^{n+1} - u_i^n}{2\Delta t} \right) + a \left(\frac{u_{i+1}^{n+1} - u_i^{n+1}}{2\Delta x} + \frac{u_{i+1}^n - u_i^n}{2\Delta x} \right) = 0.$$

The basic numerical techniques in the finite difference method have been studied in this section. The main focus of this section is on the Finite Volume Method, however, it is very important to understand these techniques because the numerical discretisation procedure of the Finite Volume Methods is also performed by using the similar numerical approximation.

3.3.2 Finite Volume Method

Numerical methods based on the differential form of a conservation law have difficulties in dealing with discontinuities because partial differential equations do not hold on discontinuous solution. In order to solve discontinuous problems, the integral form of conservation law can be used. The Finite Volume Method is based on the

integral form of conservation law. In the Finite Volume Method, the domain is divided into finite numbers of grid cells which have a finite volume as depicted in *Figure 3.1*.

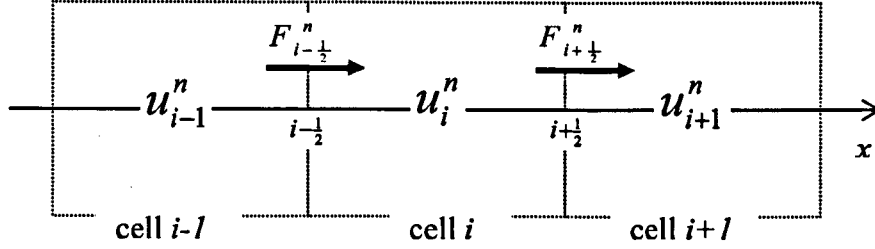


Figure 3.1 Numerical domain of the finite volume method at time $n\Delta t$

In the numerical domain, the value of the variable u_i^n at a fixed time $t^n = n\Delta t$ can be approximated by the cell average

$$u_i^n \approx \frac{1}{\Delta x} \int_{x_{i-1/2}}^{x_{i+1/2}} u(x, t^n) dx$$

and the solution u_i^{n+1} at the next time step $t^{n+1} = (n+1)\Delta t$ can be approximated by applying the integral form of the conservation law over the cell i :

$$\int_{x_{i-1/2}}^{x_{i+1/2}} u(x, t^{n+1}) dx = \int_{x_{i-1/2}}^{x_{i+1/2}} u(x, t^n) dx + \int_n^{n+1} f(u(x_{i-1/2}, t)) dt - \int_n^{n+1} f(u(x_{i+1/2}, t)) dt .$$

By using cell average values, the conservation law can be expressed in the following form

$$u_i^{n+1} = u_i^n - \frac{\Delta t}{\Delta x} (F_{i+1/2}^n - F_{i-1/2}^n) \quad (3.16)$$

where the average numerical flux across the cell interface $x_{i+1/2}$ is given by

$$F_{i+1/2}^n \approx \frac{1}{\Delta t} \int_n^{n+1} f(u(x_{i+1/2}, t)) dt .$$

Then, the problem is reduced to the calculation of numerical fluxes. In other words, if the numerical fluxes $F_{i+1/2}^n$ and $F_{i-1/2}^n$ are known functions, the solution u_i^{n+1} at the next time step can be calculated explicitly by equation (3.16). In Riemann solver based finite volume schemes, the numerical fluxes are calculated by solving a series of local Riemann problems at cell interfaces.

Riemann Problem and Solver

The Riemann problem is a special initial value problem of a hyperbolic partial differential equation system which has piecewise constant initial data with a single jump discontinuity at $x = x_i$. The initial data of a Riemann problem is given as

$$u(x,0) = u_o(x) = \begin{cases} u_L & (x < x_i) \\ u_R & (x > x_i) \end{cases},$$

and depicted in *Figure 3.2*.

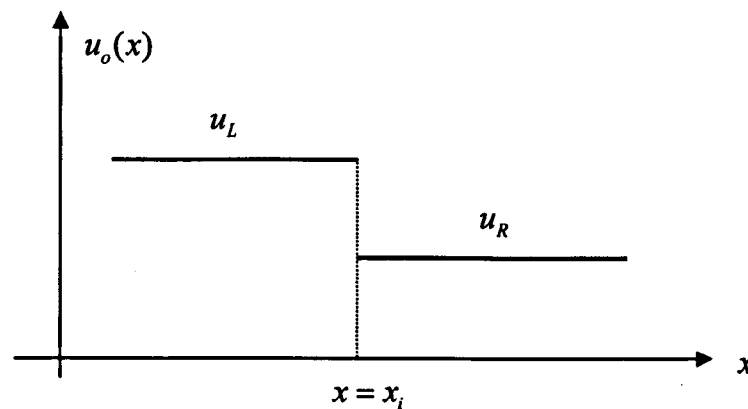


Figure 3.2 Initial data of the Riemann problem

In the finite volume method, each cell has a piecewise constant initial data which means that there is a discontinuity at each interface between neighbouring two cells as depicted in *Figure 3.3*. This discontinuity can be regarded as a local Riemann problem having discontinuous initial data at each cell interface. The solutions can be obtained by solving local Riemann problems at cell interfaces and updating with the conservation scheme (3.16). The method to solve the Riemann problem is called Riemann solver, which is broken down two categories: exact and approximate solvers. Computationally, the exact Riemann solver is often too expensive to compute for nonlinear problems such as the shallow water equations because it needs lots of iterations to find exact solutions. As a result, approximate Riemann solvers are generally used because the solutions show almost similar accuracy with much less computing resources.

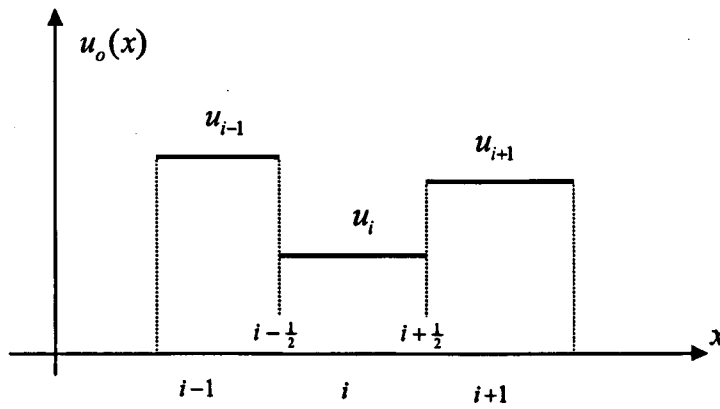


Figure 3.3 Piecewise constant distribution of initial data

Godunov's method

A general approach to solve hyperbolic conservation laws was proposed by Godunov [44]. Godunov's method was the first to introduce the idea of solving non-linear systems as a series of local Riemann problems with exact solution. Although this method was originally developed for solving the Euler equations of gas dynamics, it could be applied to other hyperbolic conservation systems such as the shallow water equations. The main idea of this method is the process of "reconstruct-evolve-average" [63].

At first, the piecewise constant initial data were approximated by calculating the cell average values by the following approximation

$$u_i^n \approx \frac{1}{\Delta x} \int_{x_{i-\frac{1}{2}}}^{x_{i+\frac{1}{2}}} u(x, t^n) dx$$

where $x_{i\pm\frac{1}{2}}$ are the cell boundaries and $u(x, t^n)$ is initial data at time t^n . This leads to a series of Riemann problems at cell interfaces. Then the exact solution $\tilde{u}(x, t^{n+1})$ at time level t^{n+1} was obtained by solving the exact solutions of the local Riemann problems. The time step Δt was chosen to be short enough the two neighbouring waves not to interact, i.e. the CFL number was chosen to be less than $\frac{1}{2}$. The solution u_i^{n+1} at next time level t^{n+1} was approximated by taking the cell average values of the exact solution $\tilde{u}(x, t^{n+1})$

$$u_i^{n+1} \approx \frac{1}{\Delta x} \int_{x_{i-\frac{1}{2}}}^{x_{i+\frac{1}{2}}} \tilde{u}(x, t^{n+1}) dx.$$

The exact solution $\tilde{u}(x, t^{n+1})$ was calculated by applying the integral form of the conservation law within a chosen cell like:

$$\int_{x_{i-\frac{1}{2}}}^{x_{i+\frac{1}{2}}} \tilde{u}(x, t_{n+1}) dx = \int_{x_{i-\frac{1}{2}}}^{x_{i+\frac{1}{2}}} \tilde{u}(x, t_n) dx + \int_n^{n+1} f(\tilde{u}(x_{i-\frac{1}{2}}, t)) dt - \int_n^{n+1} f(\tilde{u}(x_{i+\frac{1}{2}}, t)) dt.$$

Using the definition of cell average, the following conservation form was obtained

$$u_i^{n+1} = u_i^n - \frac{\Delta t}{\Delta x} [F_{i+\frac{1}{2}} - F_{i-\frac{1}{2}}] \quad (3.17)$$

where $F_{i+\frac{1}{2}}$ is the intercell flux at $x_{i+\frac{1}{2}}$ which was defined as

$$F_{i+\frac{1}{2}} = \frac{1}{\Delta t} \int_n^{n+1} f(\tilde{u}(x_{i+\frac{1}{2}}, t)) dt,$$

with $\tilde{u}(x_{i+\frac{1}{2}}, t)$ is constant over the time interval $[t^n, t^{n+1}]$ and related with u_i^n and u_{i+1}^n .

This was computed by solving the local Riemann problem, so $F_{i+\frac{1}{2}}$ was redefined as

$$F_{i+\frac{1}{2}} = f(\tilde{u}(x_{i+\frac{1}{2}}, t)) = f(u^*(u_i^n, u_{i+1}^n))$$

where $u^*(u_i^n, u_{i+1}^n)$ represents the intermediate state between cell i and $i+1$ which propagates along the emerging waves from the cell interface $i + \frac{1}{2}$. As a result, the equation (3.17) can be rewritten as

$$u_i^{n+1} = u_i^n - \frac{\Delta t}{\Delta x} [f(u^*(u_i^n, u_{i+1}^n)) - f(u^*(u_{i-1}^n, u_i^n))].$$

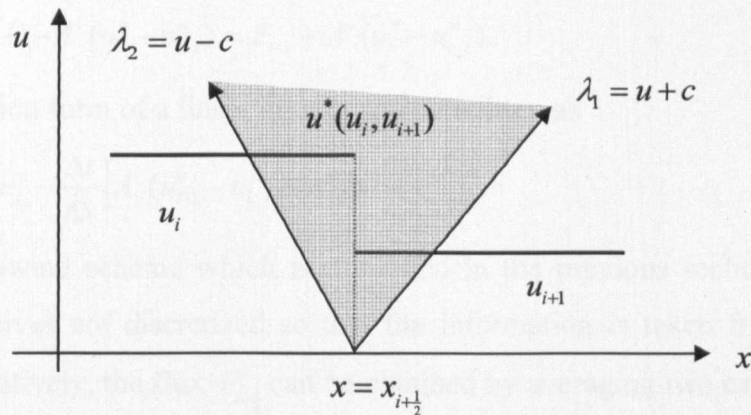


Figure 3.4 The solution structure of a Riemann problem

In *Figure 3.4*, the solution structure of the Riemann problem in the shallow water equations is depicted and, as shown in the figure, the intermediate value $u^*(u_i^n, u_{i+1}^n)$ propagates along the two eigenvalues (or waves) λ_1 and λ_2 of the Jacobian matrix A .

Godunov's Method for Linear Systems

Godunov's method can be applied to the linear system of a conservation law. For a constant coefficient linear system $u_t + Au_x = 0$, the flux $F_{i+\frac{1}{2}}$ can be described as

$$F_{i+\frac{1}{2}} = f(u^*(u_i^n, u_{i+1}^n)) = Au^*(u_i^n, u_{i+1}^n).$$

The value of $u^*(u_i^n, u_{i+1}^n)$ can be calculated by solving the Riemann problem with u_i^n (left state) and u_{i+1}^n (right state), that is

$$u^*(u_i^n, u_{i+1}^n) = u_i^n + \sum_{\lambda_k < 0} \alpha_k e_k = u_{i+1}^n - \sum_{\lambda_k > 0} \alpha_k e_k$$

where e_k is the k th eigenvector of A and α_k is the coefficient of e_k in an eigenvector expansion of $u_i^n - u_{i+1}^n$. The flux $F_{i+\frac{1}{2}}$ is

$$\begin{aligned} F_{i+\frac{1}{2}} &= A \left(u_i^n + \sum_{\lambda_k < 0} \alpha_k e_k \right) = A \left(u_{i+1}^n - \sum_{\lambda_k > 0} \alpha_k e_k \right) \\ &= Au_i^n + \sum_{\lambda_k < 0} \alpha_k \lambda_k e_k = Au_{i+1}^n - \sum_{\lambda_k > 0} \alpha_k \lambda_k e_k \\ &= F_i + A^-(u_{i+1}^n - u_i^n) = F_{i+1} - A^+(u_{i+1}^n - u_i^n). \end{aligned} \quad (3.18)$$

Similarly,

$$F_{i-\frac{1}{2}} = F_i - A^+(u_i^n - u_{i-1}^n) = F_{i-1} + A^-(u_i^n - u_{i-1}^n). \quad (3.19)$$

The conservation form of a linear system can be written as

$$u_i^{n+1} = u_i^n - \frac{\Delta t}{\Delta x} \left[A^-(u_{i+1}^n - u_i^n) + A^+(u_i^n - u_{i-1}^n) \right]. \quad (3.20)$$

This is the upwind scheme which is presented in the previous section because the spatial derivatives are discretized so that the information is taken from the side it comes. Alternatively, the flux $F_{i+\frac{1}{2}}$ can be obtained by averaging two expressions given in (3.18) and (3.19)

$$\begin{aligned}
F_{i+\frac{1}{2}} &= \frac{1}{2}(F_i + F_{i+1}) - \frac{1}{2}(A^+ - A^-)(u_{i+1}^n - u_i^n) \\
&= \frac{1}{2}(F_i + F_{i+1}) - \frac{1}{2}|A|(u_{i+1}^n - u_i^n).
\end{aligned}$$

By using this flux, the conservation form (3.20) can be rewritten as

$$u_i^{n+1} = u_i^n - \frac{\Delta t}{2\Delta x}(F_{i+1} - F_{i-1}) + \frac{\Delta t}{2\Delta x}|A|(u_{i+1}^n - 2u_i^n + u_{i-1}^n).$$

3.4 Roe's Approximate Riemann Solver

The Godunov's method requires the exact solution of the Riemann problem at every cell interface at each time level. This process is expensive and requires iterative procedures for nonlinear problems. So, many approximate solutions which are less expensive and show equally good numerical results have been developed by many researchers [32, 48, 69, 76]. Among them, the approximate Riemann solver proposed by Roe [69] is the most well known and shows robust solutions. The main concept of Roe's method is to replace the original nonlinear conservation law $u_t + F_x = 0$ with a constant coefficient linear system

$$u_t + \tilde{A}u_x = 0$$

and calculate the exact solutions of this approximate problem. $\tilde{A} = \tilde{A}(u_L, u_R)$ is the approximate Jacobian matrix having constant coefficients and satisfies the following list of properties:

- (i) It constitutes a linear mapping from the vector space u to the vector space F
- (ii) As $u_L \rightarrow u_R \rightarrow u$, $\tilde{A}(u_L, u_R) = A(u)$, where $A = \partial F / \partial u$
- (iii) For any u_L and u_R , $\tilde{A}(u_L, u_R) \times (u_R - u_L) = F_R - F_L$
- (iv) The eigenvectors of \tilde{A} are linearly independent.

These properties are collectively called "Property U " since it is intended to ensure "uniform validity" across discontinuities. According to "Property U ", the eigenvalues of the matrix \tilde{A} can be considered as the wavespeeds of the Riemann problem, and the projections of $u_R - u_L$ onto its eigenvectors are the jumps which takes place between two states (Rankine-Hugoniot Condition).

From the condition (iv), \tilde{A} can be diagonalized as

$$\tilde{A} = R\tilde{\Lambda}R^{-1}$$

where R is the matrix of right eigenvectors \tilde{e}_k and $\tilde{\Lambda}$ is the diagonal matrix of eigenvalues $\tilde{\lambda}_k$. The condition (iii) can be rewritten as

$$\tilde{A}\Delta u = \Delta F$$

where $\Delta(\bullet) = (\bullet)_R - (\bullet)_L$. Then, from the relation

$$\Delta u = \sum \tilde{\alpha}_k \tilde{e}_k,$$

the following form can be obtained

$$\Delta F = \tilde{A} \sum \tilde{\alpha}_k \tilde{e}_k = \sum \tilde{\alpha}_k \tilde{\lambda}_k \tilde{e}_k$$

where $\tilde{\alpha}_k$ is the wave strength of the k th wave travelling with speed $\tilde{\lambda}_k$.

3.4.1 The shallow water equations and Roe's Riemann Solver

Roe's method was originally developed for the Euler equations which is a hyperbolic equation system in gas dynamics. However, it could be successfully applied to the shallow water equations which is also a nonlinear hyperbolic equation system.

Glaister [43] applied Roe's method to the shallow water equations with the finite difference method. In the paper, the shallow water equations for an infinitely wide and frictionless rectangular channel was given as

$$w_t + F_x = f$$

with

$$w = (\phi, \phi u)^T,$$

$$F(w) = \left(\phi u, \phi u^2 + \frac{\phi^2}{2} \right)^T,$$

$$f(w) = (0, g\phi h'(x))^T,$$

where $\phi = \phi(x, t)$ represents g multiplied by the total height above the channel bottom. By using the approximate Jacobian matrix, the eigenvectors and wave strengths were defined as

$$\tilde{\lambda}_1 = \tilde{u} + \tilde{\psi}, \quad \tilde{e}_1 = (1, \tilde{u} + \tilde{\psi})^T,$$

$$\tilde{\lambda}_2 = \tilde{u} - \tilde{\psi}, \quad \tilde{e}_2 = (1, \tilde{u} - \tilde{\psi})^T,$$

$$\tilde{\alpha}_1 = \frac{1}{2} \Delta \phi + \frac{1}{2} \frac{\tilde{\phi}}{\tilde{\psi}} \Delta u, \quad \tilde{\alpha}_2 = \frac{1}{2} \Delta \phi - \frac{1}{2} \frac{\tilde{\phi}}{\tilde{\psi}} \Delta u$$

where the intermediate values \tilde{u} , $\tilde{\phi}$ and $\tilde{\psi}$ are

$$\tilde{u} = \frac{\sqrt{\phi_R} u_R + \sqrt{\phi_L} u_L}{\sqrt{\phi_R} + \sqrt{\phi_L}},$$

$$\tilde{\phi} = \sqrt{\phi_R \phi_L}$$

$$\tilde{\psi} = \sqrt{\frac{1}{2}(\phi_R + \phi_L)}.$$

By using the defined variables, the governing equation without source terms was numerically discretized as

$$\frac{w_P^{n+1} - w_P^n}{\Delta t} + \frac{\sum_{i=1}^2 \tilde{\lambda}_i \tilde{\alpha}_i \tilde{e}_i}{\Delta x} = 0$$

where notation P represents state L (left) or R (right). Then, upwind differencing was applied for the update procedure, which means

$$\text{added } -\frac{\Delta t}{\Delta x} \tilde{\lambda}_i \tilde{\alpha}_i \tilde{e}_i \text{ to } w_R \quad \text{when } \tilde{\lambda}_i > 0$$

or

$$\text{added } -\frac{\Delta t}{\Delta x} \tilde{\lambda}_i \tilde{\alpha}_i \tilde{e}_i \text{ to } w_L \quad \text{when } \tilde{\lambda}_i < 0.$$

The author also proposed an upwind source term treatment by using the from

$$\tilde{f} = -\frac{1}{\Delta x} \sum_{i=1}^2 \tilde{\lambda}_i \tilde{\beta}_i \tilde{e}_i$$

where the approximate vector $\tilde{f} = (0, g\tilde{\phi}(\Delta h/\Delta x))^T$ with $\tilde{\phi} = \sqrt{\phi_L \phi_R}$. Finally, the effects of the source terms were upwinded by replacing the wave strength $\tilde{\alpha}_i$ in homogeneous part of the equation with $\tilde{\lambda}_i = \tilde{\alpha}_i + \tilde{\beta}_i$. The proposed numerical scheme was applied to the idealised dam-break problem with various ratios of $\phi_{\text{upstream}}/\phi_{\text{downstream}}$. Second-order accurate solutions were obtained by using a flux limiter and the scheme produced generally good agreement with the analytical solutions even though it used the finite difference method.

The Riemann solver produces much better solution when combined with the finite volume method. Garcia-Navarro and Vazquez-Cendon [40] applied Roe's solver to the shallow water equations and presented two expressions of the explicit first-order Roe's scheme. The first expression was the "signal model" given by

$$U_n^{i+1} = U_i^n - \frac{\Delta t}{\Delta x} \left((\tilde{\lambda}_1^- \tilde{\alpha}_1 \tilde{e}_1)_{i+\frac{1}{2}} + (\tilde{\lambda}_2^- \tilde{\alpha}_2 \tilde{e}_2)_{i+\frac{1}{2}} + (\tilde{\lambda}_1^+ \tilde{\alpha}_1 \tilde{e})_{i-\frac{1}{2}} + (\tilde{\lambda}_2^+ \tilde{\alpha}_2 \tilde{e}_2)_{i-\frac{1}{2}} \right)$$

where

$$\tilde{\lambda}_k^\pm = \frac{1}{2} (\tilde{\lambda}_k \pm |\tilde{\lambda}_k|).$$

The alternative expression named "flux model" was given by

$$U_i^{n+1} = U_i^n - \frac{\Delta t}{\Delta x} (F_{i+\frac{1}{2}}^* - F_{i-\frac{1}{2}}^*)$$

where the numerical flux function $F_{i+\frac{1}{2}}^*$ at cell interface $i+\frac{1}{2}$ was obtained from the relation

$$\Delta F_{i+\frac{1}{2}} = F_{i+1} - F_i = \sum_k (\tilde{\lambda}_k \tilde{\alpha}_k \tilde{e}_k)_{i+\frac{1}{2}}$$

and expressed by the following form

$$F_{i+\frac{1}{2}}^* = \frac{1}{2} (F_i + F_{i+1}) - \frac{1}{2} \sum_k (\tilde{\lambda}_k |\tilde{\alpha}_k \tilde{e}_k|)_{i+\frac{1}{2}}.$$

Burguete and Garcia-Navarro published a series of papers [15,16,17] and proposed a new form and notations for one-dimensional conservative schemes. The authors decomposed the difference of nodal fluxes (F^T) of two neighbouring cells into two portions along the direction of waves like

$$\delta F_{i+\frac{1}{2}}^T = \delta F_{i+\frac{1}{2}}^R + \delta F_{i+\frac{1}{2}}^L$$

where δ used for the space increments and the superscripts R and L represent the direction of contribution of the flux difference. Then, the conservative scheme was expressed as the following form

$$\Delta u_i^n = \Delta t \left[S_i - \frac{1}{\Delta x} (\delta F_{i+\frac{1}{2}}^R + \delta F_{i-\frac{1}{2}}^L) \right].$$

From this form, the intercell numerical flux was expressed as

$$F_{i+\frac{1}{2}}^* = F_i^T + \delta F_{i+\frac{1}{2}}^R = F_{i+1}^T - \delta F_{i+\frac{1}{2}}^L.$$

The authors also discretized the source terms including spatial derivatives in a similar way:

$$S_{i+\frac{1}{2}}^T = S_{i+\frac{1}{2}}^R + S_{i+\frac{1}{2}}^L$$

and, finally, the conservative numerical scheme with source terms was expressed in the following simple form

$$\Delta u_i^n = \Delta t (G_{i-\frac{1}{2}}^L + G_{i+\frac{1}{2}}^R)$$

with $G_{i+\frac{1}{2}} = \left(S - \frac{\partial F}{\partial x} \right)_{i+\frac{1}{2}}$. This was also expressed as a characteristic form like

$$\Delta u_i^n = \Delta t [(R\Omega^L R^{-1}G)_{i-\frac{1}{2}} + (R\Omega^R R^{-1}G)_{i+\frac{1}{2}}]$$

with $(R^{-1}G)_{i+\frac{1}{2}} = (\Omega^L R^{-1}G)_{i+\frac{1}{2}} + (\Omega^R R^{-1}G)_{i+\frac{1}{2}}$ and $(\Omega^L + \Omega^R)_{i+\frac{1}{2}} = I$

where the matrices Ω^L and Ω^R have different forms according to the type of numerical scheme. This new form of conservative scheme represents the same form as the signal model proposed by Garcia-Navarro and Vazquez-Cendon [40] in case of the first-order Roe's upwind scheme. However, it represents a more general form of conservative scheme which can be used for any different type of numerical schemes. The authors tried to avoid the fractional step method to solve the shallow water equations with source terms and combined the flux term and source terms. However, the new form of conservative scheme is not expressed as a conservation law which leads to less applicability and, as a result, the term formed by combining the differentiation of the flux term and the source terms can not directly used for the evaluation of numerical flux at each cell interface. Moreover, the decomposition of the difference of nodal fluxes is not easily performed because the matrices Ω^L and Ω^R have complicated forms.

In [16], the authors modified the Lax-Friedrichs scheme into a conservative form by using the above definition. The decomposition of the flux difference of the Lax-Friedrichs scheme was written as

$$\delta F_{i+\frac{1}{2}}^L = \frac{1}{2} \delta F_{i+\frac{1}{2}}^n + \frac{v\Delta x}{2\Delta t} \delta u_{i+\frac{1}{2}}^n \quad \text{and} \quad \delta F_{i+\frac{1}{2}}^R = \frac{1}{2} \delta F_{i+\frac{1}{2}}^n - \frac{v\Delta x}{2\Delta t} \delta u_{i+\frac{1}{2}}^n$$

where $\nu = (1 - \alpha)/2$ is an artificial viscosity with weighting parameter α . Moreover, the authors proposed the Optimised Lax-Fridrichs scheme to be less dissipative by locally defining the parameter ν by the following form

$$\delta\nu_{i+\frac{1}{2}} = \left(\frac{\text{mod min}(\delta A, (S\delta x - \delta F + 2u\delta Q)/(u^2 - c^2))}{\delta Q} \right)_{i+\frac{1}{2}}.$$

The proposed method was applied to several test cases such as dam-break simulations and a real river flow cases and showed less dissipative results than the normal Lax-Friedrichs scheme.

Implicit schemes were also developed by many researchers because this kind of scheme, theoretically, allows unconditional stability and time steps as big as desired. Garcia-Navarro et al. [39] constructed an implicit scheme which was based on Roe's method for modelling water flows in open channels and pipes. In the paper, the discretized implicit scheme was written as

$$\frac{U_i^{n+1} - U_i^n}{\Delta t} + \frac{1}{\Delta x} \left[\theta(F_{i+\frac{1}{2}}^{*n+1} - F_{i-\frac{1}{2}}^{*n+1}) + (1 - \theta)(F_{i+\frac{1}{2}}^{*n} - F_{i-\frac{1}{2}}^{*n}) \right] = \theta S_i^{n+1} + (1 - \theta)S_i^n.$$

The numerical flux $F_{i+\frac{1}{2}}^*$ was computed by using the approximate Jacobian matrix

$$\tilde{A}_{i+\frac{1}{2}} = \tilde{R}_{i+\frac{1}{2}} \text{diag}(\tilde{\lambda}_{i+\frac{1}{2}}) \tilde{R}_{i+\frac{1}{2}}^{-1}:$$

$$F_{i+\frac{1}{2}}^* = \frac{1}{2} \left[F_{i+1} + F_i - B_{i+\frac{1}{2}} \delta U_{i+\frac{1}{2}} \right]$$

where $B_{i+\frac{1}{2}} = \tilde{R}_{i+\frac{1}{2}} \Lambda_{i+\frac{1}{2}} \tilde{R}_{i+\frac{1}{2}}^{-1}$ with $\Lambda_{i+\frac{1}{2}}$ is an diagonal vector. In the paper, flux limited second-order TVD scheme was used and $\Lambda_{i+\frac{1}{2}}$ was redefined as

$$\Lambda_{i+\frac{1}{2}} = \text{diag}[\Psi_{i+\frac{1}{2}}^k (1 - \Phi_{i+\frac{1}{2}}^k)]$$

where Ψ is the entropy correction and Φ is the flux limiter function. Then the flux and source terms at time $t = t^{n+1}$ were approximated by applying Taylor series expansion like

$$F_i^{n+1} = F_i^n + A_i^n \Delta U_i + O(\Delta t^2)$$

and

$$S_i^{n+1} = S_i^n + G_i^n \Delta U_i + O(\Delta t^2)$$

where G is the Jacobian matrix of the source term and given by

$$G = \begin{pmatrix} 0 & 0 \\ g \left[S_o + S_f \left(1 + \frac{4}{3} \frac{b}{b+2h} \right) \right] & -\frac{2gA}{Q} S_f \end{pmatrix}.$$

Finally, the implicit form of the conservative scheme was written as the form of a block tridiagonal system

$$AA_i \Delta U_{i-1} + BB_i \Delta U_i + CC_i \Delta U_{i+1} = DD_i$$

where the coefficients are 2×2 matrices with the following form:

$$AA_i = -\frac{\lambda\theta}{2} [A_{i-1} + B_{i-\frac{1}{2}}]^n$$

$$BB_i = I - \theta \Delta t G_i^n + \frac{\lambda\theta}{2} [B_{i+\frac{1}{2}} + B_{i-\frac{1}{2}}]^n$$

$$CC_i = \frac{\lambda\theta}{2} [A_{i+1} - B_{i+\frac{1}{2}}]^n$$

$$DD_i = -\lambda (F_{i+\frac{1}{2}}^* - F_{i-\frac{1}{2}}^*)^n + \Delta t G_i^n.$$

The proposed implicit scheme was applied to several test cases including open channel flows and pressurised flows in pipe networks with *CFL* values of 0.5, 1, 2 and 4. The numerical results showed that the proposed implicit scheme remained stable and produces reasonable results with some amount of numerical diffusion provided that the *CFL* does not become overly large.

Burguete and Garcia-Navarro [17] proposed a more general form of implicit scheme by using the flux difference decomposition approach. The implicit form of the conservative scheme was written as

$$\Delta u_i^n = \Delta t [(G^L)_{i-\frac{1}{2}}^{n+\theta} + (G^R)_{i+\frac{1}{2}}^{n+\theta}]$$

and the following approximation was made

$$F^{n+1} \approx F^n + \frac{\partial F^n}{\partial t} \Delta t \approx F^n + \left(\frac{\partial F}{\partial u} \frac{\partial u}{\partial t} \right)^n \Delta t \approx F^n + A^n \Delta u^n$$

$$S^{n+1} \approx S^n + \frac{\partial S^n}{\partial t} \Delta t \approx S^n + \left(\frac{\partial S}{\partial u} \frac{\partial u}{\partial t} \right)^n \Delta t \approx S^n + K^n \Delta u^n$$

where $K = \partial S / \partial u$ is the Jacobian matrix of the source term vector. Then, the implicit conservative scheme was expressed as

$$\begin{aligned} & \theta \frac{\Delta t}{\Delta x} (A^- \Delta u)_{i+1}^n + \left[1 - \theta \Delta t \left(K - \frac{A^+}{\Delta x} + \frac{A^-}{\Delta x} \right) \right]_i^n \Delta u_i^n - \theta \frac{\Delta t}{\Delta x} (A^+ \Delta u)_{i-1}^n \\ & = \Delta t [(G^L)_{i-\frac{1}{2}}^n + (G^R)_{i+\frac{1}{2}}^n] \end{aligned}$$

with $A^\pm = R\Omega^\pm R^-$. The authors introduced an artificial viscosity because the above form was unable to deal transcritical problems. The decomposed numerical fluxes with the artificial viscosity had the following form

$$\begin{aligned} F_i^T &= F_i^n + \theta (A \Delta u)_i^n \\ \delta F_{i+\frac{1}{2}}^L &= (\delta F^+)_{i+\frac{1}{2}}^n + \theta \delta (A^+ \Delta u)_{i+\frac{1}{2}}^n - (v \delta u)_{i+\frac{1}{2}}^n \\ \delta F_{i+\frac{1}{2}}^R &= (\delta F^-)_{i+\frac{1}{2}}^n + \theta \delta (A^- \Delta u)_{i+\frac{1}{2}}^n + (v \delta u)_{i+\frac{1}{2}}^n \end{aligned}$$

where the artificial viscosity was defined as

$$v_{i+\frac{1}{2}}^n = \max_k (v^k)_{i+\frac{1}{2}}^n$$

with

$$(v^k)_{i+\frac{1}{2}}^n = \begin{cases} \frac{1}{4} [\delta (\lambda^k)_{i+\frac{1}{2}}^n - 2 |\lambda^k|_{i+\frac{1}{2}}^n] & \text{if } (\lambda^k)_i^n < 0 \text{ and } (\lambda^k)_{i+\frac{1}{2}}^n \\ 0 & \text{otherwise} \end{cases}$$

3.4.2 Spatial Second-order Schemes and High Resolution Method

It is well-known that high-order linear constant coefficient schemes produce unphysical oscillations in the vicinity of large gradient or discontinuities [77]. According to Godunov's theorem, "It is not possible to construct a constant coefficient scheme that is at least second-order and will not give rise to spurious oscillations" [63]. This is the most significant disadvantage of using high-order schemes. To solve this problem, the high-resolution method was developed. The main idea of the high-resolution method is to combine the advantages of the second-order (or higher-order) scheme and the upwind scheme (or first-order) to secure better accuracy in smooth solution with non-oscillatory behaviour near discontinuous solutions.

For example, the Lax-Wendroff scheme is one of the most well-known spatial second-order schemes and has the following form

$$u_i^{n+1} = u_i^n - \frac{\Delta t}{2\Delta x} A(u_{i+1}^n - u_{i-1}^n) + \frac{1}{2} \left(\frac{\Delta t}{\Delta x} \right)^2 A^2(u_{i+1}^n - 2u_i^n + u_{i-1}^n).$$

This equation can be rewritten as a conservative form like

$$u_i^{n+1} = u_i^n - \frac{\Delta t}{\Delta x} (F_{i+\frac{1}{2}}^n - F_{i-\frac{1}{2}}^n)$$

with

$$F_{i+\frac{1}{2}}^n = \frac{1}{2} A(u_{i+1}^n + u_i^n) - \frac{1}{2} \frac{\Delta t}{\Delta x} A^2(u_{i+1}^n - u_i^n).$$

The numerical flux $F_{i+\frac{1}{2}}^n$ can be expressed in terms of the Roe's method:

$$F_{i+\frac{1}{2}}^* = \frac{1}{2} (F_i + F_{i+1}) - \frac{1}{2} \sum_k (\tilde{\alpha}_k |\tilde{\lambda}_k| \tilde{e}_k)_{i+\frac{1}{2}} + \frac{1}{2} \sum_k \tilde{\alpha}_k |\tilde{\lambda}_k| \left(1 - \frac{\Delta t}{\Delta x} |\tilde{\lambda}_k| \right) \tilde{e}_k.$$

This scheme produces more accurate results on smooth solutions than first-order schemes but fails near discontinuities where oscillations are generated. However, the Lax-Wendroff scheme can be modified to not show numerical oscillations near discontinuities while having second-order accuracy on smooth solutions. This can be implemented by decomposing the numerical flux $F_{i+\frac{1}{2}}^n$ into two parts: the first-order accurate part and a correction term corresponding to an anti-diffusive term which causes numerical oscillations on discontinuous solutions. This anti-diffusive term can be limited near discontinuities by applying a flux limiter function [77]. The flux limited version of Lax-Wendroff scheme can be expressed as

$$F_{i+\frac{1}{2}}^* = \frac{1}{2} (F_i + F_{i+1}) - \frac{1}{2} \sum_k (\tilde{\alpha}_k |\tilde{\lambda}_k| \tilde{e}_k)_{i+\frac{1}{2}} + \frac{1}{2} \sum_k \Phi_k (\tilde{\alpha}_k |\tilde{\lambda}_k| \left(1 - \frac{\Delta t}{\Delta x} |\tilde{\lambda}_k| \right) \tilde{e}_k)$$

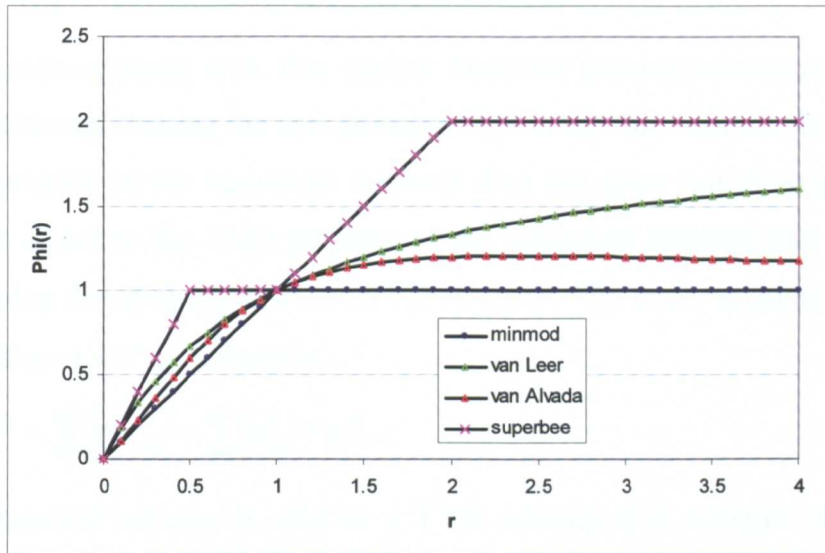
where $\Phi = \Phi(r_i)$ is the flux limiter function. The value of the flux limiter Φ can be changed according to the behaviour of the solution. To satisfy two contradictory conditions of high-resolution method, i.e. second-order accuracy and absence of unphysical oscillations, the value of Φ should be reduced to zero on the discontinuous solutions while having a non-zero value on smooth solutions.

Many researchers have developed flux limiter functions satisfying the condition for high-resolution scheme and the most commonly used limiters are

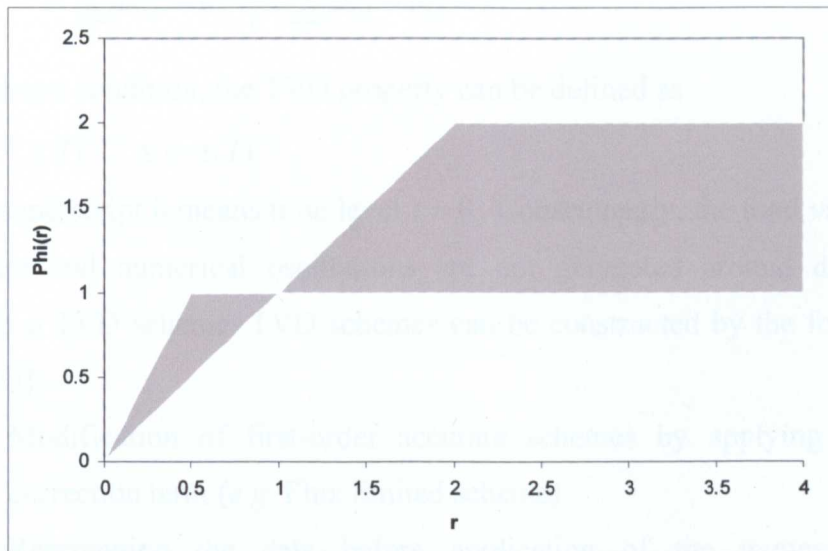
$$\text{- Roe's Minmod : } \Phi(r_i) = \max(0, \min(r_i, 1))$$

- Van Leer : $\Phi(r_i) = \frac{r_i + |r_i|}{1 + |r_i|}$
- Van Albada : $\Phi(r_i) = \frac{r_i + r_i^2}{1 + r_i^2}$
- Roe's Superbee : $\Phi(r_i) = \max(0, \min(2r_i, 1), \min(r_i, 2))$

where $r_i = \frac{u_i - u_{i-1}}{u_{i+1} - u_i}$.



(a)



(b)

Figure 3.5 (a) The Sweby digram of several flux limiters and
(b) Second order TVD region

Flux limiters must satisfy the Total Variation Diminishing(TVD) condition that means $\Phi(r) \leq \min(2r, 2)$ for $(r \geq 0)$ and pass smoothly through the point $\Phi(r) = 1$ to obtain second-order accuracy. The properties of some flux limiters are shown in the Sweby diagram in Figure 3.5. The Superbee limiter shows largest $\Phi(r)$ value while the minmod limiter has the smallest value. As a result, the minmod limiter has the dissipative property which diffuses shock waves. On the contrary, the Superbee limiter shows the anti-dissipative property which sharpens the water wave.

Total Variation Diminishing (TVD) Methods

High-resolution schemes with flux limiter functions prevent numerical oscillations and instabilities by limiting the anti-diffusive term in the flux function. In other words, the total variation of the numerical schemes does not grow but diminishes as time goes by. It is due to the TVD property of the numerical schemes and a numerical scheme having this property is called TVD schemes. The total variation of a discrete solution at time $t = t^n$ is defined as

$$TV^n = \sum_i |\Delta u_{i+\frac{1}{2}}^n| = \sum_i |u_{i+1}^n - u_i^n|.$$

Then a numerical scheme is said to a TVD scheme if it satisfies the following condition

$$TV^{n+1} = \sum_i |u_{i+1}^{n+1} - u_i^{n+1}| \leq \sum_i |u_{i+1}^n - u_i^n| = TV^n.$$

From the above condition, the TVD property can be defined as

$$TV^n \leq TV^{n-1} \leq \dots \leq TV^0$$

where the superscript 0 means time level $t = 0$. Consequently, the total variation does not increase and numerical oscillations are not generated around discontinuous solutions in a TVD scheme. TVD schemes can be constructed by the following two methods [23]:

1. Modification of first-order accurate schemes by applying the limited correction term (e.g. Flux limited scheme)
2. Rearranging the data before application of the numerical method (e.g. Monotone Upstream Scheme for Conservation Law(MUSCL) with slope limiters)

and many researchers have proposed various types of TVD schemes.

Garcia-Navarro et al. [38] proposed a TVD-MacCormack scheme by using Roe's method. The original MacCormack scheme is a two-step predictor-corrector method. It is composed of the following two-substeps in which the spatial derivatives are taken in alternate directions:

$$\text{Predictor step: } U_i^P = U_i^n - \frac{\Delta t}{\Delta x} (F_{i+1}^n - F_i^n)$$

$$\text{Corrector step: } U_i^C = U_i^P - \frac{\Delta t}{\Delta x} (F_i^P - F_{i-1}^P).$$

The updated solution at time $t = t^{n+1}$ is given by

$$U_i^{n+1} = \frac{1}{2} (U_i^P + U_i^C).$$

It has second-order accuracy and shows oscillatory behaviour near discontinuities. The authors modified the classical MacCormack scheme to have TVD property by adding TVD correction terms in the final stage:

$$U_i^{n+1} = \frac{1}{2} (U_i^P + U_i^C) + \frac{\Delta t}{\Delta x} (D_{i+\frac{1}{2}}^n - D_{i-\frac{1}{2}}^n).$$

The correction term $D_{i+\frac{1}{2}}$ was developed on the basis of Roe's method and given by

$$D_{i+\frac{1}{2}} = \frac{1}{2} \sum_k \tilde{\alpha}_{i+\frac{1}{2}}^k |\tilde{\lambda}_{i+\frac{1}{2}}^k| \left(1 - \frac{\Delta t}{\Delta x} |\tilde{\lambda}_{i+\frac{1}{2}}^k| \right) \times \left(1 - \Phi_{i+\frac{1}{2}}^k \right) \tilde{E}_{i+\frac{1}{2}}^k.$$

This term was derived from the higher-order portion of the Lax-Wendroff scheme and the function Φ is the flux limiter responsible for the smoothing of the solutions near discontinuities.

The proposed scheme showed better results in real river flow problems as well as dam-break simulations than the first-order schemes and the classical MacCormack scheme while it maintained conceptual and programming simplicity. Moreover, the authors proposed that the source terms contain spatial derivatives (S_0 and I_2) should be discretized in different direction at predictor and corrector steps

$$\text{Predictor step: } \frac{\partial b}{\partial x} \approx \frac{b_{i+1} - b_i}{\Delta x}$$

$$\text{Corrector step: } \frac{\partial b}{\partial x} \approx \frac{b_i - b_{i-1}}{\Delta x}.$$

Delis and Skeels [29] solved one-dimensional shallow water equations with various TVD schemes and compared the performance of each scheme. In the paper, the explicit conservative numerical scheme is given by

$$U_i^{n+1} = U_i^n - \frac{\Delta t}{\Delta x} (F_{i+\frac{1}{2}}^n - F_{i-\frac{1}{2}}^n) + (\Delta t) S_i^n$$

and, the numerical flux is written as

$$F_{i+\frac{1}{2}} = \frac{1}{2} (F_i + F_{i+1} + R_{i+\frac{1}{2}} D_{i+\frac{1}{2}})$$

where $R_{i+\frac{1}{2}}$ is the right eigenvector matrix and $D_{i+\frac{1}{2}}$ is the scheme-dependent vector function which have different form for each scheme. The authors used the following four Riemann solver based TVD schemes proposed by other researcher [91]:

1. Second-order symmetric TVD scheme : The elements of the vector $D_{i+\frac{1}{2}}$ had the following form

$$(d_{i+\frac{1}{2}}^k) = -(\Delta t / \Delta x) (\tilde{\lambda}_{i+\frac{1}{2}}^k)^2 L_{i+\frac{1}{2}}^k - \psi [\alpha_{i+\frac{1}{2}}^k - L_{i+\frac{1}{2}}^k]$$

where ψ is the entropy correction which is a function of eigenvalues $\tilde{\lambda}_{i+\frac{1}{2}}^k$ and $L_{i+\frac{1}{2}}^k$ is the flux limiter used to guarantee non-oscillatory behaviour near discontinuities. The flux limiter $L_{i+\frac{1}{2}}^k$ was defined as

$$L_{i+\frac{1}{2}}^k = \min \text{mod}(\alpha_{i-\frac{1}{2}}^k, \alpha_{i+\frac{1}{2}}^k) + \min \text{mod}(\alpha_{i+\frac{1}{2}}^k, \alpha_{i+\frac{3}{2}}^k) - \alpha_{i+\frac{1}{2}}^k.$$

2. Second-order upwind TVD scheme : The elements of the vector $D_{i+\frac{1}{2}}$ had the following form

$$(d_{i+\frac{1}{2}}^k) = \frac{1}{2} [\psi - (\Delta t / \Delta x) (\alpha_{i+\frac{1}{2}}^k)^2] (\tilde{\lambda}_{i+\frac{1}{2}}^k) (L_{i+1}^k + L_i^k) - \psi (\tilde{\lambda}_{i+\frac{1}{2}}^k + \gamma_{i+\frac{1}{2}}^k) \alpha_{i+\frac{1}{2}}^k.$$

The flux limiter $L_{i+\frac{1}{2}}^k$ was defined as $L_i^k = \min \text{mod}(\alpha_{i+\frac{1}{2}}^k, \alpha_{i-\frac{1}{2}}^k)$.

3. Predictor-corrector TVD schemes(TVD-McCormack) : This method was expressed as

$$U_i^{n+1} = \frac{1}{2} (U_i^C + U_i^P) + \frac{1}{2} (R_{i+\frac{1}{2}} D_{i+\frac{1}{2}} - R_{i-\frac{1}{2}} D_{i-\frac{1}{2}}).$$

The elements of the vector $D_{i+\frac{1}{2}}$ have the form

$$(d_{i+\frac{1}{2}}^k) = \psi(\tilde{\lambda}_{i+\frac{1}{2}}^k) [1 - (\Delta t / \Delta x) |\tilde{\lambda}_{i+\frac{1}{2}}^k|] (1 - L_{i+\frac{1}{2}}^k) \alpha_{i+\frac{1}{2}}^k.$$

The flux limiter $L_{i+\frac{1}{2}}^k$ was expressed as $L_i^k = \max(0, \min(1, r_{i+\frac{1}{2}}^k))$.

4. MUSCL scheme : In this method, the numerical fluxes were calculated by using $U_{i+\frac{1}{2}}^R, U_{i+\frac{1}{2}}^L$ which were modified with slope limiter rather than U_i, U_{i+1} . Then the numerical flux was expressed as

$$F_{i+\frac{1}{2}} = \frac{1}{2} [F(U_{i+\frac{1}{2}}^R) + F(U_{i+\frac{1}{2}}^L) + R_{i+\frac{1}{2}} D_{i+\frac{1}{2}}]$$

where the elements of the vector $D_{i+\frac{1}{2}}$ have the form $(d_{i+\frac{1}{2}}^k) = -\psi(\lambda_{i+\frac{1}{2}}^k) \alpha_{i+\frac{1}{2}}^k$ and are evaluated with the modified values $U_{i+\frac{1}{2}}^R, U_{i+\frac{1}{2}}^L$.

According to the numerical results, all the four schemes presented could solve the open channel flow problems with hydraulic jumps accurately. However, there were variations between them. For example, the symmetric scheme produced the most accurate solution for dam-break problem while it was the least accurate for non-transcritical problems. The TVD-MacCormack scheme showed oscillations in very severe dam-break cases though it gave generally accurate predictions with low error in other problems. This is because each scheme has different approach to avoid spurious oscillations near discontinuous solutions. In case of the symmetric scheme, the numerical flux at a cell interface is automatically reduced to a first-order accurate solution which shows more diffusive behaviour than second-order solutions. On the contrary, TVD-McCormack scheme finds solutions by adding the solutions of the first-order McCormack scheme with the correction term which is limited by the flux limiter function.

Jha et al. [55] presented a high-resolution TVD scheme which has been obtained by applying a flux limiter to the Lax-Wendroff scheme to solve the shallow water equations. This scheme has been used on a fixed grid and an adaptive grid and the results have been compared. The authors modified the Lax-Wendroff scheme to prevent numerical oscillations. The high-resolution TVD scheme was obtained by limiting the effect of the second-order term with the flux limiter function:

$$F_{i\pm\frac{1}{2}} = \frac{1}{2}(F_i + F_{i+1}) - \frac{1}{2} \sum_k (\tilde{\alpha}_k |\tilde{\lambda}_k| \tilde{e}_k)_{i\pm\frac{1}{2}} + \frac{1}{2} \sum_k \Phi_k (\tilde{\alpha}_k |\tilde{\lambda}_k| \left(1 - \frac{\Delta t}{\Delta x} |\tilde{\lambda}_k|\right) \tilde{e}_k)$$

where Φ is a flux limiter whose value varies according to the behaviour of the solution. In the paper, the authors used the Van Albada limiter.

The high-resolution scheme developed for a fixed grid was modified to be applied on a self-adjusting grid to avoid smearing of a shock. The adaptive grid was obtained by calculating the end-points of the grids at next time level with the following equation

$$\tilde{\chi}_{i\pm\frac{1}{2}}^{n+1} = \chi_{i\pm\frac{1}{2}}^n + \left[\sum_{m=-1}^i (\bar{\chi}_{i+m\pm\frac{1}{2}}^{n+1} - \chi_{i\pm\frac{1}{2}}^n) \beta_{i+m\pm\frac{1}{2}} f(\bar{\chi}_{i+m\pm\frac{1}{2}}^{n+1}; x_i, x_{i+1}) \right] / \varphi_{i\pm\frac{1}{2}}$$

where $\chi_{i\pm\frac{1}{2}} = 0.5(x_i + x_{i\pm 1})$. Other terms were calculated by

$$\begin{aligned} \bar{\chi}_{i\pm\frac{1}{2}}^{n+1} &= \chi_{i\pm\frac{1}{2}}^n + \Delta t v_{i\pm\frac{1}{2}}^n, \\ v_{i\pm\frac{1}{2}} &= \left[\sum (\alpha_{i\pm\frac{1}{2}}^k)^2 \lambda_{i\pm\frac{1}{2}}^k \right] / \beta_{i\pm\frac{1}{2}}, \\ \beta_{i\pm\frac{1}{2}} &= \sum (\alpha_{i\pm\frac{1}{2}}^k)^2, \\ \varphi_{i\pm\frac{1}{2}} &= \sum_{m=-1}^1 \beta_{i+m\pm\frac{1}{2}} f(\bar{\chi}_{i+m\pm\frac{1}{2}}^{n+1}; x_i, x_{i+1}) \end{aligned}$$

and

$$f(\bar{\chi}_{i+m\pm\frac{1}{2}}^{n+1}; x_i, x_{i+1}) = \begin{cases} 1, & x_i < \bar{\chi}_{i+m\pm\frac{1}{2}} \leq x_{i+1} \\ 0, & \text{otherwise} \end{cases}$$

The main idea of the adaptive grid was to make the location of a shock always coincides with a grid point. In shock capturing methods like Roe's approximate solver, a shock is bound to be smeared unless it lies at the ends of the cell because the values of the variables at the next time level should be calculated by cell averaging. To avoid this problem, the methods using an adaptive grid were developed. The proposed technique could calculate the propagation of a shock more accurately than the numerical schemes on a fixed grid. However, the improvement was not so significant according to the numerical results in the paper, which was mainly because the high resolution TVD scheme on a fixed grid itself produced very accurate solutions and so there was very little room for improvement. The main disadvantage of the proposed method was that the process to calculate grid points at next time level was complicated to implement.

Sanders [72] presented a MUSCL-type high-resolution scheme with mass and momentum fluxes computed using a Roe's Riemann solver. The presented MUSCL-type scheme was a two-step method: predictor and corrector steps. At first, the following form of the St. Venant equations was used for the predictor step

$$\begin{aligned}\frac{\partial A}{\partial t} + V \frac{\partial A}{\partial x} + A \frac{\partial V}{\partial x} &= 0 \\ \frac{\partial V}{\partial t} + g \frac{\partial h}{\partial x} + V \frac{\partial V}{\partial x} &= g(S_o - S_f)\end{aligned}$$

which subsequently discretized as

$$\begin{aligned}A_i^{n+\frac{1}{2}} &= A_i^n - \frac{\Delta t}{2\Delta x} (V\bar{\Delta}A + A\bar{\Delta}V)_i^n \\ V_i^{n+\frac{1}{2}} &= v_i^n - \frac{\Delta t}{2\Delta x} (g\bar{\Delta}h + V\bar{\Delta}V)_i^n + \frac{g\Delta t}{2} \left((S_o)_i^n - \frac{1}{2}(S_f)_i^n - \frac{1}{2}(S_f)_i^{n+\frac{1}{2}} \right)\end{aligned}$$

where the overbar means the average value which was defined as

$$\bar{\Delta}\bullet = \text{avg}(\bullet_{i+1} - \bullet_i, \bullet_i - \bullet_{i-1}).$$

The average values were limited by the following Superbee slope limiter function to prevent the over- and under-shoots:

$$\text{avg}(\alpha, \beta) = \begin{cases} \min \text{mod}(\max \text{mod}(\alpha, \beta), \min \text{mod}(2\alpha, 2\beta)) & \alpha\beta > 0 \\ 0 & \alpha\beta < 0 \end{cases}$$

Once the predictor step had been completed the variables at the intermediate time level $t = t^{n+\frac{1}{2}}$ were reconstructed by using the MUSCL variable extrapolation approach. The variables h and V at the left and right face of the cell interface $i + \frac{1}{2}$ were calculated by

$$\begin{aligned}h_L &= h_i + \frac{1}{2}(\bar{\Delta}h)_i, & h_R &= h_i - \frac{1}{2}(\bar{\Delta}h)_{i+1} \\ V_L &= V_i + \frac{1}{2}(\bar{\Delta}V)_i, & V_R &= V_i - \frac{1}{2}(\bar{\Delta}V)_{i+1}.\end{aligned}$$

The area A on the left and right side of each cell interface was computed by using the extrapolated water depth.

$$A_L = A(h_L), \quad A_R = A(h_R)$$

Then, in the corrector step, the mass and momentum fluxes at each cell interface were computed by using the Roe's method and the equation for the update of the solutions was given by

$$U_i^{n+1} = U_i^n - \frac{\Delta t}{\Delta x} (F_{i+\frac{1}{2}}^{n+\frac{1}{2}} - F_{i-\frac{1}{2}}^{n+\frac{1}{2}}) + \Delta t (S_F)_i^{n+\frac{1}{2}} + \frac{\Delta t}{2} ((S_s)_i^n + (S_s)_i^{n+1})$$

where

$$S_F = \begin{pmatrix} 0 \\ F_c \end{pmatrix} \text{ and } S_s = \begin{pmatrix} 0 \\ gA(S_o - S_f) \end{pmatrix}.$$

In the paper, a new definition for the hydraulic force F_c exerted by the channel walls in the streamwise direction was presented. The author defined this term as

$$F_c = g\bar{y}'\Delta A$$

where $\Delta A = A_{i+\frac{1}{2}}(h_i) - A_{i-\frac{1}{2}}(h_i)$ and \bar{y}' represents the distance from the free surface to the centroid of the wetted area ΔA . The proposed scheme was applied to triangular and trapezoidal channels with and without width variation and produced accurate solutions. The definition for the hydrostatic force F_c showed good ability to solve the flows in a channel with width variation. However, the author did not apply the scheme to the non-prismatic channel with bottom slope variation as well as width variation.

Burguete and Garcia-Navarro [15] presented general form of the conservative TVD scheme. The authors used the conservative form

$$(1 - \theta K_i^n \Delta t) \Delta U_i^n = \Delta t [(G^+)_{i-\frac{1}{2}}^n + (G^-)_{i+\frac{1}{2}}^n].$$

Then, the spatially second-order TVD conservative scheme was proposed by using the flux limiter function Ψ as

$$(1 - \theta K_i^n \Delta t) \Delta U_i^n = \Delta t \{ (G^+)_{i-\frac{1}{2}}^n + (G^-)_{i+\frac{1}{2}}^n + \frac{1}{2} [(\Psi^+ G^+)_{i-\frac{1}{2}}^n + (\Psi^- G^-)_{i+\frac{1}{2}}^n - (\Psi^+ G^+)_{i-\frac{1}{2}}^n - (\Psi^- G^-)_{i+\frac{1}{2}}^n] \}.$$

To achieve second-order accuracy without numerical oscillations, the flux limiter function was defined as the following vector form

$$\Psi_{i+\frac{1}{2}}^\pm = \begin{pmatrix} \Psi \left(\frac{(G^1)_{i+\frac{1}{2} \pm 1}^\pm}{(G^1)_{i+\frac{1}{2}}^\pm} \right) \\ \vdots \\ \Psi \left(\frac{(G^k)_{i+\frac{1}{2} \pm 1}^\pm}{(G^k)_{i+\frac{1}{2}}^\pm} \right) \end{pmatrix}.$$

As shown in the definition of the limiter function vector, the authors emphasised that the effect of the source terms should be involved in the definition of the limiter function because the flux limiter function obtained only with numerical flux term can not ensure second-order accuracy.

The second-order in space and time TVD scheme was also presented in the same paper. From the theory of Taylor series expansion

$$\begin{aligned}\Delta U_i^n &= \left(\frac{\partial U}{\partial t}\right)_i^n \Delta t + \frac{1}{2} \left(\frac{\partial^2 U}{\partial t^2}\right)_i^n \Delta t^2 + O(\Delta t^3) \\ &= \left(S - \frac{\partial F}{\partial x}\right)_i^n \Delta t + \frac{1}{2} \frac{\partial}{\partial t} \left(S - \frac{\partial F}{\partial x}\right)_i^n \Delta t^2 + O(\Delta t^3)\end{aligned}$$

and

$$\frac{\partial}{\partial t} \left(S - \frac{\partial F}{\partial x}\right)_i^n = \frac{\partial S}{\partial U} \frac{\partial U}{\partial t} - \frac{\partial}{\partial x} \left(\frac{\partial F}{\partial U} \frac{\partial U}{\partial t}\right) = K \frac{\partial u}{\partial t} - \frac{\partial}{\partial x} \left[A \left(S - \frac{\partial F}{\partial x}\right)\right]$$

Then, the TVD second-order in space and time scheme was written as

$$\begin{aligned}(1 - \frac{1}{2} K_i^n \Delta t) \Delta U_i^n &= \Delta t [(G^+)_{i-\frac{1}{2}}^n + (G^-)_{i+\frac{1}{2}}^n] \\ &\quad + \frac{\Delta t}{2} \left\{ \left[\Psi^+ \left(1 - \frac{\Delta t}{\delta x} A^+\right) G^+ \right]_{i-\frac{1}{2}}^n - \left[\Psi^+ \left(1 - \frac{\Delta t}{\delta x} A^+\right) G^+ \right]_{i-\frac{1}{2}}^n \right. \\ &\quad \left. + \left[\Psi^- \left(1 + \frac{\Delta t}{\delta x} A^-\right) G^- \right]_{i+\frac{1}{2}}^n - \left[\Psi^- \left(1 + \frac{\Delta t}{\delta x} A^-\right) G^- \right]_{i+\frac{1}{2}}^n \right\}\end{aligned}$$

with the flux limiter function matrix

$$\Psi_{i+\frac{1}{2}}^\pm = \begin{pmatrix} \Psi \left(\frac{(R^1)_{i+\frac{1}{2} \pm 1}^\pm}{(R^1)_{i+\frac{1}{2}}^\pm} \right) & & \\ & \dots & \\ & & \Psi \left(\frac{(R^k)_{i+\frac{1}{2} \pm 1}^\pm}{(R^k)_{i+\frac{1}{2}}^\pm} \right) \end{pmatrix}$$

where $R^\pm = (\delta F \pm \Delta t A G)^\pm$.

The two proposed TVD schemes were applied to some test cases including dam-break problems. The both schemes produced more accurate results in highly unsteady shallow water problems than first-order schemes while second-order in space and time

TVD scheme showed more stable results with high CFL number. However, according to the numerical results, the TVD schemes and first-order schemes produced identical solutions in steady flow problems.

3.4.3 Discretization of the Source Terms

The treatment of the source terms in inhomogeneous conservation laws like the shallow water equations has been the subject of much research. The homogeneous conservation laws without source terms can be solved by the following simple form

$$U_i^{n+1} = U_i^n - \frac{\Delta t}{\Delta x} (F_{i+\frac{1}{2}}^* - F_{i-\frac{1}{2}}^*).$$

However, the existence of the source terms which are in general an algebraic function of the variable U and other physical parameters such as the bottom gradient makes the problem complicated because it is very difficult to solve inhomogeneous partial differential equation (PDE) satisfactorily. The simplest approach is the fractional two step method in which the inhomogeneous PDE is decomposed into a homogeneous PDE and an ordinary differential equation (ODE). For example, the non-linear conservation law

$$U_t + F(U)_x = S(U)$$

can be regarded as the combination of the homogeneous advection equation system

$$U_t + F(U)_x = 0$$

and a system of ODEs

$$\frac{d}{dt}(U) = S(U).$$

There are many well-developed numerical methods to solve the system of ODEs. The ODEs for the source terms can be solved by the pointwise approach in which the bed slope and width variation terms are expressed as the following average values:

$$S_{oi} \approx \frac{1}{2} (S_{oi+\frac{1}{2}} + S_{oi-\frac{1}{2}}) \quad \text{with} \quad S_{oi+\frac{1}{2}} = -\frac{z_{i+1} - z_i}{\Delta x}$$

$$I_{2oi} \approx \frac{1}{2} (I_{2i+\frac{1}{2}} + I_{2i-\frac{1}{2}}) \quad \text{with} \quad I_{2i+\frac{1}{2}} = \frac{1}{2} h_i^2 \frac{b_{i+1} - b_i}{\Delta x} \quad \text{for rectangular channel.}$$

Unfortunately, this simple traditional method cannot solve problems satisfactorily, especially in case of steady or nearly steady flows including geometric source terms

such as bed level and width variation. This is mainly because it can not achieve a perfect balance of flux gradient(F_x) and source terms(S).

Nujic [67] specified this problem and proposed a special method for source term treatment. In the paper, the author showed that very poor results are obtained when flux-difference or flux-vector splitting methods are applied to the shallow water flow with variable bottom topography. According to the author, the numerical error was caused by the following two reasons: numerical diffusion because of the non-smooth solution (water depth h) and numerical incompatibility between bottom slope term and the $0.5gh^2$ term in the flux function. To solve this problem, two different techniques were proposed in the paper:

a) Extract the $0.5gh^2$ term from the flux function, differentiate and combine it with the bottom slope term. Then, the flux function and source terms can be written as

$$F = \begin{pmatrix} uh \\ u^2h \end{pmatrix}, \quad S = \begin{pmatrix} 0 \\ gh(S_f - S_H) \end{pmatrix}$$

where $S_H = -\frac{\partial H}{\partial x}$ with the water surface elevation $H = h + z_b$.

b) Extract the $0.5gh^2$ term from the flux function and discretize it so that it is “compatible” with the bottom slope term. Then, the shallow water equations were rewritten as

$$U_i + F_x + P_x + S = 0$$

$$\text{with } U = \begin{pmatrix} H \\ uh \end{pmatrix}, \quad F = \begin{pmatrix} uh \\ u^2h \end{pmatrix}, \quad P = \begin{pmatrix} 0 \\ 0.5gh^2 \end{pmatrix} \quad \text{and} \quad S = \begin{pmatrix} 0 \\ gh(S_f - S_o) \end{pmatrix}.$$

In the paper, the second approach was adopted and the numerical flux $P_{i+\frac{1}{2}}$ was approximated by using the average

$$P_{i+\frac{1}{2}} = 0.5(P_{i+1} + P_i).$$

By using the above method, the numerical errors could be decreased. However, this method could not solve the problem perfectly and showed small a amount of numerical error.

LeVeque [62] inserted additional discontinuity at the centre of each cell to incorporate source terms into the wave-propagation algorithm and avoid the fractional step. In the paper, the cell averaged value U_i was replaced by two values U_i^- and U_i^+ with a jump at the cell centre. The definitions of U_i^- and U_i^+ were given by

$$U_i^- = U_i - \delta_i \quad \text{and} \quad U_i^+ = U_i + \delta_i$$

to satisfy total mass conservation. The cell average values were updated by the waves from the Riemann problem at the cell centre as well as the incoming waves from each cell edge and the conservative scheme with source terms was solved by the following form

$$U_i^{n+1} = U_i^n - \frac{\Delta t}{\Delta x} (A^+ \Delta \bar{U}_{i-\frac{1}{2}} + A^- \Delta \bar{U}_{i+\frac{1}{2}}) + \Delta t \left[\psi(U_i, x_i) - \frac{1}{\Delta x} (F(U_i^+) - F(U_i^-)) \right]$$

where $\Delta \bar{U}_{i+\frac{1}{2}} = U_{i+1}^- - U_i^+$. Then, the value of vector δ_i was chosen to drop the final term and make the above form similar to the original conservation term. In other words, the vector δ_i was chosen to satisfied the condition

$$F(U_i^+) - F(U_i^-) = \psi(U_i, x_i) \Delta x.$$

The proposed method worked very well in case of steady flows with small perturbations. However, as the author stated in the paper, this method was not appropriate when the solution was far from steady state and there was numerical errors in case of transcritical steady flow including shocks.

Methods based on upwinding the source terms have been considered by many researchers as a good alternative to the traditional step method. The main idea of upwinding the source terms is to discretize the source term in a manner similar to that used for construction of the numerical flux function.

Garcia-Navarro and Vazquez-Cendon [40] presented upwind source term treatment technique for prismatic and non-prismatic rectangular channels. In the paper, the source terms were discretized by

$$S \Delta x = \sum_k \tilde{\beta}_k \tilde{e}_k,$$

and divided into two parts: forward and backward portion according to the signs of the local wave speed (eigenvalue) as depicted in *Figure 3.6*. To do this the source term vector was rewritten as

$$S\Delta x = R\beta$$

where

$$R = \begin{pmatrix} 1 & 1 \\ \lambda_1 & \lambda_2 \end{pmatrix} \quad \text{and} \quad \beta = \begin{pmatrix} \beta_1 \\ \beta_2 \end{pmatrix}.$$

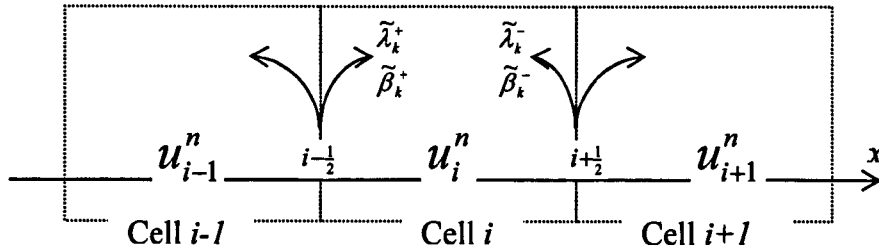


Figure 3.6 The concept of the upwind approach [80]

The diagonal matrix

$$\Lambda = R^{-1}AR = \begin{pmatrix} \lambda_1 & 0 \\ 0 & \lambda_2 \end{pmatrix}$$

was used to decompose the source term vector like

$$S = R\beta = R\Lambda\Lambda^{-1}\beta = R\Lambda^+\Lambda^{-1}\beta + R\Lambda^-\Lambda^{-1}\beta$$

where

$$\Lambda^\pm = \frac{1}{2}(\Lambda \pm |\Lambda|) \quad \text{and} \quad |\Lambda| = \begin{pmatrix} |\lambda_1| & 0 \\ 0 & |\lambda_2| \end{pmatrix}.$$

Then, the effect of the source terms at each cell interface was separated into two parts: left-hand (backward) and right-hand (forward) portion. The contribution to the nodal point i was regarded as the sum of incoming portions and expressed as the following form

$$S_i\Delta x = (R\Lambda^+\Lambda^{-1}\beta)_{i-\frac{1}{2}} + (R\Lambda^-\Lambda^{-1}\beta)_{i+\frac{1}{2}}$$

where

$$R\Lambda^+\Lambda^{-1} = \frac{1}{2} \begin{pmatrix} 1+s_1 & 1+s_2 \\ \tilde{\lambda}_1(1+s_1) & \tilde{\lambda}_2(1+s_2) \end{pmatrix}, \quad R\Lambda^-\Lambda^{-1} = \frac{1}{2} \begin{pmatrix} 1-s_1 & 1-s_2 \\ \tilde{\lambda}_1(1-s_1) & \tilde{\lambda}_2(1-s_2) \end{pmatrix}$$

and $s_k = \text{sign}(\tilde{\lambda}_k) = \tilde{\lambda}_k / |\tilde{\lambda}_k|$.

In case of shallow water flows in prismatic rectangular channel,

$$\Delta F = A\Delta U$$

and the decomposition of the source terms was given by

$$S = \left(g \left(-\tilde{A}z_{b_x} - \tilde{A}\tilde{S}_f + \frac{\tilde{A}^2}{2\tilde{b}^2} b_x \right) \right) = \frac{1}{\Delta x} \left(\tilde{\beta}_1 \begin{pmatrix} 1 \\ \tilde{u} + \tilde{c} \end{pmatrix} + \tilde{\beta}_2 \begin{pmatrix} 1 \\ \tilde{u} - \tilde{c} \end{pmatrix} \right).$$

From the above equations,

$$\tilde{\beta}_1 = -\tilde{\beta}_2 = \tilde{\beta}$$

and

$$\tilde{\beta} = \frac{g}{2\tilde{c}} \left(-\tilde{A}\Delta z_b - \tilde{A}\Delta x\tilde{S}_f + \frac{\tilde{A}^2}{2\tilde{b}^2} \Delta b \right)$$

where \tilde{A} , \tilde{b} and \tilde{S}_f represent the average values at each cell interface.

In case of non-prismatic rectangular channel,

$$\Delta F = A\Delta U + V$$

with

$$V = \left(-\frac{gA^2}{2b^2} \Delta b \right).$$

Then, the decomposition of the source terms was modified:

$$\hat{S} = S - V = \left(g \left(-\tilde{A}z_{b_x} - \tilde{A}\tilde{S}_f + \frac{\tilde{A}^2}{\tilde{b}^2} b_x \right) \right) = \frac{1}{\Delta x} \left(\tilde{\beta}_1 \begin{pmatrix} 1 \\ \tilde{u} + \tilde{c} \end{pmatrix} + \tilde{\beta}_2 \begin{pmatrix} 1 \\ \tilde{u} - \tilde{c} \end{pmatrix} \right)$$

and

$$\tilde{\beta}_1 = -\tilde{\beta}_2 = \tilde{\beta}$$

with

$$\tilde{\beta} = \frac{g}{2\tilde{c}} \left(-\tilde{A}\Delta z_b - \tilde{A}\Delta x\tilde{S}_f + \frac{\tilde{A}^2}{\tilde{b}^2} \Delta b \right).$$

The proposed decomposition technique was applied to several steady and unsteady problems and showed perfect balance of flux gradient and source terms. However,

this method was not suitable for non-rectangular channel problems and the authors used two different criteria for the average values.

Hubbard and Garcia-Navarro [51] used the upwind source term treatment and extended it to the high-resolution TVD schemes. In the paper, Roe's first-order scheme with upwind source term treatment was written as

$$U_i^{n+1} = U_i^n - \frac{\Delta t}{\Delta x} (F_{i+\frac{1}{2}}^* - F_{i-\frac{1}{2}}^*) + \frac{\Delta t}{\Delta x} (S_i^*)$$

where numerical flux $F_{i+\frac{1}{2}}^*$ is

$$F_{i+\frac{1}{2}}^* = \frac{1}{2} (F_{i+1} + F_i) - \frac{1}{2} (\tilde{R} |\tilde{\Lambda}| \tilde{R}^{-1} \Delta U)_{i+\frac{1}{2}}$$

and numerical source integral $S_i^* \approx \int S dx$ is

$$S_i^* = \tilde{S}_{i+\frac{1}{2}}^- + \tilde{S}_{i-\frac{1}{2}}^+$$

with

$$\tilde{S}_{i+\frac{1}{2}}^- = \frac{1}{2} (\tilde{R} (I - \text{sign}(I)) \tilde{R}^{-1} \tilde{S})_{i+\frac{1}{2}} = (\tilde{R} I^- \tilde{R}^{-1} \tilde{S})_{i+\frac{1}{2}}$$

$$\tilde{S}_{i-\frac{1}{2}}^+ = \frac{1}{2} (\tilde{R} (I + \text{sign}(I)) \tilde{R}^{-1} \tilde{S})_{i-\frac{1}{2}} = (\tilde{R} I^+ \tilde{R}^{-1} \tilde{S})_{i-\frac{1}{2}}.$$

According to the authors, the decomposed source terms are not able to be included within the numerical flux because the source terms can not be written as a difference. This means that the balance which is sought between flux derivatives and sources in the flux-based scheme can only be obtained locally by balancing non-zero fluxes through the edges of a control volume, and not by setting each edge flux to zero.

The upwind source term treatment was extended to TVD schemes. In case of flux-limited schemes the numerical flux has the following form

$$F_{i+\frac{1}{2}}^* = \frac{1}{2} (F_{i+1} + F_i) - \frac{1}{2} (\tilde{R} |\tilde{\Lambda}| L \tilde{R}^{-1} \Delta U)_{i+\frac{1}{2}}$$

where $L = \text{diag}(1 - \Phi(r_k)(1 - |\nu_k|))$ with $\nu_k = \tilde{\lambda} \Delta t / \Delta x$ and Φ is the flux limiter function. To maintain the balance between the flux gradient and the source terms, a corresponding high-order correction was made to the source terms approximation. The flux limited numerical source was obtained by using the same flux limiter function and given by

$$\tilde{S}_{i+\frac{1}{2}}^- = \frac{1}{2}(\tilde{R}(I - \text{sign}(I)L\tilde{R}^{-1}\tilde{S})_{i+\frac{1}{2}}) = (\tilde{R}I^- \tilde{R}^{-1}\tilde{S})_{i+\frac{1}{2}}$$

$$\tilde{S}_{i-\frac{1}{2}}^+ = \frac{1}{2}(\tilde{R}(I + \text{sign}(I)L\tilde{R}^{-1}\tilde{S})_{i-\frac{1}{2}}) = (\tilde{R}I^+ \tilde{R}^{-1}\tilde{S})_{i-\frac{1}{2}}.$$

In case of slope limited schemes like MUSCL, variables in each cell should be reconstructed and the average values of Roe's solver are evaluated from the reconstructed data. The slope-limited version of numerical flux can be written as

$$F_{i+\frac{1}{2}}^* = \frac{1}{2}(F_{i+\frac{1}{2}}^R + F_{i+\frac{1}{2}}^L) - \frac{1}{2}(\tilde{R}|\tilde{\Lambda}|\tilde{R}^{-1}\Delta U)_{i+\frac{1}{2}}$$

where the superscripts R and L represent evaluation on the right and left hand side of cell interface, respectively. Similarly, the slope-limited version of numerical source was written as

$$S_i^* = (\tilde{S}_{i+\frac{1}{2}}^- + \tilde{S}_{i-\frac{1}{2}}^+) - \tilde{S}(U_{i+\frac{1}{2}}^L, U_{i-\frac{1}{2}}^R).$$

The final term on the right hand side represents the source term integral approximated over the mesh cell.

The proposed method was applied to one- and two-dimensional shallow water flows including still water simulation and could achieve perfect balance of flux gradient and source terms except slope limited second-order scheme. According to the authors, a more sophisticated approximation was needed for the source terms in slope-limited schemes. The proposed method could not be applied to a non-rectangular channel though it showed good results even in TVD schemes for rectangular channels.

Goutal and Maurel [46] redefined source terms in the one-dimensional shallow water equations for natural river flow modelling. In the paper, the source terms were divided into two components:

1. Source terms linked to the geometry including the bed slope and variation of the river width which was expressed as

$$\left(\frac{\partial I_1(x, A)}{\partial x}\right)_{z_1=cte.} = \left(\frac{\partial I_1(x, A)}{\partial x}\right)_{A=cte.} + \frac{\partial I_1(x, A)}{\partial A} \left(\frac{\partial A}{\partial x}\right)_{z_1=cte.}.$$

2. The friction term given as $-gAS_f$.

The newly defined source terms was expressed as the sum of the following three terms:

$$(1) S_1 = \left(\frac{\partial I_1(x, A)}{\partial x} \right)_{A=cte.}$$

$$(2) S_2 = \frac{\partial I_1(x, A)}{\partial A} \left(\frac{\partial A}{\partial x} \right)_{z_s=cte.}$$

$$(3) S_3 = S_f$$

and discretized by using two different discretization techniques: term (1) was approximated by a pointwise discretization while terms (2) and (3) were upwinded.

The proposed method was applied to several one-dimensional flow problems including steady flows and a dam-break simulation and, according to the numerical results, the scheme showed that, in case of steady state, the equilibrium was correctly approximated, and the scheme was suitable for propagation over dry areas.

Burguete and Garcia-Navarro [15,16] proposed an optimal form of the one-dimensional shallow water equations for arbitrary channel geometry. In the papers, the one-dimensional hyperbolic system with source terms was given as

$$\frac{\partial U(x, t)}{\partial t} + \frac{dF(x, U)}{dx} = S(x, U)$$

with

$$U = \begin{pmatrix} A \\ Q \end{pmatrix}, \quad F = \begin{pmatrix} Q \\ Q^2/A + gI_1 \end{pmatrix} \quad \text{and} \quad S = \begin{pmatrix} 0 \\ g[I_2 + A(S_o - S_f)] \end{pmatrix}.$$

The authors used the total derivative dF/dx instead of the partial derivative in order to represent the increments due to the pure spatial variations in x and those due to the variations of the conserved variables U . From the relation between the total and partial derivatives

$$\frac{dF(x, U)}{dx} = \frac{\partial F(x, U)}{\partial x} + \frac{\partial F(x, U)}{\partial U} \frac{\partial U}{\partial x} = \frac{\partial F(x, U)}{\partial x} + A(x, U) \frac{\partial U}{\partial x},$$

the non-conservative form was written as

$$\frac{\partial U(x, t)}{\partial t} + A(x, U) \frac{\partial U(x, t)}{\partial x} = S'(x, U)$$

where the modified source term S' was given by

$$S'(x, U) = S(x, U) - \frac{\partial F(x, U)}{\partial x}.$$

In case of the shallow water equations, the following relations hold:

$$\frac{dh}{dx} = \frac{\partial h}{\partial x} + \frac{1}{b} \frac{\partial A}{\partial x}$$

$$\frac{dI_1}{dx} = \frac{\partial I_1}{\partial x} + \frac{\partial I_1}{\partial A} \frac{\partial A}{\partial x} = I_2 + A \frac{\partial h}{\partial x} + \frac{A}{b} \frac{\partial A}{\partial x} = I_2 + A \frac{dh}{dx},$$

and the new source terms of the non-conservative form was defined as

$$S'(x, U) = \begin{pmatrix} 0 \\ gA[S_o - S_f - \frac{dh}{dx} + \frac{1}{b} \frac{dA}{dx}] \end{pmatrix}.$$

Then, Roe's method and the upwind source term treatment were applied to the non-conservative form of numerical scheme. The proposed new source term discretisation produced good results in steady and unsteady problems. Especially, in case of steady flow problems including 'water at rest' test, the scheme achieved perfect balance of flux gradient and source terms and produced no numerical error. This method could be applied any type of geometry including real river channel. However, the only problem of the method was how to define the intercell average values \tilde{c} , \tilde{A} and \tilde{b} . The definition of the average values should be chosen in consideration of the balance of numerical flux and source terms. In the papers, the authors used the following definitions for average values

$$\tilde{c}_{i+\frac{1}{2}} = \sqrt{g \frac{\tilde{A}_{i+\frac{1}{2}}}{\tilde{b}_{i+\frac{1}{2}}}}, \quad \tilde{A}_{i+\frac{1}{2}} = \frac{1}{2}(A_{i+1} + A_i), \quad \text{and} \quad \tilde{b}_{i+\frac{1}{2}} = \frac{1}{2}(b_{i+1} + b_i).$$

Zhou et al. [85] proposed the surface gradient method (SGM) for the treatment of source terms in MUSCL-type schemes. In MUSCL-type numerical schemes, the initial data at each time step are reconstructed by the gradient of the geopotential $\phi = gh$ which can be expressed as

$$\delta\phi_i = G\left(\frac{\phi_{i+1} - \phi_i}{x_{i+1} - x_i}, \frac{\phi_i - \phi_{i-1}}{x_i - x_{i-1}}\right)$$

where G is the slope limiter function.. The reconstructed values on the left and right of the cell interface $i - \frac{1}{2}$ can be given by

$$\phi_{i-\frac{1}{2}}^L = \phi_{i-1} + \frac{1}{2} \Delta x_{i-1} \delta\phi_{i-1}, \quad \phi_{i-\frac{1}{2}}^R = \phi_i - \frac{1}{2} \Delta x_i \delta\phi_i$$

where $\Delta x_i = x_{i+\frac{1}{2}} - x_{i-\frac{1}{2}}$. In the paper, the authors named this approach the depth gradient method (DGM) which is suitable for homogeneous form of the equations and suggested that SGM should be used for the accurate source term treatment because DGM fails to reproduce the real variation of the water depth. In SGM, the water surface level at the left and right of the cell interface $i - \frac{1}{2}$ were given as

$$\eta_{i-\frac{1}{2}}^L = \eta_{i-1} + \frac{1}{2} \Delta x_{i-1} \delta \eta_{i-1}, \quad \eta_{i-\frac{1}{2}}^R = \eta_i - \frac{1}{2} \Delta x_i \delta \eta_i$$

where $\delta \eta_i$ represents the gradient of water surface level η . From the relation $\eta = h + z_b$, the reconstructed values of $\phi = gh$ at the left and right of the cell interface $i - \frac{1}{2}$ were calculated as

$$\phi_{i-\frac{1}{2}}^L = g(\eta_{i-\frac{1}{2}}^L - z_{bi-\frac{1}{2}}), \quad \phi_{i-\frac{1}{2}}^R = g(\eta_{i-\frac{1}{2}}^R - z_{bi-\frac{1}{2}}).$$

The main advantage of the SGM was that no special treatment was needed for the discretisation of the source terms because the gradient of the water surface elevation included the effect of bottom slope as well as water depth variation. The proposed SGM was applied to various steady and unsteady flow problems with bed slope variation and reproduced accurate solutions. However, this method is considered to be used only for MUSCL-type schemes.

Capart et al. [20] proposed a modified momentum conservation equation in the St. Venant equations to treat irregular channel geometry. The momentum balance of the control volume between two cross sections x_1 and x_2 yields the following equation:

$$\frac{\partial}{\partial t} \int_{x_1}^{x_2} Q dx + \left[\frac{Q^2}{A} \right]_{x_1}^{x_2} + \frac{1}{\rho} \int_{\Gamma} p n_x d\Gamma = - \int_{x_1}^{x_2} g A S_f dx$$

where ρ is mass density of water, p is pressure, Γ represents the control surface which consists of rigid bottom boundary Γ_0 and left and right vertical faces Γ_1, Γ_2 of the control volume, and n_x is the x component of the outward normal to Γ . The third term on the left hand side which represents the overall pressure thrust acting on control surface Γ can be decomposed into three parts

$$\int p n_x d\Gamma = \int_{\Gamma_1} p n_x d\Gamma + \int_{\Gamma_2} p n_x d\Gamma + \int_{\Gamma_0} p n_x d\Gamma = [\rho g I_1]_{x_1}^{x_2} + \int_{\Gamma_0} p n_x d\Gamma.$$

The last part of the pressure thrust which is exerted along the bottom boundary Γ_0 has very complicated form and it is very difficult to calculate accurately. To solve this problem, the authors proposed an approximation for this term. At first, the average water surface elevation $\bar{z}_s = 1/2(z_{s1} + z_{s2})$ was considered. From the equilibrium condition of static forces, the hydraulic pressure forces exerted on the new control surface $\bar{\Gamma}$ which is made by the horizontal water surface elevation \bar{z}_s is equal to zero.

It means that for arbitrary shape of channel geometry,

$$\int_{\bar{\Gamma}} pn_x d\Gamma = [\rho g I_1]_{\bar{z}_s} \Big|_{x_1}^{x_2} + \int_{\Gamma_0} pn_x d\Gamma = 0$$

where $I_1|_{\bar{z}_s} = \int_{z_b}^{\bar{z}_s - z_b} (\bar{z}_s - z_b - \eta) b(x, \eta) d\eta$. Assuming that the slope of water surface is mild and the streamwise components of the sidewall inclination is small, the following relation was considered

$$\int_{\bar{\Gamma}} pn_x d\Gamma \approx \int_{\Gamma_0} pn_x d\Gamma$$

and the pressure force for control surface Γ was rewritten as

$$\int_{\Gamma} pn_x d\Gamma \approx [\rho g I_1 - \rho g I_1]_{\bar{z}_s} \Big|_{x_1}^{x_2}.$$

By using this approximation, the integral form of the momentum conservation equation was expressed as

$$\frac{\partial}{\partial t} \int_{x_1}^{x_2} Q dx + \left[\frac{Q^2}{A} + g I_1 - g I_1 \Big|_{\bar{z}_s} \right]_{x_1}^{x_2} = - \int_{x_1}^{x_2} g A S_f dx$$

and the corresponding differential equation was given by

$$\frac{\partial Q}{\partial t} + \frac{\partial}{\partial x} \left[\frac{Q^2}{A} + g I_1 - g I_1 \Big|_{\bar{z}_s} \right] = -g A S_f.$$

The mass conservation and modified momentum conservation equations were numerically discretised as

$$A_i^{n+1} = A_i^n + \frac{\Delta t}{\Delta x} (Q_{i-\frac{1}{2}}^* - Q_{i+\frac{1}{2}}^*)$$

$$Q_i^{n+1} = Q_i^n + \frac{\Delta t}{\Delta x} (\Sigma_{i-\frac{1}{2}}^{*right} - \Sigma_{i+\frac{1}{2}}^{*left}) - (g A S_f)_i^n \Delta t$$

where

$$\Sigma_{i-\frac{1}{2}}^{*right} = \left(\frac{Q^2}{A} + gI_1 - gI_1|_{z_{st}} \right)_{i-\frac{1}{2}}^*$$

$$\Sigma_{i+\frac{1}{2}}^{*left} = \left(\frac{Q^2}{A} + gI_1 - gI_1|_{z_{st}} \right)_{i+\frac{1}{2}}^*$$

In the paper, the numerical fluxes $Q_{i+\frac{1}{2}}^*$ and $\Sigma_{i+\frac{1}{2}}^{*left}$ were calculated by using the characteristic-based flux predictor method. The proposed method was applied to dam-break problem and hydraulic jump in channel expansion problem, and showed better results than pointwise source term treatment. Moreover, the scheme was used for modelling of the Tanhui River flood in Taiwan and produced results showing good agreement with the observed data.

3.4.4 Two-dimensional Modelling

Anastasiou and Chan [1] applied the finite volume method for inviscid and viscid flows on unstructured triangular grids. In the paper, the numerical flux function was given by

$$F \cdot n = F^I - F^V = (f^I - v f^V) n_x + (g^I - v g^V) n_y,$$

with

$$f^I = \begin{pmatrix} uh \\ u^2h + gh^2/2 \\ uvh \end{pmatrix}, f^V = \begin{pmatrix} 0 \\ hu_x \\ hv_x \end{pmatrix}, g^I = \begin{pmatrix} vh \\ uvh \\ v^2h + gh^2/2 \end{pmatrix}, \text{ and } g^V = \begin{pmatrix} 0 \\ hu_y \\ hv_y \end{pmatrix}$$

where the subscripts I and V represent the inviscid and viscid fluxes, respectively, u_x , u_y and v_x , v_y are the derivatives of the velocity components in the x and y direction respectively. The inviscid flux F_{ij}^I was obtained by using Roe's flux function like

$$F_{ij}^I = \frac{1}{2} [F^I(U_{ij}^+) + F^I(U_{ij}^-) - |A|(U_{ij}^+ - U_{ij}^-)].$$

Second-order accuracy was obtained by piecewise linear reconstruction of the solution data before solving the local Riemann problem. For example, the reconstruction of the cell variables was performed by the following form

$$U(x, y) = U^A + \nabla U^A \cdot r$$

where r is the vector from cell centre A to any point (x, y) within the cell, U_A is the cell centre value and ∇U^A is the gradient of the cell. The viscous flux F_{ij}^V was evaluated by extrapolating the gradient of the velocity at each cell edge and combined with the inviscid flux. The numerical scheme was applied to several test cases including two-dimensional partial dam-break problem and oblique hydraulic jump simulation and produced accurate solutions.

Brufau and Garcia-Navarro [11] presented a two-dimensional finite volume scheme with Roe's solver. The two-dimensional shallow water equations were expressed as

$$\frac{\partial U}{\partial t} + \nabla \cdot (F, G) = S$$

$$\text{with } U = \begin{pmatrix} h \\ hu \\ hv \end{pmatrix}, \quad F = \begin{pmatrix} hu \\ hu^2 + g \frac{h^2}{2} \\ huv \end{pmatrix}, \quad G = \begin{pmatrix} hv \\ huv \\ hv^2 + g \frac{h^2}{2} \end{pmatrix}, \quad S = \begin{pmatrix} 0 \\ gh(S_{o_x} - S_{f_x}) \\ gh(S_{o_y} - S_{f_y}) \end{pmatrix}$$

where, U is the vector of conserved variables, F and G are the fluxes in x and y direction and S is the source terms. This equation was discretized by applying the finite volume method:

$$\Omega_i \frac{dU_i}{dt} + \sum_{k=1}^{N_c} (F, G)_k^* \cdot n_k dl_k = S \Omega_i$$

where, Ω_i is the area of the chosen cell, N_c is the total number of edges in the cell, $(F, G)_k^* \cdot n_k$ is the normal flux at each cell edge and dl_k is the length of each edge as shown in Figure 3.7.

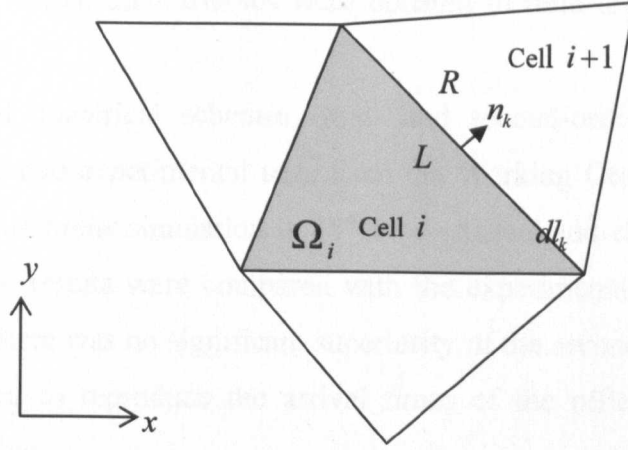


Figure 3.7 Details of the two-dimensional cells [11]

The numerical flux at each cell edge was obtained by expanding one-dimensional Roe's upwind numerical flux and expressed as

$$\begin{aligned} (F, G)^* \cdot n &= \frac{1}{2} [(F, G)_R \cdot n + (F, G)_L \cdot n] - \frac{1}{2} |\tilde{A}_{RL}| (U_R - U_L) \\ &= \frac{1}{2} [(F, G)_R \cdot n + (F, G)_L \cdot n] - \frac{1}{2} \sum_k \tilde{\alpha}_k |\tilde{\lambda}_k| \tilde{e}_k \end{aligned}$$

where \tilde{A}_{RL} is the approximate Jacobian matrix of the normal flux, R and L denote the right and left state of the cell interface, respectively. Then, the numerical discretization of the two-dimensional shallow water equations was given by

$$U_i^{n+1} = U_i^n - \frac{\Delta t}{\Omega_i} \sum_{k=1}^{N_c} [(F, G)_k^* \cdot n_k dl_k]_i^n = S_i \Delta t$$

Second-order accuracy in space was obtained by pre-processing, or reconstructing, the initial data at each time step with the following forms

$$U_L \Rightarrow U_L + r_{LR} D_L \quad \text{and} \quad U_R \Rightarrow U_R + r_{RL} D_R$$

where r_{LR} is the vector from the centroid of the cell L to the edge LR and D is the gradient operator which contains information relative to the neighbouring cells. The new left and right values of the variables were two interpolated values reconstructed from the initial cell average values. Second-order accuracy in time was obtained by updating variables in two steps. In the first step, variables were computed at time level $t = t^{n+\frac{1}{2}} = t^n + \Delta t/2$ from the extrapolated variables at time $t = t^n$. With these

intermediate values, the variables were updated to time level $t = t^{n+1}$ at the second step.

The proposed numerical schemes (first- and second-order approximations) were applied to the two experimental tests from the Working Group on Dam Break Flow Modelling: dam break simulation in 45° bend channel and channel with constriction. The numerical results were compared with the experimental data. According to the comparison, there was no significant superiority of the second-order scheme and both schemes failed to reproduce the arrival times of the reflected wave in 45° bend channel problem.

Hubbard and Garcia-Navarro [51] extended the upwind source term treatment to two-dimensional cases. The two-dimensional conservative scheme has two flux components $F = F(U)$ and $G = G(U)$ and can be written as

$$U_i^{n+1} = U_i^n - \frac{\Delta t}{\Omega_i} \sum_{l=1}^{N_e} \delta_{il} (F_{il}^*, G_{il}^*) \cdot \vec{n}_{il} + \frac{\Delta t}{\Omega_i} S_i^*$$

where Ω_i is the area of the chosen control volume, N_e is the number of cell edges, \vec{n}_{il} is the outward pointing unit normal at the cell edge between cell i and l (l represents a generic neighbouring cell) and δ_{il} is the length of the cell edge.

The first-order accurate numerical flux in two-dimensional scheme was given by

$$(F_{il}^*, G_{il}^*) \cdot \vec{n}_{il} = \frac{1}{2} (F_i + F_l, G_i + G_l) - \frac{1}{2} (\tilde{R} |\tilde{\Lambda}| \tilde{R}^{-1} \Delta U)_{il}$$

and, similarly, source integral was written as

$$S_i^* = \sum_{l=1}^{N_e} \tilde{S}_{il}^-$$

where

$$\tilde{S}_{il}^- = \frac{1}{2} (\tilde{R} (I - \text{sign}(I)) \tilde{R}^{-1} \tilde{S})_{il} = (\tilde{R} I^- \tilde{R}^{-1} \tilde{S})_{il}.$$

The source term discretization for higher-order schemes was given by a similar form to one-dimensional case. For the flux limited second-order scheme, the source term was discretized by the following form

$$\tilde{S}_{il}^- = \frac{1}{2} (\tilde{R} (I - \text{sign}(I)) L \tilde{R}^{-1} \tilde{S})_{il}$$

and the slope limited version of source term was written as

$$S_i^* = \sum_{l=1}^{N_c} (\tilde{S}_{il}^- - \tilde{S}(U_{il}, U_l)).$$

Jha et al. [54] split the two-dimensional shallow water equations into two one-dimensional problems in x and y directions, respectively. In the paper, the two-dimensional shallow water equations were broken down to a couple of one-dimensional equations which were given by:

$$\frac{\partial U}{\partial t} + \frac{\partial F}{\partial x} + S_{1x} + S_{2x} = 0$$

and

$$\frac{\partial U}{\partial t} + \frac{\partial G}{\partial y} + S_{1y} + S_{2y} = 0$$

where S_1 and S_2 are the bottom slope and the friction source term vectors, respectively. Then, the update was performed by the following two step approach: at first, the solutions were updated by solving two equations

$$U_x^{n+1} = U_{i,j}^n - \Delta t \left(\frac{\partial F}{\partial x} + S_{1x} + S_{2x} \right)$$

$$U_y^{n+1} = U_{i,j}^n - \Delta t \left(\frac{\partial G}{\partial y} + S_{1y} + S_{2y} \right)$$

and the final solution was obtained by

$$U_{i,j}^{n+1} = (U_x^{n+1} + U_y^{n+1}) - U_{i,j}^n.$$

The numerical flux for each equation was calculated by using Roe's method. Second-order accuracy was obtained by using the Lax-Wendroff numerical flux and the Van Albada flux limiter was used to secure TVD property. Source term treatment was performed by using two different approaches: the pointwise approach for the friction term and the upwind approach for the bottom slope term. The upwind treatment for the bottom slope source term S_1 was expressed as

$$S_1 = (\tilde{R}\tilde{\Lambda}\tilde{\beta})/\Delta x$$

with

$$\tilde{\beta} = \frac{g\tilde{h}\Delta z_b}{2\tilde{c}} \begin{pmatrix} 1/(\tilde{u} + \tilde{c}) \\ 0 \\ -1/(\tilde{u} - \tilde{c}) \end{pmatrix}.$$

Consequently, the following term was added to the numerical flux function

$$S_{i+\frac{1}{2},j} = -\frac{1}{2}(\tilde{R}|\tilde{\Lambda}|\tilde{\beta})_{i+\frac{1}{2},j} + \frac{1}{2}(\tilde{R}\tilde{\Lambda}\tilde{\beta})_{i+\frac{1}{2},j}.$$

The proposed schemes (first- and second-order accurate) were applied to the simulation of the flood wave due to partial dam-break and the numerical results were compared with experimental data. According to the numerical results, the both schemes predicted water depth and velocities in reservoir and floodplain with reasonable accuracy. However, there were no significant difference between the results of the two schemes.

Bradford and Sanders [10] developed a two-dimensional finite volume model featuring predictor-corrector time stepping and MUSCL data reconstruction technique.

In the predictor step, the solution at time level $t = t^{n+\frac{1}{2}}$ was obtained by solving the following primitive form of the shallow water equations

$$h_{j,k}^{n+\frac{1}{2}} = h_{j,k}^n - \frac{\Delta t}{2} [u_\xi \bar{\Delta}_\xi h + u_\eta \bar{\Delta}_\eta h + h(\xi_x \bar{\Delta}_\xi u + \xi_y \bar{\Delta}_\eta u + \eta_x \bar{\Delta}_\xi v + \eta_y \bar{\Delta}_\eta v)]_{j,k}^n$$

$$u_{j,k}^{n+\frac{1}{2}} = u_{j,k}^n - \frac{\Delta t}{2} [u_\xi \bar{\Delta}_\xi u + u_\eta \bar{\Delta}_\eta u + g(\xi_x \bar{\Delta}_\xi \varsigma + \eta_x \bar{\Delta}_\eta \varsigma + c_D u \sqrt{u^2 + v^2} / h)]_{j,k}^n$$

$$v_{j,k}^{n+\frac{1}{2}} = v_{j,k}^n - \frac{\Delta t}{2} [u_\xi \bar{\Delta}_\xi v + u_\eta \bar{\Delta}_\eta v + g(\xi_y \bar{\Delta}_\xi \varsigma + \eta_y \bar{\Delta}_\eta \varsigma + c_D v \sqrt{u^2 + v^2} / h)]_{j,k}^n$$

where ς is the free surface level and ξ and η are the directions of contiguous j and k indices, respectively. The symbol $\bar{\Delta}$ denotes cell average gradients of the variables which were computed by the Superbee slope limiter in order to preserve the monotonicity of the solution near discontinuities. Predicted values were linearly reconstructed by the MUSCL technique to obtain second-order accuracy. The corrector step was performed by the numerically discretized scheme

$$\begin{aligned} \frac{U_{j,k}^{n+1} - U_{j,k}^n}{\Delta t} + \frac{1}{\Omega_{j,k}} [(F_{\perp}^{n+\frac{1}{2}} s)_{j+\frac{1}{2},k} - (F_{\perp}^{n+\frac{1}{2}} s)_{j-\frac{1}{2},k} \\ + (F_{\perp}^{n+\frac{1}{2}} s)_{j,k+\frac{1}{2}} - (F_{\perp}^{n+\frac{1}{2}} s)_{j,k-\frac{1}{2}}] = S_{j,k}^{n+\frac{1}{2}} \end{aligned}$$

where F_{\perp} is the numerical flux at each cell interface, Ω is the area of the cell and s is the length of the cell edge. The numerical flux F_{\perp} was calculated using Roe's method and the pointwise approach with cell average values was used for the source term treatment. The proposed scheme was successfully applied to the dry bed dam-break problem and long wave runup in one- and two-dimensions.

Caleffi et al. [19] proposed a MUSCL-type scheme with HLL Riemann solver. In the paper, the numerical flux at each cell interface was calculated by the HLL approximate solver and a second-order accuracy was obtained by using the predictor-corrector and MUSCL technique respectively. Moreover, a new approach to treat source terms was proposed.

The numerical flux was calculated by the HLL Riemann solver :

$$F^* \cdot n = (s_R F_L \cdot n - s_L F_R \cdot n + s_R s_L (U_R - U_L)) / (s_R - s_L)$$

where subscript R and L represent the right and the left side of the cell interface, respectively. The wave speeds s_R and s_L were calculated by the following equations :

$$s_L = \min(q_L \cdot n - \sqrt{gh_L}, u^* - \sqrt{gh^*}) \text{ and } s_R = \min(q_R \cdot n - \sqrt{gh_R}, u^* + \sqrt{gh^*})$$

where $u^* = \frac{1}{2}(q_L + q_R) \cdot n + \sqrt{gh_L} - \sqrt{gh_R}$, $\sqrt{gh^*} = \frac{1}{2}(\sqrt{gh_L} + \sqrt{gh_R}) + \frac{1}{4}(q_L + q_R) \cdot n$

with $q = (u, v)$. To obtain second-order accuracy, the authors applied a predictor-corrector and MUSCL technique. The "minmod" slope limiter was used in the paper.

The authors used a structured quadrilateral grid. As a result, there was a problem treating bottom slope source term because the four vertices of each cell bottom did not lie on the same plane. So, the authors proposed the following four step method to solve this problem: 1) determine the planimetric position of the centroid of the four vertices 2) then, the single quadrangular cell can be splitted into four triangular cells whose common vertex coincides with a centroid 3) bottom slope along x and y directions of each triangular cell can be determined because the three vertices of the cell bottom lie on a same plane (4) the effect of the bottom slope can be calculated by adding the effect of each triangular cell. The friction slope term was discretized by using the semi-implicit method to reduce the numerical instability :

$$S_f = (1 - \beta) S_f^{n-1} + \beta S_f^n = S_f^{n-1} + \beta (S_f / \partial U) \Delta U .$$

Finally, the two-dimensional shallow water equations was expressed as :

$$\Delta U = [I - \Delta t \beta Q_f^{n-1}]^{-1} \cdot \left[-\frac{\Delta t}{\Delta V} \sum_{r=1}^4 (F_r^* \cdot n_r) dS_r + \Delta t S_f^{n-1} + \Delta t S_o^{n-1} \right].$$

The proposed scheme was verified against some well-known test cases such as two-dimensional oblique hydraulic jump and partial dam-break problems. Then the comparison between numerical results of the flood event simulation on the valley of the Toce River in Italy and available experimental data was performed. According to the comparison, a good agreement between recorded and simulated water levels was shown.

Valiani and Begnudelli [79] presented a new formulation of the bottom slope source term for the two-dimensional shallow water equations. The authors used the similar approach used by Capart et al. [20]. In the paper, the bottom slope source term was approximated by assuming horizontal free surface level over a cell and expressed as

$$S_o = \begin{pmatrix} 0 \\ -gh \frac{\partial z_b}{\partial x} = \frac{\partial}{\partial x} \left(\frac{1}{2} gh^2 \right)_{\eta=\eta^*} \\ -gh \frac{\partial z_b}{\partial y} = \frac{\partial}{\partial y} \left(\frac{1}{2} gh^2 \right)_{\eta=\eta^*} \end{pmatrix} = -gh \nabla z_b = \nabla \left(\frac{1}{2} gh^2 \right)$$

where η^* is the constant value of free surface level η . The authors named this new form of bottom slope term as the divergence form for bed slope source term (DFB). The numerically discretized form of two-dimensional shallow water equations on a structured quadrilateral grid was given by

$$\Delta U = -\frac{\Delta t}{\Omega} \sum_{r=1}^4 (F_r^* \cdot n_r) \Delta l_r + \frac{\Delta t}{\Omega} \int_{\Omega} (S_o + S_f) d\Omega$$

where l_r is the length of cell edge and n_r is the outward pointing unit vector normal to the cell edge. The homogeneous part of the equations was calculated by using the MUSCL technique and HLL Riemann solver. The divergence form of the bottom slope term was discretized as

$$\frac{\Delta t}{\Omega} \int_{\Omega} S_o d\Omega = \frac{\Delta t}{\Omega} \left(\begin{array}{c} 0 \\ \sum_{r=1}^4 \frac{1}{2} gh_r^2 \Big|_{\eta=\eta^*} \cdot n_{xr} \Delta S_r \\ \sum_{r=1}^4 \frac{1}{2} gh_r^2 \Big|_{\eta=\eta^*} \cdot n_{yr} \Delta S_r \end{array} \right)$$

where n_{xr} and n_{yr} are Cartesian components of outward pointing normal unit vector. η^* was chosen as the average free surface level and h_r was computed as the difference between η^* and the average bed elevation of the r th cell edge. The proposed scheme was applied to some classical test cases and showed good agreement between numerical and exact solution even in the case of water at rest over an irregular bed topography. However, this method was developed only for structured quadrilateral grid and further study is needed in case of unstructured or non-quadrilateral grid.

Rogers et al. [70] reformulated the two-dimensional shallow water equations to eradicate numerical imbalance of flux gradient and source terms. The two-dimensional shallow water equations can be obtained by depth-averaging the Reynolds equations and expressed as

$$\begin{aligned} \frac{\partial h}{\partial t} + \frac{\partial(uh)}{\partial x} + \frac{\partial(vh)}{\partial y} &= 0 \\ \frac{\partial(uh)}{\partial t} + \frac{\partial(u^2h)}{\partial x} + \frac{\partial(uvh)}{\partial y} - \varepsilon \left(\frac{\partial(hu_x)}{\partial x} + \frac{\partial(hu_y)}{\partial y} \right) &= \frac{\tau_{wx} - \tau_{bx}}{\rho} - gh \frac{\partial \zeta}{\partial x} + hf v \\ \frac{\partial(vh)}{\partial t} + \frac{\partial(uvh)}{\partial x} + \frac{\partial(v^2h)}{\partial y} - \varepsilon \left(\frac{\partial(hv_x)}{\partial x} + \frac{\partial(hv_y)}{\partial y} \right) &= \frac{\tau_{wy} - \tau_{by}}{\rho} - gh \frac{\partial \zeta}{\partial y} - hf u \end{aligned}$$

where ζ is the free surface elevation above the still water level h_s . $h = \zeta + h_s$ is the total water depth, τ_{wx} and τ_{wy} are surface stresses, τ_{bx} and τ_{by} are bed friction stresses, ε is the kinematic eddy viscosity coefficient and f is the Coriolis parameter. To rewrite the above equations as a hyperbolic equation system, the $gh \partial \zeta / \partial x$ term should be decomposed as

$$gh \frac{\partial \zeta}{\partial x} = \frac{\partial}{\partial x} \left(\frac{1}{2} gh^2 \right) + gh S_{ox},$$

and it means the surface gradient term is split into flux gradient and bottom slope terms. However, this method cannot simulate still water problem because of the imbalance of flux gradient and source term. In the paper, the authors proposed balancing the flux gradients and source terms by a mathematical manipulation of the surface gradient term:

$$gh \frac{\partial \zeta}{\partial x} = g(\zeta + h_s) \frac{\partial}{\partial x} \left(\frac{1}{2} g(\zeta^2 + 2\zeta h_s) \right) + g\zeta \mathcal{S}_{\alpha x}.$$

This mathematical manipulation eradicated the numerical imbalance in Roe's approximate solver, and, in case of still water simulation, the water remained quiescent throughout the domain at all times during the simulation. The two-dimensional shallow water equations were rewritten as the following integral form

$$\frac{\partial}{\partial t} \int_{\Omega} U' d\Omega + \int_{\Omega} \left(\frac{\partial F'}{\partial x} + \frac{\partial G'}{\partial y} \right) d\Omega = \int_{\Omega} S' d\Omega$$

with

$$U' = \begin{pmatrix} \zeta \\ uh \\ vh \end{pmatrix}, \quad F' = \begin{pmatrix} uh \\ u^2h + \frac{1}{2}g(\zeta^2 + 2\zeta h_s) - \epsilon h \partial u / \partial x \\ uvh - \epsilon h \partial v / \partial x \end{pmatrix},$$

$$G' = \begin{pmatrix} vh \\ uvh - \epsilon h \partial u / \partial y \\ v^2h + \frac{1}{2}g(\zeta^2 + 2\zeta h_s) - \epsilon h \partial v / \partial y \end{pmatrix}, \quad S' = \begin{pmatrix} 0 \\ (\tau_{wx} - \tau_{bx}) / \rho - g\zeta \mathcal{S}_{\alpha x} + hf v \\ (\tau_{wy} - \tau_{by}) / \rho - g\zeta \mathcal{S}_{\alpha y} - hf u \end{pmatrix}.$$

The numerical flux at each cell interface was calculated by Roe's method and second-order accuracy was obtained by using the MUSCL technique with slope limiter function. The proposed method was applied to the shallow water flows and worked successfully for still water and wind-induced circulation in a dish-like circular basin.

3.4.5 Wetting/Drying Boundary Condition

Source term treatment in the two-dimensional shallow water equations is considered easier than the one-dimensional case because it does not include the width variation term I_2 . However, wetting/drying boundaries can cause numerical imbalance of flux gradient and bottom slope term. In this section, the techniques developed for the solution of wetting/drying boundary condition are reviewed.

In two-dimensional shallow water flows such as tidal floods and wave propagation over floodplain, water usually flows over dry bed in floodplain or the edge of river channel and the boundaries between wet and dry area exist where the water depth approaches to zero. These boundaries are different from other physical boundaries because they are moving according to the state of the wave propagation. So, the wetting front advance over a dry bed is a moving boundary problem and it can not be solved by the Riemann solver itself because the shallow water equations loses its properties when the water depth approaches to zero. The numerical difficulties in wetting/drying boundary problem can be split into two categories: numerical imbalance of flux gradient and bottom slope term and numerical instability in almost dry cells. The former leads to negative water depth, artificial mass and velocity, while the latter produces unphysical high velocity because the velocity components u and v are computed by dividing the volume fluxes hu and hv by the small water depth h .

To solve correctly moving boundary problems, at first, the location of the boundary should be detected accurately and, then, a suitable numerical modification based on the physical condition of the boundary should be applied to the boundary cells.

Zhao et al. [86] modelled two-dimensional river flows with the Osher scheme and suggested a new approach for the moving boundary problem. The authors classified the elements near the moving boundary into three types (entirely dry, partially dry and wet elements) and treated with different approaches. When the water depth of an element is less than the prespecified tolerance $HTOL1$ (usually very small value), and if there is no flow across all sides of the element, then the particular element was treated as entirely dry cell and neglected in the computations for that time step. When the water depth of an element is greater than $HTOL1$ but less than $HTOL2$ ($>HTOL1$) or when the water depth of an element is less than $HTOL1$ and there are flows across one or more sides, then the element was treated as a partially dry element. In case of partially dry element, the momentum flux was neglected and only the mass conservation equation was used to update solution. Finally, a wet element having

water depth greater than HTOL2 was treated as a normal cell and the solution was updated by normal numerical methods.

Hubbard and Dodd [52] used a similar but more detailed technique for wave run-up and overtopping problems. In the paper, the distinction between wet cells and dry cells having the water depth less than a specified tolerance h_{tol} was made and the interfaces between wet and dry cells were considered as moving boundaries. At the beginning of the solution update at each time step, dry cells having bottom level lower than the water surface level of any neighbouring wet cells was wetted by setting $h = h_{tol}$ and $u = v = 0$ to prevent numerical instability. Then, the numerical fluxes through three different types of moving boundaries were computed as follows:

- wet/wet : Roe's scheme was used as normal,
- dry/dry : completely ignored,
- wet/dry : no update was made to the both cells, i.e. the solid wall boundary condition was applied to this boundary.

After the completion of the update at each time step, the cells having the water depth lower than h_{tol} were treated as dry cells and their water depth were set to zero. Moreover, cells having very small water depth (less than the second tolerance $h_{TOL} > h_{tol}$) were treated as 'almost dry' cells and their momentum components hu and hV were set to zero to secure numerical efficiency while the water depth was not altered.

Bradford and Sanders [10] presented a wetting/drying boundary solver for their MUSCL-type scheme. In the paper, cells having a water depth greater than a tolerance $\varepsilon = 0.0001m$ were treated as 'fully wet' cells. The solution was updated normally in a fully wet cell, however, in case of 'partially wet' cell, the solution was computed by extrapolation. The MUSCL reconstruction of free surface elevation $\bar{\Delta}\zeta$ was modified near a wetting/drying boundary to prevent artificial leakage into adjacent cells. $\bar{\Delta}\zeta$ in a wet cell bounded by a partially wet or dry cell is extrapolated from the neighbouring wet cell like $\bar{\Delta}\zeta_{i,j} = \bar{\Delta}\zeta_{i,j-1}$ and the free surface elevation ζ of a partially wet cell was extrapolated from the fully wet cell. At cell interfaces where both sides are dry, the

numerical fluxes were set to zero. Finally, the momentum equations were not solved in partially wet cells and the velocity components were extrapolated from the neighbouring cell with largest water depth. The extrapolation of the velocity was performed by the two forms:

$$u_{\perp f}^{n+1} = u_{\perp w}^n + 2(c_w^n - c_f^{n+1})$$

or

$$u_{\perp f}^{n+1} = u_{\perp w}^{n+1}$$

where f denotes front or partially wet cell and w denotes the wettest neighbour.

Brufau et al. [12] modified the bottom slope between the two cells neighbouring moving boundary to secure the mass balance. To solve the wet/dry cell boundary problem, the free surface level $H = h + z_b$ of the neighbouring wet and dry cells were compared and the following two situations were considered:

- $H_L < H_R$: considered as stopping condition and the bottom slope was modified,
- $H_L \geq H_R$: treated as normal condition and Riemann solver provided satisfactory solution.

The subscripts L and R represent wet and dry cells, respectively. In case of still water problem, the condition $H_L < H_R$ causes numerical imbalance of flux gradient and the bottom slope term. To solve this, the bottom level of the dry cell was modified to satisfy the following equilibrium condition

$$\Delta H_{LR} = H_L - H_R = 0.$$

From the above equilibrium condition, the modified bottom level of the dry cell was defined as

$$z'_{bR} = z_{bL} - (h_R - h_L).$$

In unsteady cases, the same procedure was used, but the velocity components u and v of the wet cell were reduced to zero to prevent leakage of the mass. The proposed method was applied to some test cases and showed generally good results. However, this method produced mass error in case of unsteady flows and this problem was solved in the authors' next paper [13].

In [13], the authors proposed a similar but more detailed method which could solve unsteady flow problems without mass error. To secure mass conservation, the authors considered the mass conservation equation near the wetting/drying boundary. The numerically discretized mass conservation equations was given by

$$\frac{h_{i,j}^{n+1} - h_{i,j}^n}{\Delta t} = -\frac{1}{\Omega} \sum_{k=1}^{N_c} (E_k^* \cdot n_k - \tilde{S}_k^-) ds_k.$$

The mass flux through the interface between wet and dry cells was calculated by using Roe's method:

$$(E^* \cdot n)_{LR} = \frac{1}{2} [F_R n_x + G_R n_y + F_L n_x + G_L n_y - \tilde{\alpha}_1 |\tilde{\lambda}_1| \tilde{e}_1 - \tilde{\alpha}_2 |\tilde{\lambda}_2| \tilde{e}_2 - \tilde{\alpha}_3 |\tilde{\lambda}_3| \tilde{e}_3]$$

and the source term contribution was computed by the upwind treatment:

$$\tilde{S}_{LR}^- = \beta_1^- + \beta_3^-$$

where L and R denote the wet and the dry cells, respectively. In case of subcritical flows,

$$\tilde{\lambda}_1 > 0 \Rightarrow |\tilde{\lambda}_1| = \tilde{\lambda}_1 \quad \text{and} \quad \tilde{\lambda}_3 < 0 \Rightarrow |\tilde{\lambda}_3| = -\tilde{\lambda}_3$$

and the numerical flux and source term contribution were given by

$$(E^* \cdot n)_{LR} = \frac{h_L}{2} [u_L n_x + v_L n_y + \tilde{c}]$$

$$\tilde{S}_{LR}^- = \frac{1}{2} \tilde{c} (z_{bR} - z_{bL}).$$

The total contribution of the LR edge to mass conservation was set to zero

$$(E^* \cdot n - \tilde{S}^-)_{LR} = \frac{1}{2} [h_L (\tilde{u}n + \tilde{c}) - \tilde{c} (z_{bR} - z_{bL})] = 0$$

to prevent mass transfer through this boundary. From the above condition, the bottom slope was redefined as

$$(z_{bR} - z_{bL}) = h_L (1 + \tilde{u}n / \tilde{c}).$$

In case of supercritical flows,

$$\tilde{\lambda}_1 > 0 \Rightarrow |\tilde{\lambda}_1| = \tilde{\lambda}_1 \quad \text{and} \quad \tilde{\lambda}_3 > 0 \Rightarrow |\tilde{\lambda}_3| = \tilde{\lambda}_3$$

and nothing had been done for bottom slope term because there was no contribution of bottom slope source term: $\tilde{S}_{LR}^- = 0$.

Moreover, the method to correct mass conservation error due to the existence of negative water depth was proposed by the following algorithm: first, the cells with negative water depth after one time step were identified and their water depth and velocity components were set to zero, then, in order to preserve mass conservation, the same volume of water was subtracted from the neighbouring cells. For example, in case of two cells L with a negative water depth and R neighbouring and having more water:

- $h_L < 0$ was redefined as $h_L = 0$ which added a volume of water $h_L A_L$
- h_R was redefined as $h_R + h_L A_L / A_R$ to deduct the added mass to the system.

The proposed method was applied to some test cases including the Malpasset dam failure simulation and produced good results. Especially, the negative depth control technique gave almost zero mass conservation error.

3.5 Application of Riemann Solver Based Scheme to Natural River Flows

In this section, some recently published literature on the application of Riemann solver to natural river flow problems has been reviewed. The powerful shock capturing ability of Riemann solver based methods induced many hydraulic researchers to apply this technique to dam-break simulations. While idealised dam break simulations such as instantaneous one-dimensional dam-break problem and two-dimensional partial dam-break problem have been the basic test examples of newly developed hydraulic models, many researchers applied newly developed numerical model to the real dam-beak events. Among these, the Malpasset dam-beak event was numerically reproduced by many researchers. The Malpasset dam was constructed in 1952 on the River Reyran, France and collapsed in 1959 due to the leakage caused by the rapid increase of water level. Hervouet and Petitjean [78] numerically simulated the Malpasset dam-break event with TELEMAC-2D program which was developed on the basis of finite difference method. After then, many researchers used Rieamn solver based hydraulic model to this real dam-break event.

Valiani et al. [65] developed a two-dimensional finite volume model with HLL (Harten, Lax, and van Leer) approximate Riemann solver. Second-order accuracy was

obtained by reconstructing data with slope limiter function. The Malpasset dam-break event was numerically simulated with this model on an unstructured quadrilateral grid.

Yoon and Kang [84] also used HLL approximate Riemann solver to simulate the Malpasset dam-break event on an unstructured triangular grid. To obtain second-order accuracy a multidimensional slope-limiting technique was used. Results of both models such as maximum water levels and wave propagation times showed good agreement with the field data recorded at the time of dam break.

Zoppou and Roberts [87] developed a Riemann solver based two-dimensional hydraulic model and used this model to simulate the sudden collapse of a water reservoir which is in the upstream area of residential areas. In the paper, a first-order accurate approximate Riemann solver was used to compute numerical fluxes. The model was used to predict the arrival time of flood wave and inundation extent caused by a sudden collapse of Lower Hackett reservoir in the suburb of Canberra, Australia. The bed elevation data of this simulation was obtained from topographic maps and the inundation area was presented at every five seconds.

Riemann solver based hydraulic modelling technique has been used in various hydraulic engineering areas recently. Leon et al. [60] developed a Riemann solver based one-dimensional hydraulic model for simulation of unsteady flows in sewers. Guinot type and HLL type approximate solvers were used to calculate numerical flux and second-order accuracy was obtained by using the minmod slope limiter function to reconstruct data. The source terms have been discretized using a second-order Runge-Kutta method. The developed model was applied to several extreme flow conditions in sewers such as hydraulic bores and roll waves. The results showed that the Riemann solver based numerical model could solve transient flows in sewers which generally have circular cross sections more accurately and efficiently than the method of characteristics which was traditionally used in the area.

Jaffe and Sanders [53] simulated the depression wave caused by engineered breaches of embankments with two-dimensional finite volume model. In the paper, the

numerical fluxes were computed by using Roe's approximate solver and second-order accuracy was obtained by reconstructing data with slope limiter function. The main topic of the paper was to study the feasibility of engineered breaches of embankments to mitigate peak flood discharges in downstream areas and the effect of various factors like breach length, breach timing and floodplain area. According to the numerical results, engineered breaches approach is more efficient for relatively short and dynamic flood wave and the breaching action caused regressive and progressive depression waves in the upstream and the downstream channels of breach, respectively, which reduced water levels both upstream and downstream. Model results showed that floodplain area and breach timing were more important factors than others. This study showed the applicability of Riemann solver based hydraulic models to complicated river engineering projects.

A Riemann solver based hydraulic model has been coupled with ground water equation. Erduran et al. [34] developed a hybrid numerical scheme to integrate shallow water flow and ground water flow. The two-dimensional shallow water equations and the two-dimensional ground water equation were numerically discretized by applying the finite volume method and linked by introducing new source and sink terms in each equation. The numerical fluxes of surface water were computed with Roe's solver and the upwind approach was applied to the bottom slope term. The numerical fluxes of ground water were calculated by using the Darcy's law. Then, various infiltration conditions were considered to integrate shallow water flows and ground water flows.

The ultimate aim of developing new hydraulic model is the application of the model to the simulation of real river flows. Riemann solver based hydraulic models have been successfully applied to the real river flow problems like prediction of flood wave propagation.

Wan et al. [82] used the finite volume method to model flood inundation of the lower Yellow River in China. The authors solved the Riemann problem at each cell interface to compute the normal flux which is essential for solving the finite volume scheme. In the paper, an irregular unstructured computational mesh was applied, because it could easily discretize the complicated natural topography of the Yellow River. Dykes and

roads in the floodplain that could influence flow were discretized as a cell interface of the mesh. Two-dimensional models are considered more appropriate for flood modelling of the big rivers like lower Yellow River which is very wide and has a vast amount of floodplain because it could provide more detailed and correct information about the flow over the floodplain.

Sanders et al. [71] solved coupled one-dimensional shallow water equations and pollutant transport equation by using the finite volume method. In the paper, coupled equations were numerically discretized by using the finite volume method and the numerical fluxes of water mass, momentum and pollutant mass were computed with Roe's approximate solver. The authors used one-dimensional and two-dimensional hybrid method to solve junction flows. In the proposed method, three channels linked to two two-dimensional junction cells which represent junction area as shown in Figure 3.8. The numerical flux between one-dimensional channel cell and two-dimensional junction cell was computed by solving the local Riemann problem.

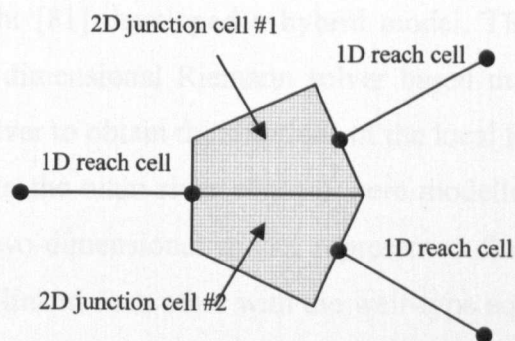


Figure 3.8 1D-2D hybrid discretization of channel junction [71]

The developed model was applied for the simulation of the urban runoff in the Talbert Channel System in Southern California, U.S.. The numerical results showed that the Riemann solver based hydraulic model could be effectively used for modelling of transport of pollutant and the model reproduced sharp pollutant pulses of urban runoff as well as water flow propagation of the channel system very correctly.

Beffa and Connell [6,7] developed a two-dimensional finite volume model, Hydro2de, to simulate floodplain flows. In the papers, Roe's solver was used and data at each

cell interface was reconstructed with slope limiters to secure second-order accuracy. The treatment of variable bed topography, friction losses including vegetation, and the boundaries between wet and dry cells were considered. The model was applied to simulate floods on the Waihao River floodplain in New Zealand. The digital terrain models (DTMs) of the floodplain having 5m and 20m resolution were obtained by aerial photogrammetric survey. The results were compared with those of MIKE11 featuring one-dimensional finite difference scheme and, according to the authors, Hydro2de model produced better results than MIKE11.

Many researchers have tried to integrate one- and two-dimensional Riemann solver based models in order to save computing resources in river modeling and solve complicated river flows more efficiently. In this approach, flows in confined or straight channels can be modelled with a one-dimensional method while complex flow conditions over floodplain or near sharp bends are solved with a two-dimensional method.

Villanueva and Wright [81] developed a hybrid model, TRENT, which links one-dimensional and two-dimensional Riemann solver based models. Both dimensional models used Roe's solver to obtain the solutions of the local Riemann problem at each cell interface. Flows in the main river channel were modelled with one-dimensional approach while the two-dimensional model represented floodplain flows. The two models were spatially linked each other with the weir-type equations which transferred mass from one-dimensional channel cells to two-dimensional floodplain cells and the coupling of the evolution time steps of both models was considered. The model was applied to 16km reach of the lower River Severn in west central England. Digital terrain models of the domain having four different resolutions (9m, 18m, 27m, 54m) were obtained from the light detection and ranging (LIDAR) data. The results of the model were compared with those of storage cell model which neglects momentum conservation equations in two-dimensional floodplain flows. According to the results, the storage cell model predicted slightly lower peak and later wave propagation on floodplains. This result was considered mainly caused by the neglect of momentum effects in the storage cell model.

A different approach of one- and two-dimensional hybrid model has been presented by Frazao and Zech [36]. The authors proposed a hybrid approach of one- and two-dimensional finite volume methods to simulate a dam-break problem in an initially dry channel with 90° bend. In the paper, a one-dimensional approach was used for the straight reaches while a two-dimensional approach applied to the bend zone. The numerical fluxes of one-dimensional and two-dimensional models were computed by using Roe's approximate Riemann solver. The results of the hybrid model were compared with those of the full one- and two-dimensional models. The pure one-dimensional model took much less computational time than other approaches. However, it could not reproduce the bore caused by the reflection process at the bend and, as a result, expected lower water depths in the upstream channel of the bend. The full two-dimensional approach showed good agreement with the experimental data while it took much more computation time than other approaches. The hybrid model could produce the two-dimensional properties including the reflection process with much less computing time than the full two-dimensional approach. The paper showed the possibility of application of hybrid approach of one- and two-dimensional models to complicated hydraulic simulations.

3.6 Conclusion

Basic information about numerical methods in hydraulic engineering has been studied and recently developed finite volume techniques published in other literature have been reviewed in this chapter. The conclusion of this chapter can be summarized that the main focus of the research in numerical river modelling has recently been on the finite volume approach and the Riemann solver based method has gained popularity due to the rigorous efforts made by other researchers. However, there is still ample room for improvement when it comes to the treatment of the source terms. While several researchers presented new techniques through rigorous research, those methods show limitations. The main limitations of the recently developed methods are their complexity and lack of universality because these follow the fractional step method. To tackle these limitations, a new approach which has a simple form and shows strong applicability to various numerical schemes will be proposed in this thesis. The main concept of the new approach is to transform the shallow water

equations into a homogeneous form and evaluate the effect of the source terms with the same method used for flux terms. The detailed techniques will be presented in the next chapter.

Chapter 4

Homogeneous Form of the Shallow Water Equations

A simple and efficient method to solve the one-dimensional shallow water equations with source terms is presented in this chapter. To avoid a fractional step method for the discretization of the source terms, the shallow water equations are transformed into a homogeneous form and well-known numerical schemes are used to solve the new form of the equations. The modification to the homogeneous equations combines the source terms with the flux term and solves them by the same solution structure of the numerical scheme. As a result, the source terms are automatically discretized to achieve balance with flux terms without any special treatment and it does not introduce numerical errors.

4.1 Introduction

The one-dimensional shallow water equations that describe the flow in an open channel can be written in the following vector form as:

$$\frac{\partial \mathbf{U}}{\partial t} + \frac{\partial \mathbf{F}}{\partial x} = \mathbf{S} \quad (4.1)$$

with

$$\mathbf{U} = \begin{pmatrix} A \\ Q \end{pmatrix}, \quad \mathbf{F} = \begin{pmatrix} Q \\ Q^2/A + gI_1 \end{pmatrix} \quad \text{and} \quad \mathbf{S} = \begin{pmatrix} 0 \\ gA(S_o - S_f) + gI_2 \end{pmatrix}$$

where A is the wetted cross-sectional area, Q is the discharge, S_o is the bed slope and S_f is the friction slope. The hydrostatic pressure terms I_1 and I_2 are defined as

$$I_1 = \int_0^h (h - \eta) \sigma d\eta \quad \text{and} \quad I_2 = \int_0^h (h - \eta) \frac{\partial \sigma}{\partial x} d\eta$$

where h is the water depth and $\sigma = \sigma(x, \eta)$ is the channel width at distance η above the channel bottom.

The shallow water equations (4.1) form an inhomogeneous hyperbolic equation system due to the existence of the source terms S . The inclusion of the source terms makes it difficult to find the correct solutions to open channel flow over irregular geometry. The causes of the difficulties can be summarized in the following two categories: complicated definition of the geometric source terms and incompatibility with the numerical methods based on homogeneous equations. First, the hydraulic pressure terms, I_1 and I_2 have complicated forms, especially the I_2 term that includes the integral of a derivative, which is very difficult to evaluate for non-rectangular channels. Consequently, the most efficient way to calculate geometric source terms is to replace the I_2 term by other terms having simpler definition. Second, most numerical methods are developed on the basis of homogeneous governing equations without source terms. As a result, the numerical techniques cannot solve the inhomogeneous equations with source terms such as the shallow water equations directly. This problem leads to a fractional step method that consists of two steps: calculation of the homogeneous part with the numerical methods based on homogeneous governing equations and subsequent addition of the source term effects. However, it is very difficult to achieve the balance of numerical flux and source terms, especially when the source terms are treated by a pointwise approach. This is because numerical balance is achieved when the following two conditions are satisfied: first, the update of the source terms should be performed with the same data used for the calculation of numerical flux and second, the discretization of the source terms should be performed in the same way as for the flux term. The simplest way to avoid this difficulty is to modify the source terms into the form of a flux, i.e. differential form, and combine it with flux term F . This modification leads to the homogeneous form of the shallow water equations.

An analogous method has been developed for nozzle flow problem by Gascon and Corberan [42]. They proposed a new flux formed by adding the primitive of the source terms to the flux terms, which was used to modify the governing equations for a compressible gas. The new flux can be written as

$$G(x, U) = F(U) - \int_0^x S(y) dy$$

where $F(U)$ is the flux vector and $S(y)$ is the source vector.

Then, the inhomogeneous governing equations for a compressible gas can be written as the following homogeneous form

$$\frac{\partial U}{\partial t} + \frac{\partial G(U)}{\partial x} = 0.$$

The problem is how to find the value of the primitive of the source terms and, in the paper, the authors replaced the integral by the average values. However, difficulties arise when this method is applied to the shallow water equations because it is difficult to define appropriate values for the integral of the source terms, especially in case of a nonprismatic channel. Moreover, their method needs complicated algebraic manipulation to obtain higher-order schemes.

An alternative method is developed here for the shallow water equations. This differs from Gascon and Coberan [42] in that the modification is performed by changing the source terms into a differential form similar to the flux term, which leads to a simpler and more efficient form of numerical scheme. Moreover, to secure exact numerical balance, new expressions for the source flux terms and corresponding channel geometry are presented. Consequently, the source terms are treated as a flux term and combined with the original numerical flux to form an integrated numerical flux representing real flow conditions. The integrated intercell numerical flux function including source term effects is obtained by modifying the well-known conservative numerical schemes.

In the next section, the shallow water equations are modified to a homogeneous form and a new definition for the source flux term will be presented.

4.2 Homogeneous Form of the Shallow Water Equations

The shallow water equations (4.1) can be modified to the following homogeneous form

$$\frac{\partial U}{\partial t} + \frac{\partial F}{\partial x} - \frac{\partial R}{\partial x} = 0$$

or

$$\frac{\partial U}{\partial t} + \frac{\partial H}{\partial x} = 0 \text{ with } H = (F - R). \quad (4.2)$$

where $\mathbf{R} = (0, R)^T$ represents the flux vector related to the source terms, which can drive or impede the flow of water. By modification to the homogeneous form, the source terms can be regarded as a flux and solved by the same solution structure used for the flux vector \mathbf{F} .

The modified shallow water equations (4.2) can be numerically discretized conservatively by using a finite volume method

$$\mathbf{U}_i^{n+1} = \mathbf{U}_i^n - \frac{\Delta t}{\Delta x} (\mathbf{H}_{i+\frac{1}{2}}^* - \mathbf{H}_{i-\frac{1}{2}}^*) \quad (4.3)$$

with $\mathbf{H}_{i+\frac{1}{2}}^* = \mathbf{F}_{i+\frac{1}{2}}^* - \mathbf{R}_{i+\frac{1}{2}}^*$, where $\mathbf{F}_{i+\frac{1}{2}}^*$ and $\mathbf{R}_{i+\frac{1}{2}}^*$ are the intercell numerical fluxes corresponding to momentum flux \mathbf{F} and source flux \mathbf{R} , respectively. The integrated numerical flux $\mathbf{H}_{i+\frac{1}{2}}^*$ represents the net flow of mass and momentum through the cell interface including the effect of the source terms. The integrated numerical flux $\mathbf{H}_{i+\frac{1}{2}}^*$ can be calculated by modifying the numerical flux functions developed for homogeneous governing equations because the equation system (4.2) and (4.3) have similar form to the homogeneous conservation law

$$\frac{\partial \mathbf{U}}{\partial t} + \frac{\partial \mathbf{F}}{\partial x} = 0,$$

and its discretized form

$$\mathbf{U}_i^{n+1} = \mathbf{U}_i^n - \frac{\Delta t}{\Delta x} (\mathbf{F}_{i+\frac{1}{2}}^* - \mathbf{F}_{i-\frac{1}{2}}^*). \quad (4.4)$$

Definition of source flux vector \mathbf{R}

While formulating the equations in homogeneous form is relatively straightforward, establishing the components of \mathbf{R} correctly requires more careful consideration. In fact, it is the latter that is the crucial aspect of the method proposed here. To obtain the correct expression of R , which is a component of the source flux vector \mathbf{R} , first of all, the channel geometry should be reconstructed to be compatible with the homogeneous form equations. The transformation of the equations into homogeneous form effectively removes the external forces on the control volume and instead represents these through the flux term: this implies that there is no additional source

of mass or momentum inside a control volume (or, cell) and only the flux terms can contribute to the update of the conserved variables, U . To satisfy this condition, a piecewise constant channel geometry as shown in *Figure 4.1* is considered. In the figure, all the factors of the channel geometry, i.e. bed level, width, shape, etc., have constant values in a cell and the interface between two neighbouring cells is considered as a discontinuity because any variation of the channel geometry in a cell causes the addition of momentum, which is contradictory to the assumption of the homogeneous form equations. The flux term R can be defined based on the piecewise constant channel geometry by using the following two steps: defining ΔR at cell interface and decomposing it properly into two nodal forces.

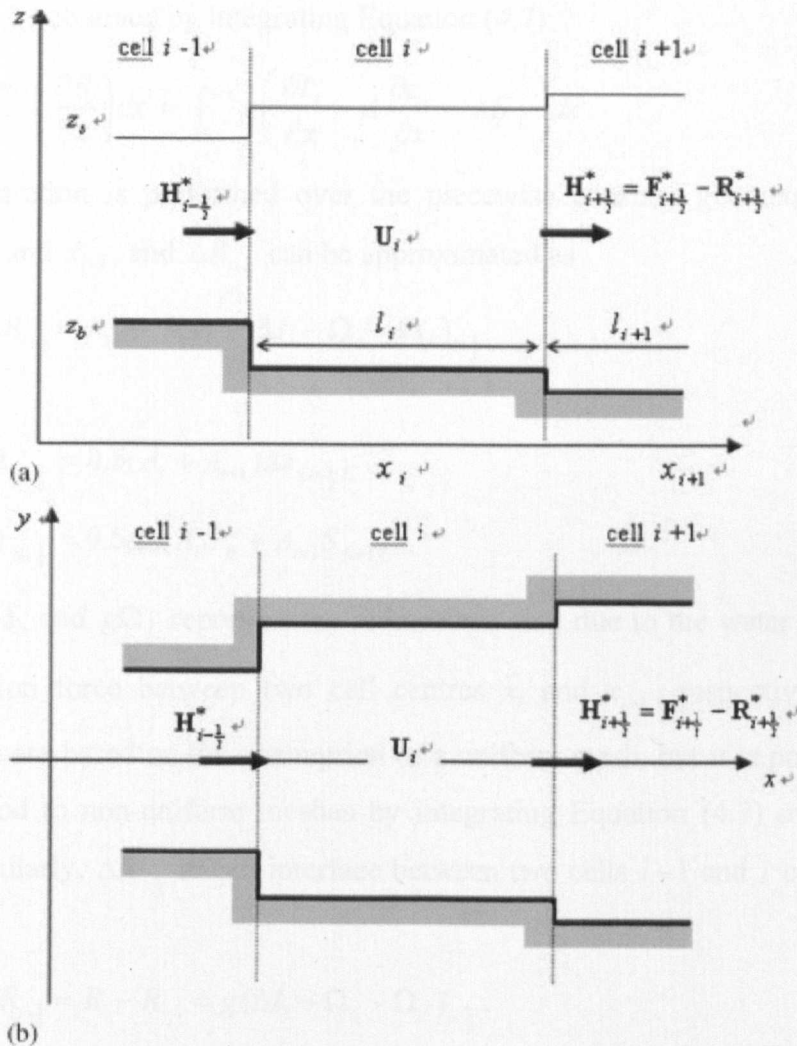


Figure 4.1 Reconstruction of geometry: (a) section view and (b) plan view

First, the definition of force ΔR can be obtained by comparing Equation (4.1) and (4.2):

$$\frac{\partial R}{\partial x} = gA(S_o - S_f) + gI_2. \quad (4.5)$$

To avoid complicated calculation of I_2 term, it should be modified by using the Leibnitz theorem for differentiation of an integral [28] :

$$I_2 = \frac{\partial I_1}{\partial x} - A \frac{\partial h}{\partial x}. \quad (4.6)$$

Consequently, Equation (4.5) can be rewritten as

$$\frac{\partial R}{\partial x} = g \left(\frac{\partial I_1}{\partial x} - A \frac{\partial z_s}{\partial x} - AS_f \right) \quad (4.7)$$

where $\partial z_s / \partial x$ is the slope of free surface elevation $z_s = z_b + h$. ΔR at cell interface $i + \frac{1}{2}$ can be obtained by integrating Equation (4.7):

$$\int_{x_i}^{x_{i+1}} \left(\frac{\partial R}{\partial x} \right) dx = \int_{x_i}^{x_{i+1}} g \left(\frac{\partial I_1}{\partial x} - A \frac{\partial z_s}{\partial x} - AS_f \right) dx.$$

The integration is performed over the piecewise constant geometry between two nodes x_i and x_{i+1} , and $\Delta R_{i+\frac{1}{2}}$ can be approximated as

$$\Delta R_{i+\frac{1}{2}} = R_{i+1} - R_i = g(\Delta I_1 - \Omega_o - \Omega_f)_{i+\frac{1}{2}}$$

with

$$\Omega_{o_{i+\frac{1}{2}}} = 0.5(A_i + A_{i+1})\Delta z_{s_{i+\frac{1}{2}}},$$

$$\Omega_{f_{i+\frac{1}{2}}} = 0.5\Delta x(A_i S_{f_i} + A_{i+1} S_{f_{i+1}})$$

where $g\Omega_o$ and $g\Omega_f$ represent the momentum flux due to the water level difference and friction force between two cell centres x_i and x_{i+1} , respectively. The above equations are based on the assumption of a uniform mesh, but it is possible to extend the method to non-uniform meshes by integrating Equation (4.7) over the relevant cells. Similarly, $\Delta R_{i-\frac{1}{2}}$ at cell interface between two cells $i-1$ and i can be expressed as

$$\Delta R_{i-\frac{1}{2}} = R_i - R_{i-1} = g(\Delta I_1 - \Omega_o - \Omega_f)_{i-\frac{1}{2}}.$$

The next step is to decompose $\Delta R_{i+\frac{1}{2}}$ and $\Delta R_{i-\frac{1}{2}}$ terms into the three ideal forces R_{i+1} , R_i and R_{i-1} , which are essential to update the conserved variable U_i . The decomposition can be performed by the following algebraic manipulations.

From the definitions of $\Delta R_{i+\frac{1}{2}}$ and $\Delta R_{i-\frac{1}{2}}$,

$$R_{i+1} - R_i = gI_{li+1} - gI_{li} - g(\Omega_o + \Omega_f)_{i+\frac{1}{2}} \quad (4.8)$$

$$R_i - R_{i-1} = gI_{li} - gI_{li-1} - g(\Omega_o + \Omega_f)_{i-\frac{1}{2}}. \quad (4.9)$$

To decide the values of each force, R_{i+1} , R_i and R_{i-1} can be considered as follows:

$$R_{i+1} = a_{i+1}gI_{li+1} + b_{i+1}gI_{li} + c_{i+1}gI_{li-1} + d_{i+1}g(\Omega_o + \Omega_f)_{i+\frac{1}{2}} + e_{i+1}g(\Omega_o + \Omega_f)_{i-\frac{1}{2}} \quad (4.10)$$

$$R_i = a_i gI_{li+1} + b_i gI_{li} + c_i gI_{li-1} + d_i g(\Omega_o + \Omega_f)_{i+\frac{1}{2}} + e_i g(\Omega_o + \Omega_f)_{i-\frac{1}{2}} \quad (4.11)$$

$$R_{i-1} = a_{i-1}gI_{li+1} + b_{i-1}gI_{li} + c_{i-1}gI_{li-1} + d_{i-1}g(\Omega_o + \Omega_f)_{i+\frac{1}{2}} + e_{i-1}g(\Omega_o + \Omega_f)_{i-\frac{1}{2}} \quad (4.12)$$

where, a , b , c , d and e represent the coefficients of each term. By substituting (4.10-12) into (4.8) and (4.9),

$$a_{i+1} - a_i = 1, \quad a_i - a_{i-1} = 0,$$

$$b_{i+1} - b_i = -1, \quad b_i - b_{i-1} = 1,$$

$$c_{i+1} - c_i = 0, \quad c_i - c_{i-1} = -1,$$

$$d_{i+1} - d_i = -1, \quad d_i - d_{i-1} = 0,$$

$$e_{i+1} - e_i = 0, \quad e_i - e_{i-1} = -1.$$

By considering the conditions of the numerical domain, the values of several coefficients can be decided. In other words, R_{i+1} can not be influenced by gI_{li-1} and $g(\Omega_o + \Omega_f)_{i-\frac{1}{2}}$ terms, while R_{i-1} has no relationship with gI_{li+1} and $g(\Omega_o + \Omega_f)_{i-\frac{1}{2}}$ terms. This is because the characteristic informations of the cell $i-1$ can not be transferred to cell $i+1$ at each time step, and vice versa. As a result,

$$c_{i+1} = e_{i+1} = 0, \quad a_{i-1} = d_{i-1} = 0$$

and

$$a_{i+1} = 1, a_i = 0, c_i = 0, c_{i-1} = 1, d_{i+1} = -1, d_i = 0, e_i = 0, e_{i-1} = 1.$$

Then,

$$R_{i+1} = gI_{li+1} + b_{i+1}gI_{li} - g(\Omega_o + \Omega_f)_{i+\frac{1}{2}}$$

$$R_i = b_i gI_{li}$$

$$R_{i-1} = b_{i-1}gI_{li} + gI_{li-1} + g(\Omega_o + \Omega_f)_{i-\frac{1}{2}}$$

and, it is reasonable to consider the gI_{li} term and a force related to the shape of the cross section of each cell. while $g(\Omega_o + \Omega_f)$ term is about the bottom slope and friction. As a result, the coefficient b_{i+1} , b_i and b_{i-1} can be decided as

$$b_i = 1, b_{i+1} = b_{i-1} = 0.$$

Finally, R_{i+1} , R_i and R_{i-1} can be defined as

$$R_{i+1} = gI_{li+1} + g(\Omega_o + \Omega_f)_{i+\frac{1}{2}},$$

$$R_i = gI_{li},$$

$$R_{i-1} = gI_{li-1} - g(\Omega_o + \Omega_f)_{i-\frac{1}{2}}.$$

In case of prismatic rectangular channel with width b and depth h , R_{i+1} , R_i and R_{i-1} is expressed as

$$R_{i+1} = \frac{g}{2}bh_{i+1}^2 + \frac{g}{2}(b(h_i + h_{i+1}))(z_{i+1} - z_i) + \Delta xb(h_i S_{f_i} + h_{i+1} S_{f_{i+1}})$$

$$R_i = \frac{g}{2}bh_i^2$$

$$R_{i-1} = \frac{g}{2}bh_{i-1}^2 - \frac{g}{2}(b(h_i + h_{i-1}))(z_i - z_{i-1}) - \Delta xb(h_i S_{f_i} + h_{i-1} S_{f_{i-1}}).$$

The $g(\Omega_o + \Omega_f)$ term representing the momentum flux due to the water level difference and friction force is not included in R_i term because it should be considered as a pressure force exerted by the neighbouring cells R_{i+1} and R_{i-1} . As a result, the momentum flux R does not have an absolute value but a relative value. For example, to update the variable U_{i+1} , the values of the three ideal forces R_i , R_{i+1} and R_{i+2} are needed and these can be calculated by decomposing two terms $\Delta R_{i+\frac{1}{2}}$ and

$\Delta R_{i+\frac{3}{2}}$ and the value of the term R_i will be changed to $R_i = gI_{ii} + g(\Omega_o + \Omega_f)_{i+\frac{1}{2}}$. Similarly, to update the variable U_{i-1} , the three terms U_{i-2} , U_{i-1} and U_i are needed and the value of the term R_i will be changed to $R_i = gI_{ii} - g(\Omega_o + \Omega_f)_{i-\frac{1}{2}}$.

4.3 Conservative Schemes

In the previous section, a homogeneous form of the shallow water equations and the definition of the source flux have been presented. This section is devoted to the solution of the homogeneous form equations and it can be performed through simple modification of the well-known numerical schemes developed on the basis of the shallow water equations without source terms. The modification can be performed by replacing the flux term F and the variable difference ΔU with the integrated flux H and the modified difference $\Delta U'$. $\Delta U'$ represents the net difference of the conserved variables ΔU including the effect of the channel geometry and can be obtained from the relation between ΔH and ΔF . To verify the applicability of the proposed method to various numerical schemes, approximate Riemann solver-based schemes (Roe and HLL) and classical schemes (Lax-Friedrichs, Lax-Wendroff and MacCormack) are presented. In order to demonstrate the modification process, the original numerical scheme is introduced first and, then, changed to the homogeneous form.

To show the property of each scheme, the numerical results of the one-dimensional ideal dam-break problem in 100m long prismatic rectangular channel are also presented. The initial conditions of the dam-break problem are two water depths, $h_1 = 20m$ upstream ($x < 50m$) and $h_2 = 1m$ downstream ($x \geq 50m$) and the numerical results at time $t = 2s$ are compared with analytical solution [23].

4.3.1 Roe's Approximate Riemann solver

Original Roe's Solver

The details of Roe's solver have been presented in Section 3.4.1. Roe [69] constructed an approximate Jacobian \tilde{J} which satisfies the relation $\Delta F = \tilde{J}\Delta U$ and is

diagonalizable with real eigenvalues. The main idea of Roe's method is to split the flux difference at each cell interface by using the approximate Jacobian matrix and which can be expressed as

$$\Delta \mathbf{F} = \tilde{\mathbf{J}} \Delta \mathbf{U} = \tilde{\mathbf{J}}^+ \Delta \mathbf{U} + \tilde{\mathbf{J}}^- \Delta \mathbf{U}$$

where $\tilde{\mathbf{J}}^\pm$ represents the positive or negative portion of the Jacobian matrix. $\tilde{\mathbf{J}}^\pm$ can be obtained by using the diagonal matrix of the eigenvalues

$$\tilde{\mathbf{J}}^\pm = \mathbf{R} \Lambda^\pm \mathbf{R}^{-1}$$

where \mathbf{R} is the matrix of right eigenvectors and Λ^\pm represents the matrix having only the positive or negative eigenvalues on the diagonal. \mathbf{R} and Λ^\pm satisfy the following relations:

$$\tilde{\mathbf{J}} = \tilde{\mathbf{J}}^+ + \tilde{\mathbf{J}}^- = \mathbf{R}(\Lambda^+ + \Lambda^-)\mathbf{R}^{-1}.$$

By using these relations, the numerical flux at the cell interface $i + \frac{1}{2}$ between two cells i and $i + 1$, $\mathbf{F}_{i+\frac{1}{2}}^*$, can be written as

$$\mathbf{F}_{i+\frac{1}{2}}^* = \mathbf{F}_i + \tilde{\mathbf{J}}_{i+\frac{1}{2}}^- (\mathbf{U}_{i+1} - \mathbf{U}_i), \quad (4.13)$$

$$\mathbf{F}_{i+\frac{1}{2}}^* = \mathbf{F}_{i+1} - \tilde{\mathbf{J}}_{i+\frac{1}{2}}^+ (\mathbf{U}_{i+1} - \mathbf{U}_i) \quad (4.14)$$

or by averaging (4.13) and (4.14)

$$\mathbf{F}_{i+\frac{1}{2}}^* = \frac{1}{2}(\mathbf{F}_{i+1} + \mathbf{F}_i) - \frac{1}{2} |\tilde{\mathbf{J}}_{i+\frac{1}{2}}| \Delta \mathbf{U}_{i+\frac{1}{2}}. \quad (4.15)$$

By projecting onto the right eigenvectors, the variable differences $\Delta \mathbf{U}$ and $\Delta \mathbf{F}$ can be rewritten as

$$\Delta \mathbf{U}_{i+\frac{1}{2}} = \mathbf{U}_{i+1} - \mathbf{U}_i = \sum_k (\tilde{\alpha}_k \tilde{\mathbf{e}}_k)_{i+\frac{1}{2}}, \quad (4.16)$$

$$\Delta \mathbf{F}_{i+\frac{1}{2}} = \mathbf{F}_{i+1} - \mathbf{F}_i = \sum_k (\tilde{\alpha}_k \tilde{\lambda}_k \tilde{\mathbf{e}}_k)_{i+\frac{1}{2}}$$

and the numerical flux function (4.15) can be rewritten as the following characteristic form as:

$$\mathbf{F}_{i+\frac{1}{2}}^* = \frac{1}{2}(\mathbf{F}_{i+1} + \mathbf{F}_i) - \frac{1}{2} \sum_k (\tilde{\alpha}_k |\tilde{\lambda}_k| \tilde{\mathbf{e}}_k)_{i+\frac{1}{2}}.$$

The approximate Jacobian matrix has eigenvalues and eigenvectors of the form

$$\tilde{\lambda}_{1,2} = \tilde{u} \pm \tilde{c},$$

$$\tilde{e}_{1,2} = (1, \tilde{\lambda}_{1,2})^T$$

where the average values \tilde{u} and \tilde{c} can be obtained from the condition $\Delta F = \tilde{J}\Delta U$:

$$\tilde{u}_{i+\frac{1}{2}} = \frac{Q_{i+1}/\sqrt{A_{i+1}} + Q_i/\sqrt{A_i}}{\sqrt{A_{i+1}} + \sqrt{A_i}} \quad (4.17)$$

$$\tilde{c}_{i+\frac{1}{2}}^2 = \begin{cases} g \frac{l_{i+1}-l_i}{A_{i+1}-A_i} & \text{if } A_{i+1} - A_i \neq 0 \\ gh & \text{if } A_{i+1} - A_i = 0 \end{cases}$$

Note that Equation (4.17) can be used only for a prismatic channel case because, in case of a non-prismatic channel, $\frac{l_{i+1}-l_i}{A_{i+1}-A_i}$ and $\tilde{c}_{i+\frac{1}{2}}^2$ can have a negative value.

Alternatively, several expressions for \tilde{c} are found in available literature and the one presented by Garcia-Navarro and Vazquez-Cendon [40] is used in this paper:

$$\tilde{c}_{i+\frac{1}{2}}^2 = \sqrt{\frac{g}{2} \left(\frac{A_i}{B_i} + \frac{A_{i+1}}{B_{i+1}} \right)}$$

The wavenumbers $\tilde{\alpha}_{1,2}$ can be computed from Equation (4.16):

$$\tilde{\alpha}_1 = \frac{(\tilde{c} - \tilde{u})\Delta A + \Delta Q}{2\tilde{c}},$$

$$\tilde{\alpha}_2 = \frac{(\tilde{c} + \tilde{u})\Delta A - \Delta Q}{2\tilde{c}}.$$

Roe's solver, under certain circumstances, can lead to entropy violating solutions with spurious oscillation near a transcritical point. To rectify this problem, the 'entropy fix' proposed by Harten and Hyman [47] is used

$$|\tilde{\lambda}| = \begin{cases} |\tilde{\lambda}| & (|\tilde{\lambda}| \geq \varepsilon) \\ \varepsilon & (|\tilde{\lambda}| < \varepsilon) \end{cases}$$

where ε is given by

$$\varepsilon = \max(0, \tilde{\lambda}_{i+\frac{1}{2}} - \lambda_i, \lambda_{i+1} - \tilde{\lambda}_{i+\frac{1}{2}}).$$

The water depth profile of the dam-break simulation with Roe's solver are presented in *Figure 4.2*. As shown in the figure, Roe's solver reproduces the shock wave well. However the results show diffusive solutions for the rarefaction waves and it

demonstrates that Roe's solver is first-order accurate. The entropy correction removes the unphysical solutions near transcritical point.

Homogeneous form of Roe's Solver

The integrated intercell numerical flux $\mathbf{H}_{i+\frac{1}{2}}^*$ can be easily obtained by modifying $\mathbf{F}_{i+\frac{1}{2}}^*$

$$\mathbf{H}_{i+\frac{1}{2}}^* = \frac{1}{2}(\mathbf{H}_{i+1} + \mathbf{H}_i) - \frac{1}{2}|\tilde{\mathbf{J}}|\Delta\mathbf{U}'_{i+\frac{1}{2}}$$

where the flux term \mathbf{F} is replaced by \mathbf{H} and $|\tilde{\mathbf{J}}|\Delta\mathbf{U}$ term related to the splitting of the flux difference $\Delta\mathbf{F}$ is replaced by $|\tilde{\mathbf{J}}|\Delta\mathbf{U}'$ corresponding to the splitting of $\Delta\mathbf{H}$. The definition of the term $\Delta\mathbf{U}'_{i+\frac{1}{2}} = (\Delta\mathbf{A}', \Delta\mathbf{Q}')_{i+\frac{1}{2}}^T$ can be obtained by considering the relation

$$\Delta\mathbf{H}_{i+\frac{1}{2}} = \Delta\mathbf{F}_{i+\frac{1}{2}} - \Delta\mathbf{R}_{i+\frac{1}{2}} = \tilde{\mathbf{J}}_{i+\frac{1}{2}}\Delta\mathbf{U}'_{i+\frac{1}{2}} \quad (4.18)$$

because the effect of the source flux \mathbf{R} propagates along the eigenvalues $\tilde{\lambda}_{1,2}$ of Jacobian $\tilde{\mathbf{J}}$. The term $\Delta\mathbf{U}'$ represents the spatial difference of the conserved variables due to the source flux $\Delta\mathbf{R}$ as well as the momentum flux $\Delta\mathbf{F}$ while $\Delta\mathbf{U}$ is only related to $\Delta\mathbf{F}$. From Equation (4.18),

$$\begin{pmatrix} \Delta\mathbf{Q} \\ \Delta\left(\frac{\rho^2}{A}\right) + g\Delta I_1 \end{pmatrix}_{i+\frac{1}{2}} - \begin{pmatrix} 0 \\ g\Delta I_1 - g(\Omega_o + \Omega_f) \end{pmatrix}_{i+\frac{1}{2}} = \begin{pmatrix} 0 & 1 \\ -\tilde{\lambda}_1 \cdot \tilde{\lambda}_2 & \tilde{\lambda}_1 + \tilde{\lambda}_2 \end{pmatrix}_{i+\frac{1}{2}} \begin{pmatrix} \Delta\mathbf{A}' \\ \Delta\mathbf{Q}' \end{pmatrix}_{i+\frac{1}{2}}$$

and

$$\Delta\mathbf{Q}'_{i+\frac{1}{2}} = \Delta\mathbf{Q}_{i+\frac{1}{2}},$$

$$\Delta\mathbf{A}'_{i+\frac{1}{2}} = -\frac{\Delta\left(\frac{\rho^2}{A}\right)_{i+\frac{1}{2}} + g(\Omega_o + \Omega_f)_{i+\frac{1}{2}} - (\tilde{\lambda}_1 + \tilde{\lambda}_2)\Delta\mathbf{Q}_{i+\frac{1}{2}}}{\tilde{\lambda}_1 \cdot \tilde{\lambda}_2}.$$

Finally, the integrated flux \mathbf{H}^* can be expressed as the following characteristic form:

$$\mathbf{H}_{i+\frac{1}{2}}^* = \frac{1}{2}(\mathbf{H}_{i+1} + \mathbf{H}_i) - \frac{1}{2} \sum_k (\tilde{\alpha}'_k |\tilde{\lambda}'_k| \tilde{\mathbf{e}}_k)_{i+\frac{1}{2}}$$

where the modified wave strengths $\tilde{\alpha}'_{1,2}$ are obtained from $\Delta\mathbf{U}' = \sum_k (\tilde{\alpha}'_k \tilde{\mathbf{e}}_k)$ and given

by

$$\tilde{\alpha}'_1 = \frac{(\tilde{c} - \tilde{u})\Delta A' + \Delta Q}{2\tilde{c}}, \quad \tilde{\alpha}'_2 = \frac{(\tilde{c} + \tilde{u})\Delta A' - \Delta Q}{2\tilde{c}}.$$

The wavestrengths $\tilde{\alpha}'_{1,2}$ represent the real state of the flow including the effect of the source terms. For example, in the case of the still water problem, $\Delta A' = 0$, $\Delta Q' = 0$ and, consequently, $\tilde{\alpha}'_{1,2} = 0$, which means that there is no flow through the cell interface.

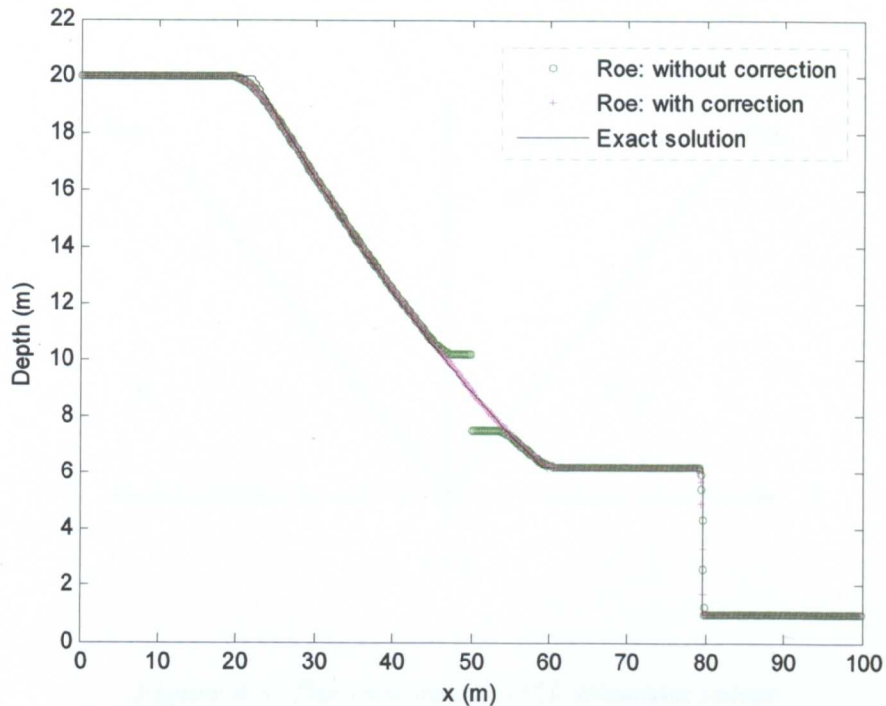


Figure 4.2 Ideal dam-break problem with Roe's solver

4.3.2 HLL Approximate Riemann solver

Original HLL Solver

The HLL solver was proposed by Harten *et al.* [48] and has been widely used because it has a simple structure and does not need complicated characteristic decomposition of the flux difference. The solution of the HLL solver consists of three constant states separated by two characteristics λ_{\min} and λ_{\max} as shown in *Figure 4.3*. The numerical

flux in the intermediate region $F(U^*)$ can be obtained by considering the following two Rankine–Hugoniot conditions

$$F(U^*) - F(U_i) = \lambda_{\min}(U^* - U_i)$$

$$F(U_{i+1}) - F(U^*) = \lambda_{\max}(U_{i+1} - U^*)$$

and by eliminating the U^* term

$$F(U^*) = \frac{\lambda_{\max}F(U_i) - \lambda_{\min}F(U_{i+1})}{\lambda_{\max} - \lambda_{\min}} - \frac{\lambda_{\max}\lambda_{\min}(U_{i+1} - U_i)}{\lambda_{\max} - \lambda_{\min}}.$$

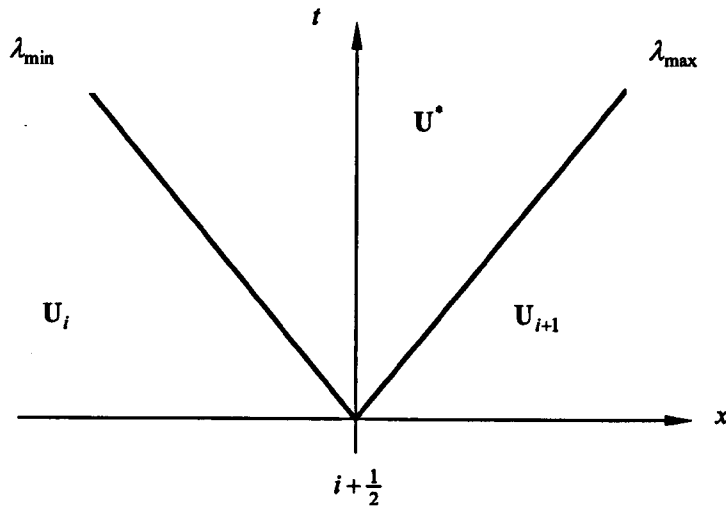


Figure 4.3 The structure of HLL Riemann solver

The intercell numerical flux $F_{i+\frac{1}{2}}^*$ has different values according to the sign of the wave speeds and is given by

$$F_{i+\frac{1}{2}}^* = \begin{cases} F(U_i) & \text{if } \lambda_{\min} \geq 0 \\ F(U_{i+1}) & \text{if } \lambda_{\max} \leq 0 \\ F(U^*) & \text{otherwise} \end{cases}$$

The two wave speeds λ_{\min} and λ_{\max} should be chosen carefully so as not to cause entropy violation and, in this thesis, those suggested by Einfeldt [31] which use Roe's average values \tilde{u} and \tilde{c} are used

$$\lambda_{\min} = \min(u_i - c_i, \tilde{u}_{i+\frac{1}{2}} - \tilde{c}_{i+\frac{1}{2}}),$$

$$\lambda_{\max} = \max(u_{i+1} + c_{i+1}, \tilde{u}_{i+\frac{1}{2}} + \tilde{c}_{i+\frac{1}{2}})$$

where u and c represent velocity and wave speed, respectively.

The HLL solver produces results very similar to Roe's solver and it is also first-order accurate. The HLL solver does not need entropy correction.

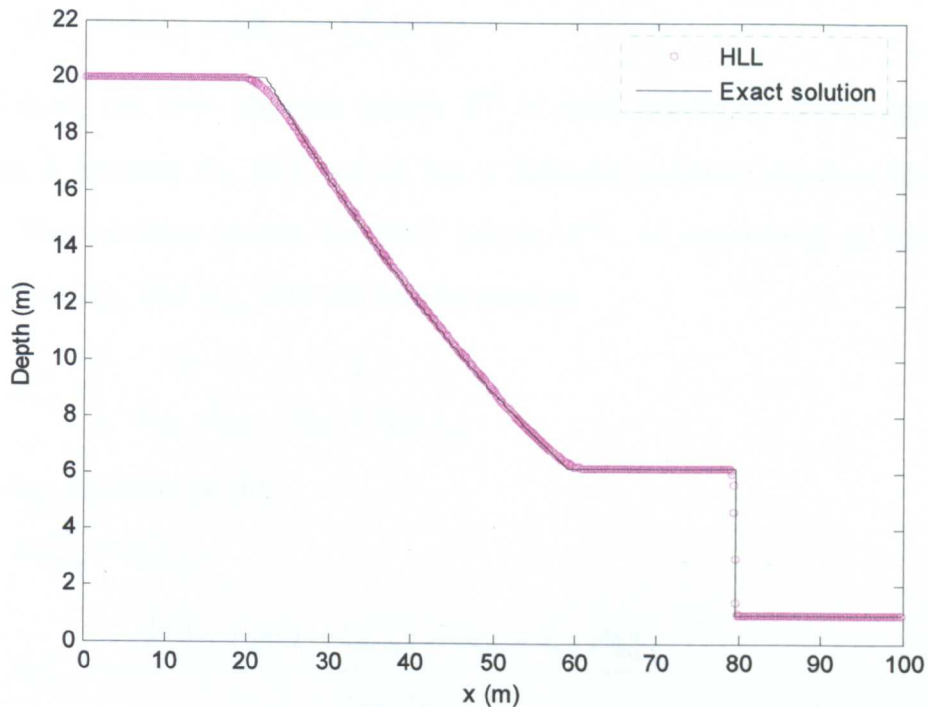


Figure 4.4 Ideal dam-break problem with HLL solver

Homogeneous form of HLL Solver

The integrated numerical flux $\mathbf{H}_{i+\frac{1}{2}}^*$ can be easily obtained by modifying the solution for the numerical flux $\mathbf{F}_{i+\frac{1}{2}}^*$

$$\mathbf{H}_{i+\frac{1}{2}}^* = \begin{cases} \mathbf{H}_i & \text{if } \lambda_{\min} \geq 0 \\ \mathbf{H}_{i+1} & \text{if } \lambda_{\max} \leq 0 \\ \mathbf{H}^* & \text{otherwise} \end{cases}$$

with

$$\mathbf{H}^* = \frac{\lambda_{\max} \mathbf{H}_i - \lambda_{\min} \mathbf{H}_{i+1}}{\lambda_{\max} - \lambda_{\min}} - \frac{\lambda_{\min} \lambda_{\max} \Delta \mathbf{U}'_{i+\frac{1}{2}}}{\lambda_{\max} - \lambda_{\min}}$$

where $\Delta \mathbf{U}'_{i+\frac{1}{2}} = (\Delta \mathcal{A}', \Delta \mathcal{Q}')_{i+\frac{1}{2}}^T$ can be defined by using a technique similar to that used for Roe's solver. In other words, $\Delta \mathbf{U}'_{i+\frac{1}{2}}$ satisfy the following relation:

$$\Delta \mathbf{H}_{i+\frac{1}{2}} = \Delta \mathbf{F}_{i+\frac{1}{2}} - \Delta \mathbf{R}_{i+\frac{1}{2}} = \mathbf{J}^{hll} \Delta \mathbf{U}'_{i+\frac{1}{2}}. \quad (4.19)$$

In this case, the new Jacobian matrix \mathbf{J}^{hll} is used instead of Roe's approximate Jacobian $\tilde{\mathbf{J}}$ because the HLL solver has a different solution structure from Roe's solver. The Jacobian matrix for HLL solver, \mathbf{J}^{hll} , is considered as having two eigenvalues λ_{\min} and λ_{\max} and can be expressed as

$$\mathbf{J}^{hll}_{i+\frac{1}{2}} = \begin{pmatrix} 0 & 1 \\ -\lambda_{\min} \cdot \lambda_{\max} & \lambda_{\min} + \lambda_{\max} \end{pmatrix}_{i+\frac{1}{2}}.$$

By solving Equation (4.19),

$$\Delta \mathcal{Q}'_{i+\frac{1}{2}} = \Delta \mathcal{Q}_{i+\frac{1}{2}},$$

$$\Delta \mathcal{A}'_{i+\frac{1}{2}} = -\frac{\Delta \left(\frac{\mathcal{Q}}{\mathcal{A}} \right)_{i+\frac{1}{2}} + g(\Omega_o + \Omega_f)_{i+\frac{1}{2}} - (\lambda_{\min} + \lambda_{\max}) \Delta \mathcal{Q}_{i+\frac{1}{2}}}{\lambda_{\min} \cdot \lambda_{\max}}.$$

4.3.3 Lax-Friedrichs Scheme

Original Lax-Friedrichs scheme

The Lax-Friedrichs scheme is a classical first-order accurate scheme presented by Lax [58] and can be derived by using the following first-order accurate approximation of derivatives

$$\frac{\partial \mathbf{U}}{\partial t} \approx \frac{\mathbf{U}_i^{n+1} - \left[a \mathbf{U}_i^n + \frac{1-a}{2} (\mathbf{U}_{i+1}^n - \mathbf{U}_{i-1}^n) \right]}{\Delta t} \quad (0 \leq a < 1) \quad (4.20)$$

$$\frac{\partial \mathbf{F}}{\partial x} \approx \frac{\mathbf{F}_{i+1}^n - \mathbf{F}_{i-1}^n}{2\Delta x}. \quad (4.21)$$

By substituting (4.20) and (4.21) into Equations (4.4), the Lax-Friedrichs scheme can be expressed as

$$\mathbf{U}_i^{n+1} = a\mathbf{U}_i^n + \frac{1-a}{2}(\mathbf{U}_{i+1}^n + \mathbf{U}_{i-1}^n) - \frac{1}{2} \frac{\Delta t}{\Delta x} (\mathbf{F}_{i+1}^n - \mathbf{F}_{i-1}^n)$$

or

$$\mathbf{U}_i^{n+1} = \mathbf{U}_i^n + \frac{1-a}{2}(\Delta \mathbf{U}_{i+\frac{1}{2}} - \Delta \mathbf{U}_{i-\frac{1}{2}}) - \frac{1}{2} \frac{\Delta t}{\Delta x} (\mathbf{F}_{i+1}^n - \mathbf{F}_{i-1}^n).$$

The value of a is related to the numerical diffusion of the solutions and the stability of the scheme. $a=1$ makes the scheme unconditionally unstable while the higher a value leads to more diffusive solutions. Usually, $a=0.1$ is used for open channel flow problems [38].

The conservative form of the Lax-Friedrichs scheme can be obtained through simple algebraic manipulations and expressed as

$$\mathbf{U}_i^{n+1} = \mathbf{U}_i^n - \frac{\Delta t}{\Delta x} (\mathbf{F}_{i+\frac{1}{2}}^* - \mathbf{F}_{i-\frac{1}{2}}^*)$$

with intercell numerical flux

$$\mathbf{F}_{i+\frac{1}{2}}^* = \frac{1}{2}(\mathbf{F}_i + \mathbf{F}_{i+1}) - \frac{1-a}{2} \frac{\Delta t}{\Delta x} \Delta \mathbf{U}_{i+\frac{1}{2}},$$

which has similar form to the numerical flux of Roe's scheme, i.e. the $|\tilde{\mathcal{J}}|$ term in Roe's flux is replaced by a constant value $(1-a)(\Delta t/\Delta x)$. Consequently, the Lax-Friedrichs scheme cannot split the flux difference $\Delta \mathbf{F}$ according to the eigenvalues of the Jacobian matrix and shows diffusive solutions.

The numerical results for the dam-break problem with the Lax-Friedrichs scheme are shown in *Figure 4.5*. As shown in the figure, the Lax-Friedrichs scheme shows more diffusive results than the two Riemann solver based schemes (Roe and HLL which are shown in *Figure 4.2* and *4.3* respectively) and the large value of the coefficient a makes the scheme unstable near discontinuities while it produces less diffusive results.

Homogeneous form of Lax-Friedrichs scheme

The homogeneous form of the Lax-Friedrichs scheme can be constructed by replacing the flux term F with the integrated flux H . Moreover, the ΔU term should be changed to $\Delta U'$ which can be calculated by the relation $\Delta U' = J^{-1}H$. In this case, the approximate Jacobian matrix used for Roe's scheme can be adopted.

For non-conservative form of Lax-Friedrichs scheme, it can be expressed as

$$U_i^{n+1} = U_i^n + \frac{1-a}{2}(\Delta U'_{i+\frac{1}{2}} - \Delta U'_{i-\frac{1}{2}}) - \frac{1}{2} \frac{\Delta t}{\Delta x} (H_{i+1}^n - H_{i-1}^n)$$

The conservative form of the Lax-Friedrichs scheme can be written as

$$U_i^{n+1} = U_i^n - \frac{\Delta t}{\Delta x} (H_{i+\frac{1}{2}}^* - H_{i-\frac{1}{2}}^*)$$

with integrated intercell numerical flux

$$H_{i+\frac{1}{2}}^* = \frac{1}{2}(H_i + H_{i+1}) - \frac{1-a}{2} \frac{\Delta t}{\Delta x} \Delta U'_{i+\frac{1}{2}}.$$

This scheme shows good results for smooth solutions, however, it can not solve transcritical flow correctly because the $\frac{1-a}{2} \frac{\Delta t}{\Delta x} \Delta A'$ term has a singular value at the transcritical point. The sign of $\Delta A'$ term is changed at transcritical point and Lax-Friedrichs scheme cannot capture this because it does not use eigenvalues but constant term $(1-a)(\Delta t/\Delta x)$ for flux splitting. This problem can be solved by smoothing solutions near the transcritical point. In this thesis, the method used by Burguete and Garcia-Navarro [16] to construct 'Optimised Lax-Friedrichs scheme' is adopted and it can be expressed by

$$\Delta A' = \text{mod min} \left(\Delta A, - \frac{\Delta \left(\frac{Q^2}{\lambda} \right) + g(\Omega_o + \Omega_f)_{i+\frac{1}{2}} - (\tilde{\lambda}_1 + \tilde{\lambda}_2) \Delta Q_{i+\frac{1}{2}}}{\tilde{\lambda}_1 \tilde{\lambda}_2} \right)$$

with the definition

$$\text{mod min}(a,b) = \begin{cases} 0 & \text{if } ab \leq 0 \\ a & \text{if } |a| < |b| \text{ and } ab > 0. \\ b & \text{if } |a| \geq |b| \text{ and } ab > 0 \end{cases}$$

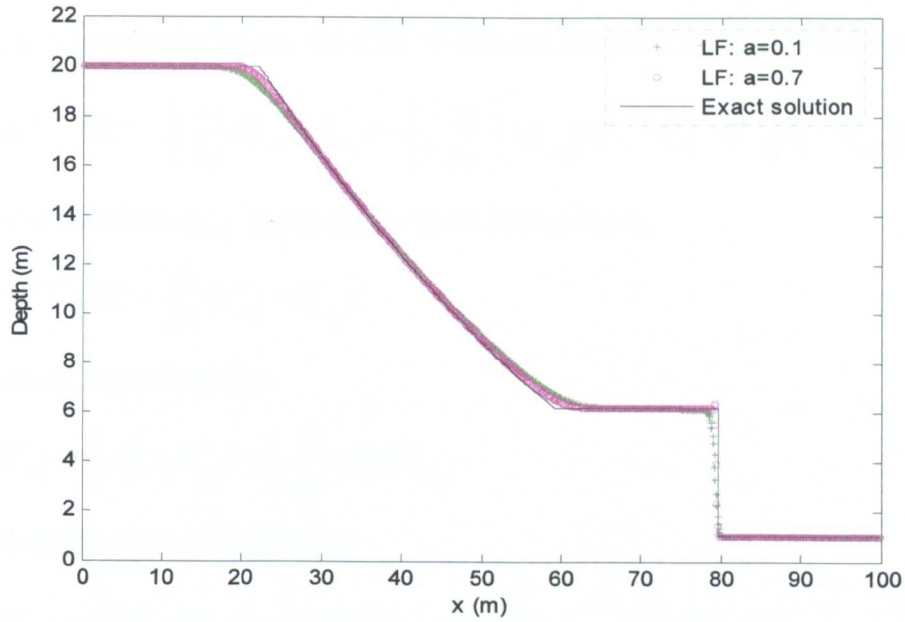


Figure 4.5 Ideal dam-break problem with Lax-Friedrichs (LF) scheme

4.3.4 Lax-Wendroff Scheme

Original Lax-Wendroff scheme

The Lax–Wendroff scheme is second-order accurate and was initially presented by Lax and Wendroff [59]. The scheme can be derived based on the Taylor series expansion:

$$\mathbf{U}_i^{n+1} = \mathbf{U}_i^n + \left(\frac{\partial \mathbf{U}}{\partial t} \right) \Delta t + \left(\frac{\partial^2 \mathbf{U}}{\partial t^2} \right) \frac{(\Delta t)^2}{2} + O(\Delta t)^3. \quad (4.22)$$

In case of a conservation law without source terms

$$\frac{\partial \mathbf{U}}{\partial t} = - \frac{\partial \mathbf{F}}{\partial x} \quad (4.23)$$

and

$$\frac{\partial^2 \mathbf{U}}{\partial t^2} = - \frac{\partial}{\partial t} \frac{\partial \mathbf{F}}{\partial x} = \frac{\partial}{\partial x} \left(- \mathbf{J} \frac{\partial \mathbf{U}}{\partial t} \right) = \frac{\partial}{\partial x} \left(\mathbf{J} \frac{\partial \mathbf{F}}{\partial x} \right). \quad (4.24)$$

By substituting (4.23) and (4.24) into (4.22),

$$\mathbf{U}_i^{n+1} = \mathbf{U}_i^n - \left(\frac{\partial \mathbf{F}}{\partial x} \right) \Delta t + \frac{\partial}{\partial x} \left(\mathbf{J} \frac{\partial \mathbf{F}}{\partial x} \right) \frac{(\Delta t)^2}{2} + O(\Delta t)^3.$$

Finally, by using a central difference approximation for the spatial derivatives and neglecting higher-order terms, the Lax–Wendroff scheme can be expressed as

$$\mathbf{U}_i^{n+1} = \mathbf{U}_i^n - \frac{1}{2} \frac{\Delta t}{\Delta x} (\mathbf{F}_{i+1} - \mathbf{F}_{i-1}) + \frac{1}{2} \left(\frac{\Delta t}{\Delta x} \right)^2 (\mathbf{J}_{i+\frac{1}{2}} [\mathbf{F}_{i+1} - \mathbf{F}_i] - \mathbf{J}_{i-\frac{1}{2}} [\mathbf{F}_i - \mathbf{F}_{i-1}]).$$

This can be rewritten as a conservative form and given by

$$\mathbf{U}_i^{n+1} = \mathbf{U}_i^n - \frac{\Delta t}{\Delta x} (\mathbf{F}_{i+\frac{1}{2}}^* - \mathbf{F}_{i-\frac{1}{2}}^*)$$

with intercell numerical flux

$$\mathbf{F}_{i+\frac{1}{2}}^* = \frac{1}{2} (\mathbf{F}_i + \mathbf{F}_{i+1}) - \frac{1}{2} \frac{\Delta t}{\Delta x} (\mathbf{J} \Delta \mathbf{F})_{i+\frac{1}{2}}. \quad (4.25)$$

Equation (4.20) can be rewritten as

$$\mathbf{F}_{i+\frac{1}{2}}^* = \frac{1}{2} (\mathbf{F}_i + \mathbf{F}_{i+1}) - \frac{1}{2} (\mathbf{J} \Delta \mathbf{U})_{i+\frac{1}{2}} + \frac{1}{2} \left(\mathbf{J} \left[1 - \frac{\Delta t}{\Delta x} |\mathbf{J}| \right] \Delta \mathbf{U} \right)_{i+\frac{1}{2}} \quad (4.26)$$

which can be considered as a first-order accurate scheme with a second-order correction term. The main defect of using Lax–Wendroff scheme is that it produces spurious oscillations near discontinuous solutions. This problem can be solved by limiting the second-order correction term in Equation (4.26), which causes numerical oscillations near discontinuities. By using the characteristic decomposition technique used for Roe’s scheme, the numerical flux function for TVD Lax–Wendroff scheme can be written as [51, 55]

$$\mathbf{F}_{i+\frac{1}{2}}^* = \frac{1}{2} (\mathbf{F}_i + \mathbf{F}_{i+1}) - \frac{1}{2} \sum_k (\tilde{\alpha}_k |\tilde{\lambda}_k| \tilde{\mathbf{e}}_k)_{i+\frac{1}{2}} + \frac{1}{2} \sum_k (\tilde{\alpha}_k \Phi_k |\tilde{\lambda}_k| [1 - \frac{\Delta t}{\Delta x} |\tilde{\lambda}_k|] \tilde{\mathbf{e}}_k)_{i+\frac{1}{2}}$$

where $\Phi_k = \Phi(r_k)$ is a nonlinear flux limiter function and the argument r_k represents the behaviour of the solution. The value of r_k is calculated from the ratio of wave strength $\tilde{\alpha}_k$ such as

$$r_k = \frac{\tilde{\alpha}_k^{upwind}}{\tilde{\alpha}_k^{local}}.$$

The numerical results for the dam-break problem with the Lax-Wendroff and TVD Lax-Wendroff schemes are shown in *Figure 4.6* and *4.7*. As shown in *Figure 4.6*, the entropy correction removes unphysical solutions near transcritical point, however, it still shows oscillatory behaviour near shock wave front. This oscillation is removed

by using TVD Lax-Wendroff scheme as shown in *Figure 4.7* and the results show good agreement with the exact solutions.

Homogeneous form of Lax-Wendroff scheme

The homogeneous form of Lax-Wendroff scheme can be constructed by replacing the flux term \mathbf{F} with the integrated flux term \mathbf{H} . The modification is simpler than first-order schemes because it does not include the ΔU term. The conservative form of Lax-Wendroff scheme can be rewritten as

$$\mathbf{U}_i^{n+1} = \mathbf{U}_i^n - \frac{\Delta t}{\Delta x} (\mathbf{H}_{i+\frac{1}{2}}^* - \mathbf{H}_{i-\frac{1}{2}}^*)$$

with integrated intercell numerical flux

$$\mathbf{H}_{i+\frac{1}{2}}^* = \frac{1}{2} (\mathbf{H}_i + \mathbf{H}_{i+1}) - \frac{1}{2} \frac{\Delta t}{\Delta x} (\mathbf{J}\Delta\mathbf{H})_{i+\frac{1}{2}}.$$

Similarly, the TVD version of the Lax-Wendroff numerical flux can be expressed as

$$\mathbf{H}_{i+\frac{1}{2}}^* = \frac{1}{2} (\mathbf{H}_i + \mathbf{H}_{i+1}) - \frac{1}{2} \sum_k (\tilde{\alpha}'_k |\tilde{\lambda}_k| \tilde{e}_k)_{i+\frac{1}{2}} + \frac{1}{2} \sum_k (\tilde{\alpha}'_k \Phi_k |\tilde{\lambda}_k| [1 - \frac{\Delta t}{\Delta x} |\tilde{\lambda}_k|] \tilde{e}_k)_{i+\frac{1}{2}}.$$

where $\tilde{\alpha}'_k$ is the same modified wavenumber used for homogeneous form of Roe's scheme in Section 4.3.1. The flux limiter function $\Phi_k = \Phi(r_k)$ should also be modified to deliver the effect of the source terms into the TVD correction term and the argument r_k is calculated by using the ratio of modified wave strength $\tilde{\alpha}'_k$ like

$$r_k = \frac{\tilde{\alpha}'_k^{upwind}}{\tilde{\alpha}'_k^{local}}.$$

It is important to use $\tilde{\alpha}'_k$, instead of $\tilde{\alpha}_k$, to calculate the value of r_k because $\tilde{\alpha}'_k$ represents the real behaviour of the solutions including the effects of channel geometry and the using of $\tilde{\alpha}_k$ does not guarantee oscillation-free second-order solutions. A similar expression was mentioned by Burguete and Garcia-Navarro [15].

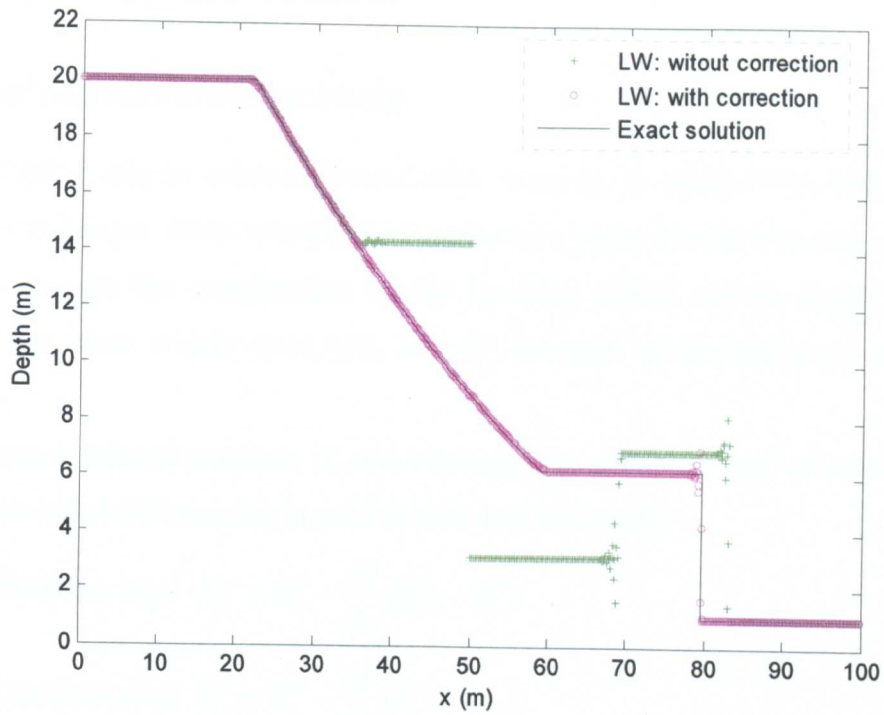


Figure 4.6 Ideal dam-break problem with Lax-Wendroff (LW) scheme

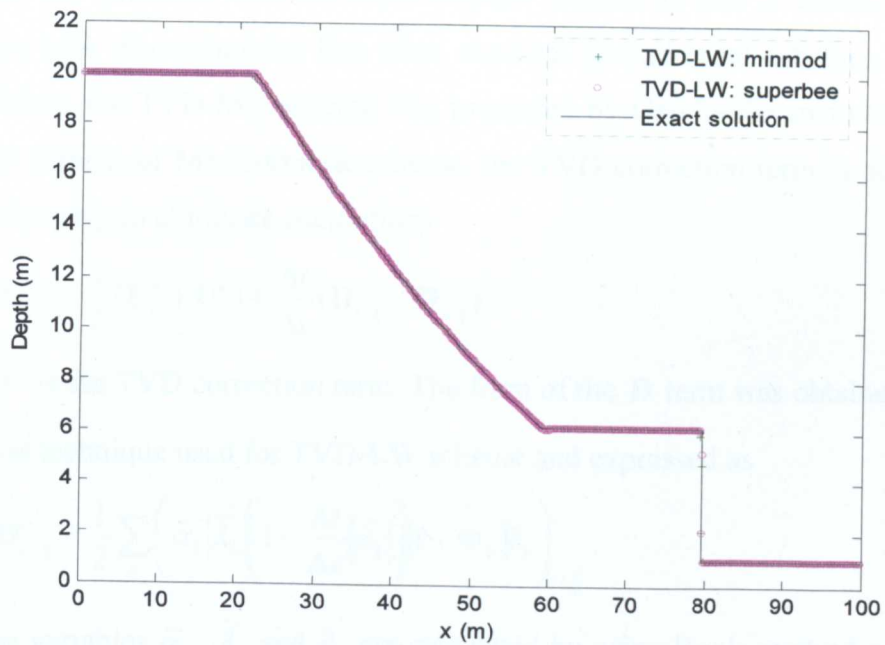


Figure 4.7 Ideal dam-break problem with TVD Lax-Wendroff (TVD-LW) scheme

4.3.5 MacCormack Scheme

Original MacCormack scheme

An alternative way to achieve second-order accuracy is using a two-step predictor–corrector technique. MacCormack [64] presented a second-order two-step method that does not require the computation of the Jacobian matrix and its eigenvalues. The scheme has been widely used [38, 39, 41] because of its efficiency and simple structure.

MacCormack scheme consists of two substeps: i.e. predictor and corrector steps, in which one-sided differencing is used in alternate directions:

$$\text{Predictor step: } \mathbf{U}_i^p = \mathbf{U}_i^n - \frac{\Delta t}{\Delta x} (\mathbf{F}_{i+1}^n - \mathbf{F}_i^n)$$

$$\text{Corrector step: } \mathbf{U}_i^c = \mathbf{U}_i^p - \frac{\Delta t}{\Delta x} (\mathbf{F}_i^p - \mathbf{F}_{i-1}^p).$$

Finally, the updated solution is given by

$$\mathbf{U}_i^{n+1} = \frac{1}{2} (\mathbf{U}_i^n + \mathbf{U}_i^c).$$

However, the problem with the MacCormack scheme is that it shows oscillatory behaviour near discontinuities like other classical second-order schemes. To rectify this problem, the TVD-MC scheme was presented by Garcia-Navarro *et al.* [22]. In the TVD version of MacCormack scheme, the TVD correction term is added to the final update step to eliminate oscillations

$$\mathbf{U}_i^{n+1} = \frac{1}{2} (\mathbf{U}_i^n + \mathbf{U}_i^c) + \frac{\Delta t}{\Delta x} (\mathbf{D}_{i+\frac{1}{2}}^n - \mathbf{D}_{i-\frac{1}{2}}^n)$$

where \mathbf{D}^n is the TVD correction term. The form of the \mathbf{D} term was obtained by using the similar technique used for TVD-LW scheme and expressed as

$$\mathbf{D}_{i+\frac{1}{2}}^n = \frac{1}{2} \sum_k \left(\tilde{\alpha}_k |\tilde{\lambda}_k| \left[1 - \frac{\Delta t}{\Delta x} |\tilde{\lambda}_k| \right] [1 - \Phi_k] \tilde{\epsilon}_k \right)_{i+\frac{1}{2}}$$

where the variables $\tilde{\alpha}_k$, $\tilde{\lambda}_k$ and $\tilde{\epsilon}_k$ are calculated by using Roe's method and Φ_k is a flux limiter function.

The numerical results of the dam-break problem with MacCormack and TVD MacCormack schemes are presented in *Figure 4.8*. As shown in the figure, the oscillatory solutions of MacCormack scheme is removed by using TVD MacCormack scheme and shows almost similar results to the TVD Lax-Wendroff scheme.

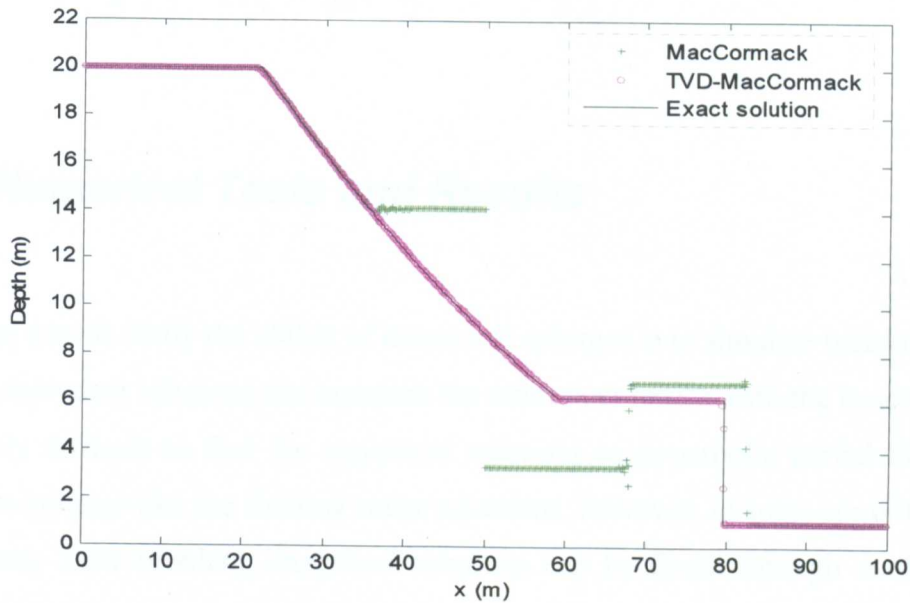


Figure 4.8 Ideal dam-break problem with MacCormack and TVD MacCormack scheme

Homogeneous form of MacCormack scheme

The homogeneous form of the MacCormack scheme can be easily obtained by replacing the flux term \mathbf{F} with the integrated flux term \mathbf{H} in each step:

$$\text{Predictor step: } \mathbf{U}_i^p = \mathbf{U}_i^n - \frac{\Delta t}{\Delta x} (\mathbf{H}_{i+1}^n - \mathbf{H}_i^n)$$

$$\text{Corrector step: } \mathbf{U}_i^c = \mathbf{U}_i^p - \frac{\Delta t}{\Delta x} (\mathbf{H}_i^p - \mathbf{H}_{i-1}^p).$$

Then, the updated solution is given by

$$\mathbf{U}_i^{n+1} = \frac{1}{2} (\mathbf{U}_i^n + \mathbf{U}_i^c).$$

By using the integrated flux term \mathbf{H} , the contribution of the source terms is automatically evaluated in a different direction at each step and no special treatment is

needed. In the case of the TVD-MC scheme, the TVD correction term should be modified to calculate the effect of the source terms correctly. This can be done by using the same expressions of $\tilde{\alpha}'$ and Φ_k used for TVD-LW scheme and the TVD correction term is expressed as

$$\mathbf{D}_{i+\frac{1}{2}}^n = \frac{1}{2} \sum_k \left(\tilde{\alpha}'_k |\tilde{\lambda}_k| \left[1 - \frac{\Delta t}{\Delta x} |\tilde{\lambda}_k| \right] [1 - \Phi_k] \tilde{e}_k \right)_{i+\frac{1}{2}}.$$

4.4 Numerical Tests and Results

The best way to verify the ability of numerical schemes is to simulate benchmark tests having analytical solutions and compare the numerical results with the exact solutions. It is very difficult to find the analytical solutions to hyperbolic partial differential equation systems like the shallow water equations, however, in some simplified cases like steady flow problem, analytical solutions can be found through mathematical manipulations.

In this section, the proposed homogeneous form of conservative numerical schemes is applied to several benchmark tests that are taken from the available literature. All the test problems are simulated with a rectangular or trapezoidal channel as shown in *Figure 4.9*. The side slope of the trapezoidal channel is defined as $1:m$ and, in case of rectangular channel, m is set to zero. To ensure numerical stability $CFL = 0.9$ is used and the minmod flux limiter function that is given by $\Phi(r) = \max[0, \min(1, r)]$ is used for TVD schemes. The convergence criterion for steady problems is defined as $R < 1 \times 10^{-6}$, where R is the relative error defined by

$$R = \sqrt{\sum_i \left(\frac{h_i^n - h_i^{n-1}}{h_i^n} \right)^2}.$$

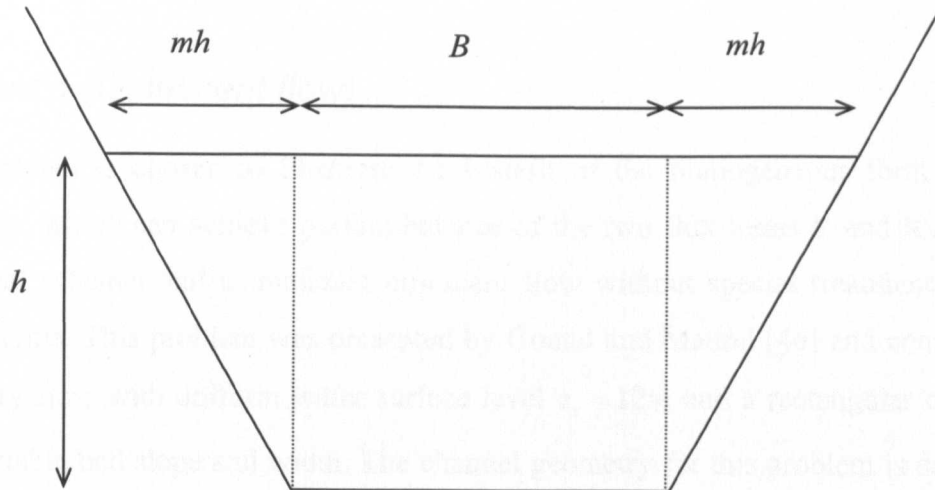


Figure 4.9 Cross section used for test problems

The boundary conditions are described by using a ghost-cell approach in which the conditions are implemented by creating dummy cells at the end of the reach. For example, the values for the dummy cells to describe transmissive downstream boundary are defined as

$$A_{N+1} = A_N, \quad Q_{N+1} = Q_N$$

and

$$A_{N+2} = A_{N-1}, \quad Q_{N+2} = Q_{N-1}$$

4.4.1 Test Problems

Problem 1 (Quiescent flow)

This problem is chosen to illustrate the benefit of the homogeneous form of the equations, which can achieve perfect balance of the two flux terms F and R . Many numerical schemes fail to maintain quiescent flow without special treatment of the source terms. This problem was presented by Goutal and Maurel [46] and consists of stationary flow with uniform water surface level $z_s = 12m$ and a rectangular channel with variable bed slope and width. The channel geometry for this problem is depicted in *Figure 4.10*. The length of the channel is $1,500m$ and 600 uniform cells ($\Delta x = 2.5m$) are used.

Problem 2 (Tidal wave flow over an irregular bed)

To verify the ability to solve flow over an irregular bed, the proposed schemes are applied to a test case initially presented by Goutal and Maurel [46]. The same geometry (bed level and base width) as in *Problem 1* is used. The initial conditions are the same as the previous problem

$$Q(x,0) = 0m^3 / s ,$$

$$h(x,0) + z_b = 12m$$

and the boundary conditions are

$$h(0,t) = h(0,0) + \phi(t) ,$$

$$Q(L,t) = 0m^3 / s$$

where $\phi(t)$ is the time-dependent tidal flow entering the boundary $x=0$ and given by

$$\phi(t) = 4 + 4 \sin\left(\pi\left(\frac{4t}{86400} + \frac{1}{2}\right)\right)$$

which represents a slow wave with long period $T = 43,200s$. The friction term is included by setting Manning's roughness coefficient $n = 0.1$. The analytical solutions were presented by Bermudez and Vazquez [9] and are obtained by the first-order approximation of the mass conservation equation:

$$h(x, t) = h(x, 0) + \phi(t),$$

$$Q(x, t) = \phi'(t) \int_x^L (B(s) + 2mh) ds.$$

The numerical simulations were performed with both a rectangular ($m = 0$) and a trapezoidal channel ($m = 1$) using 200 uniform cells with $\Delta x = 7.5m$. It should be noted that the analytical solutions are only asymptotically exact as the speed of flow tends to zero.

Problem 3 (Steady flow over an irregular bed with friction)

MacDonald [65] presented an analytical solutions for steady open channel flow problems including a friction force term by calculating the bed slope S_o corresponding to a hypothetical water depth \hat{h} . In [65], the bed slope function $S_o(x)$ was obtained from the steady flow equation and given by

$$S_o = \left(1 - \frac{Q^2 T}{gA^3}\right) \hat{h}'(x) + \frac{Q^2 n^2 P^{4/3}}{A^{10/3}}$$

where $T = B + 2m\hat{h}(x)$ is the top width of the wetted cross section, $P = B + 2\hat{h}(x)\sqrt{1+m^2}$ is the wetted perimeter and Q represents constant discharge. A set of test cases that consist of steady flows over rectangular or trapezoidal rough channel were presented in [65] and, among them, two problems with prismatic channels were chosen to verify the ability of the proposed numerical schemes. In *Problem 3-1*, a subcritical and smooth water depth profile is used in a rectangular channel, while a transcritical flow consisting of four hydraulic jumps is simulated in *Problem 3-2*. The bed and free surface profiles for both problems are depicted in *Figure 4.11* and *4.12*.

Problem 4 (Steady flow over a hump in a non-prismatic channel)

A steady flow in a 3m-long rectangular non-prismatic channel with a hump is simulated with the proposed schemes. This test case was presented by Hubbard and Garcia-Navarro [51] and the channel geometry is given by

$$z_b(x) = \begin{cases} 0.1 \cos^2(\pi(x-1.5)) & 1.0 \leq x \leq 2.0 \\ 0.0 & \text{otherwise} \end{cases}$$

$$b(x) = \begin{cases} 1.0 - 0.1 \cos^2(\pi(x-1.5)) & 1.0 \leq x \leq 2.0 \\ 1.0 & \text{otherwise} \end{cases}$$

and shown in *Figure 4.13*. A uniform 150 cell grid with $\Delta x = 0.02m$ is used for the two flows, each defined by a local Froude No. Fr : subcritical ($Fr = 0.5$) flow and transcritical ($Fr = 0.6$) flow. The downstream boundary condition is $h_{dn} = 1m$.

Problem 5 (Wave propagation)

The test problem presented by LeVeque [62] is chosen to demonstrate the ability of the proposed schemes to solve wave propagation problems over variable geometry. A 1m-long rectangular channel with variable bed elevation, which is given by

$$z_b(x) = \begin{cases} 0.25 \cos(\pi(x-0.5)/0.1) + 1.0 & 0.4 \leq x \leq 0.6 \\ 0.0 & \text{otherwise} \end{cases}$$

is used and the initial condition is stationary flow ($Q = 0$) with the following water surface profile:

$$z_s(x) = \begin{cases} 1.0 + \varepsilon & 0.1 \leq x \leq 0.2 \\ 0.0 & \text{otherwise} \end{cases}$$

where ε is a small perturbation. According to [62], the reduced gravitational acceleration $g = 1m^2/s$ and perturbation depth $\varepsilon = 0.01$ are used. The initial perturbation of water depth causes two waves, right- and left-going, which propagates at the speed $\pm \sqrt{gh}$, respectively. The right-going wave propagates over the hump located at the middle area of the channel, whereas the left-going wave leaves the domain through the boundary $x = 0$. The numerical results are obtained at $t = 0.7s$ on a uniform grid with 500 cells.

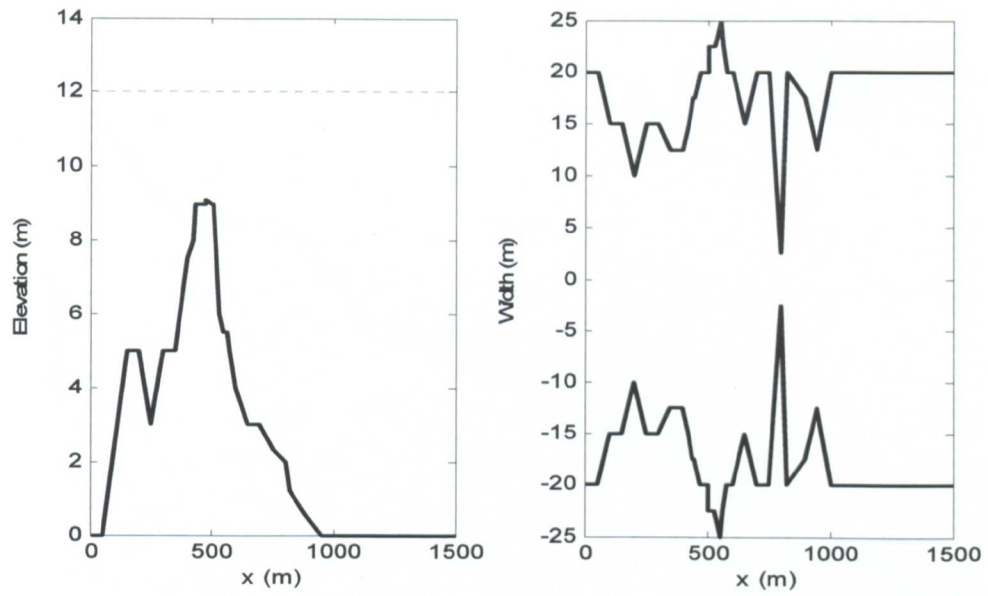


Figure 4.10 Bed elevation and width variation for Problems 1 and 2

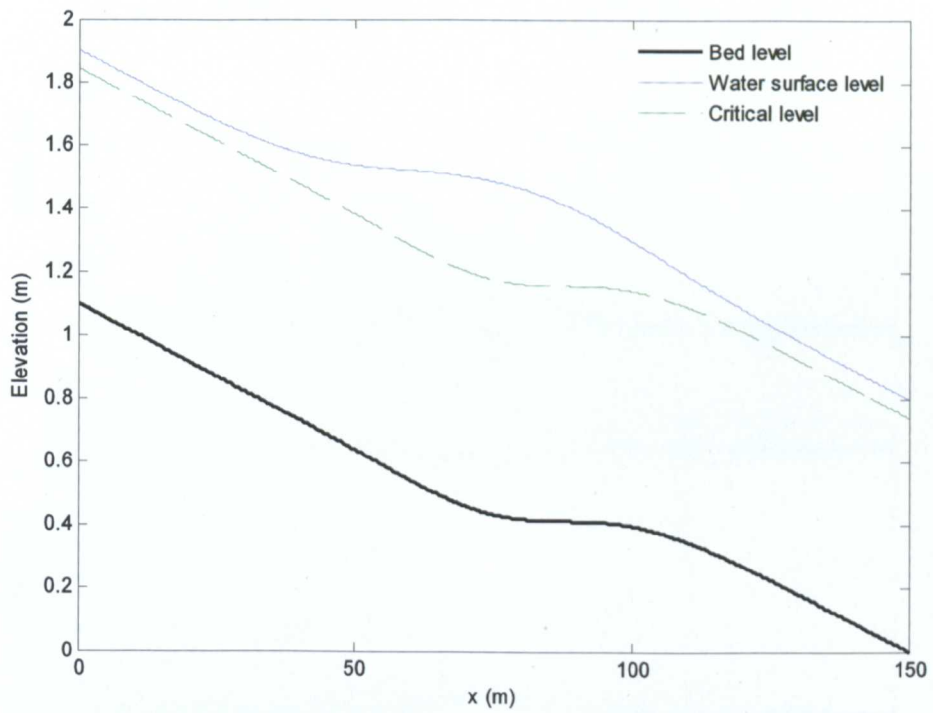


Figure 4.11 Water surface and bed elevation for Problem 3-1

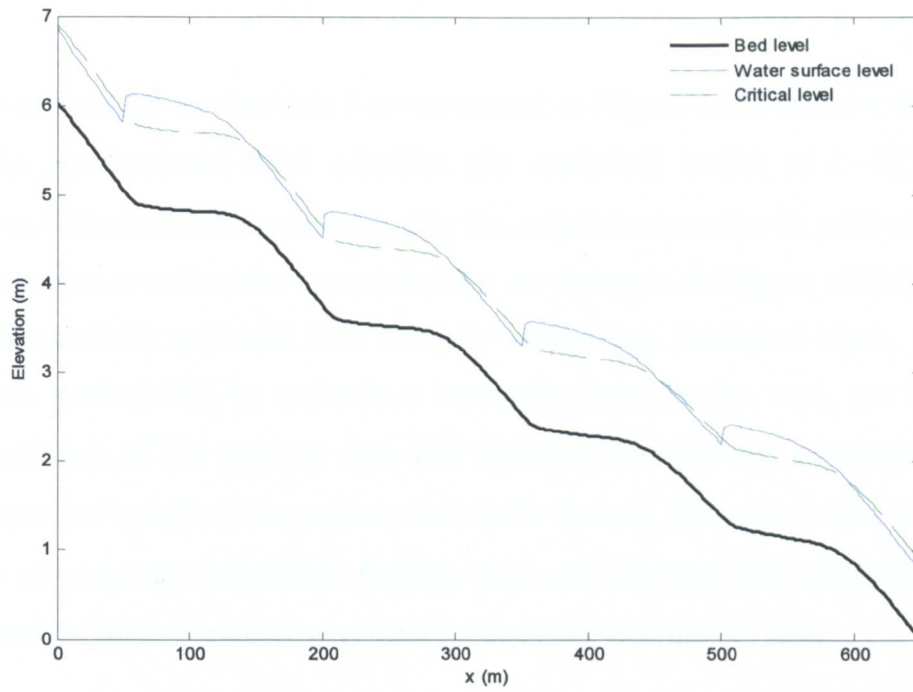


Figure 4.12 Water surface and bed elevation for Problem 3-2

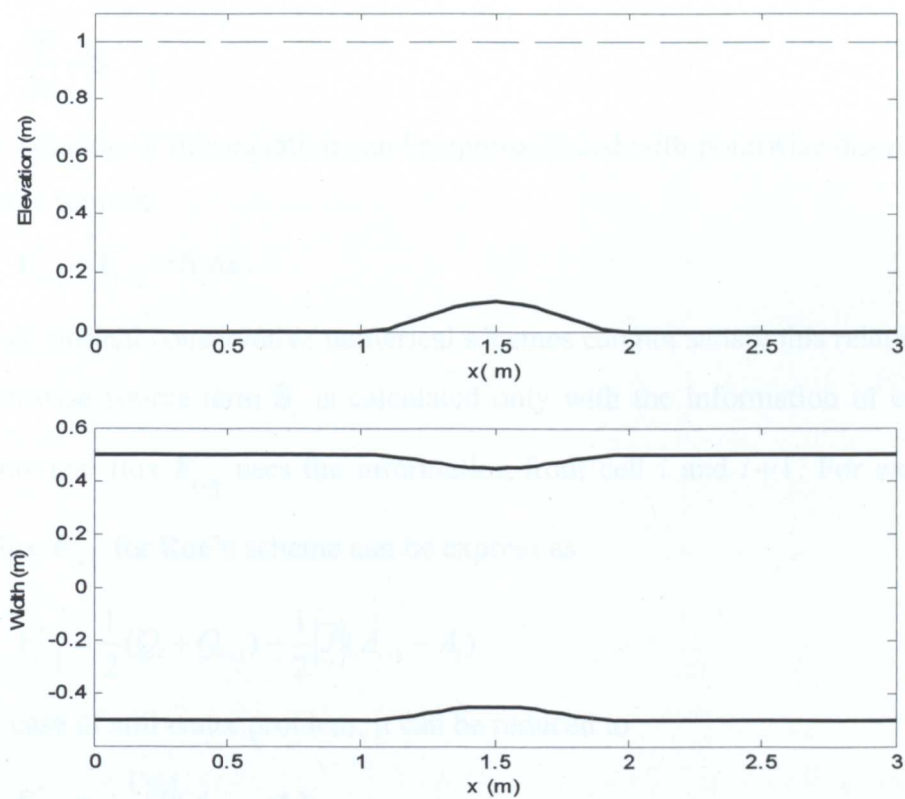


Figure 4.13 Bed level and width variation for Problem 4

4.4.2 Results and Discussion

Numerical solutions to *Problem 1* are presented in *Figure 4.14*. To show the benefit of using homogeneous form schemes, the numerical results at $t=10,000s$ are compared with the solutions calculated by the original schemes with pointwise source term treatment as well as the exact solutions. As shown in the figure, all the proposed schemes reproduce quiescent flow correctly without any numerical errors, while the pointwise method fails to maintain a stationary state. In this case, the integrated numerical flux \mathbf{H}^* is zero at each cell interface because the modified variable differences $\Delta A' = \Delta Q' = 0$ throughout the whole domain. This shows that there is no transfer of mass and momentum through each cell interface and, consequently, the homogeneous form of numerical schemes can ensure a stationary state.

To study how the homogeneous form conservative schemes work for steady state flow problems, the comparison with the original scheme with pointwise source term treatment is considered. In case of steady problem, the original shallow water equations can be reduced to

$$\frac{\partial \mathbf{F}}{\partial x} = \mathbf{S}$$

and the solution of this equation can be approximated with pointwise discretization of the source term as

$$\mathbf{F}_{i+\frac{1}{2}}^* - \mathbf{F}_{i-\frac{1}{2}}^* = \mathbf{S}_i \Delta x.$$

However, normal conservative numerical schemes can not satisfy this relation because the pointwise source term \mathbf{S}_i is calculated only with the information of cell i while the numerical flux $\mathbf{F}_{i+\frac{1}{2}}^*$ uses the information from cell i and $i+1$. For example, the mass flux $\mathbf{F}_{i+\frac{1}{2}}^*$ for Roe's scheme can be express as

$$\mathbf{F}_{i+\frac{1}{2}}^* = \frac{1}{2}(Q_i + Q_{i+1}) - \frac{1}{2}|\tilde{\mathcal{J}}|(A_{i+1} - A_i)$$

and, in case of still water problem, it can be reduced to

$$\mathbf{F}_{i+\frac{1}{2}}^* = -\frac{1}{2}|\tilde{\mathcal{J}}|(A_{i+1} - A_i),$$

which has non-zero value except for the case $A_{i+1} = A_i$ while the source term for mass equations is zero. This discrepancy leads to numerical errors and makes it difficult to find correct solutions to steady state problems. However, in case of the homogeneous form shallow water equations, the solution of steady state problem can be given as

$$\frac{\partial \mathbf{H}}{\partial x} = 0$$

and

$$\mathbf{H}_{i+\frac{1}{2}}^* - \mathbf{H}_{i-\frac{1}{2}}^* = 0,$$

which represents that the influx and the outflux of the mass and momentum are the same, i.e. the net increase (or, decrease) of the mass and momentum stored in a control volume is zero. The source terms are included in the integrated numerical flux \mathbf{H}^* and evaluated by the same information used for the calculation of flux terms. For example, the mass flux $\mathbf{H}_{i+\frac{1}{2}}^*$ for the homogeneous form of Roe's scheme can be express as

$$\mathbf{H}_{i+\frac{1}{2}}^* = \frac{1}{2}(Q_i + Q_{i+1}) - \frac{1}{2}|\tilde{J}|\Delta A'$$

and, in case of still water problem

$$\mathbf{H}_{i+\frac{1}{2}}^* = 0 \text{ with } \Delta A' = 0.$$

This means that there is no transfer of mass through each cell interface and it perfectly represents the real physical condition of stationary flow.

Numerical solutions to *Problem 2* are presented in *Figure 4.15* (rectangular channel) and *4.16* (trapezoidal channel). The velocity profiles at $t = 10,800s$ corresponding to a half-risen tide with maximum positive velocity are compared with exact solutions. As shown in the figures, all the proposed schemes calculate the effect of the extreme irregularity of the channel geometry correctly and show good agreement with the analytical solutions for both rectangular and trapezoidal channels. Especially, the TVD second-order schemes do not show numerical errors due to the imbalance of high-order numerical flux and source terms. This is because the high-order correction terms using the modified wave strength $\tilde{\alpha}'$ can deliver the effect of geometry and friction force to the high-order term and also because the numerical schemes

automatically calculate the high-order source flux that is well balanced with the flux term F .

The numerical solutions to *Problem 3* are presented in *Figure 4.17-18*. The numerical water depth and discharge profiles are compared with the hypothetical depth \hat{h} and steady discharge Q . The numerical solutions to *Problems 3-1* are presented in *Figure 4.17*. As shown in the figures, all the proposed schemes produce very accurate solutions to this subcritical flow problem. The numerical solutions to *Problems 3-2* are presented in *Figure 4.18*. This problem is a very severe test case including multiple hydraulic jumps and transcritical points. While the Lax-Friedrichs scheme produces diffusive results near the hydraulic jumps correctly, all other schemes predicted the position and magnitude of the hydraulic jumps, except small discrepancies at the discharge profiles at the shock positions (which is a common numerical behaviour for most conservative schemes). The convergence histories for both cases are shown in *Figure 4.19 and 4.20* and it shows that the TVD-MC scheme that is two-step predictor-corrector method converges to steady state faster than the other schemes. Generally, the two-step approach shows faster convergence than normal methods, while the former has a more complicated structure. It is clear that there is a tradeoff between accuracy and complexity.

The numerical results for *Problem 4* are presented in *Figure 4.21-22*. Similar to the results of previous problems, all the proposed schemes predicted the water depth and discharge profiles correctly in the subcritical flow case. In case of transcritical flow problem, the proposed schemes reproduce the position and strength of the hydraulic jump very correctly. The convergence histories for this problems are shown in *Figure 4.23 and 4.24*. Similar to *Problems 3-1* and *3-2*, the TVD-MC scheme converges to steady state faster than other schemes.

The numerical solutions for *Problem 5* are presented in *Figure 4.25*. Owing to the absence of analytical solutions, the computed solutions are compared with the reference solution obtained with TVD-LW scheme on a finer grid (2500 cell). As shown in the figure, the proposed schemes reproduce wave propagation of very small

perturbation without any noticeable distortions or oscillations and the two TVD second-order schemes show more accurate solutions than the first-order schemes. In this case, a series of runs has been carried out to indicate the accuracy of the presented schemes. The l_2 errors are plotted against the corresponding cell numbers and shown in *Figure 4.26*. According to the numerical results, the second-order accurate schemes produce more accurate solutions and show higher sensitivity to the variation of the grid size. To show the ability and accuracy of the proposed method, The root mean square errors of water surface levels in *Problem 2* are calculated and summarized in *Table 4.1*. As presented in the table, the proposed method, i.e. homogeneous form scheme, produces accurate solutions while the pointwise method shows much bigger numerical errors. Similar analysis has been performed on the *Problem 3-1* and *5* which are a steady flow problem and a flood wave propagation problem respectively. The root mean square errors are presented in *Table 4,2*. According to the table, the two second-order accurate schemes produce smaller numerical errors than the other schemes for the transient problem(*Problem 5*), while no significant difference is presented for the steady flow problem(*Problem 3-1*).

	Homogeneous	Pointwise
Roe	4.840×10^{-4}	8.327×10^{-1}
HLL	4.740×10^{-4}	5.241×10^{-1}
LF	4.250×10^{-4}	8.294×10^{-1}
TVD-LW	4.990×10^{-4}	8.313×10^{-1}
TVD-MC	5.210×10^{-4}	7.141×10^{-1}

Table 4.1 The root mean square errors of water surface level at $t = 10,800s$ with rectangular channel in Problem 2

	<i>Problem 3-1</i>	<i>Problem 5</i>
Roe	2.131×10^{-2}	5.505×10^{-4}
HLL	2.172×10^{-2}	5.505×10^{-4}
LF	1.957×10^{-2}	7.621×10^{-4}
TVD-LW	2.131×10^{-2}	1.743×10^{-4}
TVD-MC	2.128×10^{-2}	1.732×10^{-4}

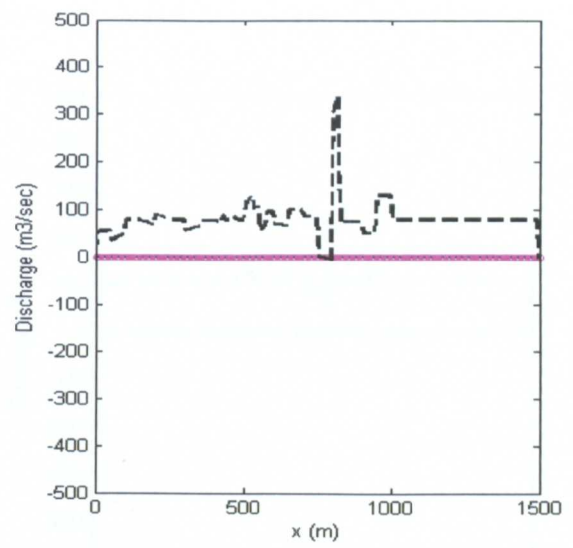
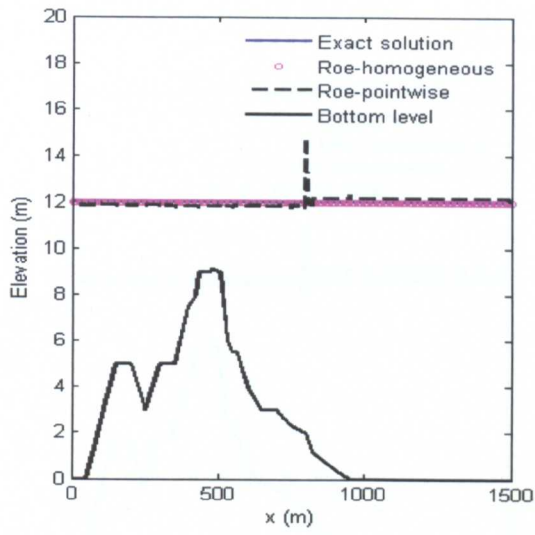
Table 4.2 The root mean square errors of water surface level in Problem 3-1 and 5

4.5 Conclusion

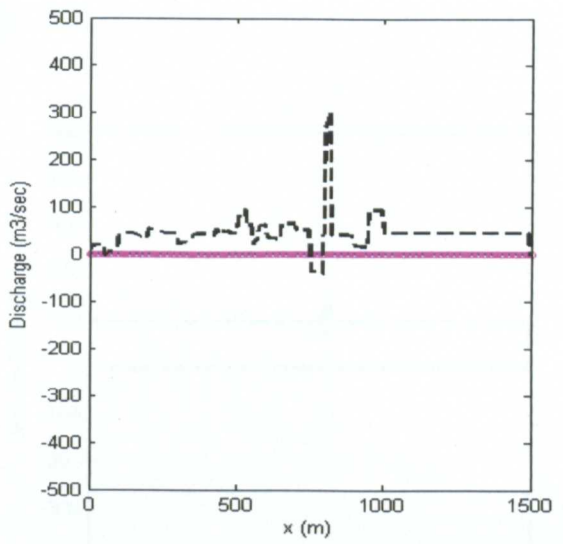
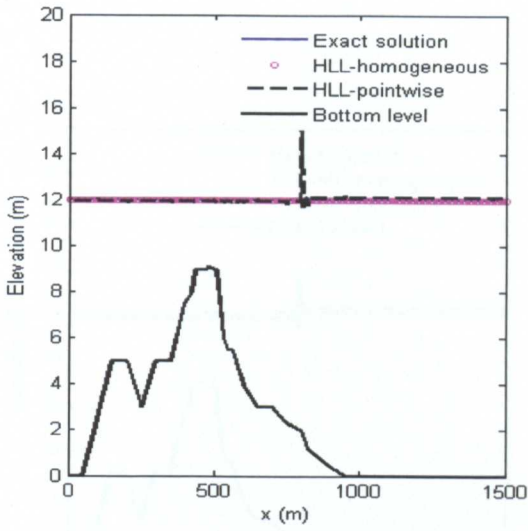
A simple and accurate method to solve open channel flow over irregular geometry has been presented. The modification of the shallow water equations to the homogeneous form enables one to use numerical methods developed for homogeneous conservations laws and avoid a cumbersome fractional step method for source term treatment. An integrated numerical flux, which includes the representation of the source terms, has been obtained by straightforward modification of the governing equations. The well-known conservative numerical schemes have then been amended to solve these newly proposed equations. The numerical results show that the proposed schemes are highly conservative and accurate while having simple forms. The proposed schemes produce excellent agreement with the analytical solutions.

The proposed method has several advantages. First, it can solve steady flows over highly nonprismatic channels without numerical errors, thus demonstrating that the proposed schemes achieve perfect numerical balance of the two flux terms **F** and **R**. Second, it can compute the numerical flux corresponding to the real state of water

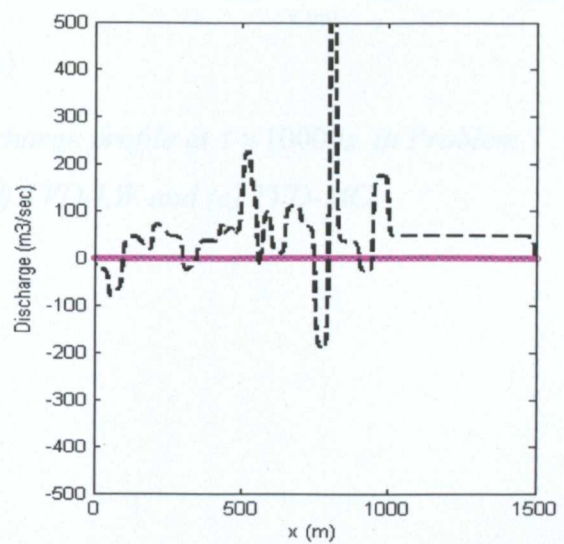
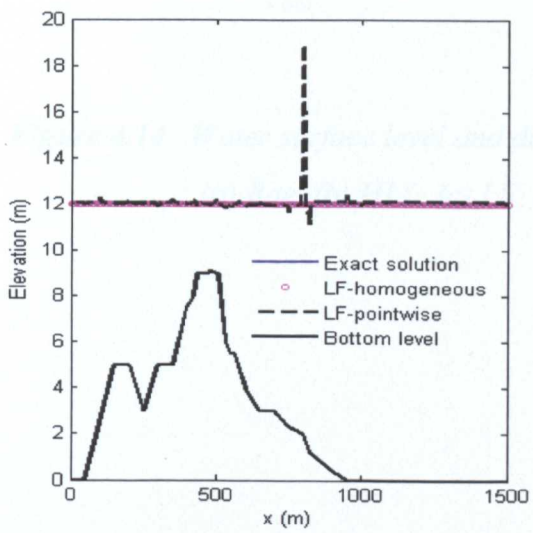
flow and give straightforward results. For example, in the still water simulation problem, the integrated numerical flux \mathbf{H}^* is equal to zero at every cell interface, which represents no transfer of mass and momentum. Third, high-order accuracy can be obtained easily and no special treatment is needed to maintain a numerical balance, because it is performed automatically in the integrated numerical flux function. Finally, the proposed approach has strong applicability to various conservative numerical schemes as shown in the numerical results. Moreover, it can be easily expanded for higher-dimensional problems. In the next chapter, the application of this approach to two-dimensional cases is presented.



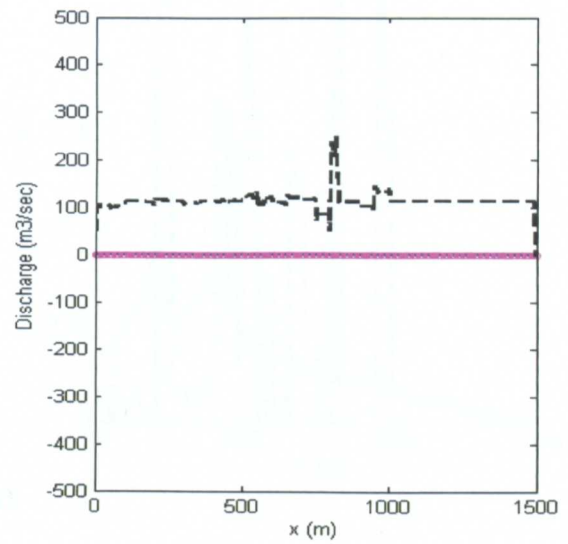
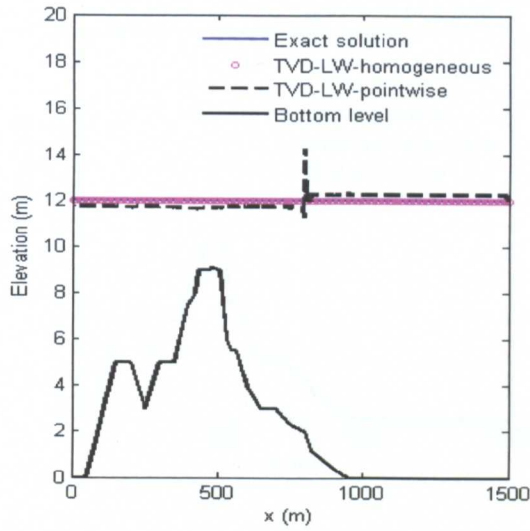
(a)



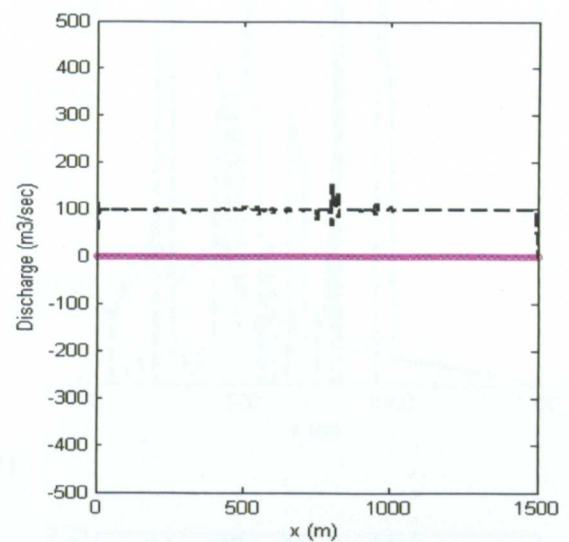
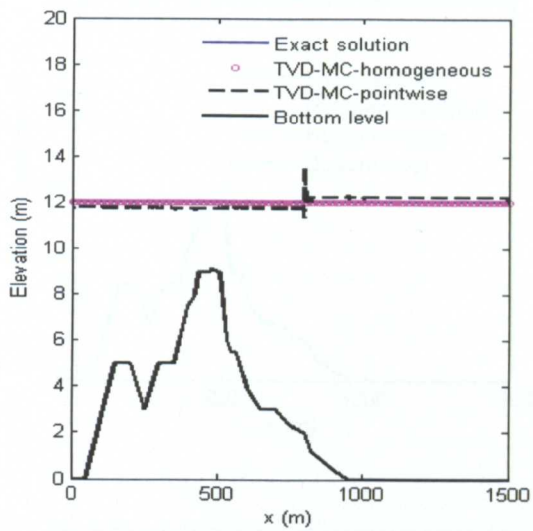
(b)



(c)

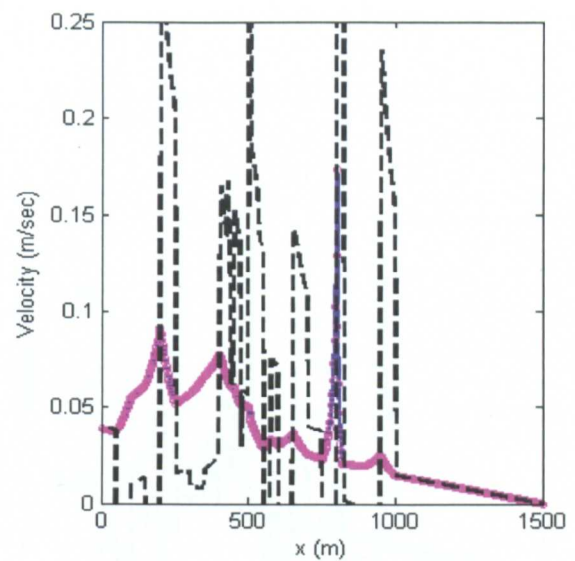
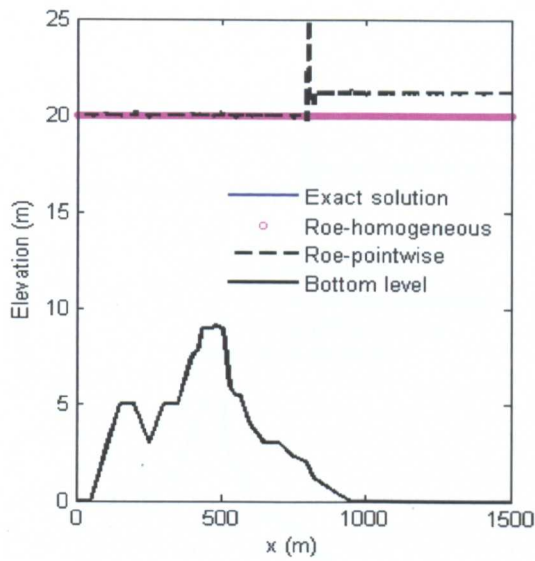


(d)

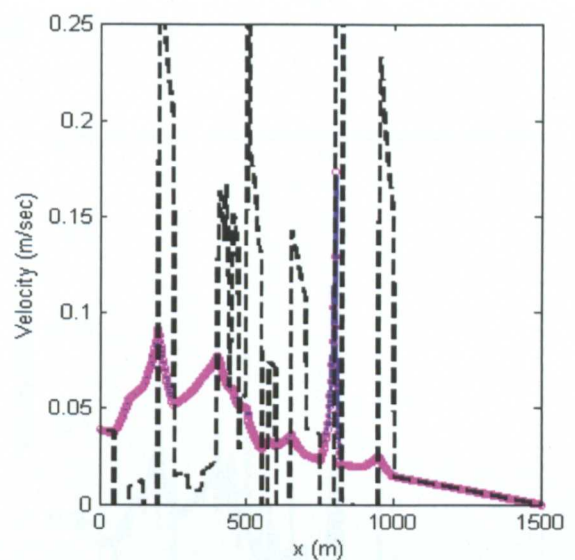
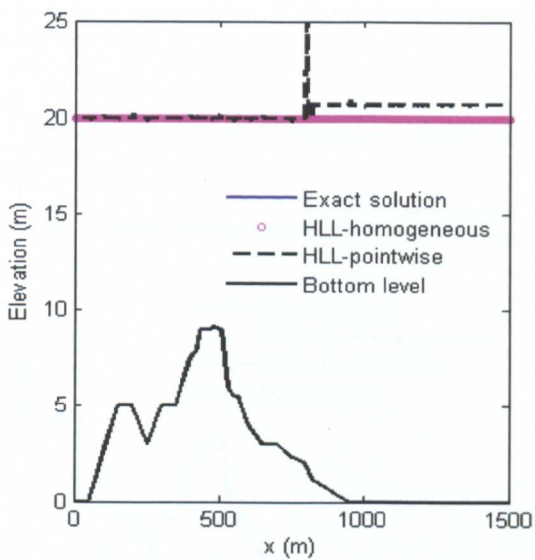


(e)

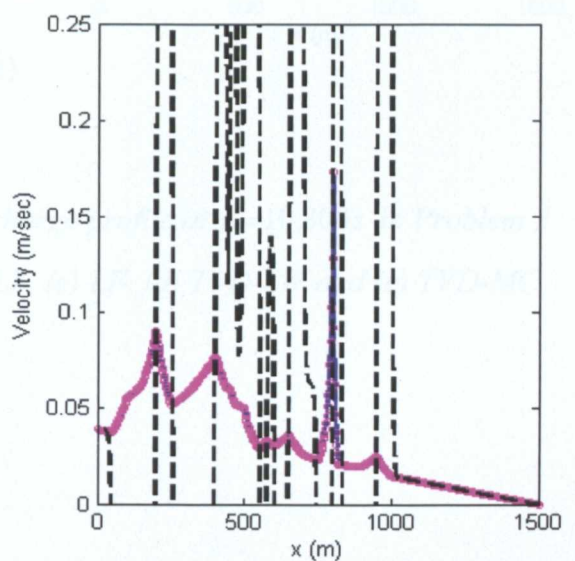
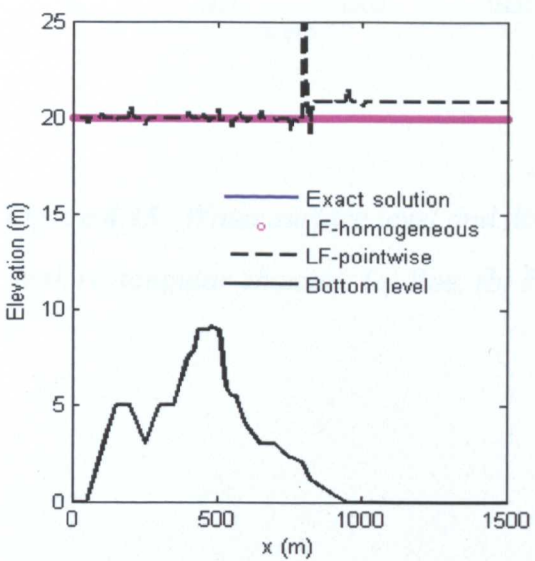
Figure 4.14 Water surface level and discharge profile at $t = 10000s$ in Problem 1 : (a) Roe, (b) HLL, (c) LF, (d) TVD-LW and (e) TVD-MC



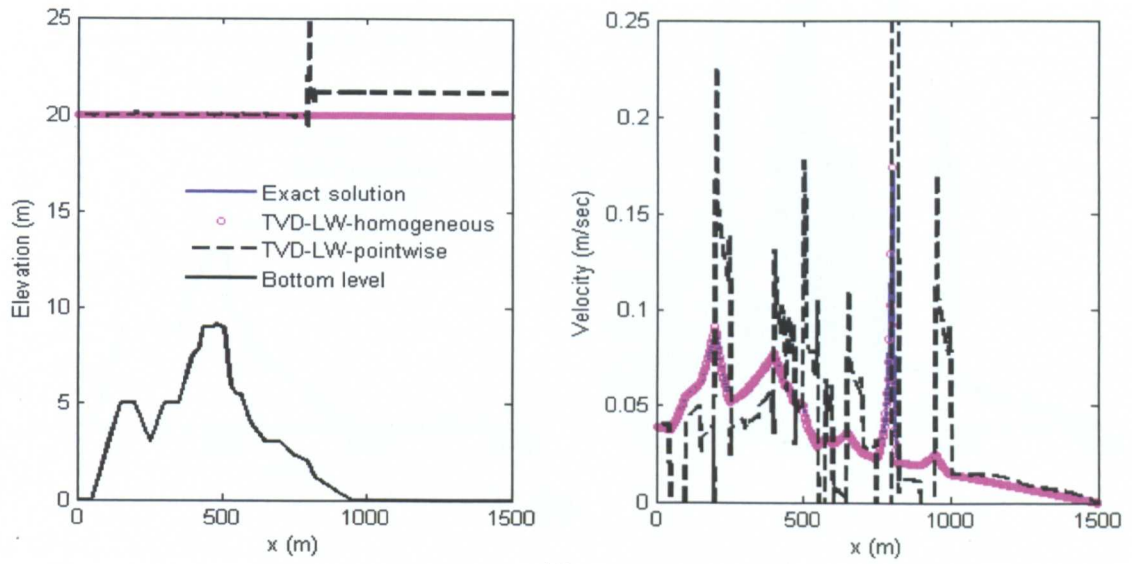
(a)



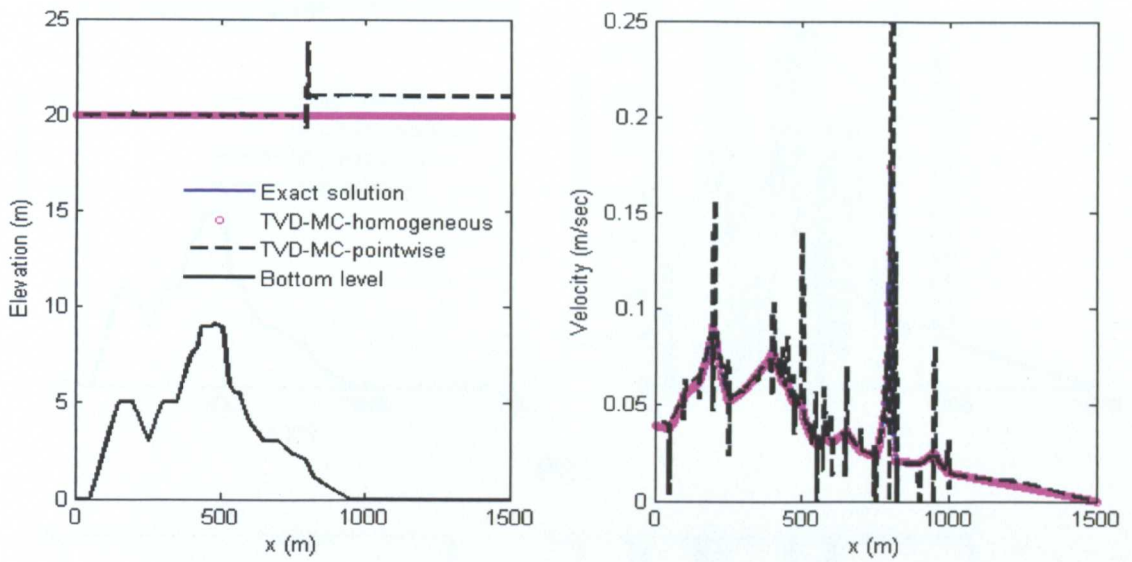
(b)



(c)

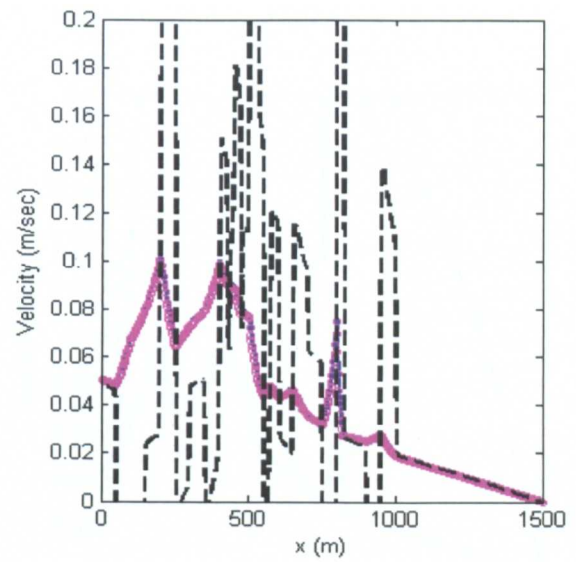
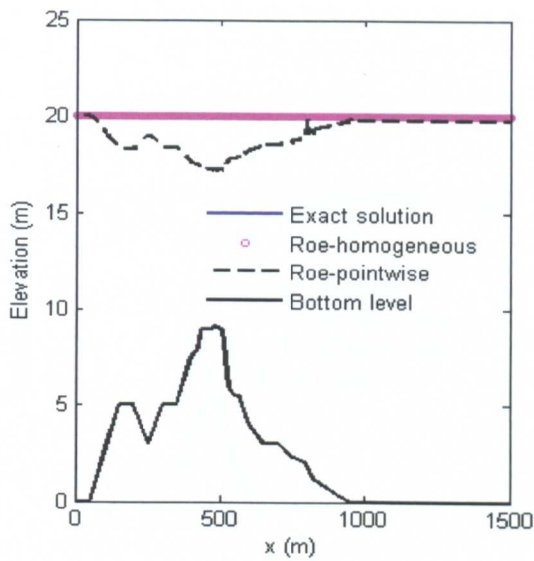


(d)

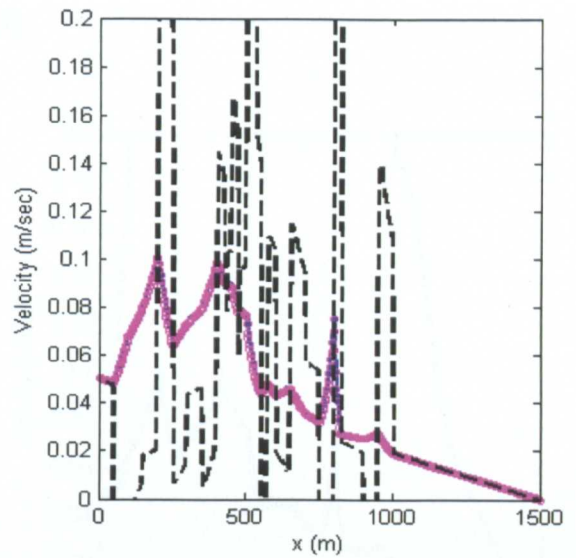
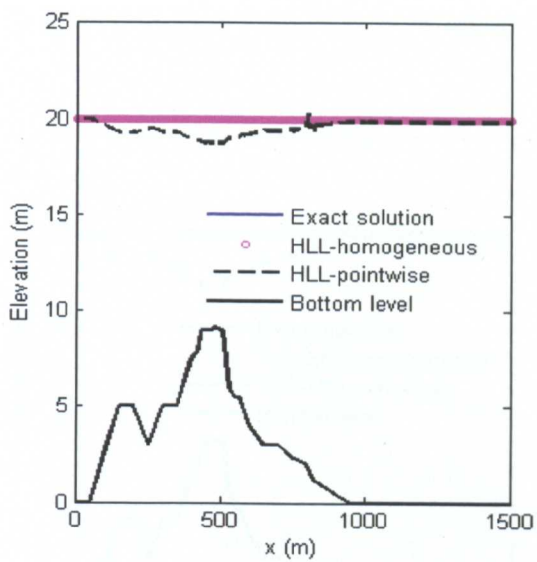


(e)

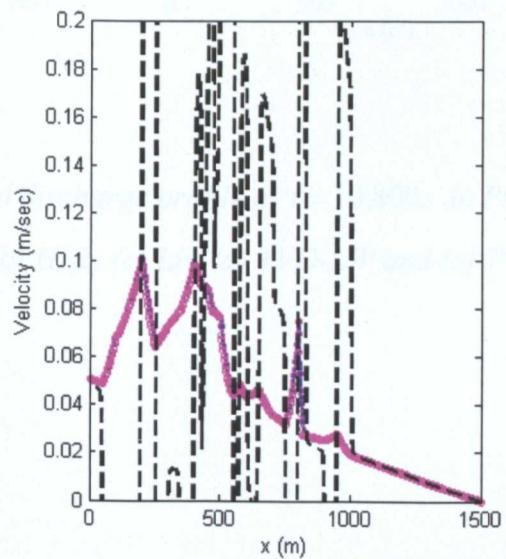
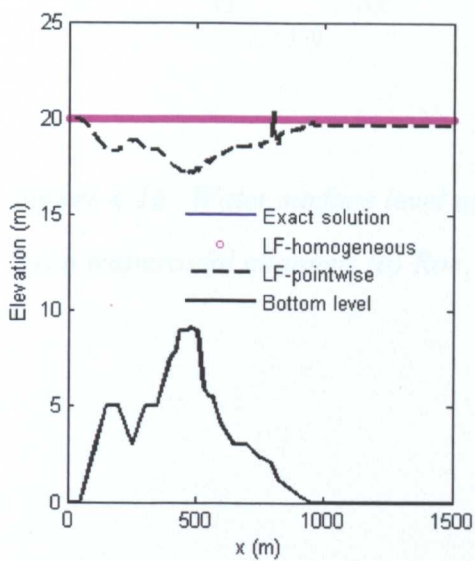
Figure 4.15 Water surface level and discharge profile at $t = 10,800s$ in Problem 2 with rectangular channel: (a) Roe, (b) HLL, (c) LF, (d) TVD-LW and (e) TVD-MC



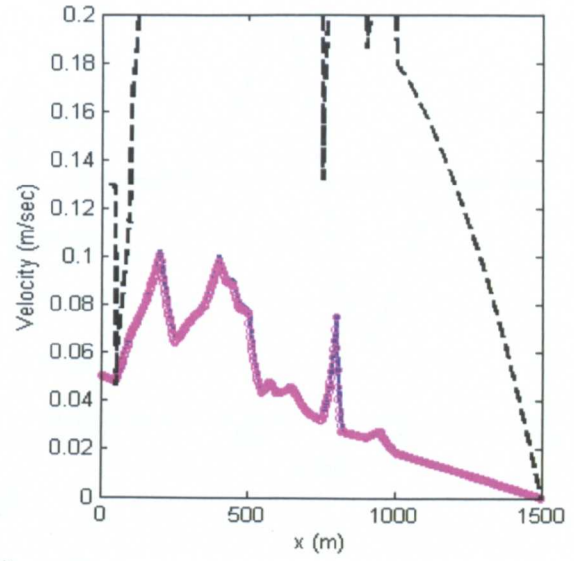
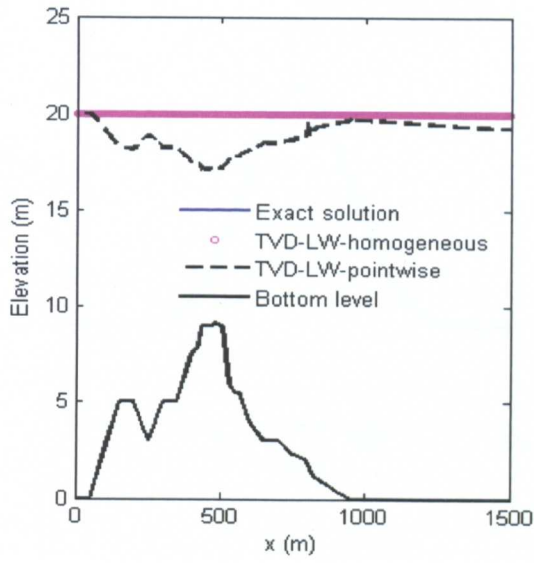
(a)



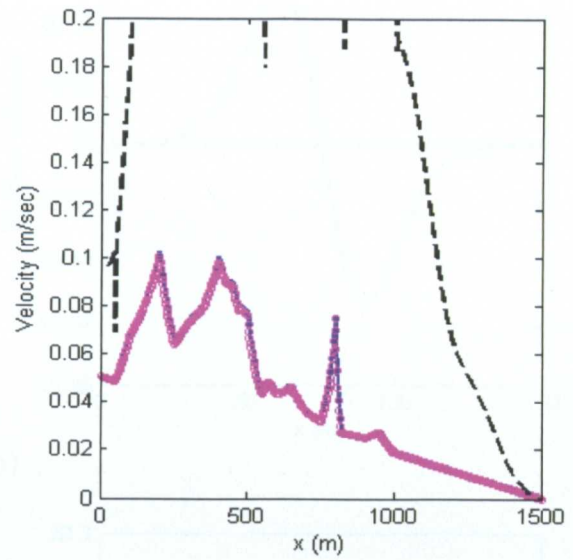
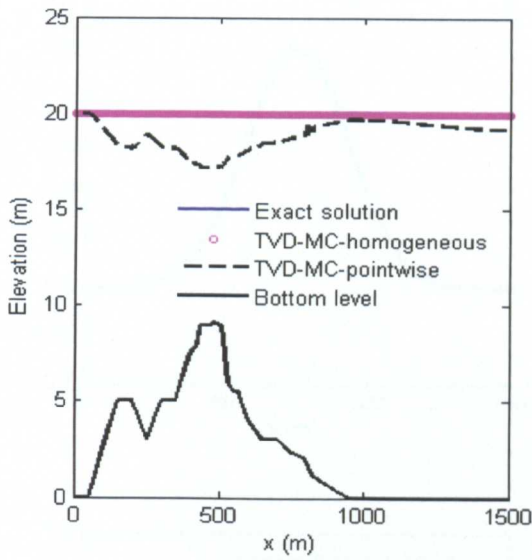
(b)



(c)

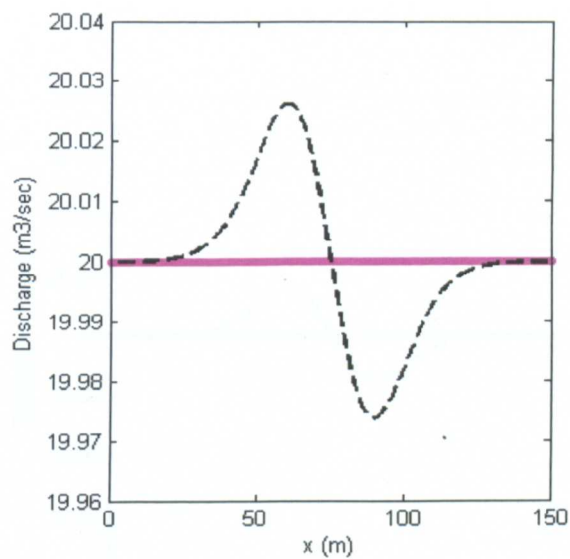
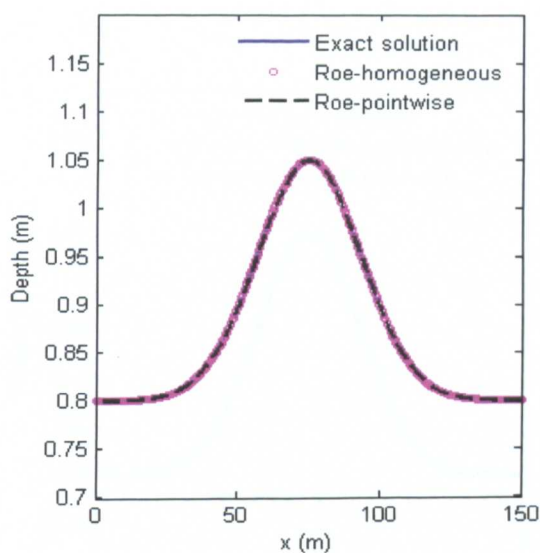


(d)

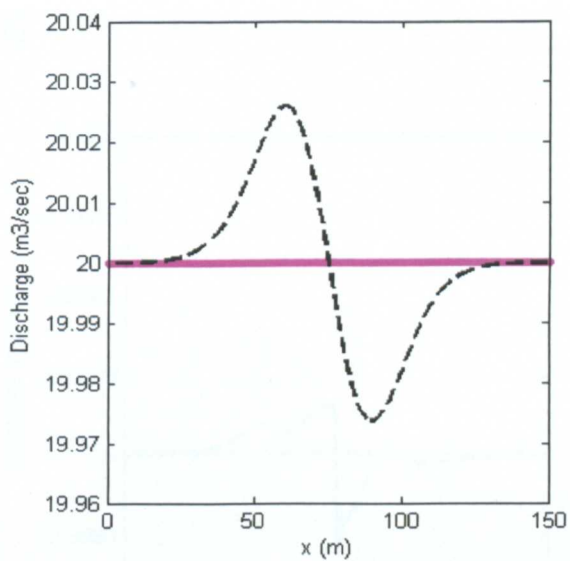
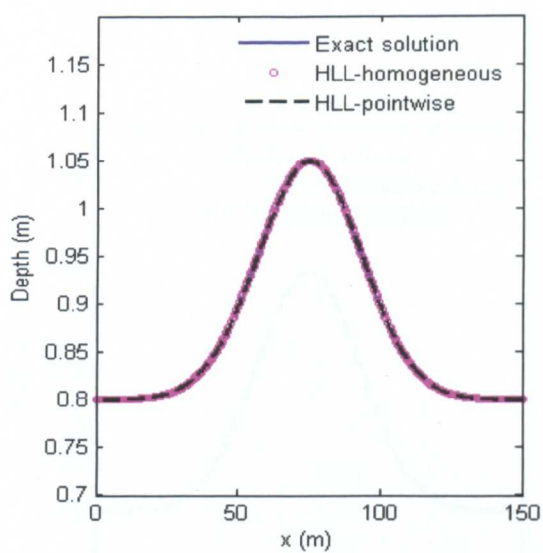


(e)

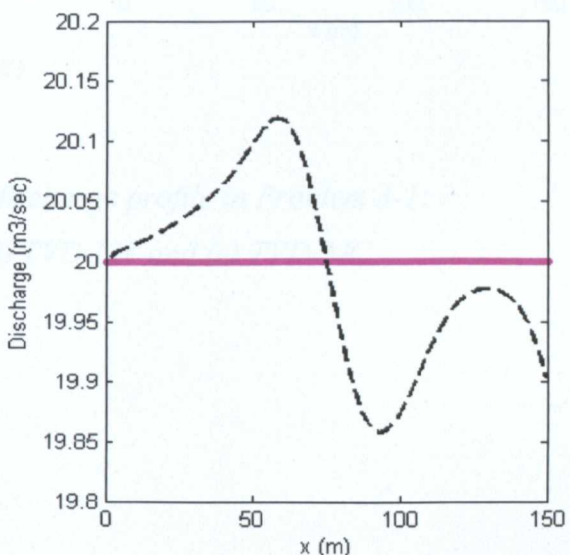
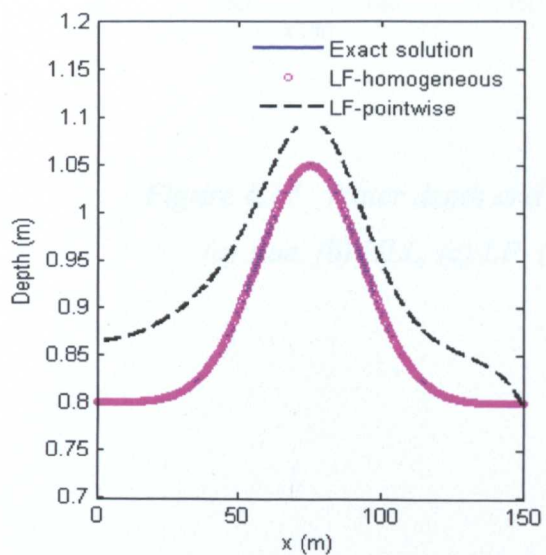
Figure 4.16 Water surface level and discharge profile at $t = 10,800s$ in Problem 2 with trapezoidal channel: (a) Roe, (b) HLL, (c) LF, (d) TVD-LW and (e) TVD-MC



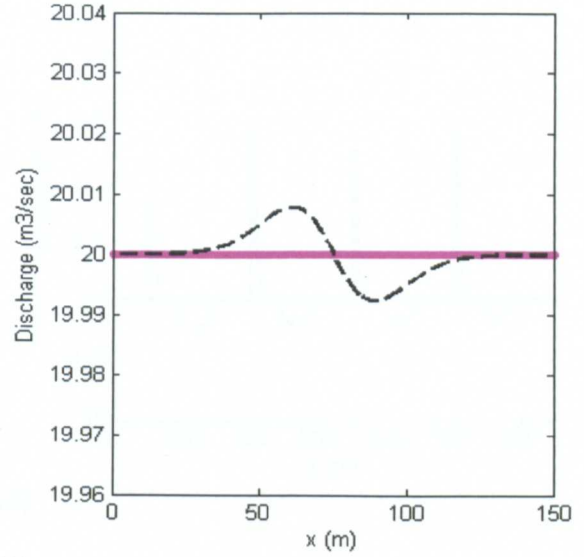
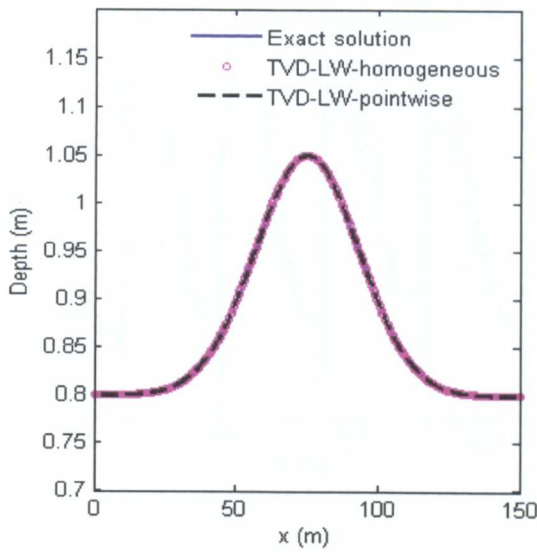
(a)



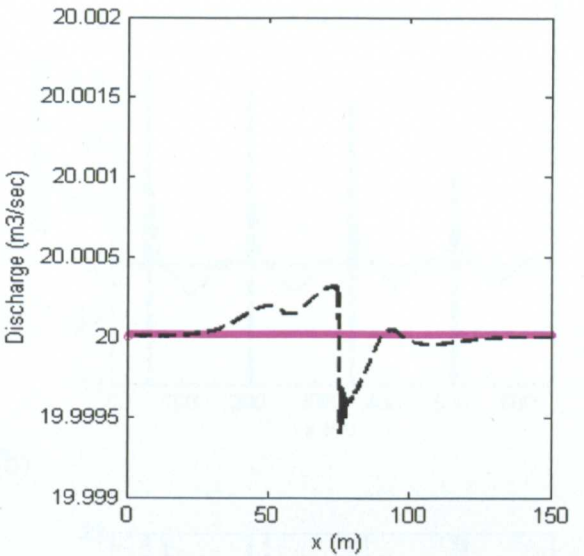
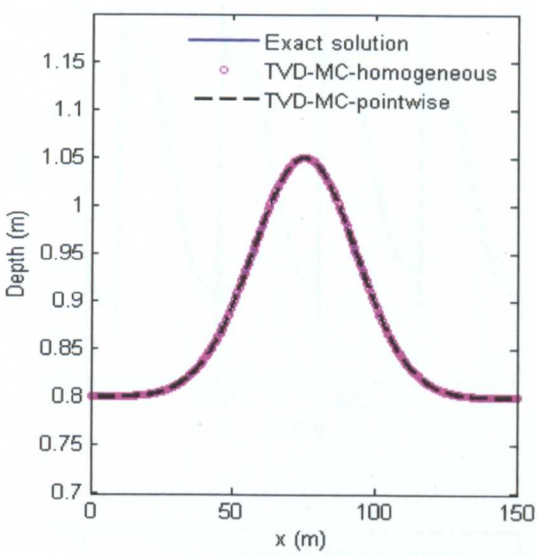
(b)



(c)

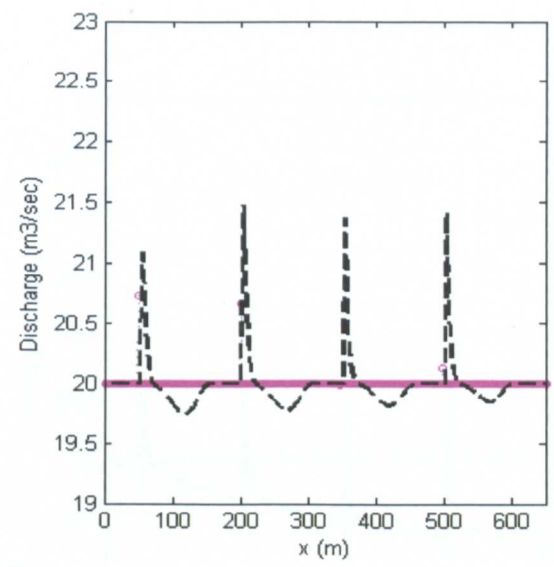
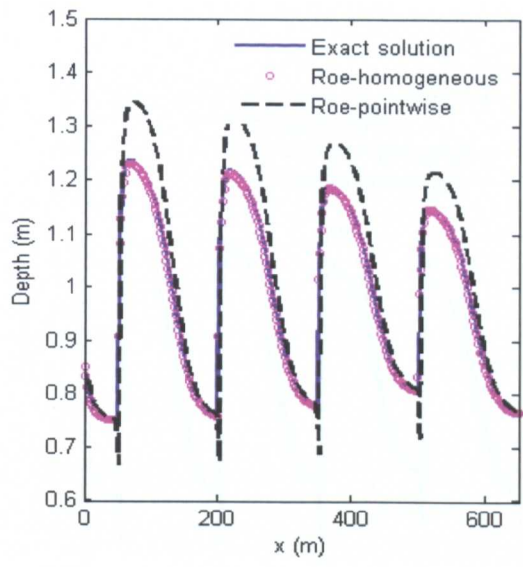


(d)

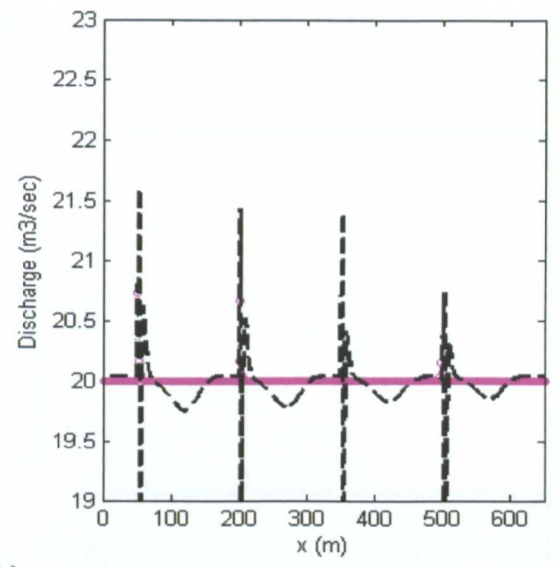
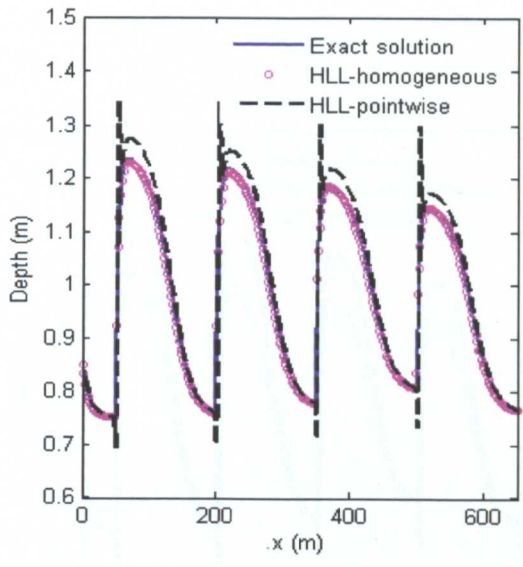


(e)

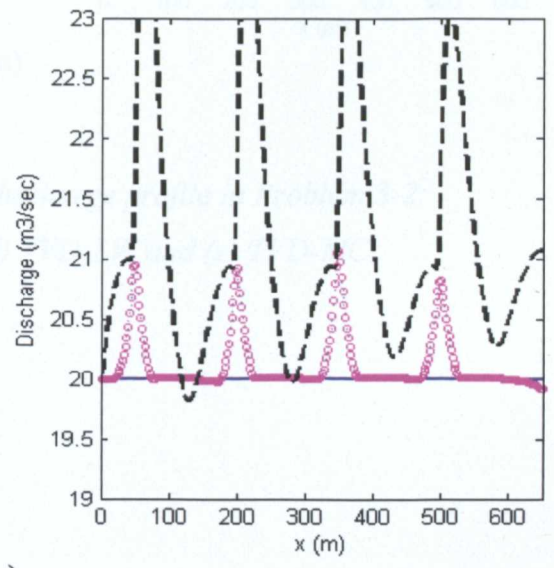
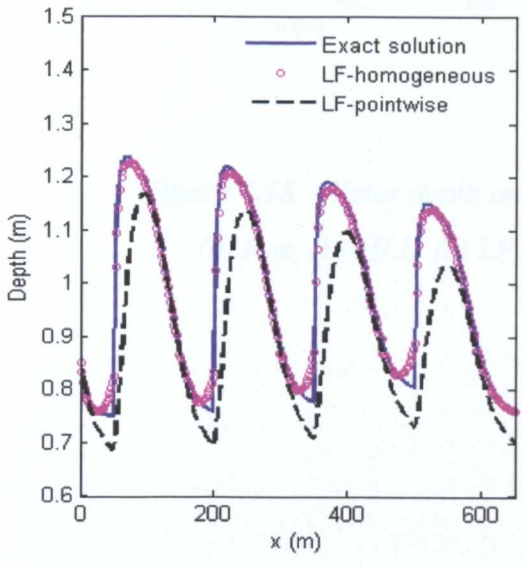
Figure 4.17 Water depth and discharge profile in Problem 3-1:
 (a) Roe, (b) HLL, (c) LF, (d) TVD-LW and (e) TVD-MC



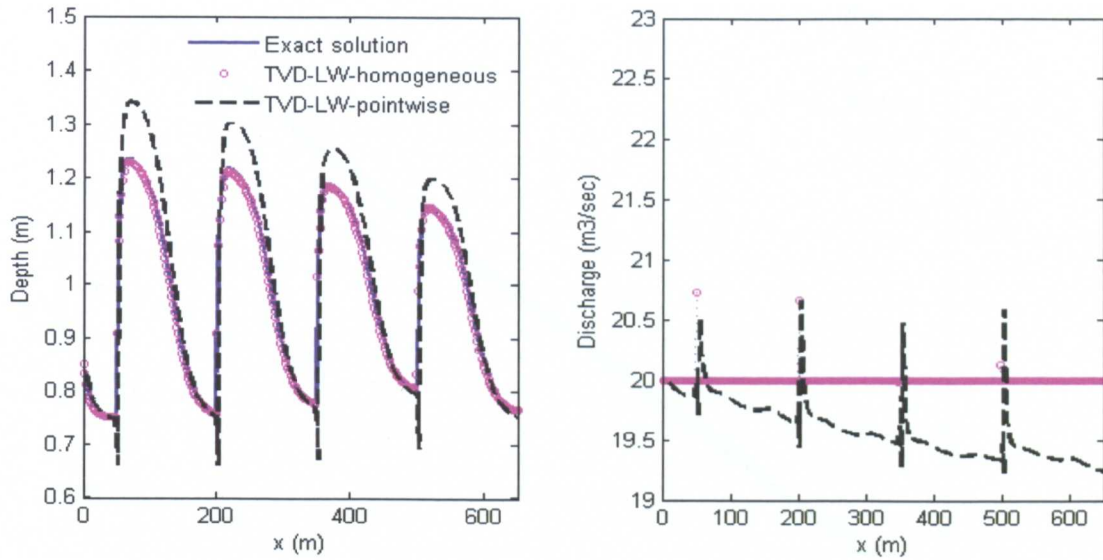
(a)



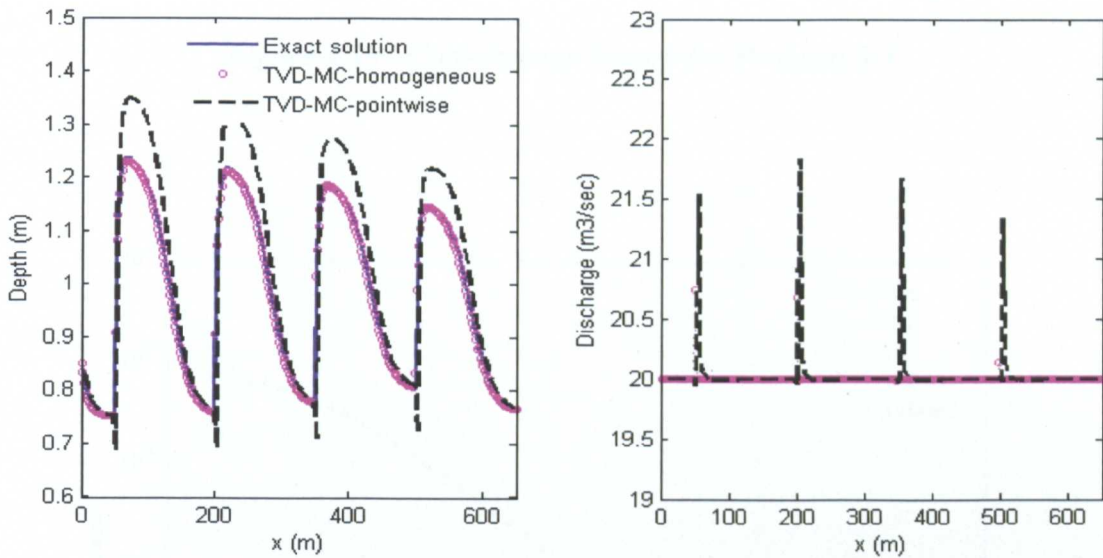
(b)



(c)



(d)



(e)

Figure 4.18 Water depth and discharge profile in Problem 3-2:

(a) Roe, (b) HLL, (c) LF, (d) TVD-LW and (e) TVD-MC

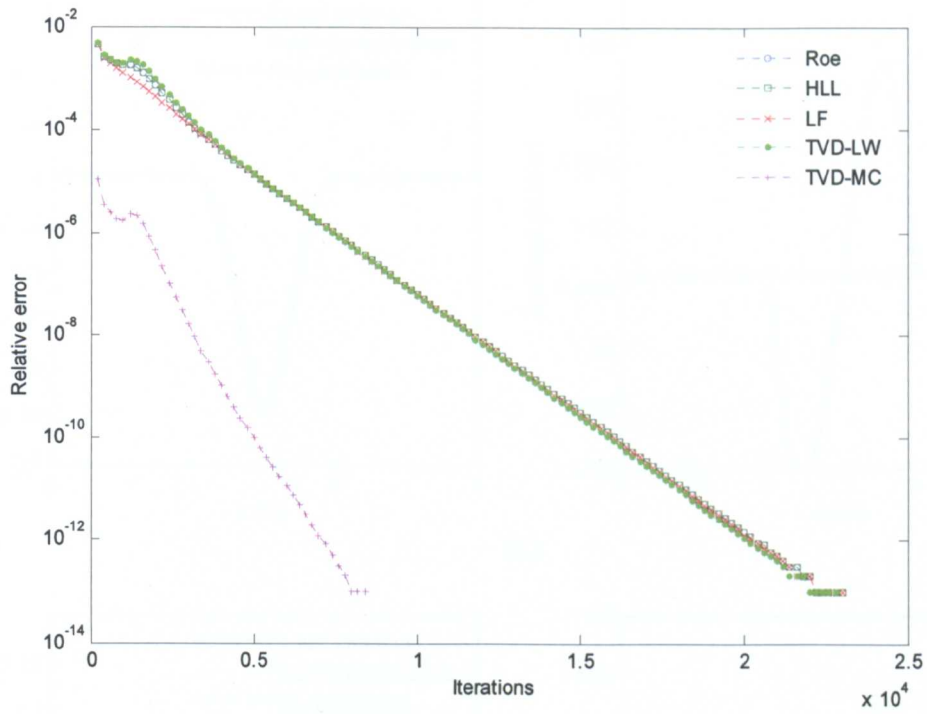


Figure 4.19 Convergence history for Problem 3-1

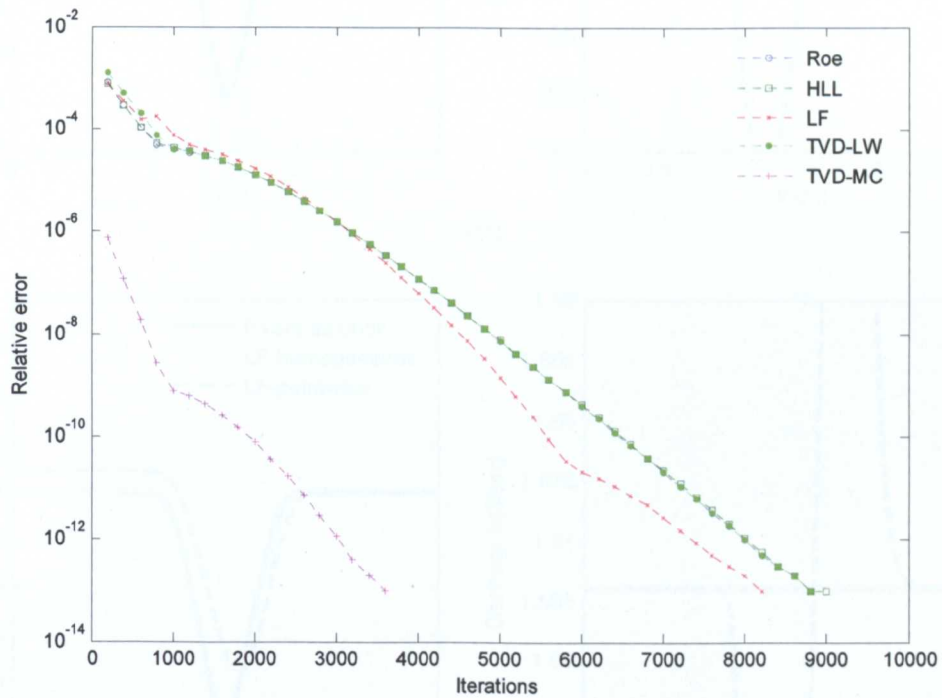
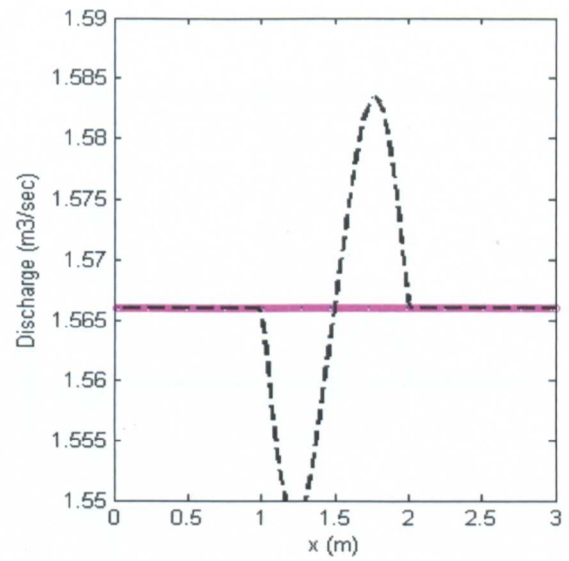
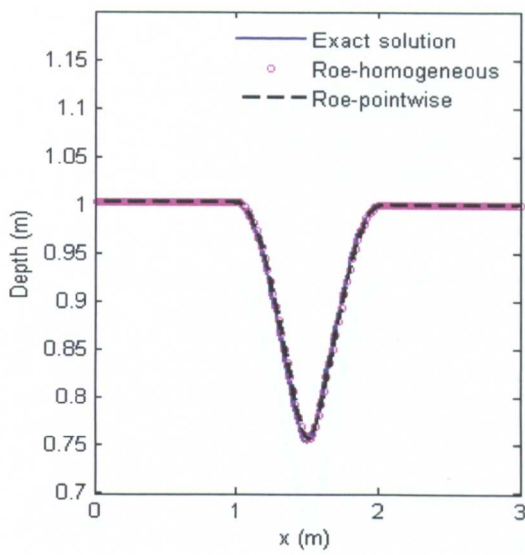
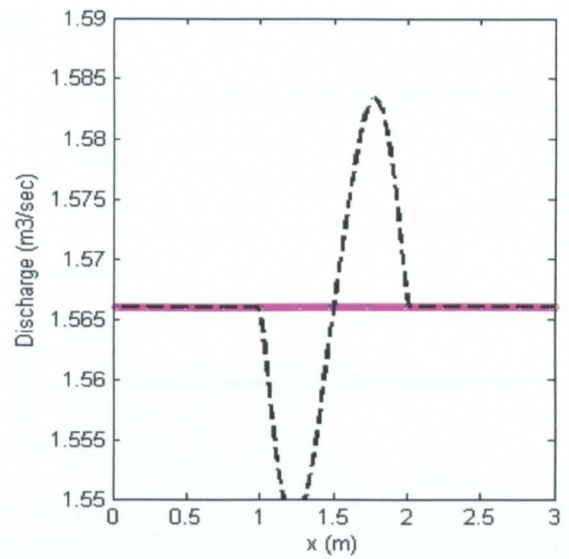
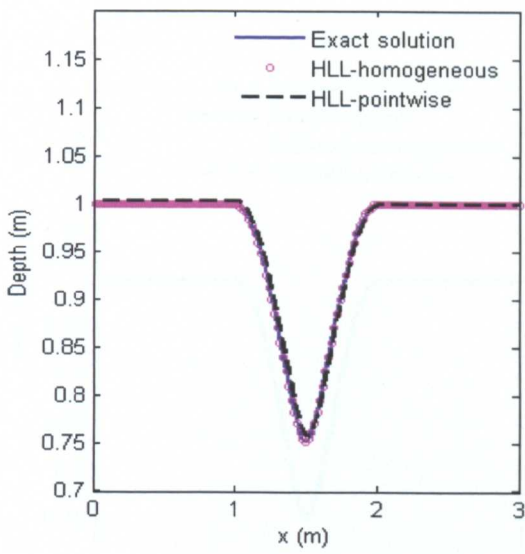


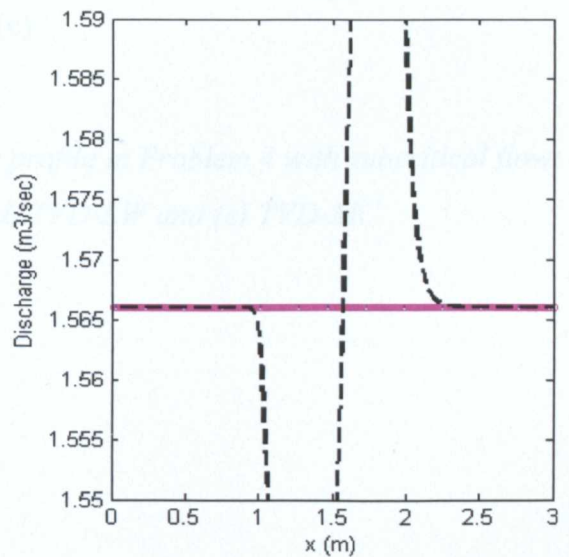
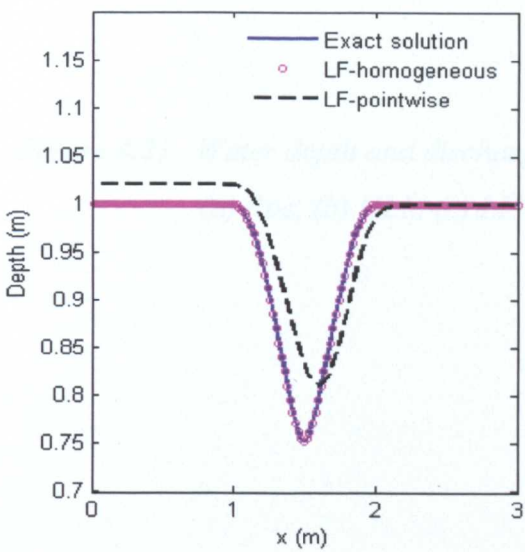
Figure 4.20 Convergence history for Problem 3-2



(a)



(b)



(c)

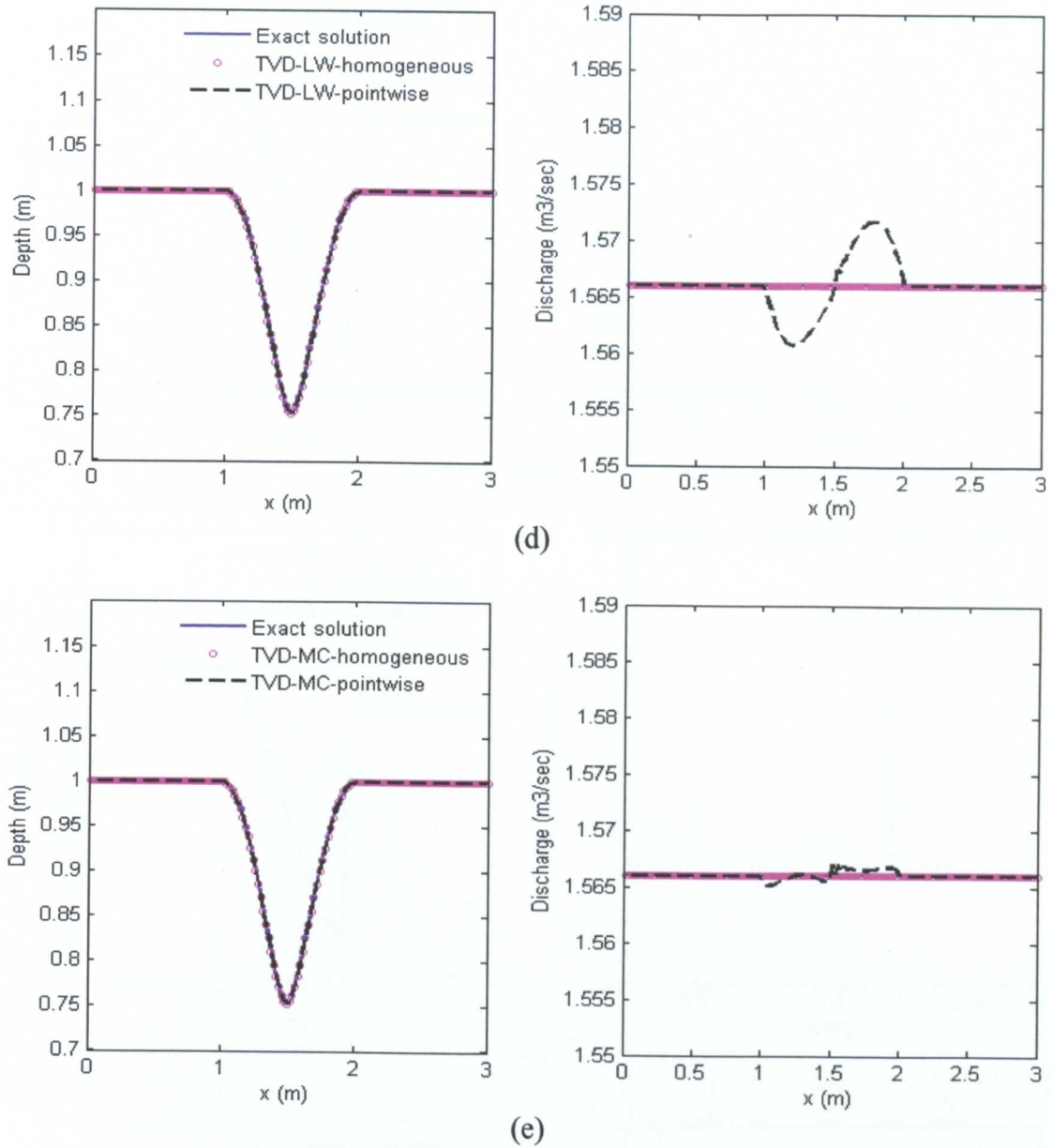
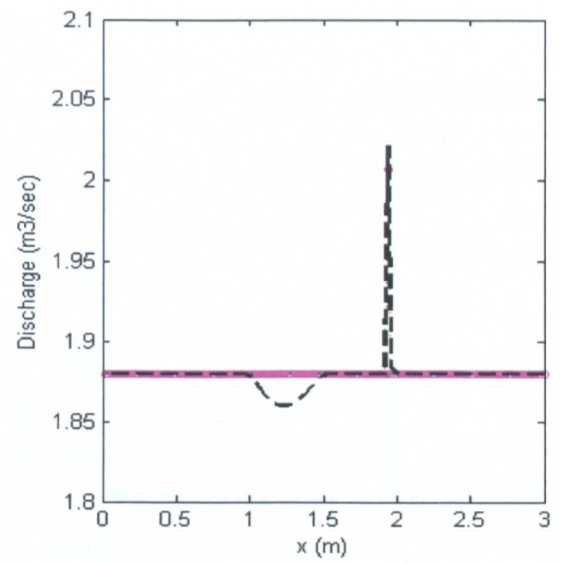
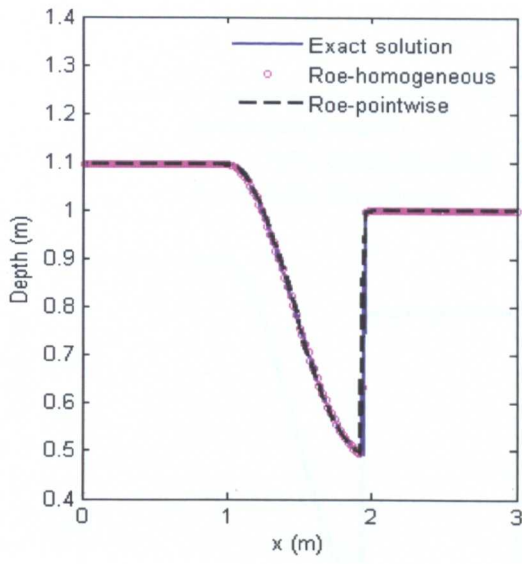
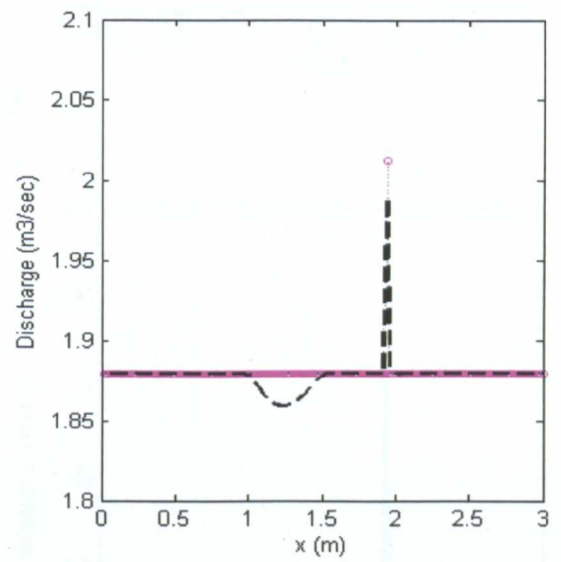
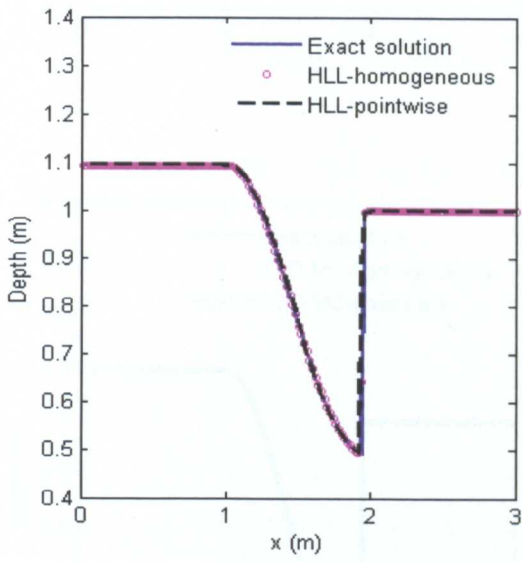


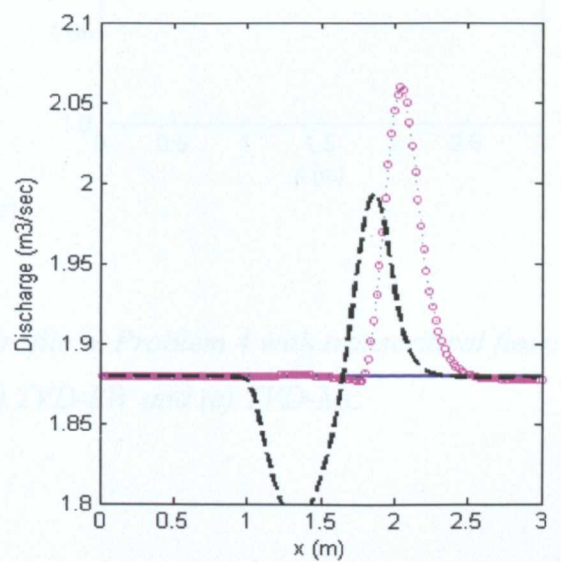
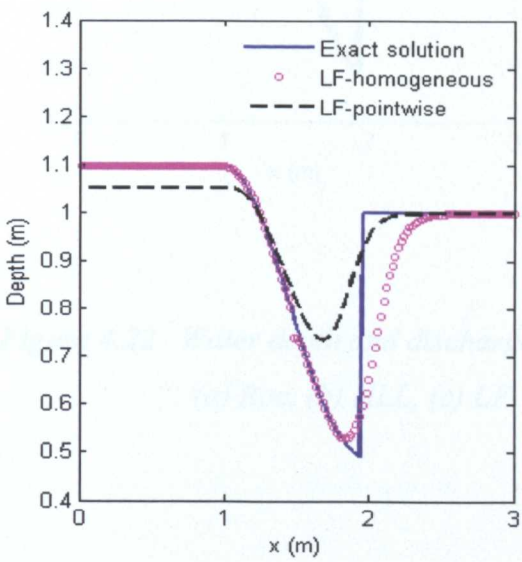
Figure 4.21 Water depth and discharge profile in Problem 4 with subcritical flow:
 (a) Roe, (b) HLL, (c) LF, (d) TVD-LW and (e) TVD-MC



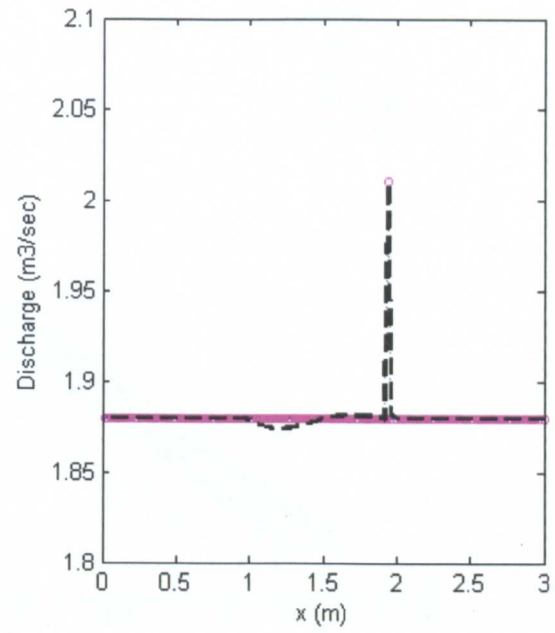
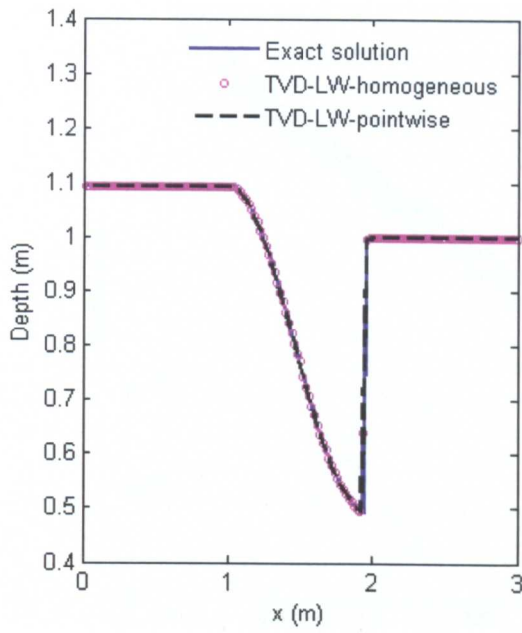
(a)



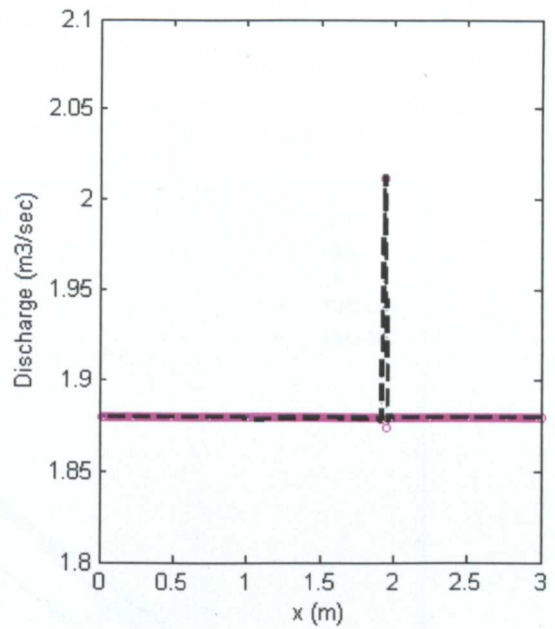
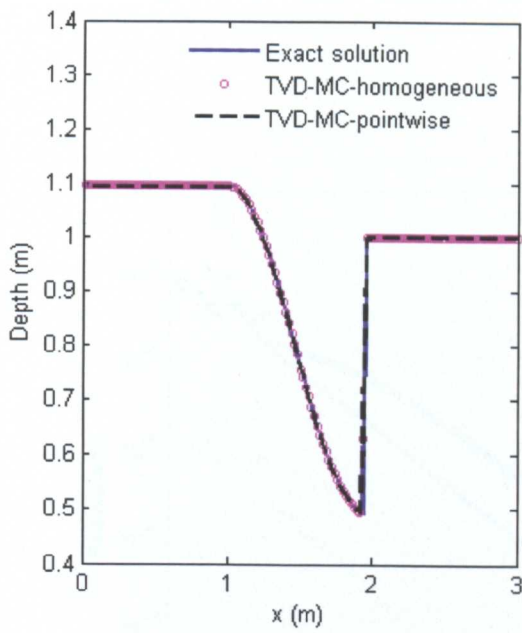
(b)



(c)



(d)



(e)

Figure 4.22 Water depth and discharge profile in Problem 4 with transcritical flow:
 (a) Roe, (b) HLL, (c) LF, (d) TVD-LW and (e) TVD-MC

Figure 4.24 Convergence history for Problem 4 (transcritical flow)

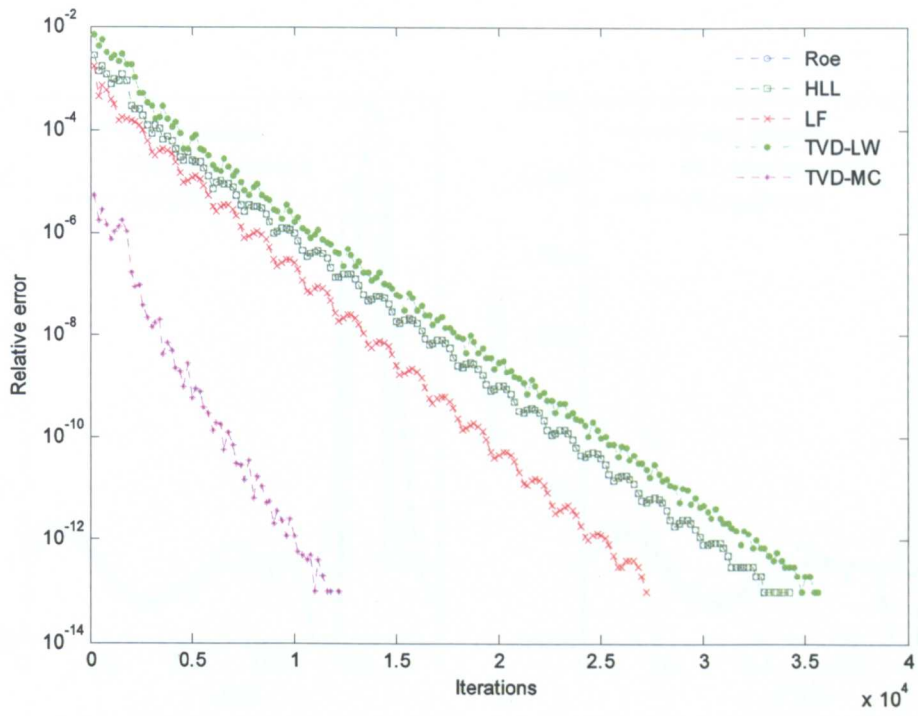


Figure 4.23 Convergence history for Problem 4 (subcritical flow)

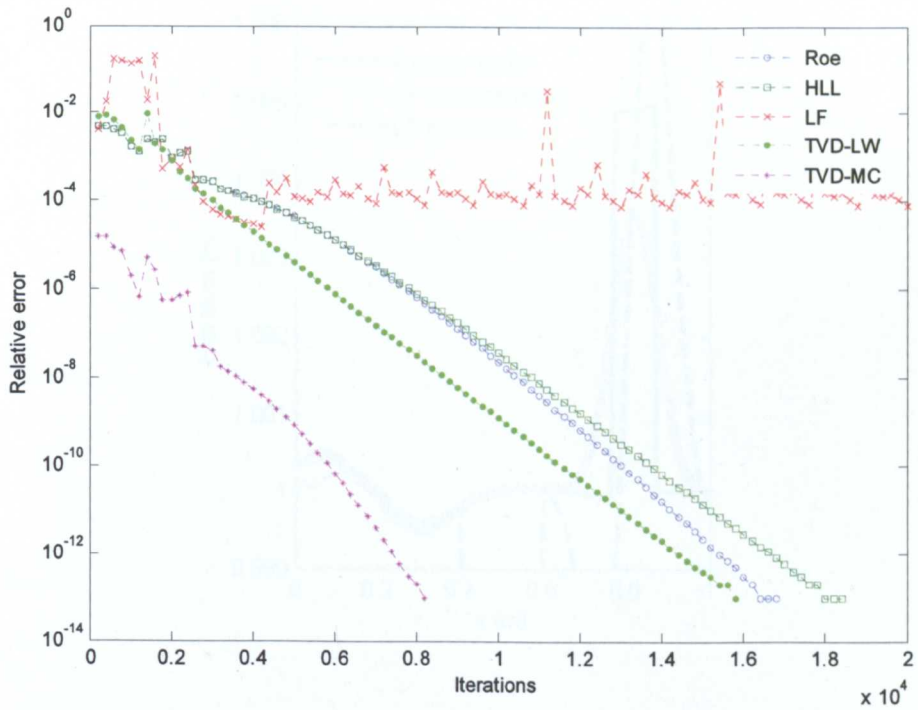
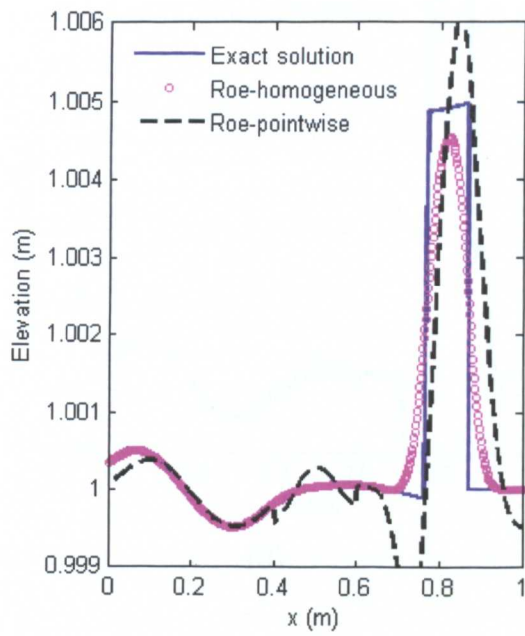
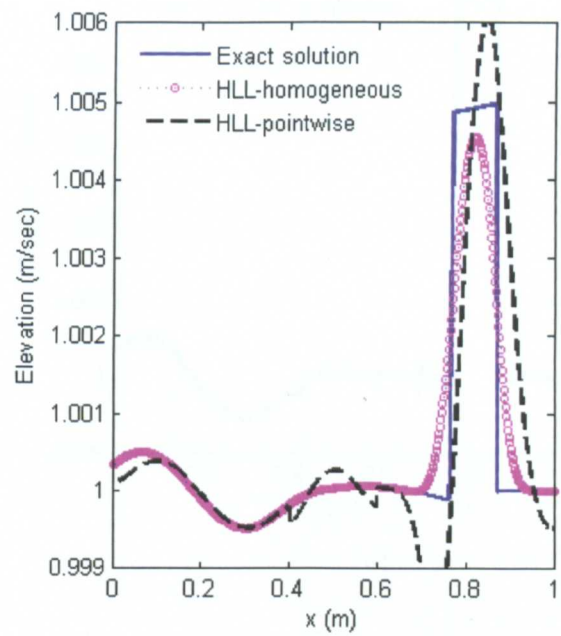


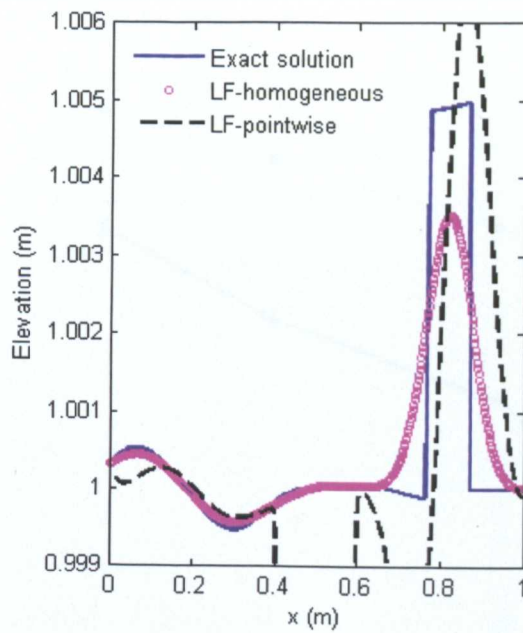
Figure 4.24 Convergence history for Problem 4 (transcritical flow)



(a)



(b)



(c)

Figure 4.24 Graph of L_2 error against number of cells (N) in Problem 3

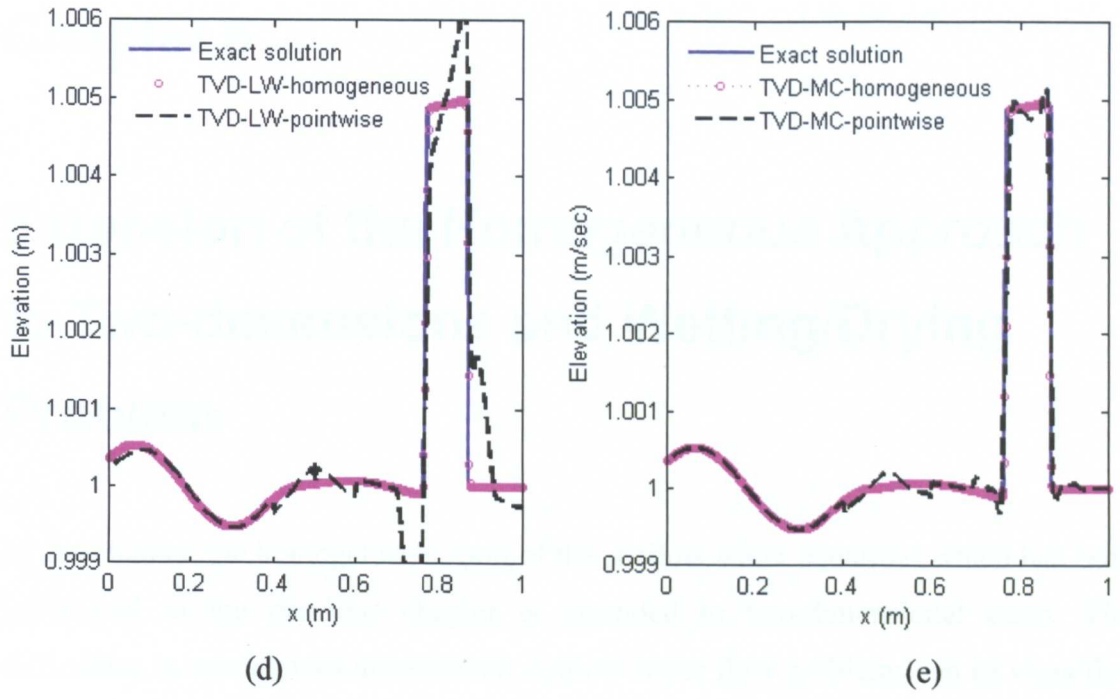


Figure 4.25 Water surface profile in Problem 5:
 (a) Roe, (b) HLL and (c) LF, (d) TVD-LW and (e) TVD-MC

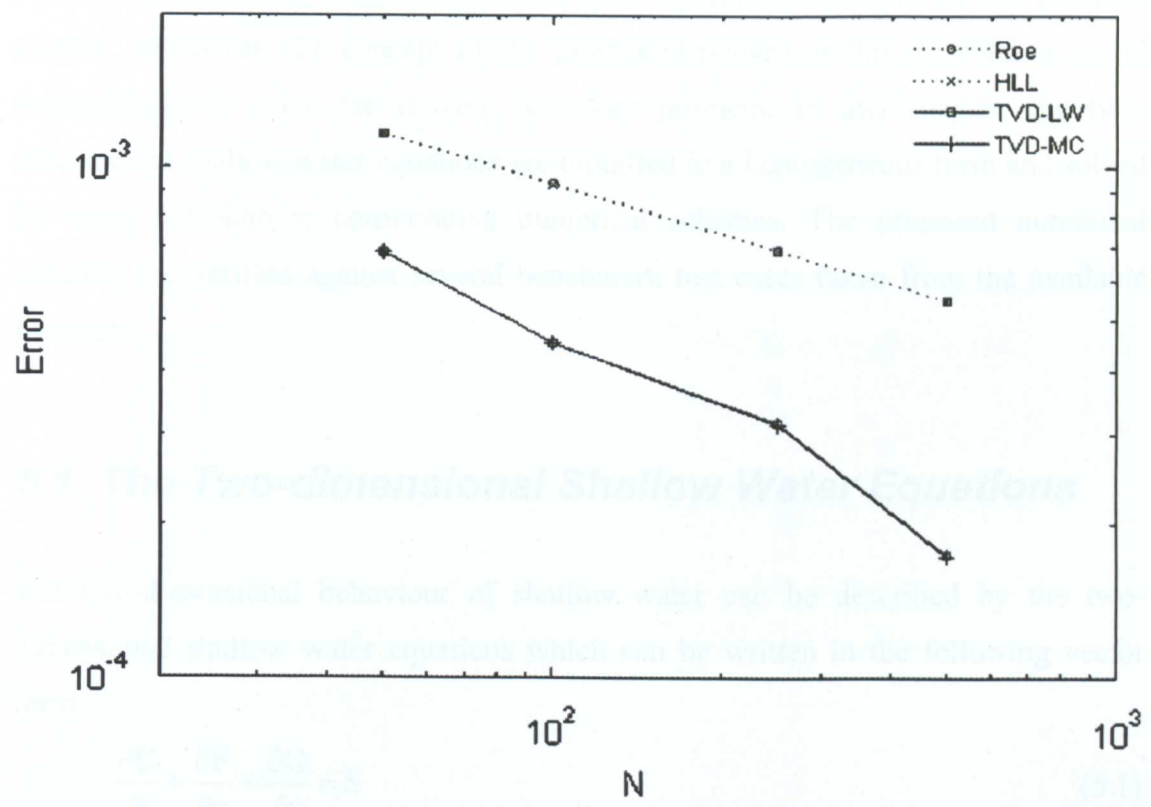


Figure 4.26 Graph of l_2 error against number of cells (N) in Problem 5

Chapter 5

Extension of the Homogeneous Approach to Two-dimensions and Wetting/Drying Problem

In this chapter, the homogeneous form of the shallow water equations which has been introduced in the previous chapter is extended to two-dimensional cases. The difficulties in solving two-dimensional shallow water flow problems can be classified into the following two categories: the numerical imbalance of the flux and the source terms and the solution of the moving boundary problem. These can be solved correctly and efficiently by adopting the homogeneous approach presented in the previous chapter. It is straightforward to solve the numerical balance problem in two-dimensions extending the homogeneous form equations as shown in the previous chapter. Moreover, the concept of the integrated numerical flux provides a useful methodology to solve the moving boundary problem. In this chapter, the two-dimensional shallow water equations are modified to a homogeneous form and solved by using well-known conservative numerical schemes. The proposed numerical schemes are verified against several benchmark test cases taken from the available literature.

5.1 *The Two-dimensional Shallow Water Equations*

The two-dimensional behaviour of shallow water can be described by the two-dimensional shallow water equations which can be written in the following vector form

$$\frac{\partial \mathbf{U}}{\partial t} + \frac{\partial \mathbf{F}}{\partial x} + \frac{\partial \mathbf{G}}{\partial y} = \mathbf{S} \quad (5.1)$$

$$\text{with } \mathbf{U} = \begin{pmatrix} h \\ hu \\ h\nu \end{pmatrix}, \mathbf{F} = \begin{pmatrix} hu \\ hu^2 + \frac{1}{2}gh^2 \\ hu\nu \end{pmatrix}, \mathbf{G} = \begin{pmatrix} h\nu \\ hu\nu \\ h\nu^2 + \frac{1}{2}gh^2 \end{pmatrix} \text{ and } \mathbf{S} = \begin{pmatrix} 0 \\ gh(S_{ox} - S_{fx}) \\ gh(S_{oy} - S_{fy}) \end{pmatrix}$$

where h is the water depth, u and ν are the velocity components in the x and y directions respectively. The variation of the bottom elevation is represented by the x - and y - components of the bed slopes, S_{ox} , S_{oy} which is given by

$$S_{ox} = -\frac{\partial z_b}{\partial x}, \quad S_{oy} = -\frac{\partial z_b}{\partial y},$$

and the components of the friction slopes, S_{fx} , S_{fy} are defined with the Manning's roughness coefficients n :

$$S_{fx} = \frac{n^2 u \sqrt{u^2 + \nu^2}}{h^{4/3}}, \quad S_{fy} = \frac{n^2 \nu \sqrt{u^2 + \nu^2}}{h^{4/3}}.$$

The two-dimensional equations have a more complicated form than the one-dimensional ones because they have two flux terms and consist of three equations. However, it is conceptually easier to evaluate the effects of the source terms in the two-dimensional equations because they do not include the I_2 term related to the channel width variation.

5.2 Homogeneous Form of the Shallow Water Equations

The homogeneous form of the two-dimensional shallow water equations can be obtained by using the same approach used for the one-dimensional ones and given by

$$\frac{\partial \mathbf{U}}{\partial t} + \frac{\partial \mathbf{H}}{\partial x} + \frac{\partial \mathbf{K}}{\partial y} = 0 \quad (5.2)$$

with $\mathbf{H} = \mathbf{F} - \mathbf{R}_1$, $\mathbf{K} = \mathbf{G} - \mathbf{R}_2$, where $\mathbf{R}_1 = (0, R_1, 0)^T$ and $\mathbf{R}_2 = (0, 0, R_2)^T$ are the flux terms corresponding to the source terms in the x and y directions respectively. The shallow water equations (5.2) can be rewritten in the following conservative form by using the divergence operator:

$$\frac{\partial \mathbf{U}}{\partial t} + \nabla \cdot \mathbf{E} = 0 \quad (5.3)$$

with $\mathbf{E} = (\mathbf{H}, \mathbf{K}) = (\mathbf{F} - \mathbf{R}_1, \mathbf{G} - \mathbf{R}_2)$. To apply the finite volume technique, Equation (5.3) should be written as the following integral form over a control volume V ,

$$\int_V \frac{\partial \mathbf{U}}{\partial t} dV + \int_V (\nabla \cdot \mathbf{E}) dV = 0. \quad (5.4)$$

The application of the Gauss's divergence theorem to Equations (5.4) leads to the following conservation equation with surface integral:

$$\int_V \frac{\partial \mathbf{U}}{\partial t} dV + \oint_{\partial V} (\mathbf{E} \cdot \mathbf{n}) ds = 0 \quad (5.5)$$

where ∂V represents the boundary of control volume V and \mathbf{n} is the outward-pointing normal vector to the boundary ∂V .

5.2.1 Numerical Discretization

In case of two-dimensional modelling of shallow water flows, a two-dimensional domain can be discretized into a finite number of grid cells as shown in *Figure 5.1*. Each discretized cell (control volume) has a finite volume encompassed by the boundaries (control surface), and the cell L represents the control volume considered while the cell R denotes neighbouring cells.

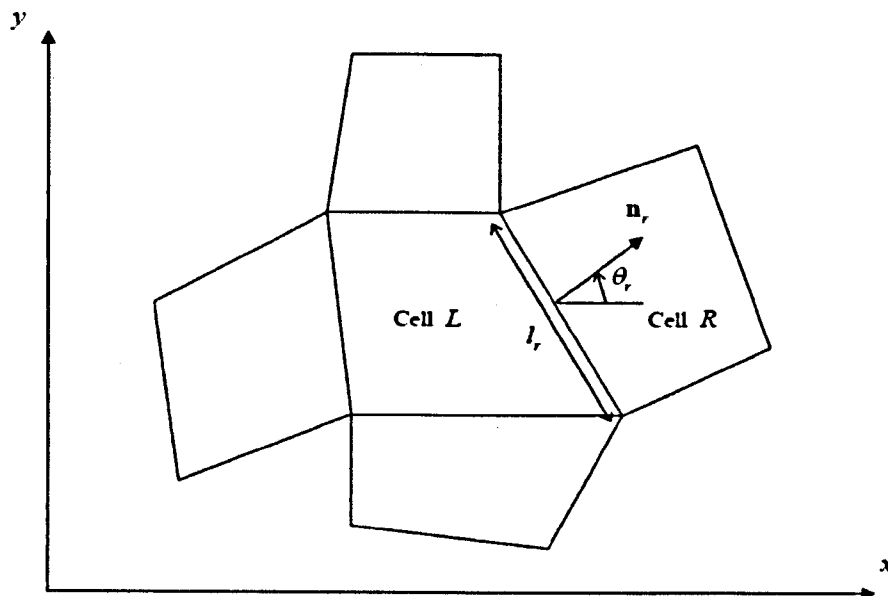


Figure 5.1 Finite volume grid in two-dimensional domain

By using the discretized two-dimensional grid, the surface integral in equation (5.5) can be approximated by the following form:

$$\oint_{\partial V} (\mathbf{E} \cdot \mathbf{n}) ds \approx \sum_r^N (\mathbf{E}_r^* \cdot \mathbf{n}_r \cdot l_r) \quad (5.6)$$

where $\mathbf{E}_r^* = \mathbf{E}_r^*(\mathbf{U}_L, \mathbf{U}_R)$ is the vector of the intercell numerical flux through boundary r , \mathbf{n}_r is the outward-pointing unit vector normal to the boundary, N is the total number of the boundaries and l_r is the length of the boundary. Consequently, $\mathbf{E}_r^* \cdot \mathbf{n}_r \cdot l_r$ represents the total outgoing numerical flux normal to the cell boundary r .

The components of the vector \mathbf{n}_r can be defined in terms of the angle θ_r :

$$\mathbf{n}_r = (\cos \theta_r, \sin \theta_r),$$

and the intercell numerical flux normal to the cell boundary r can be written as

$$\mathbf{E}_r^*(\mathbf{U}_L, \mathbf{U}_R) \cdot \mathbf{n}_r = \cos \theta_r \mathbf{H}_r^*(\mathbf{U}_L, \mathbf{U}_R) + \sin \theta_r \mathbf{K}_r^*(\mathbf{U}_L, \mathbf{U}_R).$$

Finally, Equation (5.5) can be rewritten as the following discretized form by applying explicit time evolution technique:

$$\mathbf{U}_i^{n+1} = \mathbf{U}_i^n - \frac{\Delta t}{A_i} \sum_r^N (\cos \theta_r \mathbf{H}_r^* + \sin \theta_r \mathbf{K}_r^*) l_r \quad (5.7)$$

where A_i is the area of the considered control volume. The discretized conservation law (5.7) means that the time evolution of the conserved variable \mathbf{U}_i depends only on the intercell numerical fluxes through the boundaries which can be calculated by producing numerical fluxes in Cartesian coordinates with the unit vector normal to each boundary. However, the solution of Equation (5.7) needs calculation of the two numerical fluxes \mathbf{H}^* and \mathbf{K}^* in the x and y directions respectively. The alternative and more efficient way to construct the intercell numerical flux is to use the rotation matrix [77] which is given by

$$\mathbf{T}(\theta) = \begin{pmatrix} 1 & 0 & 0 \\ 0 & \cos \theta & \sin \theta \\ 0 & -\sin \theta & \cos \theta \end{pmatrix}.$$

By introducing the rotation matrix, the following relation can be obtained:

$$\begin{aligned} \mathbf{E}_r^*(\mathbf{U}_L, \mathbf{U}_R) \cdot \mathbf{n}_r &= \mathbf{H}^*(\mathbf{U}_L, \mathbf{U}_R) \cos \theta_r + \mathbf{K}^*(\mathbf{U}_L, \mathbf{U}_R) \sin \theta_r \\ &= \mathbf{T}_r^{-1} \cdot \mathbf{H}^*(\mathbf{T}_r \cdot \mathbf{U}_L, \mathbf{T}_r \cdot \mathbf{U}_R) \end{aligned} \quad (5.8)$$

where $\mathbf{T}_r = \mathbf{T}(\theta_r)$ is the rotation matrix for the boundary r . Note that $\mathbf{T}_r \mathbf{U}$ represents the vector of the transformed variables corresponding to the normal and tangential directions to the boundary r and $\mathbf{H}^*(\mathbf{T}_r \cdot \mathbf{U}_L, \mathbf{T}_r \cdot \mathbf{U}_R)$ is the intercell numerical flux normal to the boundary and evaluated with the transformed variables $\mathbf{T}_r \cdot \mathbf{U}_L$ and $\mathbf{T}_r \cdot \mathbf{U}_R$. Finally, by substituting (5.8) into Equations (5.7), the conservative scheme is rewritten as

$$\mathbf{U}_i^{n+1} = \mathbf{U}_i^n - \frac{\Delta t}{A_i} \sum_r^N [\mathbf{T}_r^{-1} \cdot \mathbf{H}^*(\mathbf{T}_r \cdot \mathbf{U}_L, \mathbf{T}_r \cdot \mathbf{U}_R) \cdot l_r]. \quad (5.9)$$

As a result, the solution of the conservative scheme (5.9) can be obtained by calculating the intercell numerical flux at each boundary with the transformed variables and re-transforming it to the Cartesian coordinate. The integrated numerical flux \mathbf{H}^* can be calculated by using the same conservative numerical schemes used for one-dimensional problems in the previous chapter.

5.2.2 Definition of Source Flux Vector

To solve Equation (5.2), the definitions of ΔR_2 as well as ΔR_1 are needed. However, by using the discretized form (5.9) with the rotation matrix, the definition of ΔR_2 and R_2 are not needed because Equation (5.9) only needs the numerical flux normal to the cell interface. The definition of the source flux term R_1 which is essential to calculate numerical flux \mathbf{H}^* can be obtained by using the similar method to the one-dimensional case. By comparing Equation (5.1) and (5.2):

$$\frac{\partial R_1}{\partial x} = gh(S_{\alpha x} - S_{fx}). \quad (5.10)$$

To obtain a similar form to the one-dimensional problem, the bed slope $S_{\alpha x}$ should be rewritten as

$$S_{\alpha x} = -\frac{\partial z_b}{\partial x} = \frac{\partial}{\partial x}(h - z_s)$$

where $z_s = z_b + h$ is the free surface elevation. Then, Equations (5.10) can be expressed as

$$\frac{\partial R_1}{\partial x} = gh \left(\frac{\partial h}{\partial x} - \frac{\partial z_s}{\partial x} - S_{fx} \right). \quad (5.11)$$

The difference of the source flux, ΔR_1 , at the boundary between the cell L and R can be obtained by integrating Equation (5.11) over the domain of the two-cell system:

$$\int_{V_{LR}} \frac{\partial R_1}{\partial x} dV = \int_{V_{LR}} gh \left(\frac{\partial h}{\partial x} - \frac{\partial z_s}{\partial x} - S_{fx} \right) dV$$

where V_{LR} represents the domain consisting of the two cells L and R . Then ΔR_1 is given by

$$\Delta R_{1LR} = \Delta \left(\frac{g}{2} h^2 \right)_{LR} - g(\Omega_o + \Omega_f)_{LR}$$

where $g\Omega_o$ and $g\Omega_f$ are the momentum flux due to the water level difference and the friction force between the two cells respectively and expressed as

$$\begin{aligned} g\Omega_o &= g\Delta z_s \frac{h_L A_L + h_R A_R}{A_L + A_R}, \\ g\Omega_f &= g \frac{h_L A_L S_{fxL} + h_R A_R S_{fxR}}{A_L + A_R} \end{aligned} \quad (5.12)$$

where A_L , A_R and h_L , h_R represent the areas and water depths of the cell L and R respectively.

Note that Equation (5.12) is effective on unstructured grids as well as structured ones because it is derived by averaging over the domain of the two-cell system. In case of structured grid, (5.12) is reduced to

$$\begin{aligned} g\Omega_o &= g\Delta z_s \frac{h_L + h_R}{2}, \\ g\Omega_f &= g \frac{h_L S_{fxL} + h_R S_{fxR}}{2}. \end{aligned}$$

Then, the nodal flux term R_1 in each cell is calculated by splitting the flux difference ΔR_{1LR} :

$$R_{1L} = \frac{g}{2} h_L^2,$$

$$R_{1R} = \frac{g}{2} h_R^2 - g(\Omega_o + \Omega_f)_{LR}.$$

The momentum terms, $g(\Omega_o + \Omega_f)$, due to the water surface difference and the friction are allocated to the outside cell because it should be considered as a force exerted by the neighbouring cells.

5.3 Conservative Schemes

The homogeneous form of the conservation law system (5.9) can be solved by using the well-known conservative numerical schemes as shown in the previous chapter. Several numerical schemes including Roe and HLL approximate solvers, Lax-Friedrichs scheme and TVD Lax-Wendroff scheme are modified to solve the homogeneous form equations. As all the schemes are already introduced in the previous chapter, only the homogeneous form schemes are presented here. To show the numerical properties of each scheme, the numerical solutions to the two-dimensional circular dam-break problem are presented at the end of this section.

Roe's Solver

The approximate Jacobian matrix of the two-dimensional shallow water equations is given by

$$\tilde{\mathbf{J}} = \begin{pmatrix} 0 & 1 & 0 \\ \tilde{c}^2 - \tilde{u}^2 & 2\tilde{u} & 0 \\ -\tilde{u}\tilde{v} & \tilde{v} & \tilde{u} \end{pmatrix}$$

which have the following eigenvalues and eigenvectors:

$$\tilde{\lambda}_1 = \tilde{u} + \tilde{c}, \quad \tilde{\lambda}_2 = \tilde{u}, \quad \tilde{\lambda}_3 = \tilde{u} - \tilde{c},$$

$$\tilde{\mathbf{e}}_1 = (1, \tilde{u} + \tilde{c}, \tilde{v})^T, \quad \tilde{\mathbf{e}}_2 = (0, 0, \tilde{c})^T, \quad \tilde{\mathbf{e}}_3 = (1, \tilde{u} - \tilde{c}, \tilde{v})^T.$$

The average values \tilde{u} , \tilde{v} and \tilde{c} are calculated from the condition $\Delta \mathbf{F} = \tilde{\mathbf{J}} \Delta \mathbf{U}$:

$$\tilde{u}_{LR} = \frac{u_R / \sqrt{h_R} + u_L / \sqrt{h_L}}{\sqrt{h_R} + \sqrt{h_L}},$$

$$\tilde{v}_{LR} = \frac{v_R/\sqrt{h_R} + v_L/\sqrt{h_L}}{\sqrt{h_R} + \sqrt{h_L}},$$

$$\tilde{c}_{LR} = \sqrt{\frac{g}{2}(h_R + h_L)}.$$

The integrated numerical flux \mathbf{H}_{LR}^* at the boundary between two cells L and R is expressed as

$$\mathbf{H}_{LR}^* = \frac{1}{2}(\mathbf{H}_R + \mathbf{H}_L) - \frac{1}{2}|\tilde{\mathbf{J}}_{LR}|\Delta\mathbf{U}'_{LR},$$

or, in a characteristic form:

$$\mathbf{H}_{LR}^* = \frac{1}{2}(\mathbf{H}_R + \mathbf{H}_L) - \frac{1}{2}\sum_k(\tilde{\alpha}'_k|\tilde{\lambda}_k|\tilde{e}_k)_{LR}$$

where the modified wavestrength $\tilde{\alpha}'$ is obtained from the relation $\Delta\mathbf{H}_{LR} = \tilde{\mathbf{J}}_{LR}\Delta\mathbf{U}'_{LR}$:

$$\begin{aligned} \begin{pmatrix} \Delta(hu) \\ \Delta(hu^2) + \Delta(gh^2/2) \\ \Delta(huv) \end{pmatrix}_{LR} - \begin{pmatrix} 0 \\ \Delta(gh^2/2) - g(\Omega_o + \Omega_f) \\ 0 \end{pmatrix}_{LR} \\ = \begin{pmatrix} 0 & 1 & 0 \\ -\tilde{\lambda}_1\tilde{\lambda}_3 & \tilde{\lambda}_1 + \tilde{\lambda}_3 & 0 \\ -\frac{1}{2}(\tilde{\lambda}_1 + \tilde{\lambda}_3)\tilde{v} & \tilde{v} & \frac{1}{2}(\tilde{\lambda}_1 + \tilde{\lambda}_3) \end{pmatrix}_{LR} \begin{pmatrix} \Delta(h)' \\ \Delta(hu)' \\ \Delta(hv)' \end{pmatrix}_{LR} \end{aligned}$$

and

$$\Delta(h)'_{LR} = \frac{\Delta(hu^2)_{LR} + g(\Omega_o + \Omega_f)_{LR} - (\tilde{\lambda}_1 + \tilde{\lambda}_3)\Delta(hu)'_{LR}}{\tilde{\lambda}_1\tilde{\lambda}_3}, \quad (5.12a)$$

$$\Delta(hu)'_{LR} = \Delta(hu)_{LR}, \quad (5.12b)$$

$$\Delta(hv)'_{LR} = \Delta(hv)_{LR} - \tilde{v}\Delta(h)_{LR} + \tilde{v}\Delta(h)'_{LR}. \quad (5.12c)$$

The modified wavestrength $\tilde{\alpha}'_{1,2,3}$ can be obtained by using the modified variable difference (5.12a-c):

$$\tilde{\alpha}'_1 = \frac{(\tilde{c} - \tilde{u})\Delta(h)' + \Delta(hu)}{2\tilde{c}}, \quad (5.13a)$$

$$\tilde{\alpha}'_2 = \frac{\Delta(hv)' - \Delta(h)'\tilde{v}}{\tilde{c}}, \quad (5.13b)$$

$$\tilde{\alpha}'_3 = \frac{(\tilde{c} + \tilde{u})\Delta(h)' - \Delta(hu)}{2\tilde{c}}. \quad (5.13c)$$

HLL Solver

The integrated intercell numerical flux \mathbf{H}^* has the same form as the one-dimensional scheme:

$$\mathbf{H}_{LR}^* = \begin{cases} \mathbf{H}_L & \text{if } \lambda_{\min} \geq 0 \\ \mathbf{H}_R & \text{if } \lambda_{\max} \leq 0 \\ \mathbf{H}^* & \text{otherwise} \end{cases}$$

where the two wave speeds λ_{\min} and λ_{\max} is given by

$$\lambda_{\min} = \min(u_L - c_L, \tilde{u}_{LR} - \tilde{c}_{LR}),$$

$$\lambda_{\max} = \max(u_R + c_R, \tilde{u}_{LR} + \tilde{c}_{LR}).$$

The numerical flux in the intermediate state is expressed as

$$\mathbf{H}^* = \frac{\lambda_{\max} \mathbf{H}_i - \lambda_{\min} \mathbf{H}_{i+1}}{\lambda_{\max} - \lambda_{\min}} - \frac{\lambda_{\min} \lambda_{\max} \Delta \mathbf{U}'_{i+\frac{1}{2}}}{\lambda_{\max} - \lambda_{\min}}$$

where $\Delta \mathbf{U}'_{i+\frac{1}{2}} = (\Delta A', \Delta Q')_{i+\frac{1}{2}}^T$ calculated from the condition $\Delta \mathbf{H}_{LR} = \mathbf{J}_{LR}^{hll} \Delta \mathbf{U}'_{LR}$. The

Jacobian matrix for HLL solver, \mathbf{J}^{hll} , is constructed by using the two wavespeeds

λ_{\min} and λ_{\max} :

$$\mathbf{J}^{hll} = \begin{pmatrix} 0 & 1 & 0 \\ -\tilde{\lambda}_{\max} \tilde{\lambda}_{\min} & \tilde{\lambda}_{\max} + \tilde{\lambda}_{\min} & 0 \\ -\frac{1}{2}(\tilde{\lambda}_{\max} + \tilde{\lambda}_{\min}) \tilde{v} & \tilde{v} & \frac{1}{2}(\tilde{\lambda}_{\max} + \tilde{\lambda}_{\min}) \end{pmatrix},$$

and the modified variable differences can be expressed as

$$\Delta(hu)'_{LR} = \Delta(hu)_{LR},$$

$$\Delta(h)'_{LR} = \frac{\Delta(hu^2)_{LR} + g(\Omega_o + \Omega_f)_{LR} - (\tilde{\lambda}_{\max} + \tilde{\lambda}_{\min}) \Delta(hu)'_{LR}}{\tilde{\lambda}_{\max} \tilde{\lambda}_{\min}},$$

$$\Delta(hv)'_{LR} = \Delta(hv)_{LR} - \tilde{v} \Delta(h)_{LR} + \tilde{v} \Delta(h)'_{LR}.$$

Lax-Friedrichs scheme (LF)

The integrated numerical flux for the two-dimensional Lax-Friedrichs scheme can be obtained by modifying the one-dimensional scheme

$$\mathbf{H}_{LR}^* = \frac{1}{2}(\mathbf{H}_R + \mathbf{H}_L) - \frac{1-a}{N} \frac{\Delta t}{\Delta x} \Delta \mathbf{U}'_{LR}$$

where N is the number of the boundaries of each computing cell, i.e. $N = 4$ for a quadrilateral grid cell. The same variable difference $\Delta \mathbf{U}'_{LR}$ used for Roe's scheme which is given as (5.12a-c) is used for the Lax-Friedrichs scheme.

TVD Lax-Wendroff scheme (TVD-LW)

The integrated numerical flux for the TVD version of Lax-Wendroff scheme is expressed as

$$\mathbf{H}_{LR}^* = \frac{1}{2}(\mathbf{H}_L + \mathbf{H}_R) - \frac{1}{2} \sum_k (\tilde{\alpha}'_k |\tilde{\lambda}_k| \tilde{e}_k)_{LR} + \frac{1}{2} \sum_k (\tilde{\alpha}'_k \Phi_k |\tilde{\lambda}_k| [1 - \frac{\Delta t}{\Delta x} |\tilde{\lambda}_k|] \tilde{e}_k)_{LR}$$

where $\tilde{\alpha}'$ is the modified wavestrength as defined in (5.13a-c) and Φ is the flux limiter function.

Each conservative scheme is applied to the hypothetical circular dam-break problem to demonstrate the properties of each scheme. The initial conditions of this problem are two regions of stationary water separated by a thin circular dam with radius $11m$. The water depths inside and outside of the dam are $10m$ and $1m$ respectively. The problem domain is $50m \times 50m$ square frictionless flat bottom which is discretized by a rectangular grid with $\Delta x = \Delta y = 0.5m$. The numerical results at $t = 0.69s$ after the collapse of the circular dam are obtained and presented in *Figure 5.2* and *5.3*. As shown in the figures, TVD-LW scheme presents a sharper advancing wave front than Roe's and HLL schemes while the LF scheme shows a diffusive solution with a smooth water depth profile.

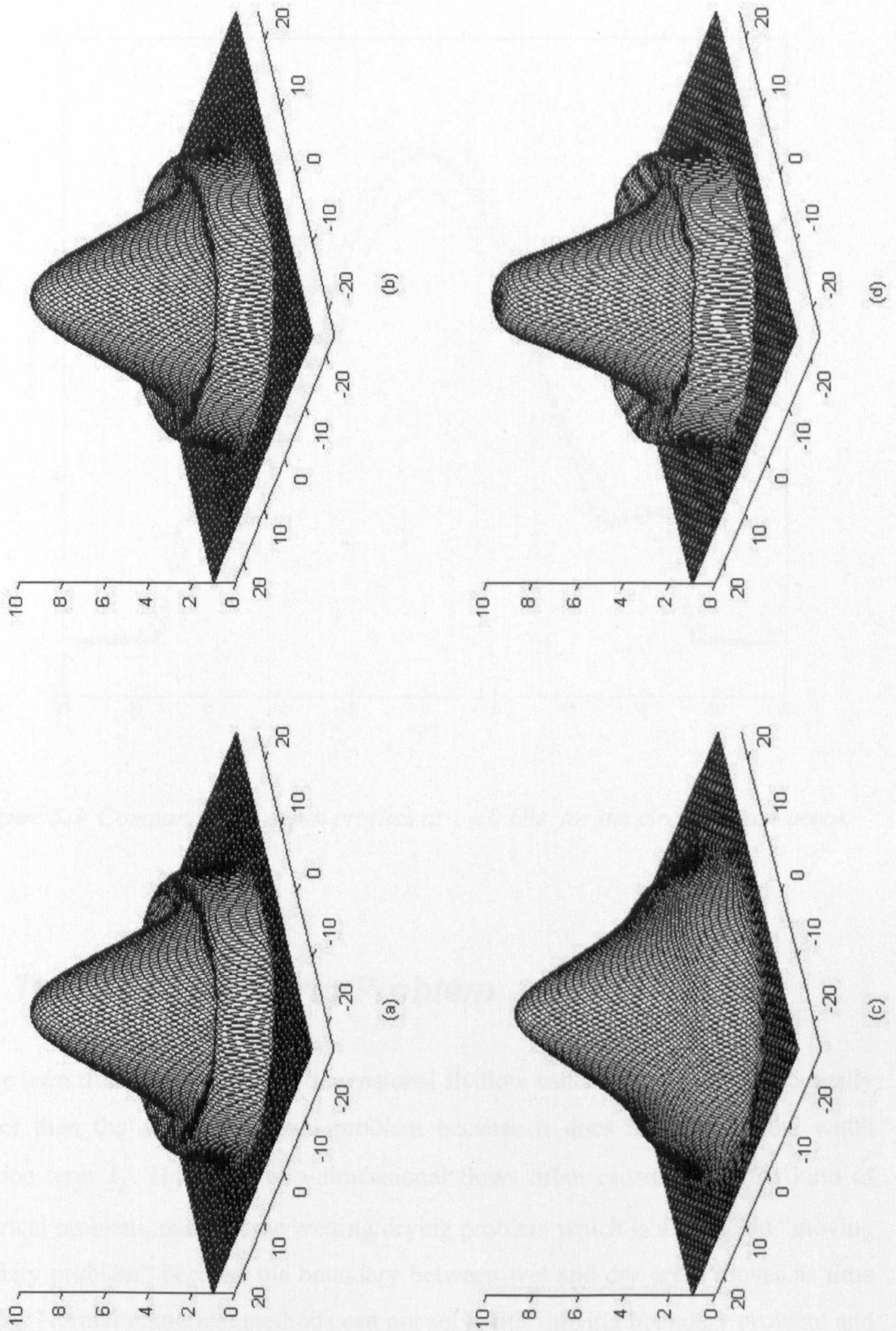


Figure 5.2 Water surface profiles at $t = 0.69s$ after the breaking of a circular dam:
 (a)Roe, (b)HLL, (c)LF and (d)TVD-LW

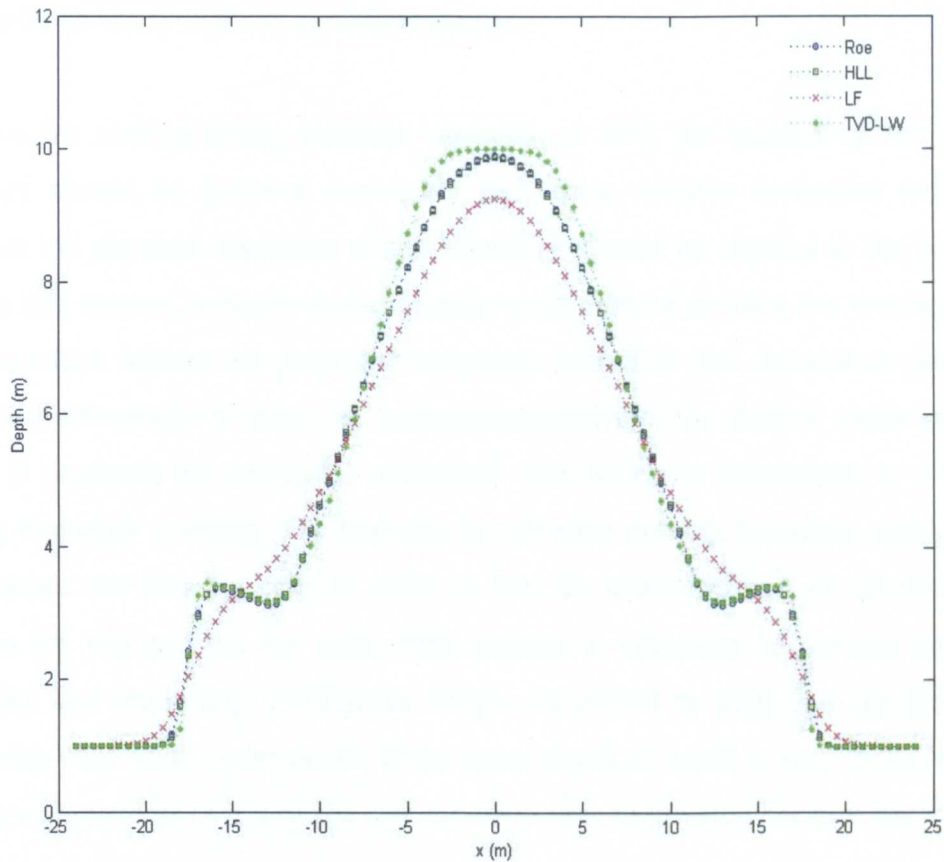


Figure 5.3 Comparison of depth profiles at $t = 0.69s$ for the circular dam-break

5.4 The Wetting/Drying Problem

Source term treatment in the two-dimensional shallow water equations is conceptually simpler than the one-dimensional problem because it does not include the width variation term I_2 . However, two-dimensional flows often cause a different kind of numerical problem, namely, the wetting/drying problem which is also called “moving boundary problem” because the boundary between wet and dry areas moves as time goes by. Normal numerical methods can not solve this moving boundary problem and cause numerical errors without the adoption of special methods. This is mainly because the shallow water equations lose their properties when the water depth

approaches to zero and the numerical schemes cannot automatically detect moving boundaries correctly without special treatment.

To solve the wetting/drying problem correctly, at first, the location of the moving boundary should be detected accurately and, then, suitable numerical techniques based on the physical condition of the boundary should be applied to the boundary cells. In this section, a simple and straightforward method to solve the wetting/drying problem which utilises the proposed integrated numerical flux function is presented. One of the advantages of using the homogeneous form of the shallow water equations is that it produces an integrated numerical flux which is convenient to solve the moving boundary problem. The first step to solve the moving boundary problem is to discriminate wet and dry cells in order to find the exact location of the boundaries between the wet and the dry cells. This process is necessary to prevent numerical instability and computing inefficiency which are caused by cells that are almost dry i.e. having very small water depth. If the water depth of a cell is very small, then the velocity components (u, v) of the cell can have very high value because the values of u and v are obtained by dividing hu and hv by the water depth h . The extremely high values of the velocity components can cause numerical instability and the numerical scheme would need very small update time step which subsequently leads to longer computing time. To prevent numerical inefficiency, cells having smaller water depth than a specified tolerance h_{tol} should be detected and given zero velocity components, i.e. $u = v = 0$. These cells are considered as cells on the moving boundary. The tolerance $h_{tol} = 10^{-5}$ is used throughout this thesis. Then, the numerical flux between a wet and a dry cell can be obtained by considering the following two cases:

1. The water surface level of a wet cell is higher than the bottom level of the adjacent dry cell as shown in *Figure 5.4(a)*: $h_{wet} + z_{bwet} \geq z_{bdry}$. In this case, no special treatment is needed, in other words, the numerical flux \mathbf{H}^* can be calculated by the same method used in normal wet cells.
2. The water surface level of a wet cell is lower than the bottom level of the adjacent dry cell as shown in *Figure 5.4(b)*: $h_{wet} + z_{bwet} < z_{bdry}$. In this case,

there is no physical contact between two cells, so the numerical flux H^* should be set to zero to prevent leakage or inflow of mass and momentum through the cell interface.

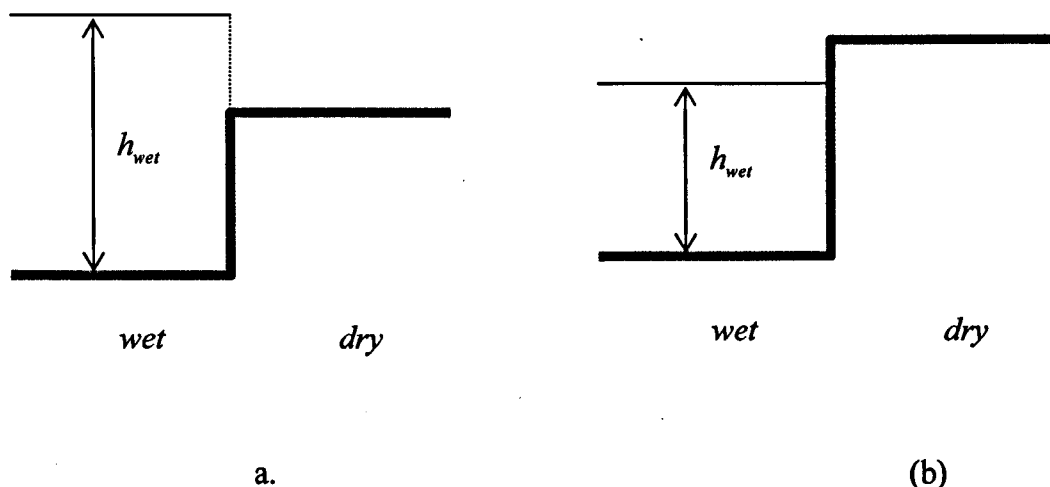


Figure 5.4 Two categories of wetting/drying boundary

Flux correction method for mass conservation

Having completed an update at each time step, the water depth of some cells near receding waves can have negative values as shown in Figure 5.5. This is unphysical and can violate global mass conservation because the value of the water depth is given as zero for the update at next time step and this causes an increase of the mass. The unphysical negative water depth is caused by the fact that the numerical fluxes have constant values during the time step Δt even after the water depth of the cell gone below 0, and this leads to the addition of artificial mass and momentum to the neighbouring cells and the increase of total mass volume. To remove this artificial mass and momentum, the numerical fluxes should be set to zero after the water surface level goes down below the bottom level. This process can be performed by calculating the modified flux H'^* which has been reduced from the flux H^* by multiplying the ratio of the time that the cell remained wet, tr , i.e.

$$\mathbf{H}^* = \mathbf{H} \times tr$$

where

$$tr = \frac{h_i^n}{h_i^n - h_i^{n+1}}$$

For example, if the cell (i, j) in a quadrilateral grid as shown in *Figure 5.6* has water depth $h_{i,j}^{n+1} < 0$ at time $t = t^{n+1}$, it means that some amount of artificial mass and momentum has been added to the neighbouring cells. To remove this artificial mass and momentum, the cell (i, j) should be treated as a dry cell at time $t = t^{n+1}$, i.e. $h_{i,j}^{n+1} = 0$ and $u_{i,j}^{n+1} = v_{i,j}^{n+1} = 0$. Then the variables in the neighbouring 4 cells, $(i+1, j)$, $(i-1, j)$, $(i, j+1)$, and $(i, j-1)$, should be recalculated with the reduced numerical flux \mathbf{H}^* .

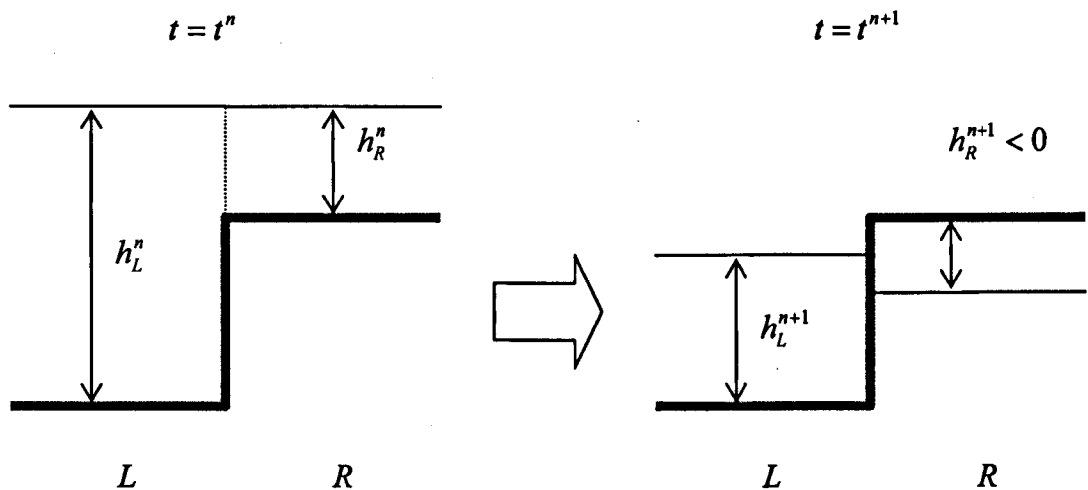


Figure 5.5 Decrease of water depth after a time step Δt

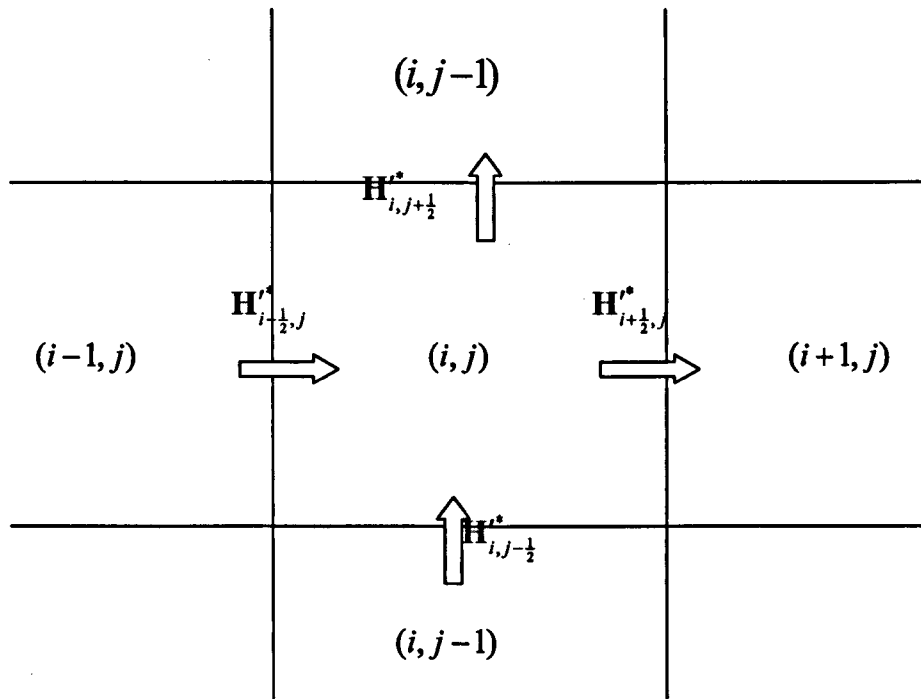


Figure 5.6 Recalculation of numerical fluxes on a quadrilateral grid

5.5 Numerical Tests and Results

In this section, the proposed numerical schemes are applied to several well-known test problems taken from the literature. The test cases presented here are chosen to demonstrate the ability of the schemes to achieve numerical balance and solve the wetting/drying problem. To secure numerical stability, $CFL = 0.9$ is used and the problem domains are discretized by using rectangular structured grids.

Problem 1 (Wave propagation)

Leveque [62] presented this test problem to demonstrate wave propagation caused by a small perturbation of a steady-state solution over variable topography. The frictionless variable bed elevation is defined by

$$z_b(x, y) = 0.5 \exp(-50((x - 0.1)^2 + (y - 0.1)^2))$$

for rectangular domain $0 < x, y < 1$. The initial conditions are stationary water with $u = v = 0$ and a perturbed free surface profile given by

$$z_s = \begin{cases} 1.01 & (0.1 < x < 0.2) \\ 1.0 & (\text{otherwise}) \end{cases}$$

At the beginning of the simulation, the perturbation leads to two waves propagating with characteristic speeds $\pm \sqrt{gh}$ and the left moving wave leaves the domain while the right moving one propagates over the two-dimensional hump. All the boundaries are regarded as transmissive open boundaries and the gravitational acceleration is set to $g = 1m^2/s$ according to Leveque [62]. The water surface level profiles at $t = 0.69s$ are obtained on a uniform 100×100 square grid.

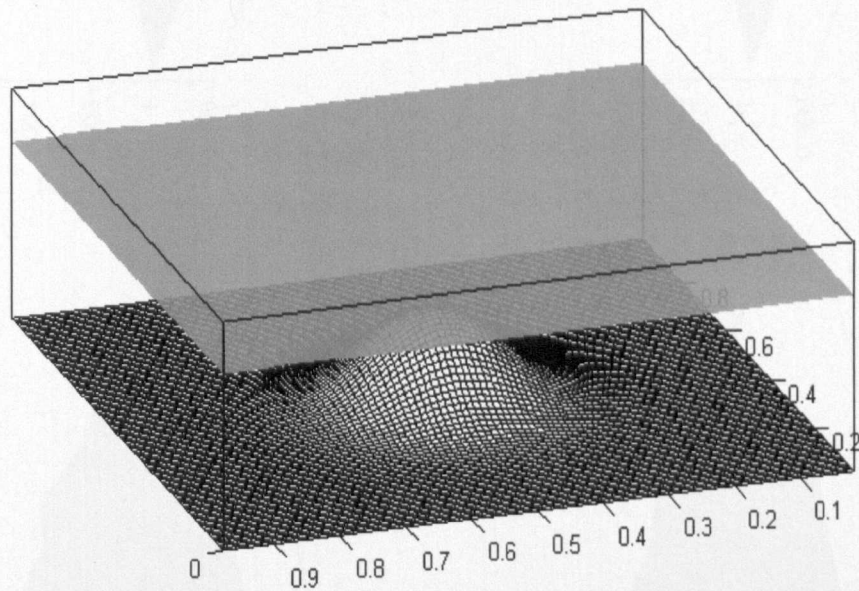


Figure 5.7 Geometry and initial condition for Problem 1.

The numerical solutions to *Problem 1* are presented in *Figure 5.8* and *5.9*. As shown in the figures, all the proposed schemes show well-balanced water surface profiles and contours without any numerical noise. The two approximate Riemann solver based schemes show similar results and TVD-LW scheme reproduces the sharpest advancing wave while LF scheme presents the smoothest water surface profile. To show the property of each scheme, the water surface level at $y = 0.5m$ and $x = 0.8m$ are compared in *Figure 5.10* and *5.11*. The numerical results show good agreement with those presented in other literature [51, 70].

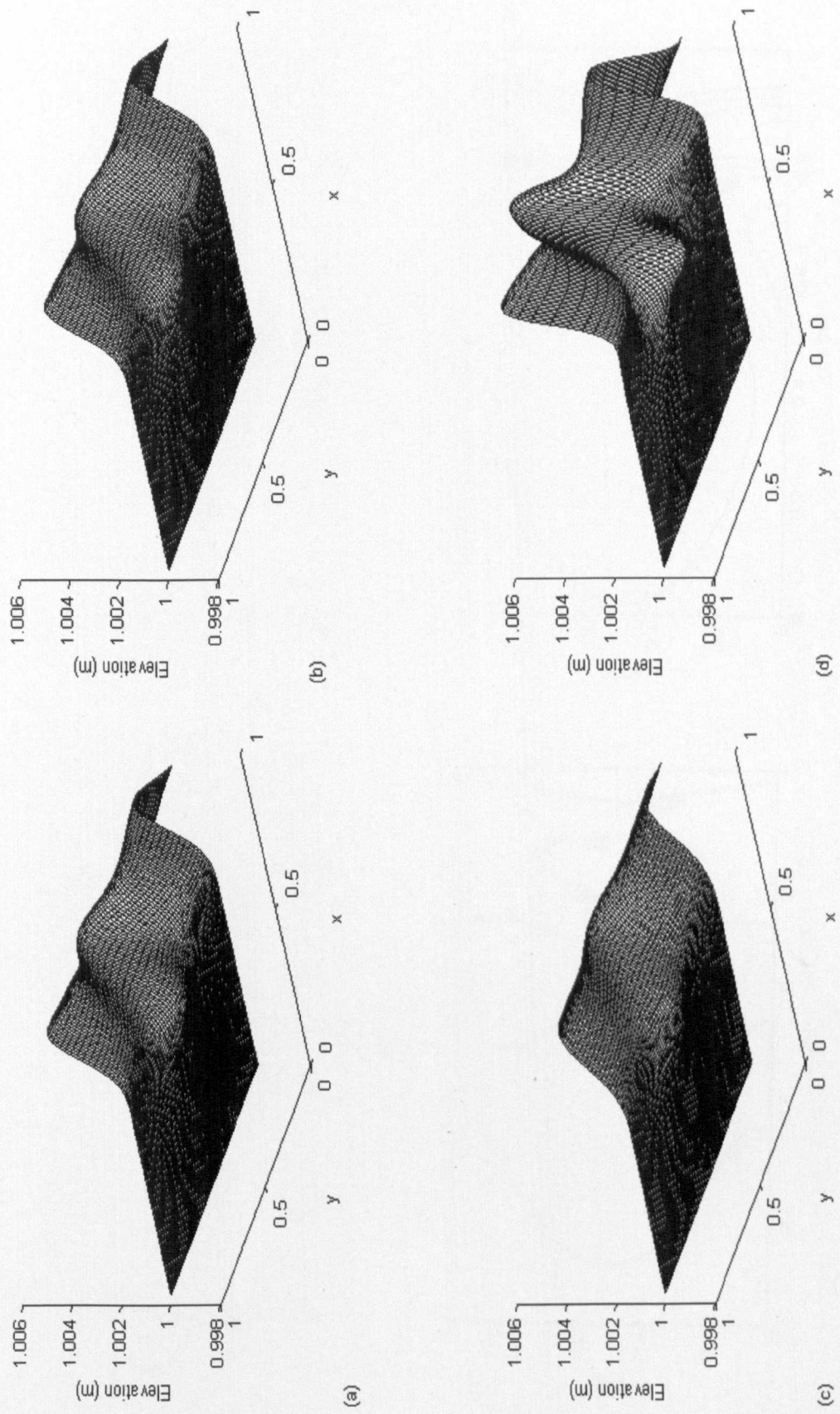


Figure 5.8 Water surface profiles for Problem 1: (a)Roe, (b)HLL, (c)LF and (d)TVD-LW

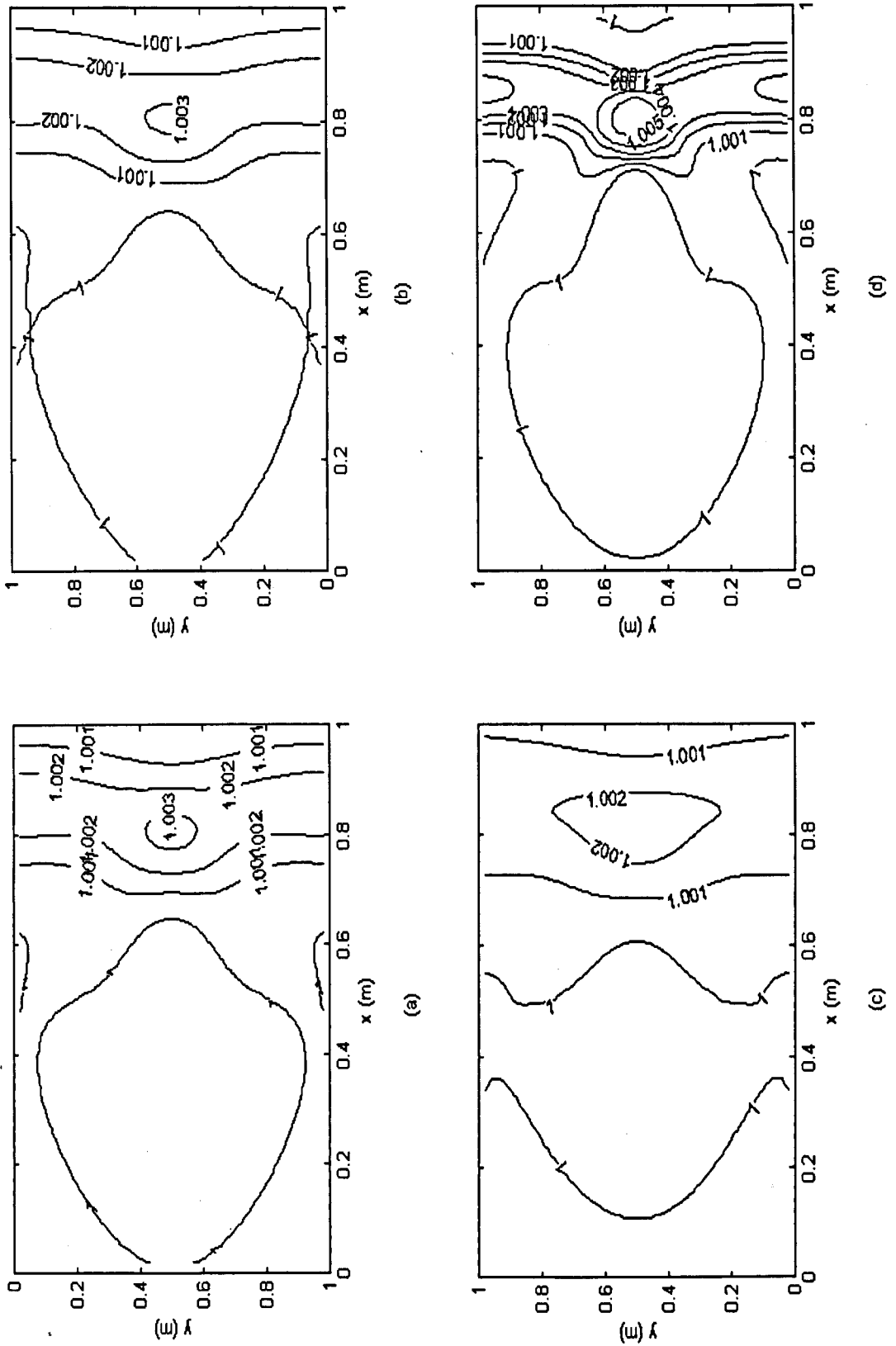


Figure 5.9 Water surface contours for Problem 1: (a)Roe, (b)HLL, (c)LF and (d)TVD-LW

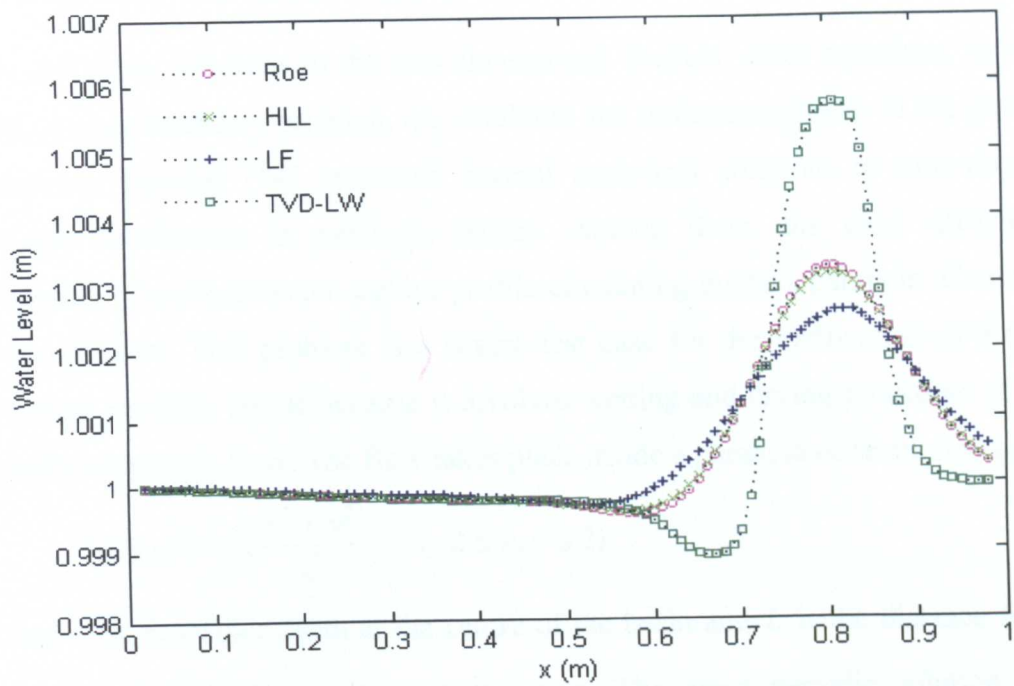


Figure 5.10 Water surface profiles at $y = 0.5m$

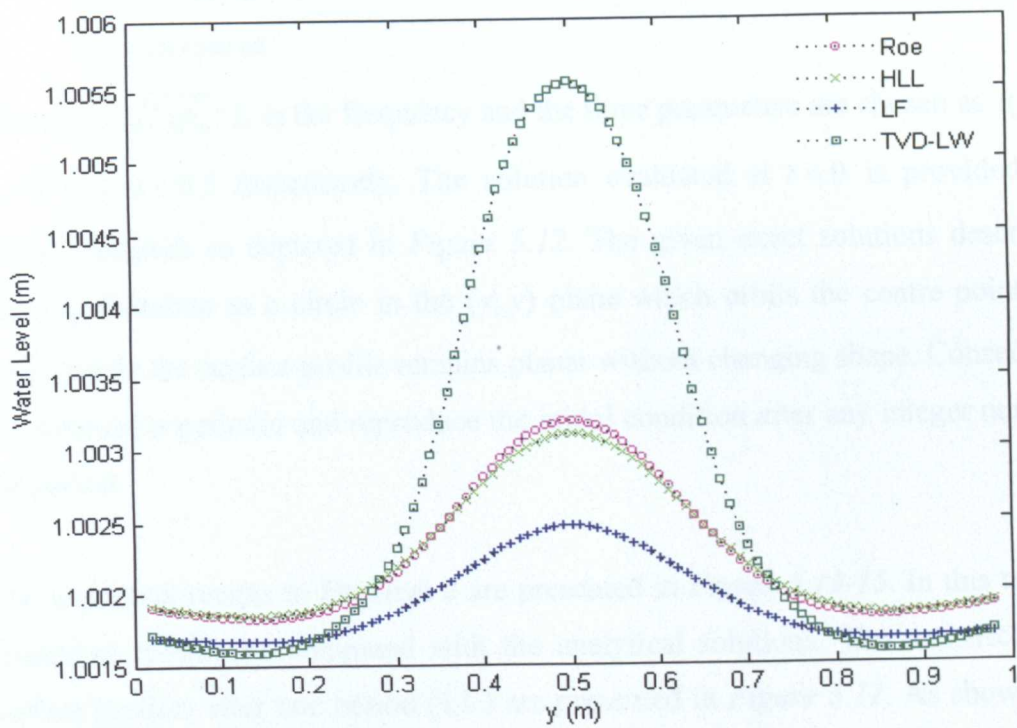


Figure 5.11 Water surface profiles at $x = 0.8m$

Problem 2 (Flow around parabolic basin)

Few analytical solutions to the two-dimensional shallow water equations, especially with moving boundary problem, are available due to the complexity of the governing equations. Thacker [74] presented several analytical solutions to time-dependent periodic oscillations in parabolic basins. Among them, the most difficult one consisting of a planar water surface profile circulating inside a parabola of revolution is chosen here. This problem is a severe test case for the verification of a moving boundary problem solver because it involves wetting and drying procedure of a non-radially symmetric flow. The flow takes place inside a parabola of revolution given by

$$z_b(x, y) = -h_o \frac{x^2 + y^2}{L^2} \quad (-2 \leq x, y \leq 2)$$

where h_o is the water depth at the centre of the basin and L is the distance from the centre to the shoreline with zero elevation. The exact periodic solution can be expressed as the following water surface and velocity profiles:

$$z_s(x, y, t) = \frac{\eta h_o}{L^2} (2x \cos \omega t + 2y \sin \omega t - \eta),$$

$$u = -\eta \omega \sin \omega t,$$

$$v = -\eta \omega \cos \omega t$$

where $\omega = \sqrt{2gh_o} / L$ is the frequency and the three parameters are chosen as $h_o = 0.1$, $L = 1$ and $\eta = 0.5$ respectively. The solution evaluated at $t = 0$ is provided as an initial condition as depicted in *Figure 5.12*. The given exact solutions describe the moving shoreline as a circle in the (x, y) plane which orbits the centre point of the basin, while the surface profile remains planar without changing shape. Consequently, the solution is periodic and reproduce the initial condition after any integer number of the period.

The numerical results to *Problem 2* are presented in *Figure 5.13-15*. In this test case, numerical results are compared with the analytical solutions. The numerical water surface profiles after one period ($1T$) are presented in *Figure 5.11*. As shown in the figure, the proposed numerical schemes show good agreement with the analytical solutions except LF schemes which produces diffusive solutions. The numerical

velocity components and water depth contours are shown in *Figure 5.14* and *5.15* and show similar trends. The second-order scheme (TVD-LW) produces very accurate solutions while LF scheme shows distorted results. It is because the second-order accurate scheme produces less diffusive solution than first-order accurate schemes while LF scheme shows bigger diffusion than Riemann solver based schemes. The diffusive property has similar effect to the introduction of artificial viscosity for the domain and, as a result, the body of water moves slowly.

Problem 3 (Tidal wave over an variable adverse slope)

This test was presented by Heniche et al. [49] and Brufau et al. [12]. Heniche et al. simulated this problem with a finite element model while Brufau et al. used a Riemann solver based finite volume model. In this test, the wave run-up and run-down process driven by a tidal wave in a rectangular channel with a variable slope is reproduced and the performance of the wetting/drying problem solver is tested. The 500m long and 25m wide rectangular channel has the following variable bed slope:

$$S_o = -0.001 \quad (x \leq 100m)$$

$$S_o = -0.01 \quad (100m < x \leq 200m)$$

$$S_o = -0.001 \quad (200m < x \leq 500m).$$

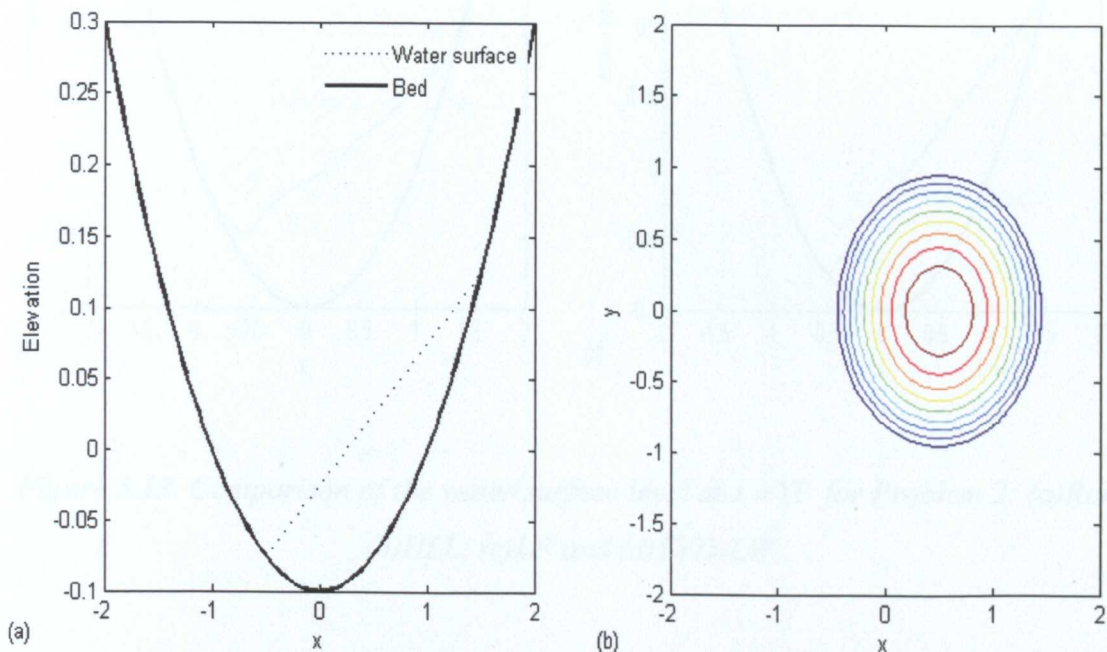


Figure 5.12 Initial condition for Problem 3: (a) surface profile and (b) depth contour

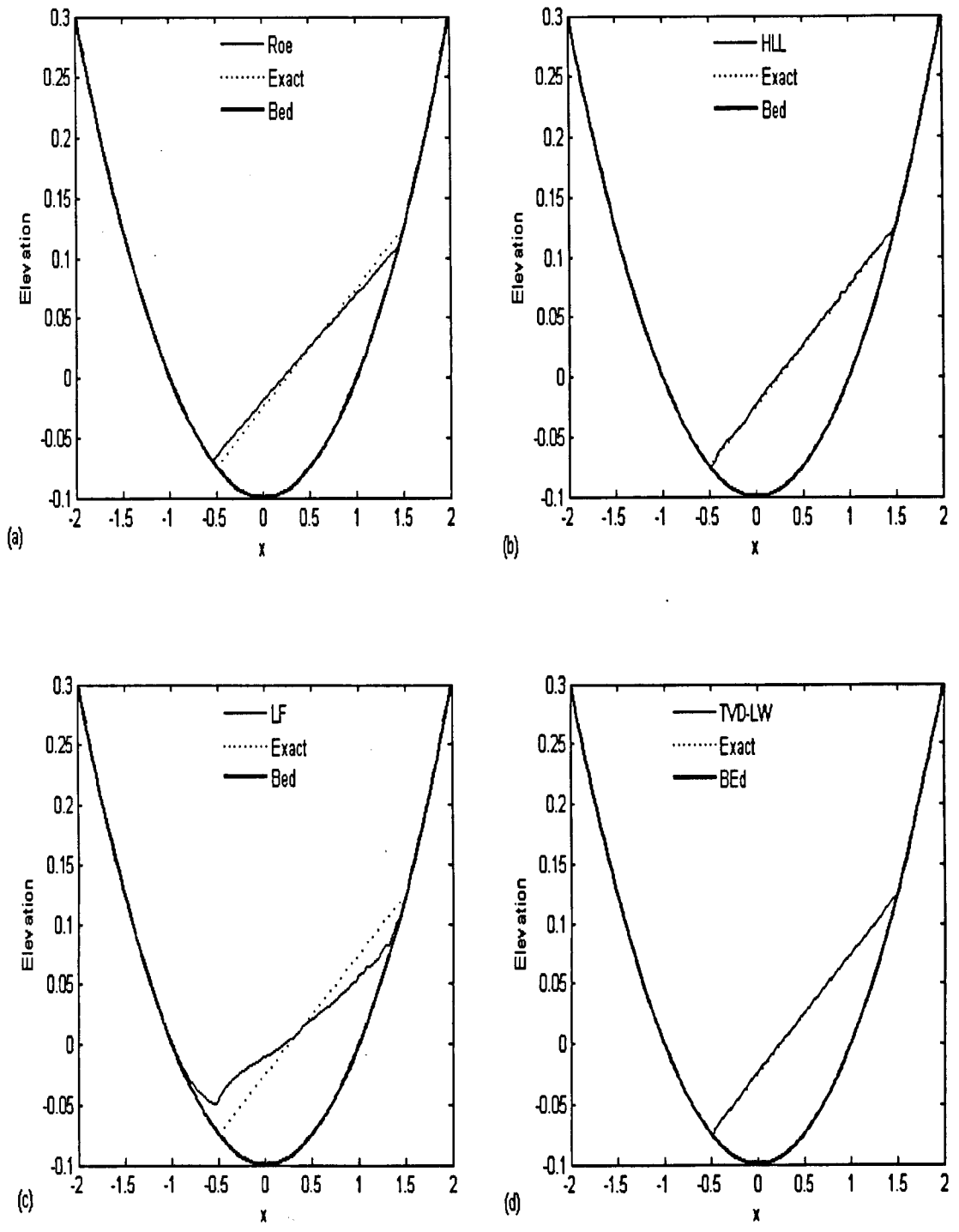


Figure 5.13 Comparison of the water surface level at $t = 1T$ for Problem 2: (a)Roe, (b)HLL, (c)LF and (d)TVD-LW

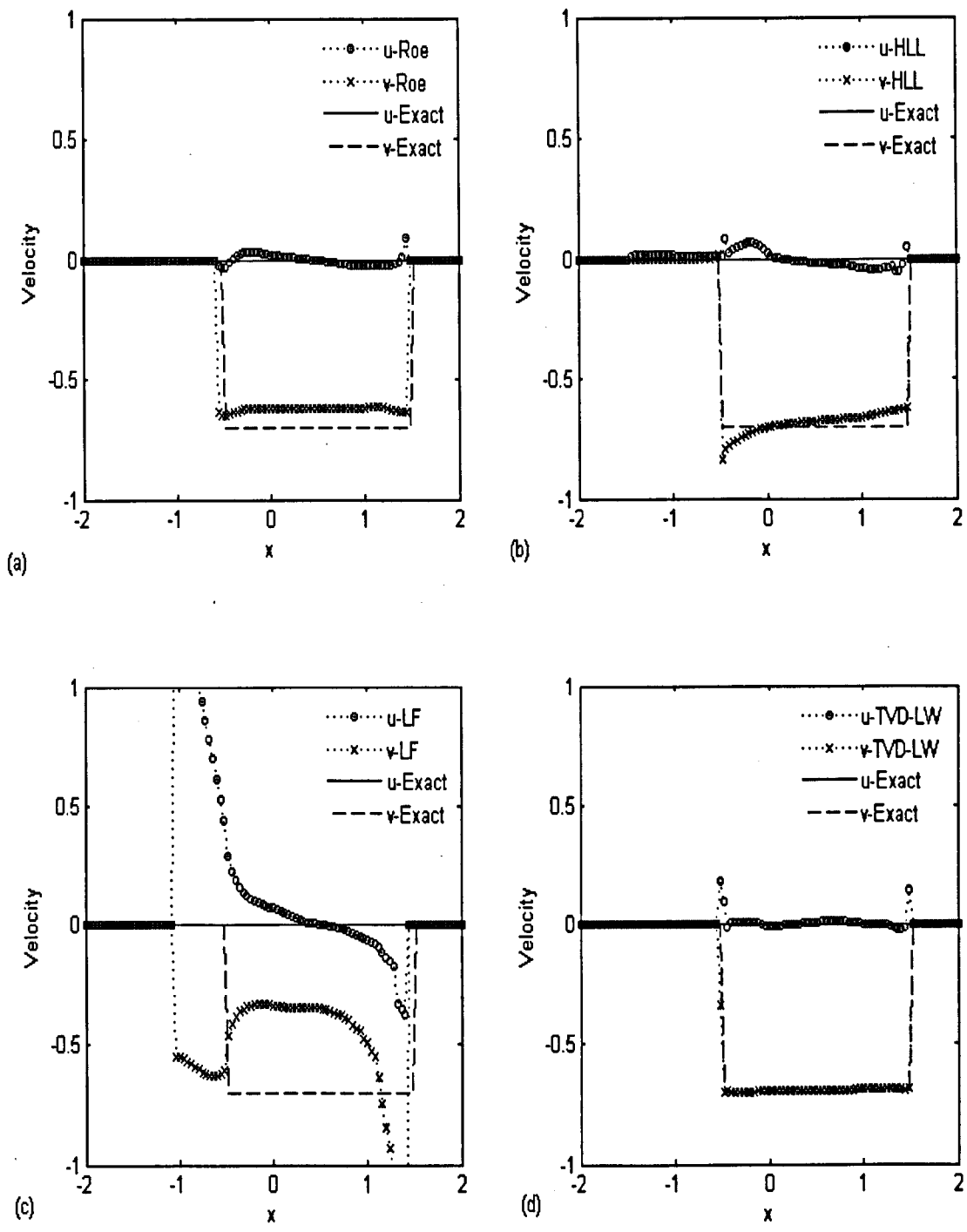


Figure 5.14 Comparison of the velocity components at $t = 1T$ for Problem 2: (a)Roe, (b)HLL, (c)LF and (d)TVD-LW

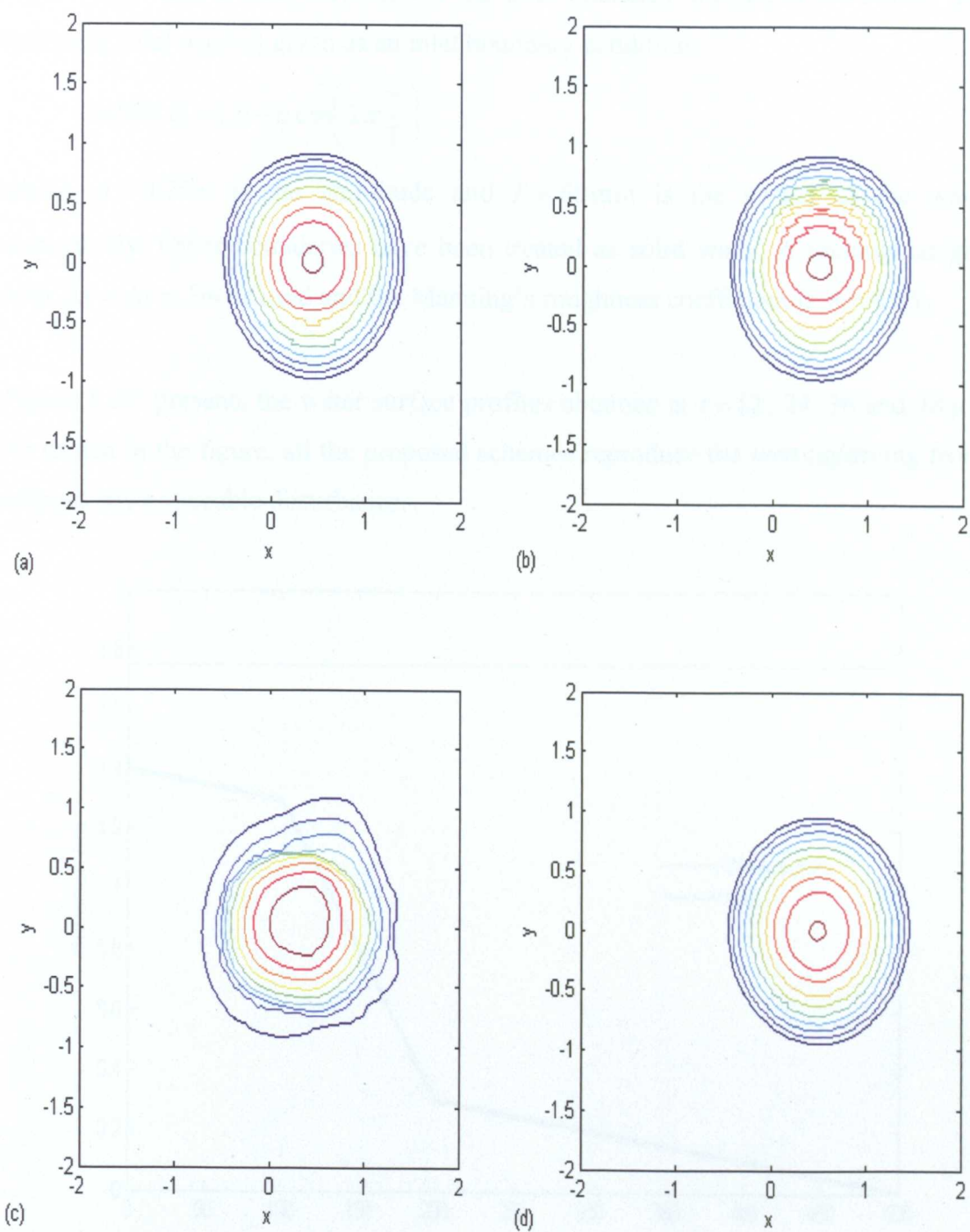


Figure 5.15 Water depth contours at $t=1T$ for Problem 2: (a)Roe, (b)HLL, (c)LF and (d)TVD-LW

The initial condition is a still water with free surface $H = 1.75m$ as shown in *Figure 5.16*. and a tidal wave enters the inlet boundary located at $x = 500m$. The following tidal wave is given as an inlet boundary condition:

$$h(500,t) = 1.0 + \eta \cos\left(2\pi \frac{t}{T}\right)$$

where, $\eta = 0.75m$ is the amplitude and $T = 60min$ is the period of the wave, respectively. Other boundaries have been treated as solid walls. A rectangular grid with $\Delta x = \Delta y = 5m$ is used and the Manning's roughness coefficient is $n = 0.03$.

Figure 5.17 presents the water surface profiles obtained at $t = 12, 24, 36$ and $48min$. As shown in the figure, all the proposed schemes reproduce the wetting/drying fronts without any noticeable disturbance.

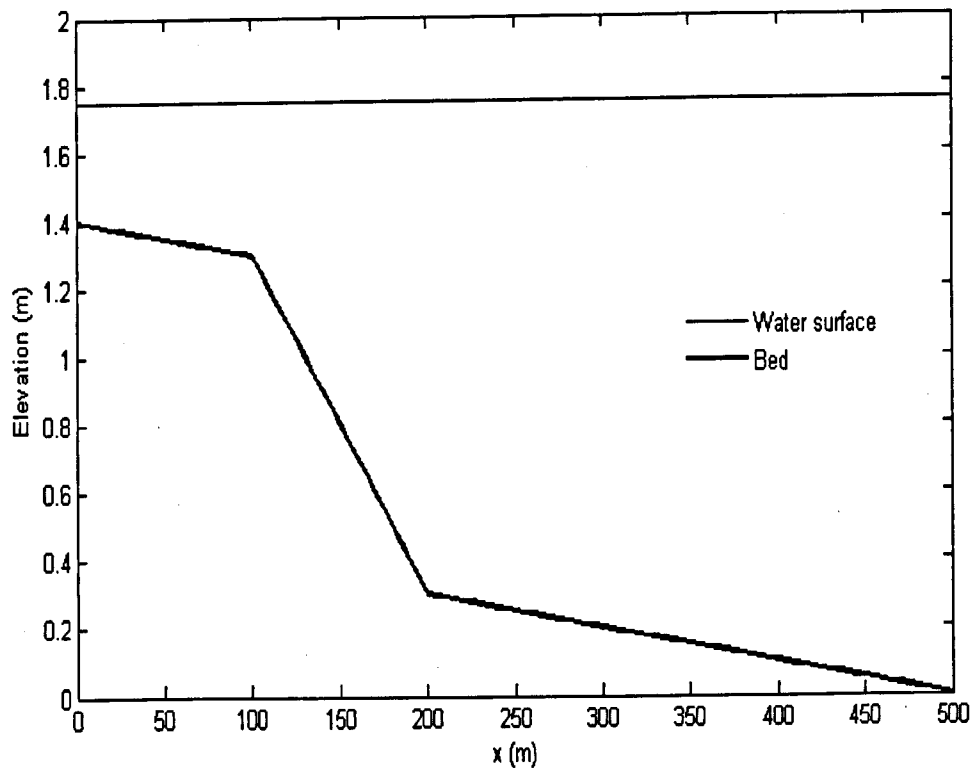


Figure 5.16 Geometry and initial condition for Problem 3.

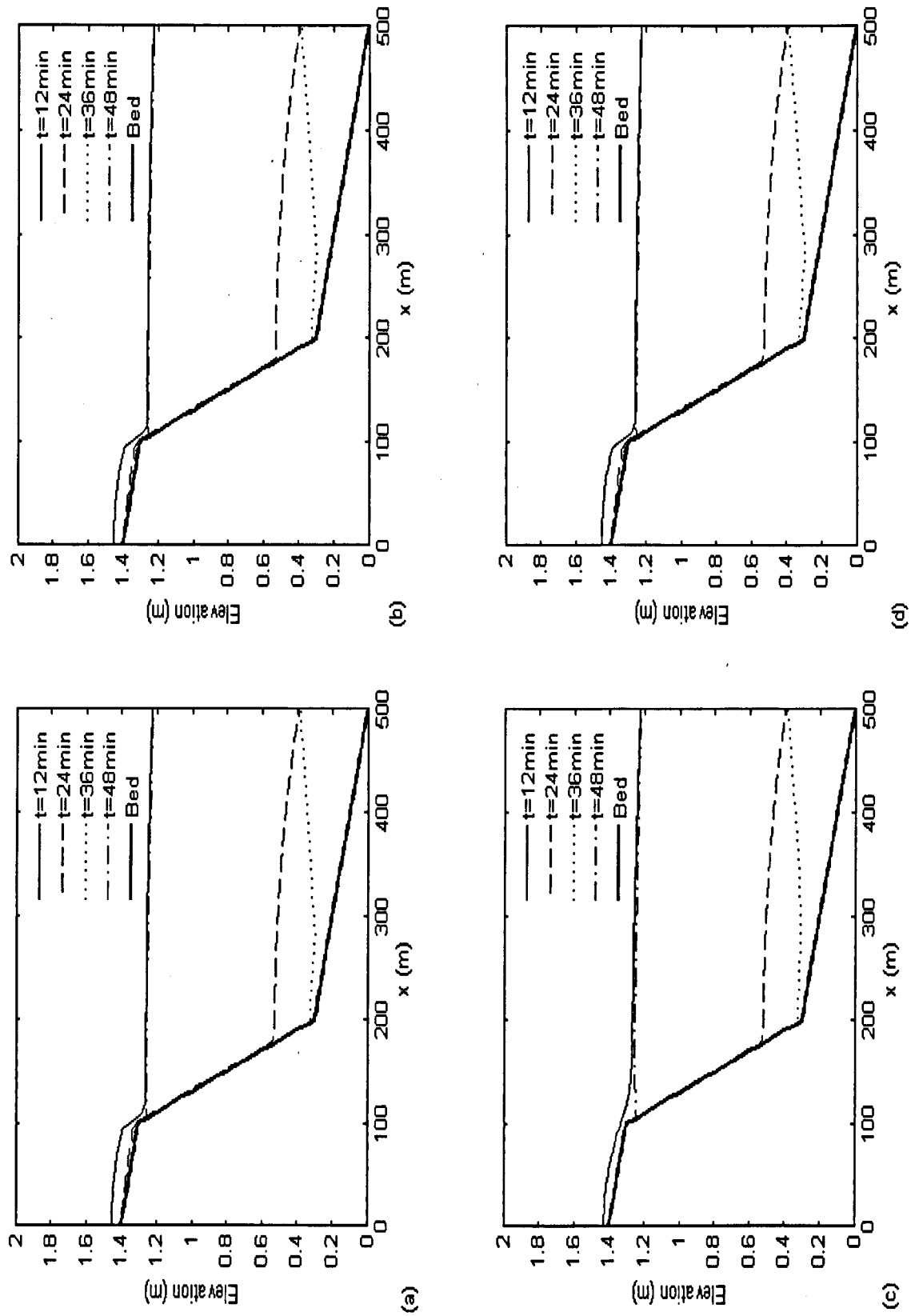


Figure 5.17 Water depth profiles for Problem 3: (a)Roe, (b)HLL, (c)LF and (d)TVD-LW

To demonstrate the benefit of using the flux correction method for negative water depth, mass conservation errors are computed by using the following:

$$\text{Mass error (\%)} = \frac{V_i + Q_{net} - V_f}{V_i} \times 100$$

where, V_i is the initial total mass volume, V_f is the sum of the mass volume remaining in the domain and Q_{net} is the net inflow of mass through the boundaries. The time history of mass conservation error of this problem is depicted in *Figure 5.18*. According to the figure, the mass conservation error due to the negative water depth is removed by using the flux correction method proposed in this chapter.

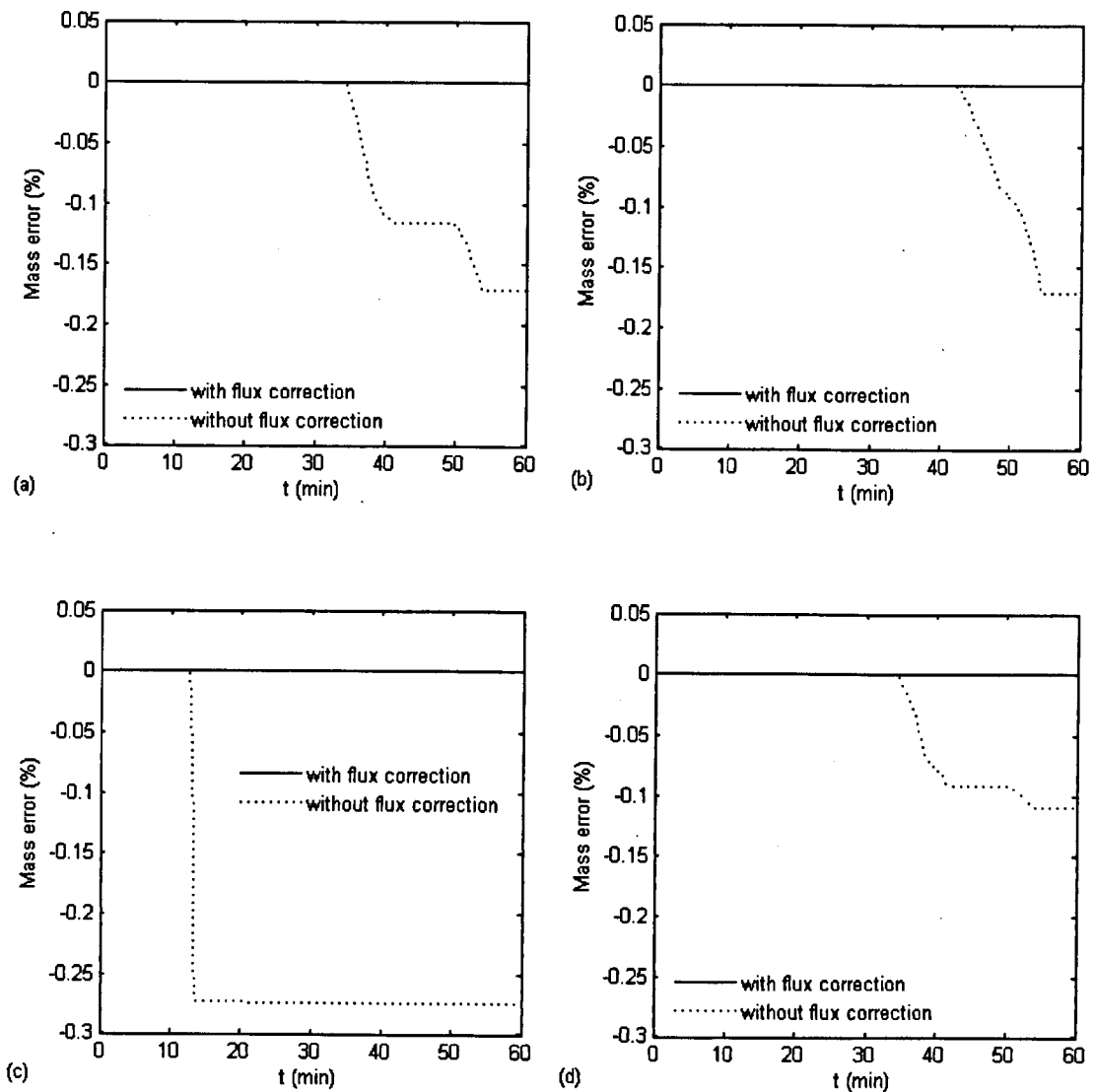


Figure 5.18 Mass conservation error histories for Problem 3: (a)Roe, (b)HLL, (c) LF and (d)TVD-LW

Problem 4 (Dam-break over a channel with three mounds)

This test was proposed by Kawahara and Umetsu [56] and used by Brufau et al. [12] and Begnudelli and Sanders [8]. In this problem, the propagation of the flood wave caused by a sudden collapse of a dam over a complicated channel geometry consisting of three mounds is simulated. The channel geometry used in [8] is chosen here because the detailed geometry is not specified in other literature. The channel is $75m$ long and $30m$ -wide and includes three mounds, two small and one big, which are located at $(x,y) = (30,6)$, $(30,24)$, and $(47.5,15)m$, as shown in *Figure 5.19*. The bottom radius and side slope of each mound is $8, 8, \text{ and } 10m$ and $1/8, 1/8, \text{ and } 3/10$, respectively. The dam is located at $x = 11m$ and the initial upstream water depth is set $h = 1.875m$. The downstream area is considered as a dry bed and the Manning's roughness coefficient is $n = 0.018$. A rectangular grid with $\Delta x = \Delta y = 0.5m$ is used and numerical simulation is performed during the time $t = 0 \sim 30\text{sec}$.

Figure 5.20 and *5.21* present the numerical water surface profiles and contours for this problem. To show the property of each scheme, the water surface level at $y = 15m$ and $y = 5m$ are compared in *Figure 5.22* and *5.23*. The time history of mass conservation error of this problem is depicted in *Figure 5.24* and show similar results to Problem 3, which means that most of the mass conservation error is removed by using the flux correction method developed in this thesis.

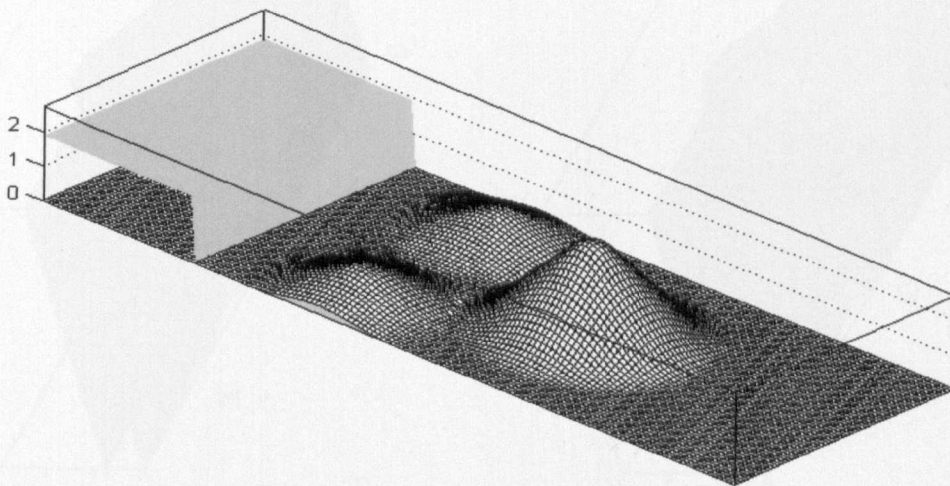


Figure 5.19 Channel geometry and initial water depth for Problem 4

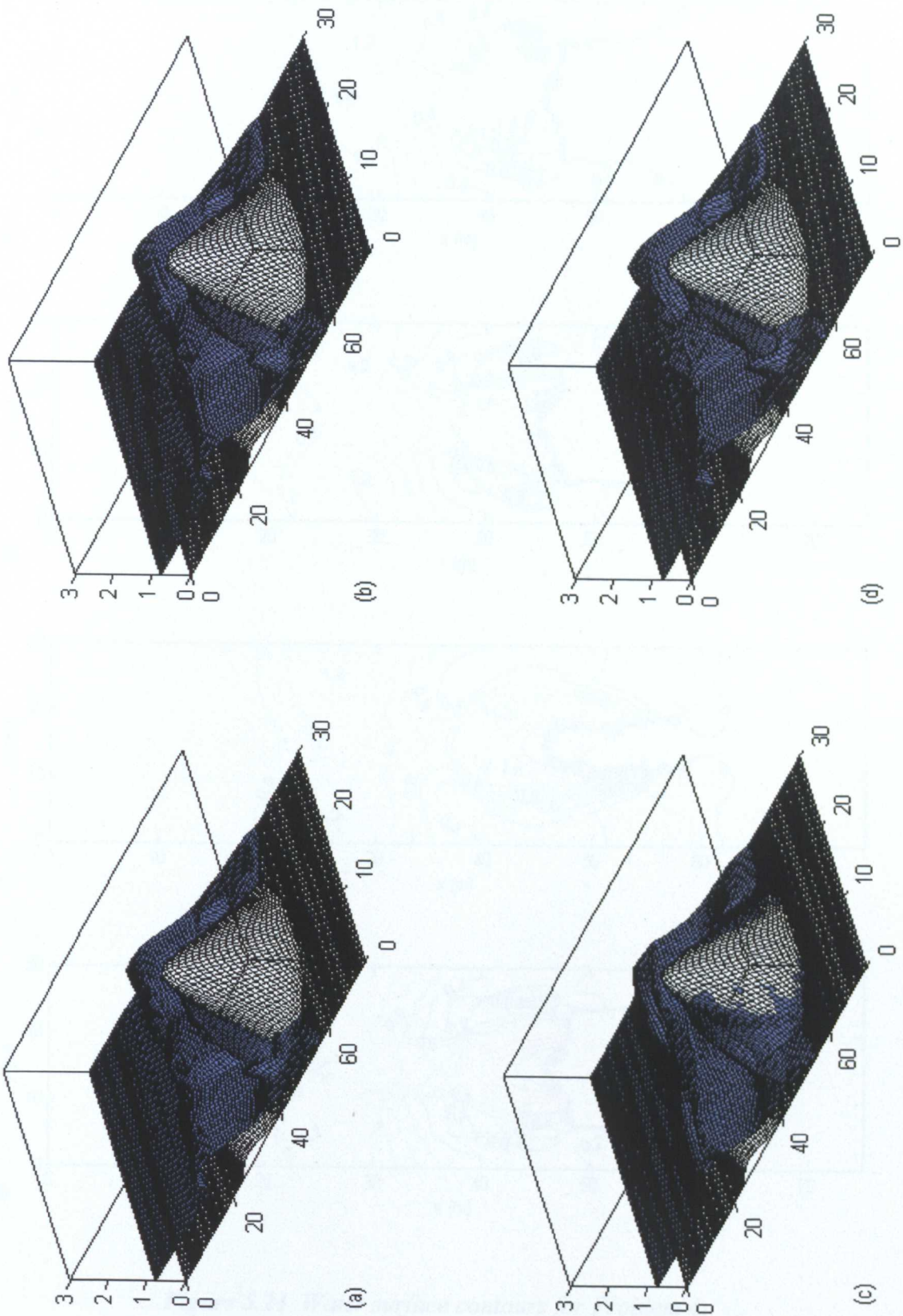


Figure 5.20 Water surface profiles for Problem 4: (a)Roe, (b)HLL, (c)LF and (d)TVD-LW

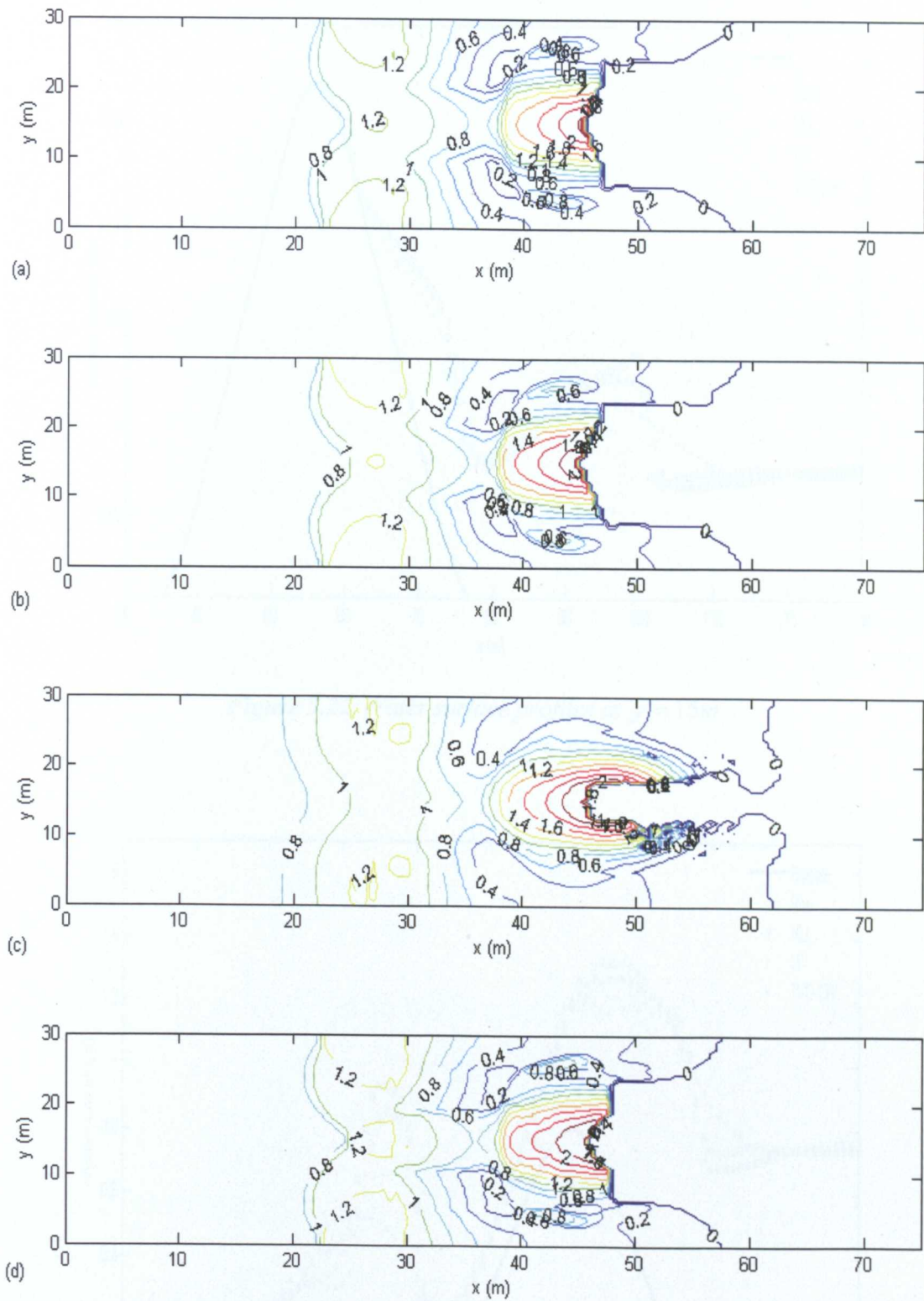


Figure 5.21 Water surface contours for Problem 4:

(a)Roe, (b)HLL, (c)LF and (d)TVD-LW

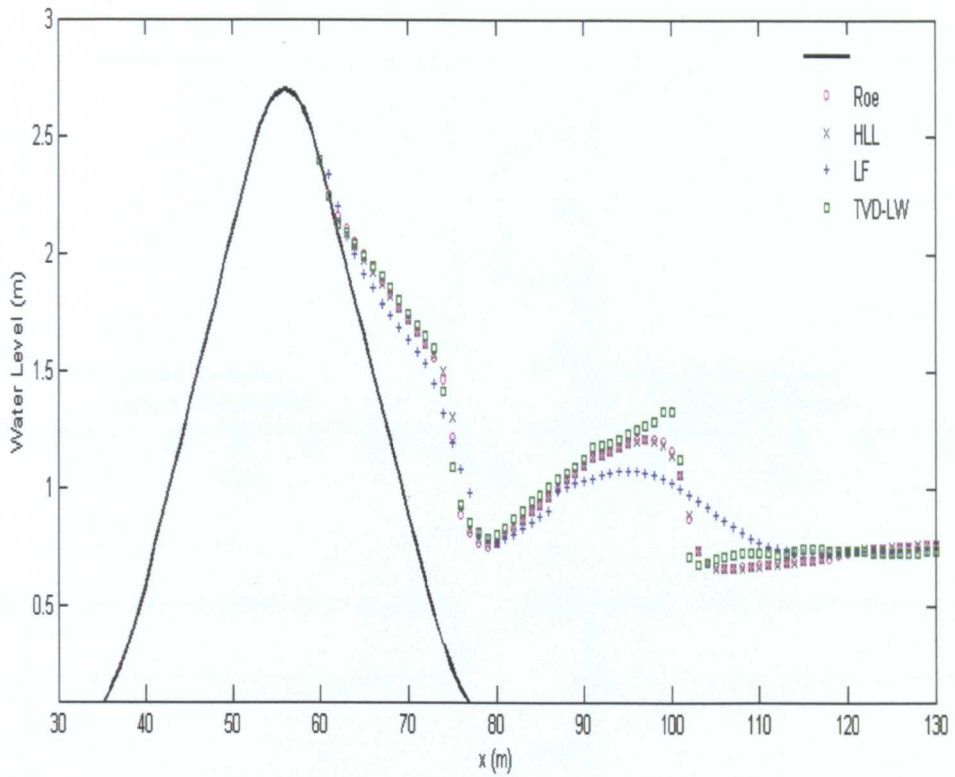


Figure 5.22 Water surface profiles at $y = 15m$

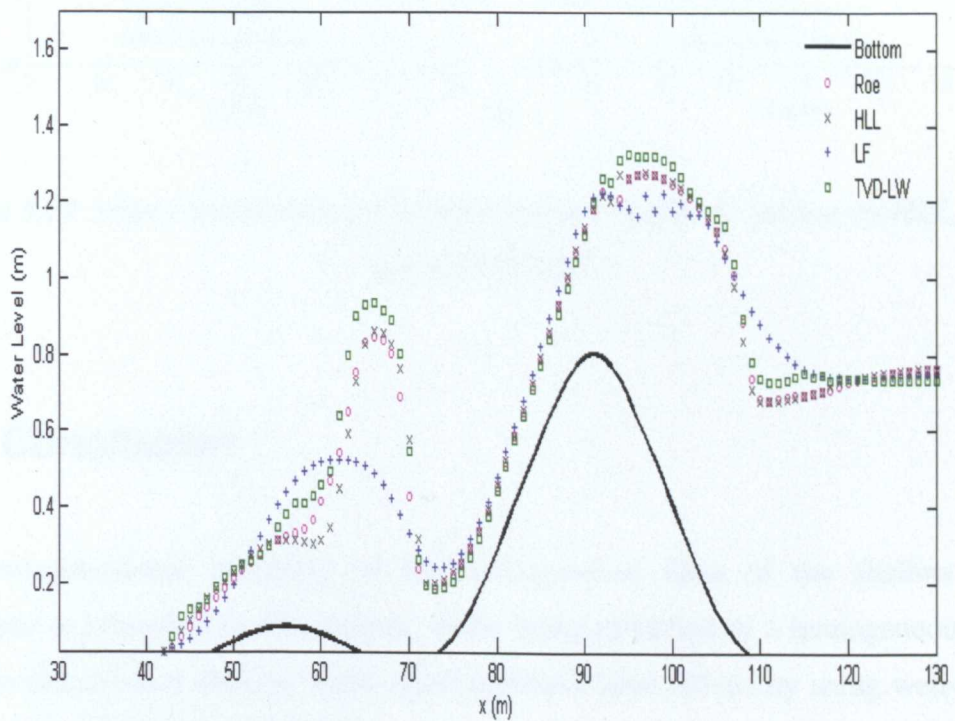


Figure 5.23 Water surface profiles at $y = 5m$

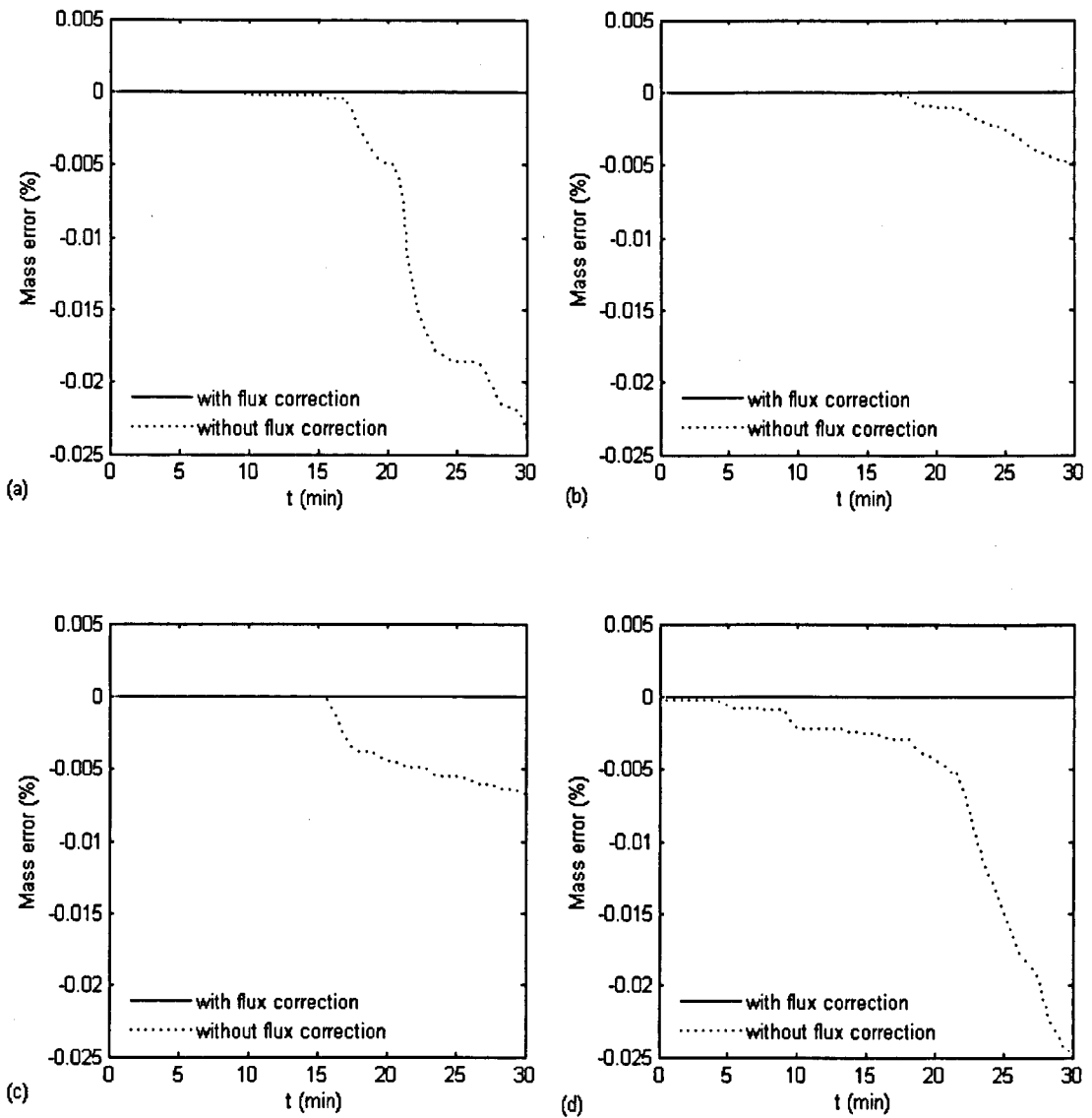


Figure 5.24 Mass conservation error histories for Problem 4: (a)Roe, (b)HLL, (c)LF and (d)TVD-LW

5.6 Conclusion

The two-dimensional extension of the homogeneous form of the shallow water equations is presented in this chapter. After being modified to a homogeneous form the two-dimensional shallow water equations have been solved by using well-known conservative numerical schemes.

The homogeneous form numerical schemes have been applied to several bench-mark test cases and produced numerically well-balanced results to the flow over an irregular channel geometry. Moreover, the proposed wetting/drying problem condition solver which uses the integrated numerical flux shows good results and almost zero mass conservation errors. Through Chapter 4 and 5, the homogeneous form of the shallow water equations and its solutions in both one- and two-dimension are presented. As shown in the numerical results, the proposed method solves numerical problems caused by the existence of the geometric source terms very accurately. It is straightforward for the proposed technique to be implemented as a useful methodology to model natural river flow problems which consist of severe variation of channel geometry and rapidly varying flow conditions. In the next chapter, the application of this approach to the natural river flow problems is presented.

Chapter 6

Application: flood modelling over natural geometry

In the previous chapters, the homogeneous form shallow water equations which can solve one- and two-dimensional open channel flows over irregular geometry have been proposed. The proposed numerical schemes based on the homogeneous form shallow water equations were applied to several benchmark problems and produced very accurate results. The ultimate goal of developing a new numerical method is to model real flood events in which maximum water depth or inundation extent can be obtained. In this chapter, the conservative finite volume schemes presented in the previous chapters are applied to several flood events including one- and two-dimensional cases. The 1996 and 1999 floods in the Im-jin River, Korea which has highly irregular channel geometry is chosen for one-dimensional flood modelling whilst a hypothetical flood caused by a sudden breach of the embankment in the Sung-seo district of Korea near the Nak-dong river is modeled by the two-dimensional numerical scheme. Finally, an urban flood event in a small catchment within the city of Glasgow, U.K. is modelled with the proposed numerical schemes.

6.1 One-dimensional modelling of the Im-jin river Flood

6.1.1 Introduction

The floods events in 1996 and 1999 in the Im-jin river basin are modelled with the proposed homogeneous form numerical schemes. The Im-jin River is located in the middle of the Korean peninsula and has its origin in the mountainous area of North Korea. The river receives inflows from the mountainous catchment areas upstream and its main tributary, the Han-tan River, which has very steep bed slope and highly irregular channel geometry. The river basin has repeatedly suffered severe floods mainly due to the rapidly rising flood waves caused by heavy rainfalls and steep mountainous upstream catchment area. Moreover, the main channel and tributaries

have few floodplains and very confined channel geometry, which makes the flood wave propagate very fast. The recent severe flood events occurred in 1996 and 1999 and were caused by the sudden torrential rainfall all over the basin. The recorded rainfalls and losses are summarized in *Table 6.1*.

	1996	1999
Date	July 26 ~ 28	July 31 ~ August 3
Average rainfall (mm)	600	700
Loss (£)	162 million	177 million
Inundated area (ha.)	10,799	40,978
Casualties (person)	18	9

Table 6.1 The recorded rainfalls and losses in 1996 and 1999 flood events



(a)



(b)

Figure 6.1 1999 flood event : (a) Downstream area of the Im-jin River, (b) An inundated village near the Im-jin River

6.1.2 Overview of the Study Site and Input Data

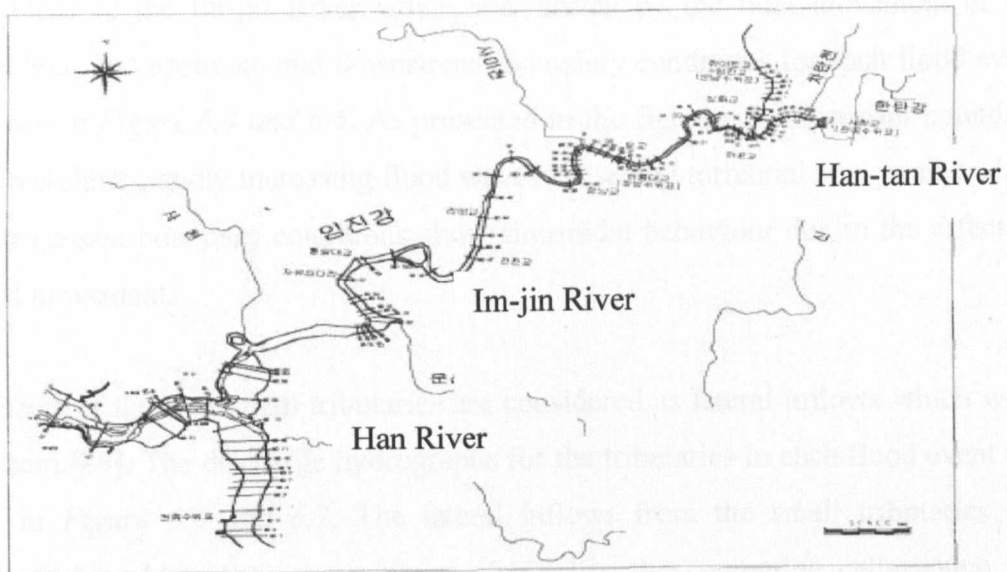
The length of the main channel considered in this simulation is 79.5 km which is a third of the total length of the Im-jin River. Two big tributaries, the Han-tan and Han Rivers, join the main channel at 13.5 and 67.3 km from the upstream boundary, respectively. The downstream boundary is the Yellow Sea. Inflows from four small tributaries, the Cha-tan, Sa-mi, Sa and Gok-reung Creeks, are also considered. The plan view and the simplified view of the Im-jin River system are shown in *Figure 6.2*.

The data needed for modelling open channel flows can be classified into the following two categories: topographic and hydraulic [28]. The topographic data describes physical properties of the modelled river system while the hydraulic data provides water levels, discharges and velocities which can be used for boundary conditions. All the topographic and hydraulic data are taken from the Ministry of the Construction and Transportation [88] who carried out a ground survey across the basin in 2001.

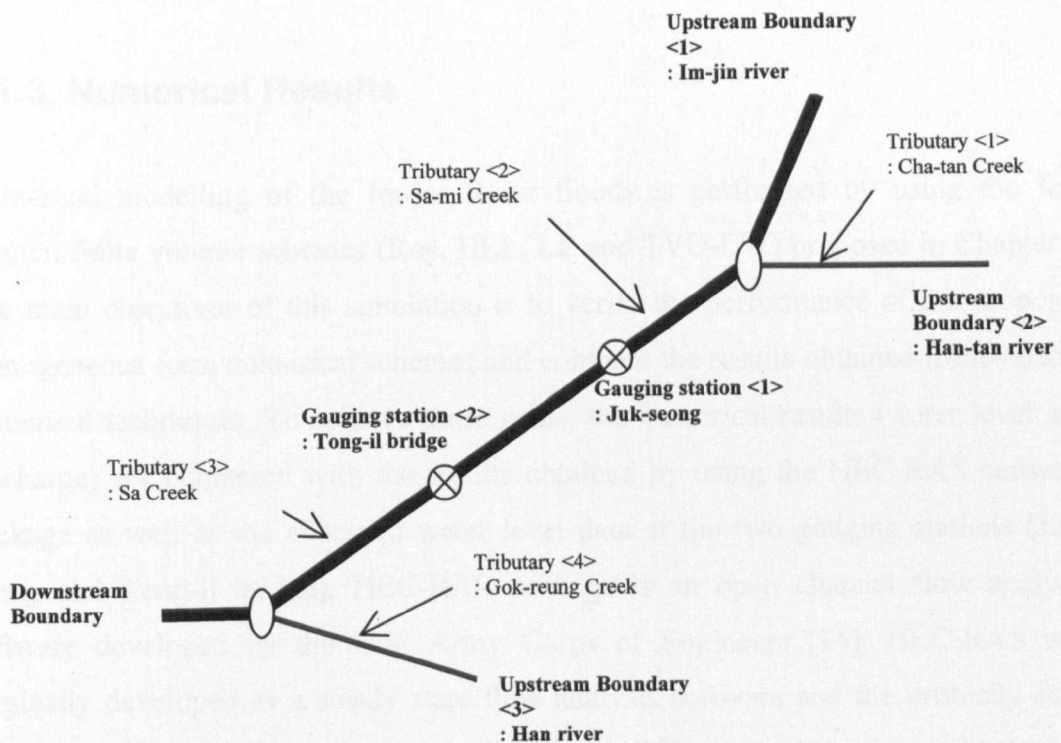
The most important topographic data for one-dimensional modelling of open channel flows is the channel geometry including the transverse profiles across river channels and friction coefficients. The transverse profiles are obtained at a uniform distance 100m apart for the main channel and two big tributaries. The Manning's friction coefficients which vary from 0.020 to 0.038 are given by [88] in which the friction coefficients were evaluated by the ground surveying and calibrated through the flood modelling performed by the Ministry of Construction and Transportation. The samples of channel geometry for the main channel (the Im-jin River) are shown in *Figure 6.3*. As shown in the figures, the upstream part of the Im-jin River has very confined and narrow channels while the lower part of the river has relatively wide and flat channel geometry.

Boundary conditions are given at the three upstream boundaries and one downstream boundary. Water level and discharge hydrographs which were recorded hourly in each flood event are used for upstream boundary conditions. The water level histories recorded at the Gun-nam and Jeon-gok gauging stations are used for the upstream

boundary conditions of the Im-jin and Han-tan Rivers respectively while the discharge history is used as the upstream boundary condition of the Han River.



(a)



(b)

Figure 6.2 Diagram of the Im-jin River network: (a) planview and (b) simplified view of the river network [88]

The downstream boundary condition is imposed as the water level hydrograph at the river mouth of the Im-jin River which was driven by the tidal movement of the Yellow Sea. The upstream and downstream boundary conditions for each flood event are shown in *Figure 6.4 and 6.5*. As presented in the figures, the upstream boundary conditions show rapidly increasing flood waves caused by torrential heavy rains while the downstream boundary conditions show sinusoidal behaviour due to the effect of the tidal movement.

The effects of the four small tributaries are considered as lateral inflows which were taken from [89]. The discharge hydrographs for the tributaries in each flood event are shown in *Figure 6.6 and 6.7*. The lateral inflows from the small tributaries are considered by adding the same amount of mass to the computing cells which are closest to the points where the tributaries join.

6.1.3. Numerical Results

Numerical modelling of the Im-jin River floods is performed by using the four explicit finite volume schemes (Roe, HLL, LF and TVD-LW) proposed in Chapter 4. The main objectives of this simulation is to verify the performance of the proposed homogeneous form numerical schemes and compare the results obtained from various numerical techniques. To achieve these goals, the numerical results (water level and discharge) are compared with the results obtained by using the HEC-RAS software package as well as the observed water level data at the two gauging stations (Juk-seong and Tong-il bridge). HEC-RAS package is an open channel flow analysis software developed by the U.S. Army Corps of Engineers [14]. HEC-RAS was originally developed as a steady state flow analysis software and the unsteady state flow analysis module featuring an implicit finite difference scheme was added later. In this simulation, the unsteady state flow module of the HEC-RAS version 3.1.3 which was initially presented in 2005 is used. To secure numerical stability of the

proposed explicit schemes 0.9 is used as *CFL* number and the computing time step of the HEC-RAS package is set to 30s.

The numerical results for 1996 flood event are presented in *Figure 6.8 and 6.9*. In *Figure 6.8*, the water level and discharge histories at the Juk-seong station are compared with those obtained by using HEC-RAS as well as the observed water level data. As presented in the figures, all the proposed finite volume schemes produce similar results and show good agreement with the observed data. According to the numerical results there is no significant difference between the results of each finite volume scheme. However, HEC-RAS package produces unstable results with oscillatory behaviour. The numerical results at Tong-il bridge station are presented in *Figure 6.9* and show similar tendency to the previous figure. In this case, the observed water level data are not available.

The numerical results for 1999 flood event are shown in *Figure 6.10 and 6.11*. As shown in the figures, the proposed finite volume schemes produce almost similar results and HEC-RAS shows slightly lower water levels and discharges than the proposed schemes at both stations. In case of 1999 flood, most of the observed data are not available due to the malfunctioning of the gauging stations and only a part of the water level history at the Tong-il bridge station is available. The proposed finite volume schemes and HEC-RAS produces lower water levels than the observed data.

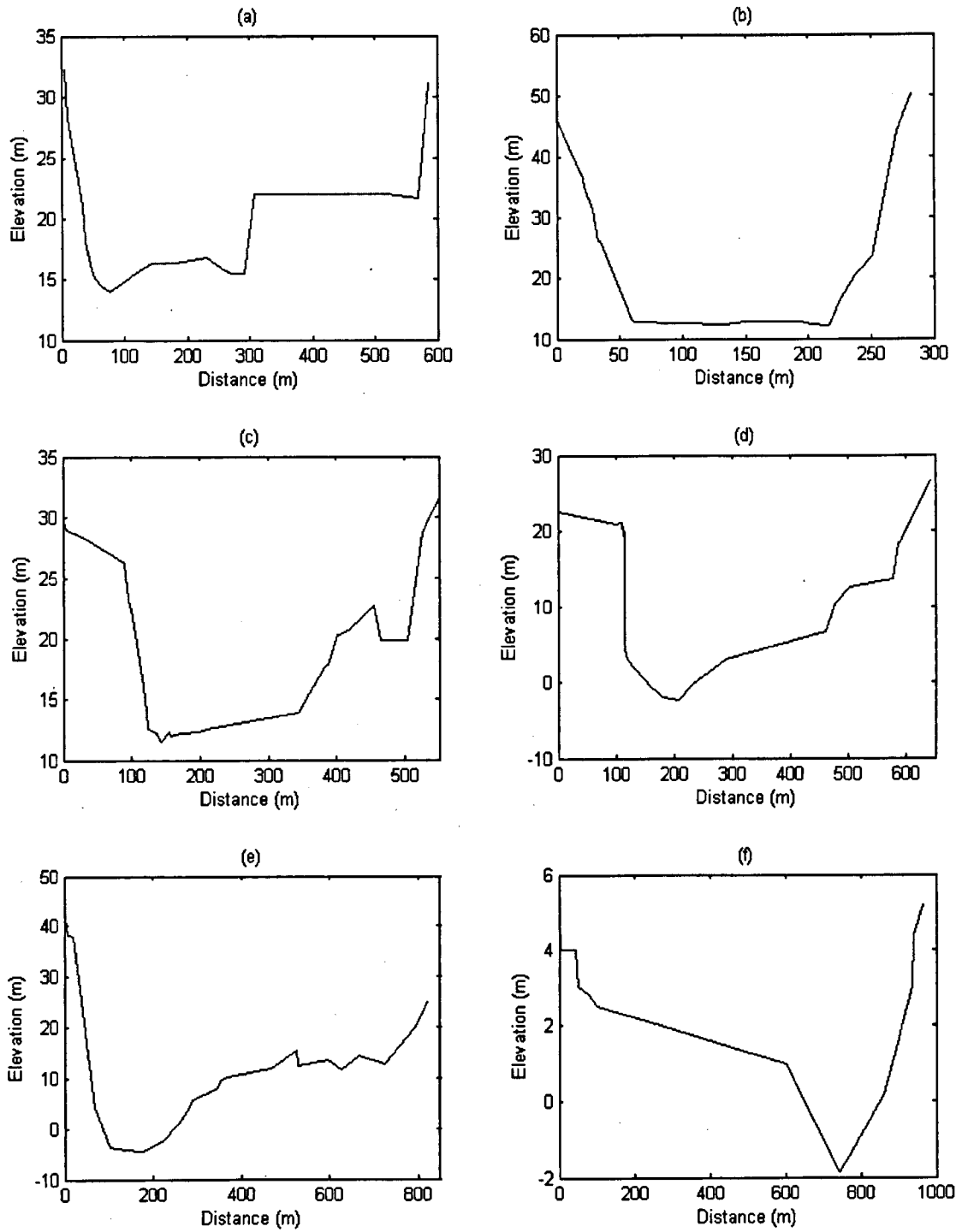


Figure 6.3 Cross-sectional profiles at different locations: (a) 3.2km, (b) 4.8km, (c) 5.9km, (d) 26.2km, (e) 35.8km and (f) 53.8km from the upstream boundary

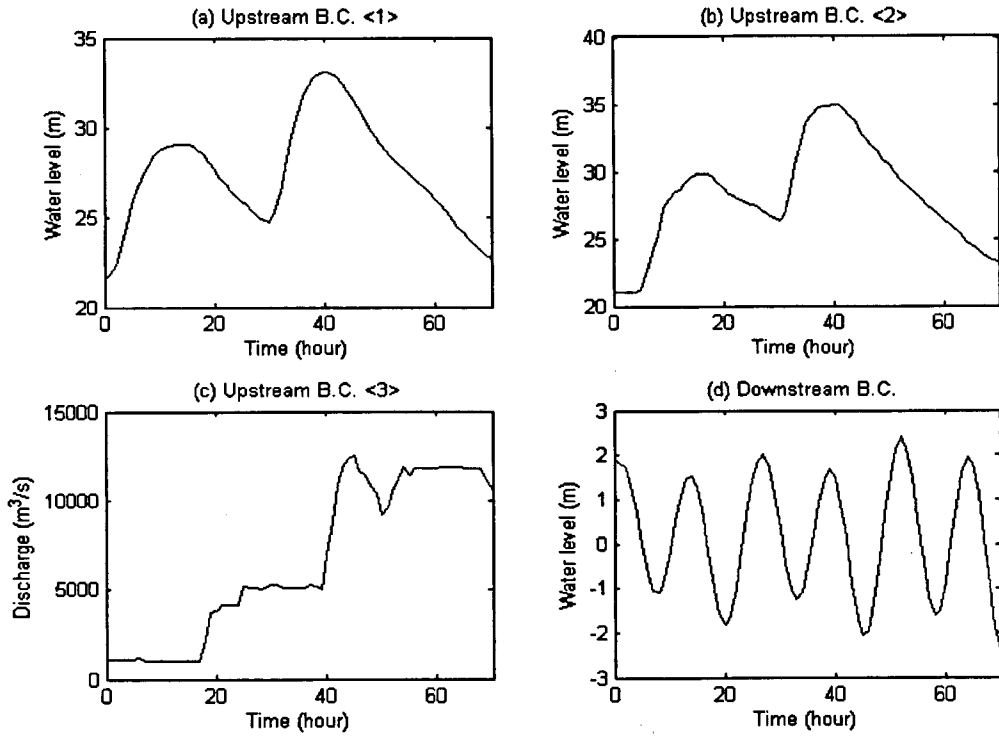


Figure 6.4 Boundary conditions for 1996 flood event

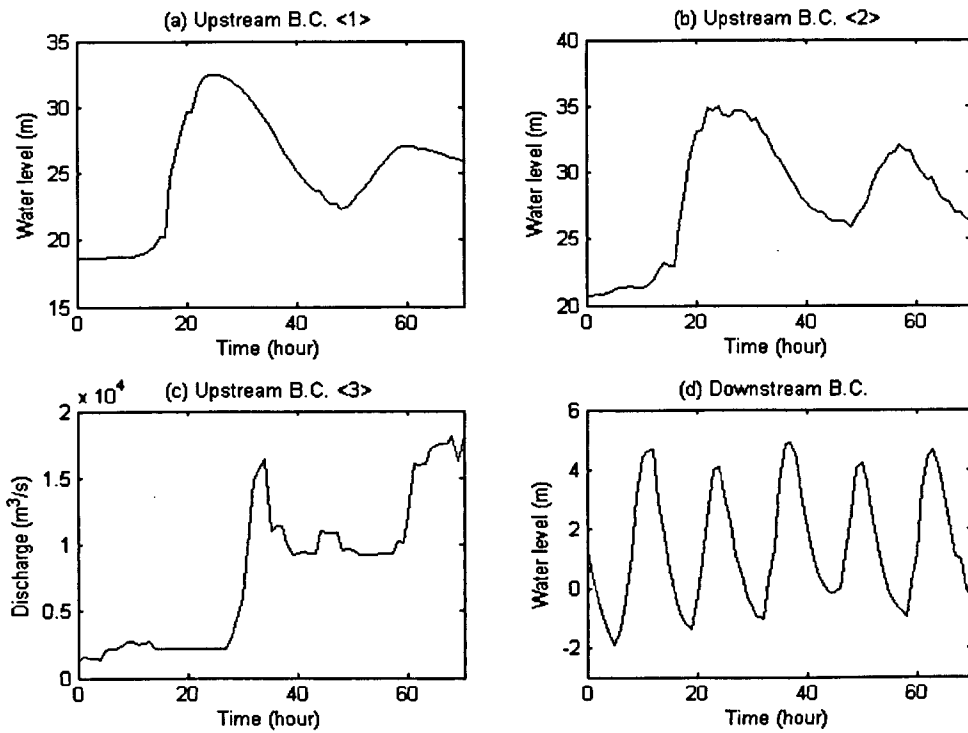


Figure 6.5 Boundary conditions for 1999 flood event

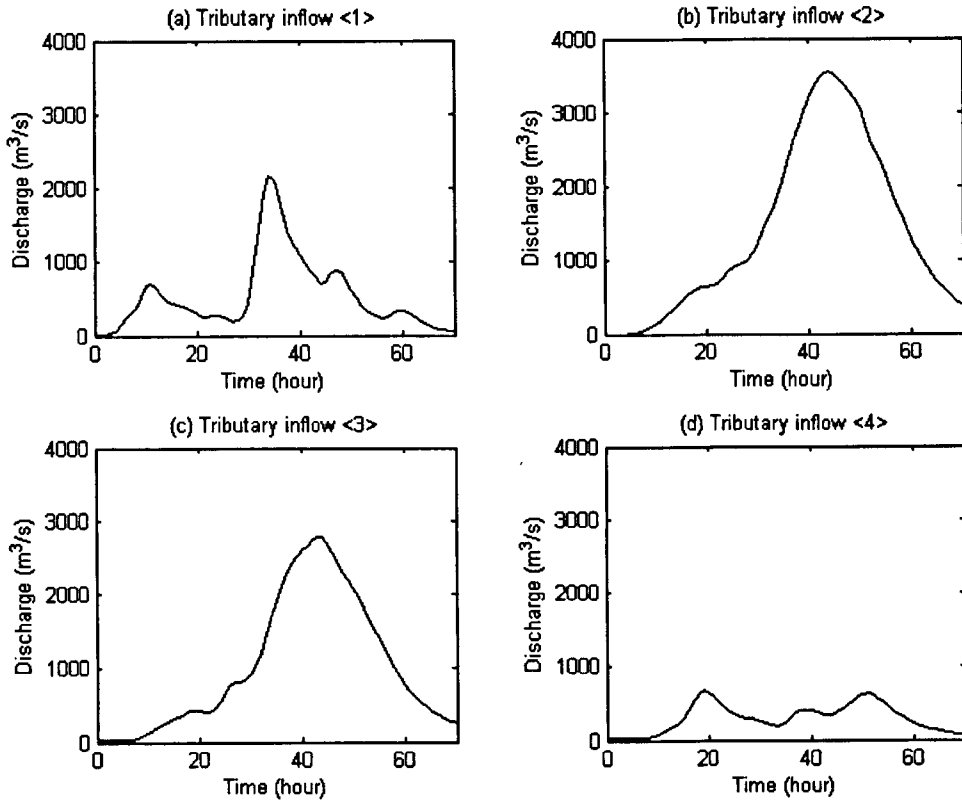


Figure 6.6 Tributary inflow data for 1996 flood event

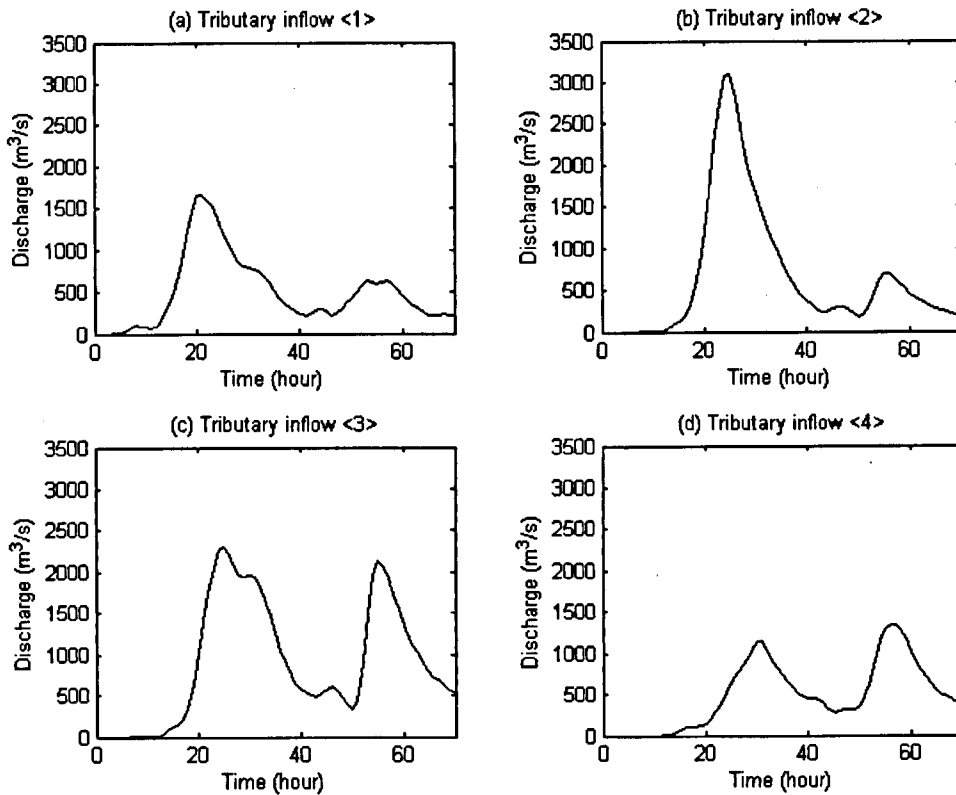


Figure 6.7 Boundary conditions for 1999 flood event

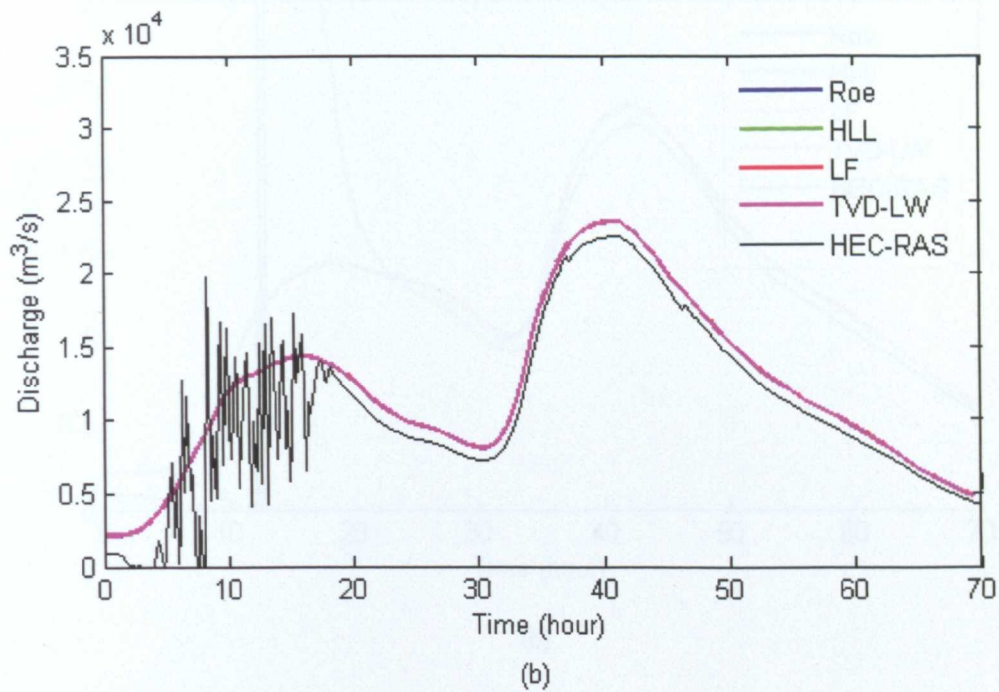
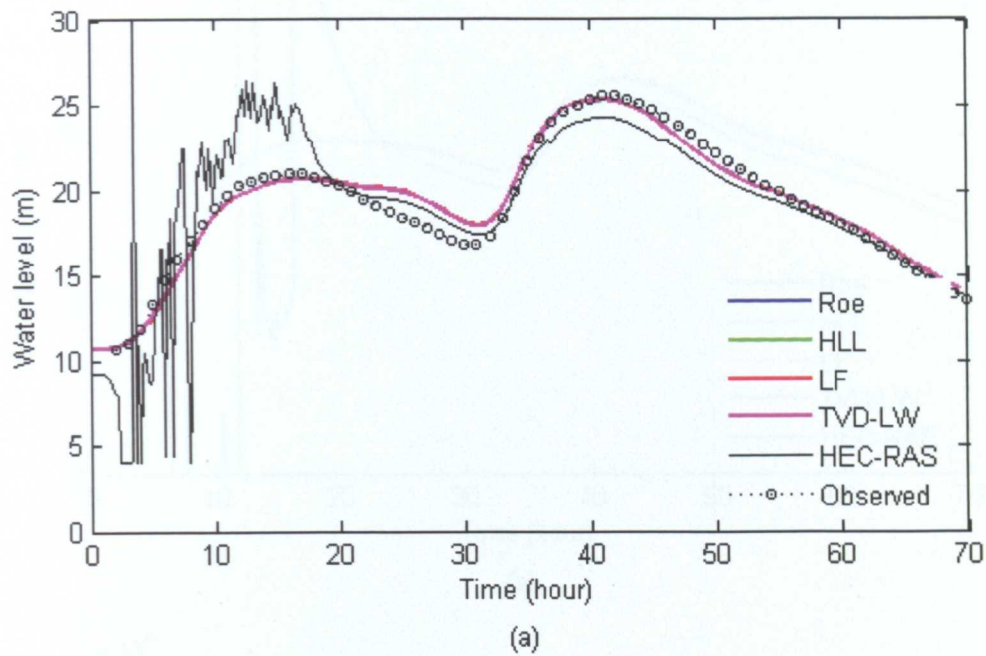
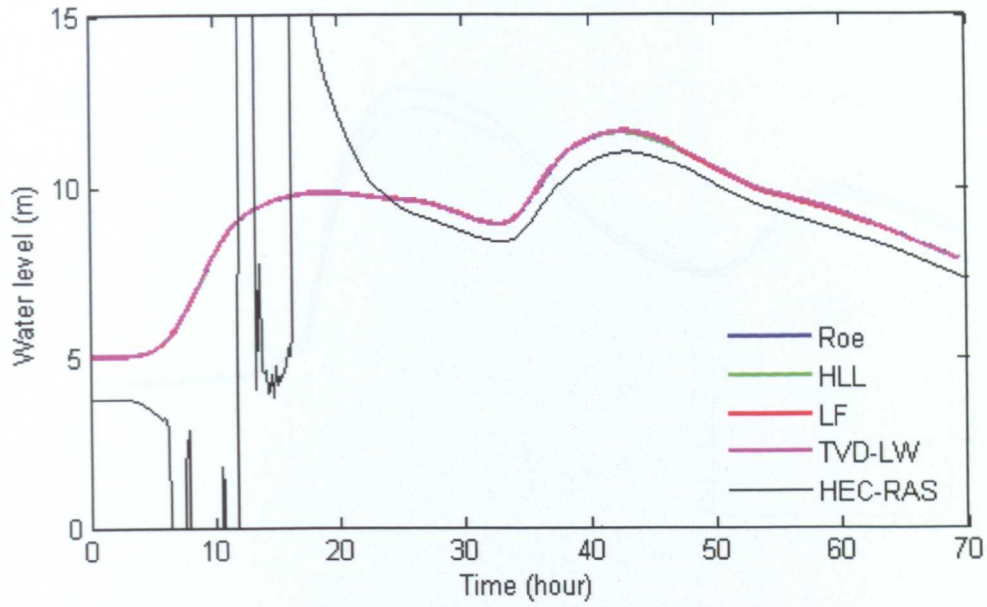
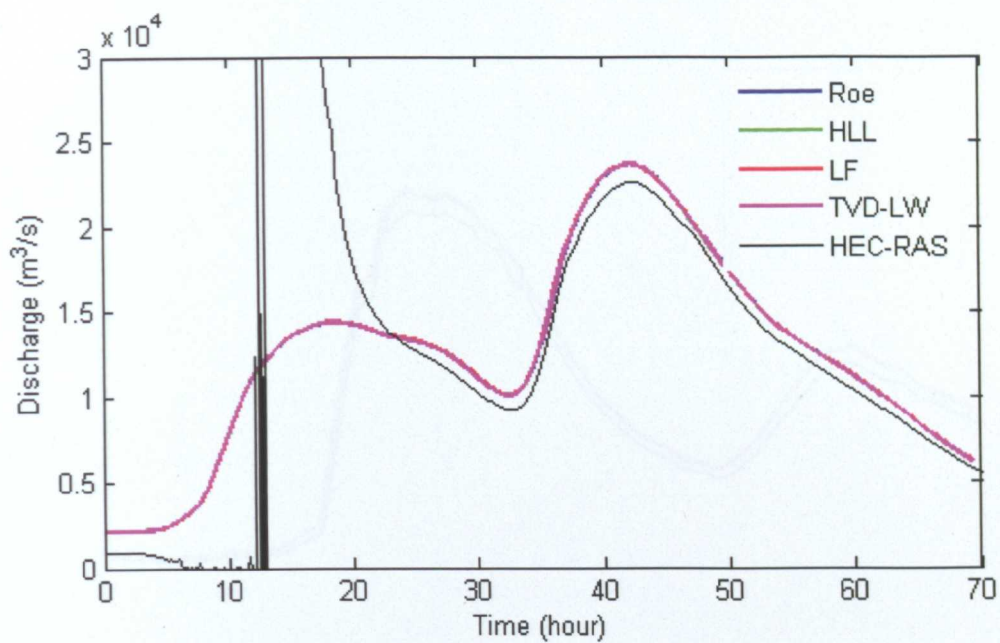


Figure 6.8 Numerical results for 1996 flood event: (a) water level and (b) discharge history at the Juk-seong station

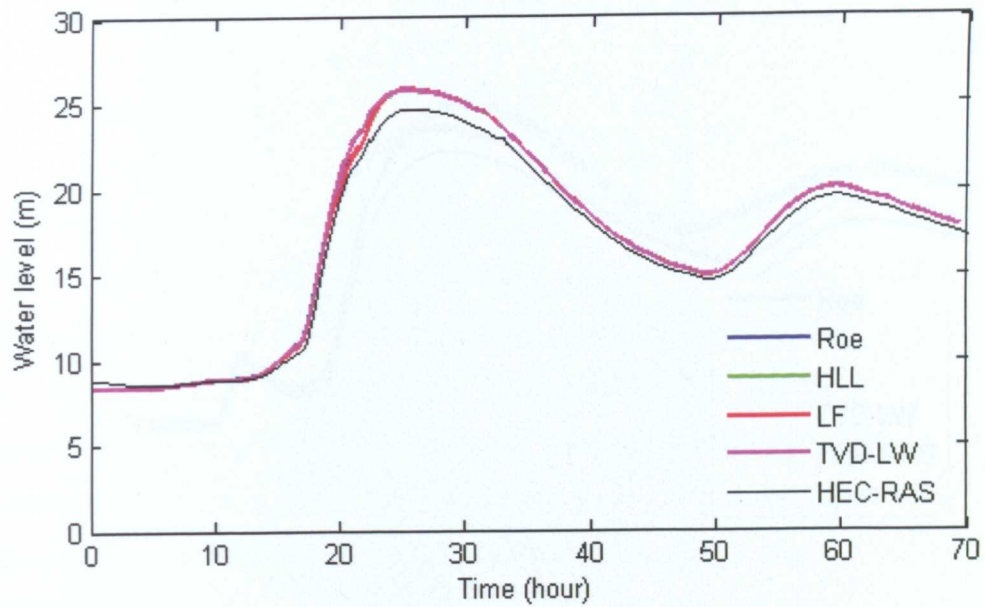


(a)

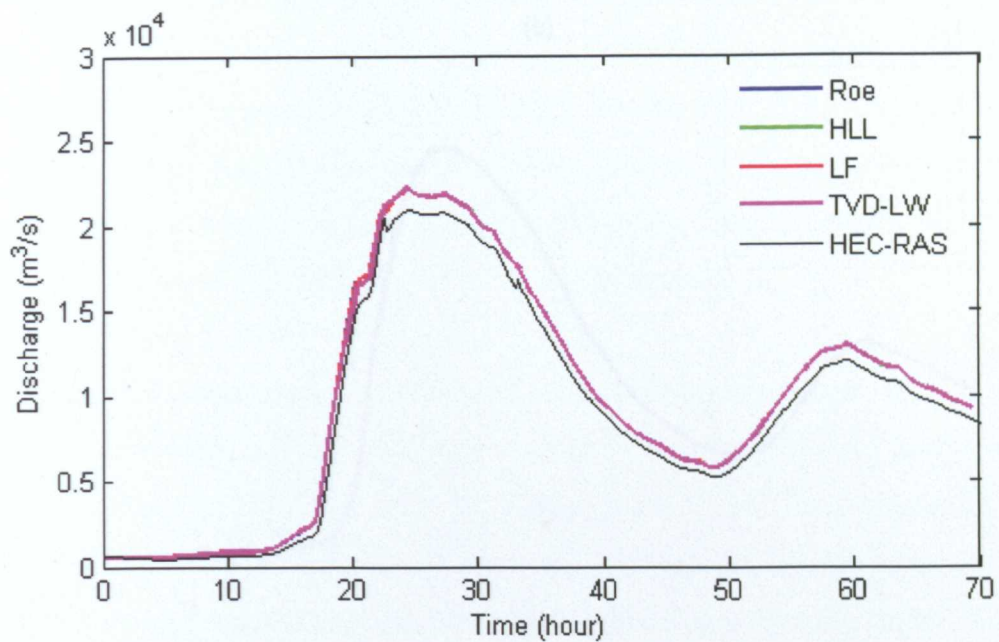


(b)

Figure 6.9 Numerical results for 1996 flood event: (a) water level and (b) discharge history at the Tong-il bridge station



(a)



(b)

Figure 6.10 Numerical results for 1999 flood event: (a) water level and (b) discharge history at the Juk-seong station

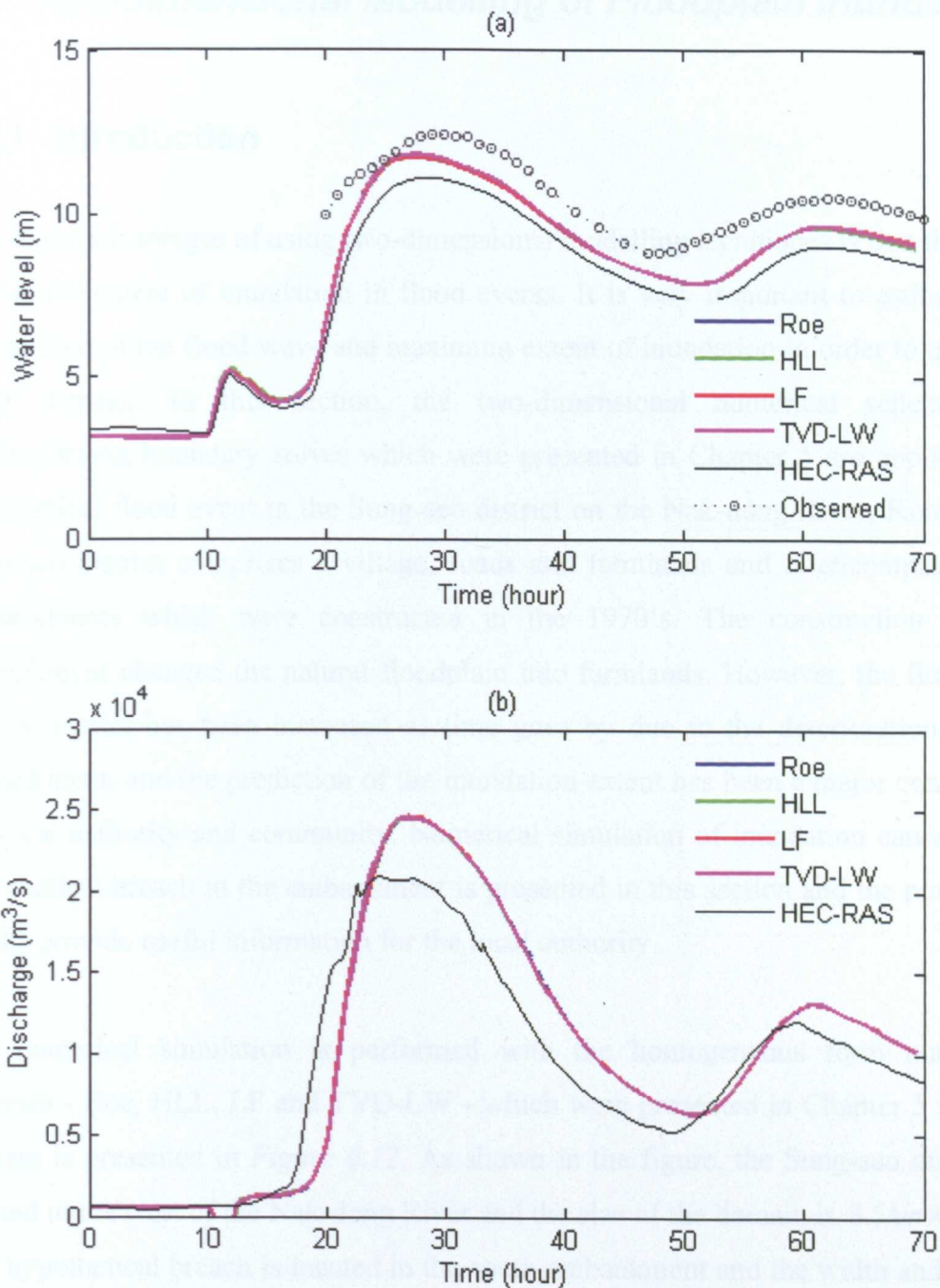


Figure 6.11 Numerical results for 1999 flood event: (a) water level and (b) discharge history at the Tong-il bridge station

6.2 Two-dimensional Modelling of Floodplain Inundation

6.2.1 Introduction

One of the advantages of using two-dimensional modelling techniques is that they can predict the extent of inundation in flood events. It is very important to estimate the arrival time of the flood wave and maximum extent of inundation in order to mitigate flood damage. In this section, the two-dimensional numerical scheme and wetting/drying boundary solver which were presented in Chapter 5 are applied to a hypothetical flood event in the Sung-seo district on the Nak-dong River, Korea. The Sung-seo district comprises a village, roads and farmlands and is encompassed by embankments which were constructed in the 1970's. The construction of the embankment changed the natural floodplain into farmlands. However, the flood risk to this district has been increased as time goes by due to the deterioration of the embankment, and the prediction of the inundation extent has been a major concern of the local authority and community. Numerical simulation of inundation caused by a hypothetical breach in the embankment is presented in this section and the numerical results provide useful information for the local authority.

The numerical simulation is performed with the homogeneous form numerical schemes - Roe, HLL, LF and TVD-LW - which were presented in Chapter 5 and the domain is presented in *Figure 6.12*. As shown in the figure, the Sung-seo district is located in the west of the Nak-dong River and the size of the domain is $8.5\text{km} \times 9.0\text{km}$. The hypothetical breach is located in the south embankment and the width and height of the hypothetical breach are 20m and 2m respectively. The water surface level of the Nak-dong River is maintained 1m higher than the bottom of the breach. The geometry of the domain is provided as a DEM (Digital Elevation Model) which was obtained by LiDAR (Light Detection and Ranging) survey. The resolution of the DEM is $10\text{m} \times 10\text{m}$ and, as a result, the domain consists of 850×900 square cells. The friction effect is considered by setting the Manning's friction coefficients of the farmland and roads as 0.035 and 0.015 respectively. The propagation of the flood

wave after the instantaneous breach of the embankment is calculated and the numerical simulation is performed up to 5 hours after the breach.

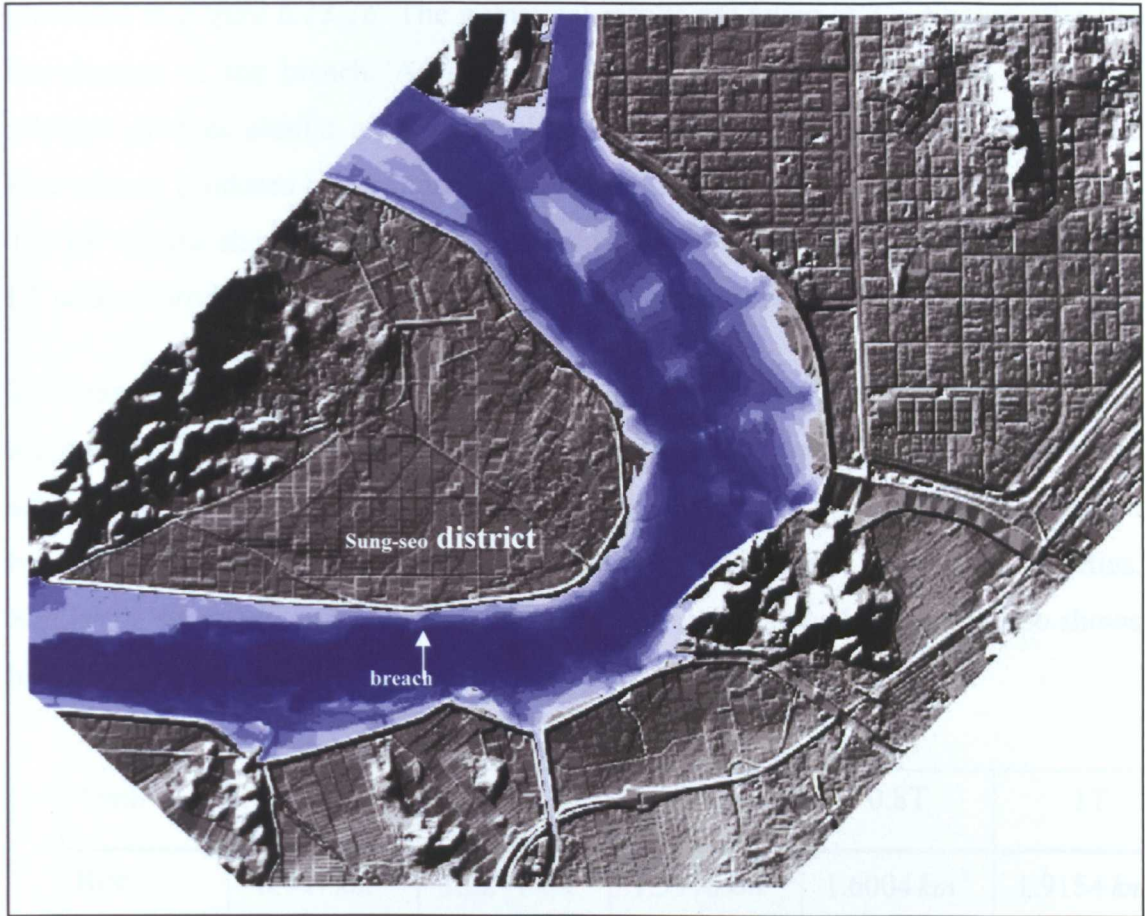


Figure 6.12 Planview of the Sung-seo district and the Nak-dong River

	0.1349 km ²	1.1614 km ²	1.3104 km ²	1.5390 km ²	1.7376 km ²
1954.5	1.1078 km ²	1.2966 km ²	2.1396 km ²	1.6582 km ²	2.2271 km ²

Table 6.2 The variation of the inundated area during the flood simulation (T = 5 hours)

6.2.2 Numerical Results

The inundation extents predicted by using the four different numerical schemes are presented in *Figure 6.13-16*. The numerical results are taken at $T = 5$ hours after the introduction of the breach. As shown in the figures, all the proposed numerical schemes produce similar and reasonable results without any unphysical errors. The Roe scheme produces larger inundation extent than the HLL and TVD-LW schemes. The LF scheme shows smallest extent and this means that the diffusive property of the LF scheme produced slightly slower wave propagation speed.

To compare the property of each scheme, the time variations of the inundated areas are presented in *Table 6.2*. As shown in the table, the two Riemann solver based schemes show similar inundated areas as time goes by, while the flood wave modelled by the second-order accurate scheme(TVD-LW) moves faster than other schemes. Similar to other numerical results in the previous sections, the LF scheme also shows highly diffusive results and the smallest inundation area.

Time	0.2T	0.4T	0.6T	0.8T	1T
Roe	0.997 km^2	1.2271 km^2	1.3976 km^2	1.6004 km^2	1.9154 km^2
HLL	0.9451 km^2	1.1869 km^2	1.3690 km^2	1.5750 km^2	1.8239 km^2
LF	0.8249 km^2	1.1614 km^2	1.3164 km^2	1.5390 km^2	1.7376 km^2
TVD-LW	1.1078 km^2	1.2969 km^2	1.5396 km^2	1.8253 km^2	2.2271 km^2

Table 6.2 The variation of the inundated area during the flood simulation($T = 5$ hours)

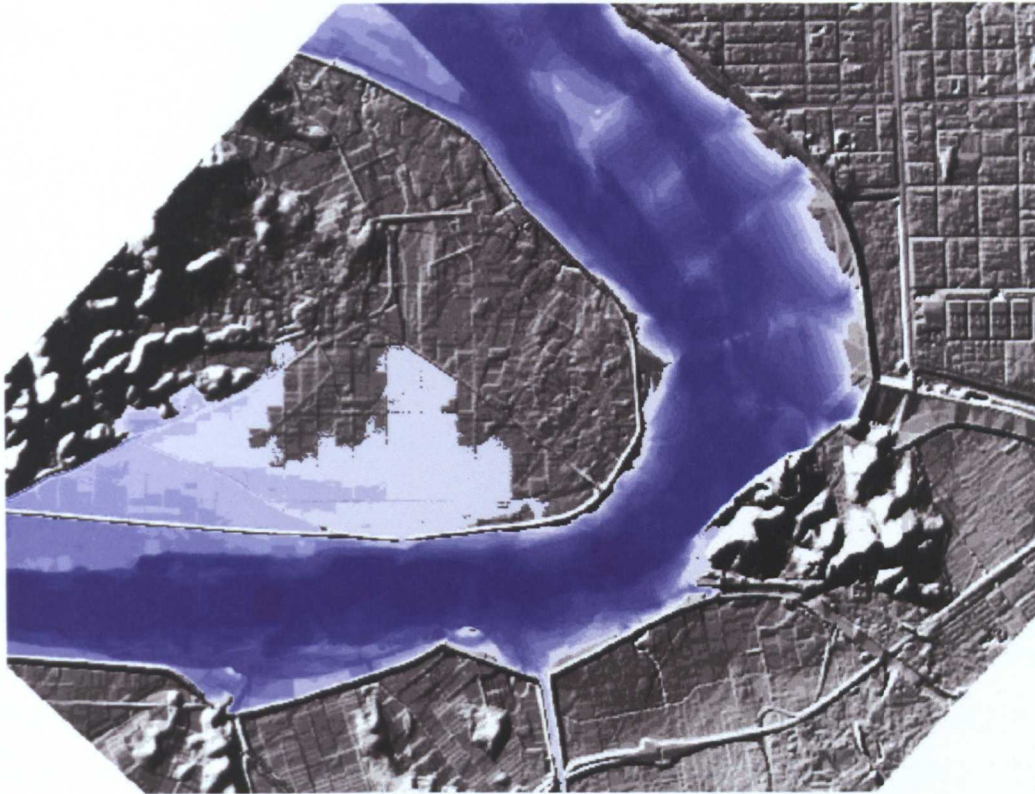


Figure 6.13 Inundation extent predicted by Roe's scheme at 5 hours into the event

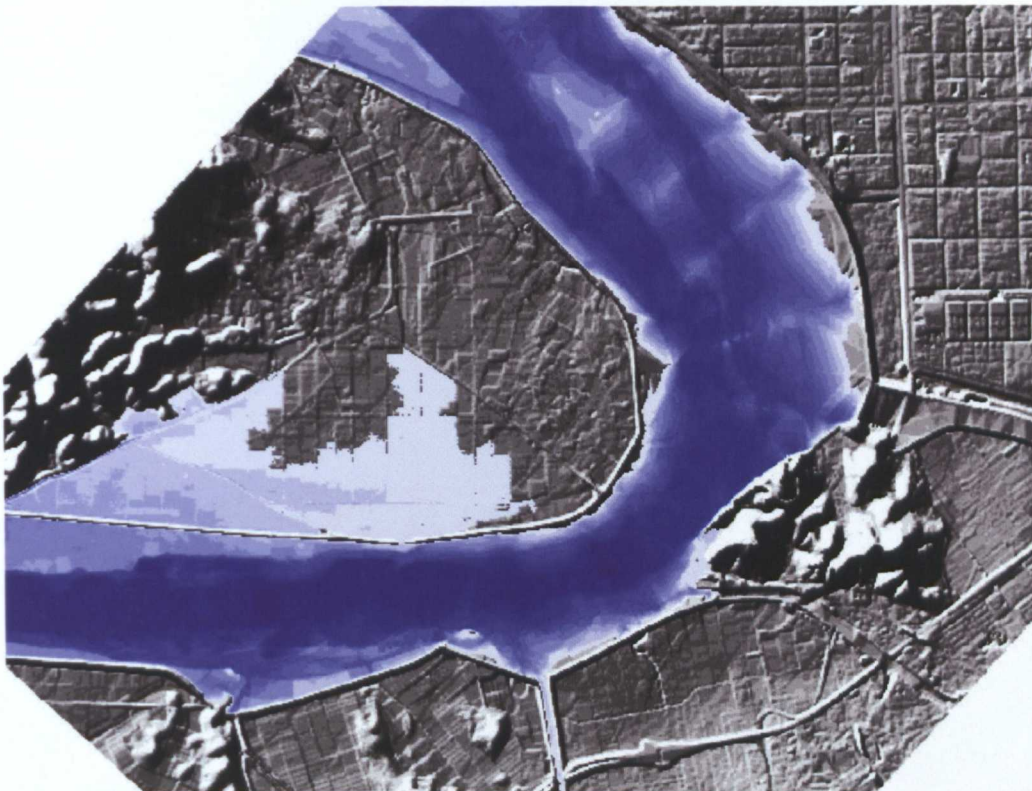


Figure 6.14 Inundation extent predicted by HLL scheme at 5 hours into the event

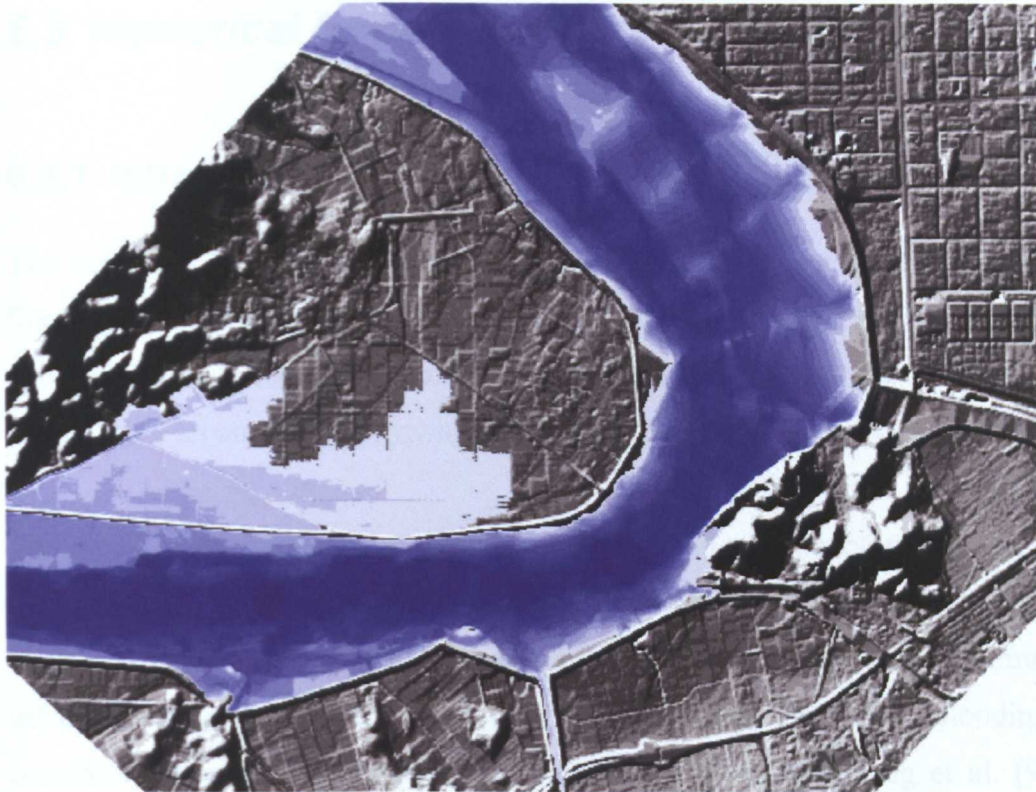


Figure 6.15 Inundation extent predicted by LF scheme at 5 hours into the event

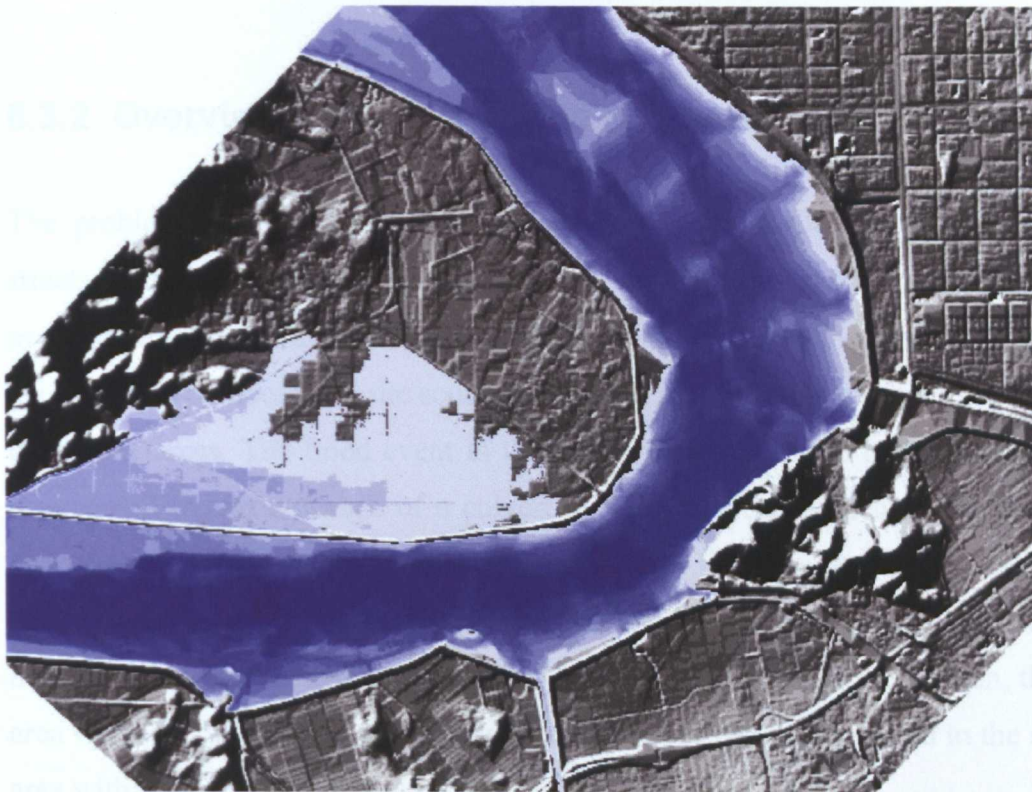


Figure 6.16 Inundation extent predicted by TVD-LW scheme at 5 hours into the event

6.3 Numerical Modelling of Urban Flooding

6.3.1 Introduction

The numerical schemes presented in the previous chapters are applied to an urban flooding event in this section. The modelling of urban flood is considered as a typical two-dimensional problem because it includes two-dimensional flow factors over the complicated urban topography which consists of roads, buildings, parks and etc.

The flood wave propagation problem in an urban catchment within the city of Glasgow, U.K. is modelled with the homogeneous form numerical schemes presented in the previous chapters. The Roe and TVD-LW scheme are used to simulate the urban flooding event and the results are compared. The urban flooding event considered here has been studied by Hunter et al. [89] and Liang et al. [90]. The numerical modelling in this chapter is performed with the same topographic and hydraulic data used in [89] and [90].

6.3.2 Overview of the Study Site and Input Data

The problem domain consists of vegetated areas and buildings located along the streets within the $968m \times 404m$ rectangle site as presented in *Figure 6.17*. As shown in the figure, the main road runs through the middle area of the domain and most of the buildings are located at the south of the main road where the ground level is lower than other areas. The flood event in this urban area took place on 30 July 2002 and was caused by the blockage of a culvert in a small stream which enters the domain near the north-east corner. The overflowed water from the stream spilled over the nearby street and the flood wave propagated through the road network which played the role of an open channel. As the flood wave propagated over the domain, the urban area with lots of buildings were inundated and water was accumulated in the southern area with a low ground level.



Figure 6.17 Map of the study site and some relevant locations

The geometry of this site is described by using the DEM with $2m$ resolution. The DEM was initially obtained from the LiDAR survey which produced the base ground elevation and modified to include the information about the buildings by using the Ordnance Survey Mastermap. The land cover information was also extracted from the Ordnance Survey Mastermap and specified as the two Manning's roughness coefficient: 0.015 for the roads and streets and 0.05 for the rest of the domain, respectively. The domain is discretized into 484×202 rectangular grid cells and each cell has a single value of ground elevation and roughness coefficient.

The flood event occurred on 30 July 2002 is described by the simplified hydrograph and total water volume history shown in *Figure 6.18*. The inflow is imposed as a point source and introduced at point Q_0 as specified in *Figure 6.17*. All the outer boundaries of the domain are considered as solid walls. [89][90] The numerical simulation is performed for 120 minutes and the histories of the water depths at the four designated gauging points denoted G1, G2, G3 and G4 in *Figure 6.17* are computed.

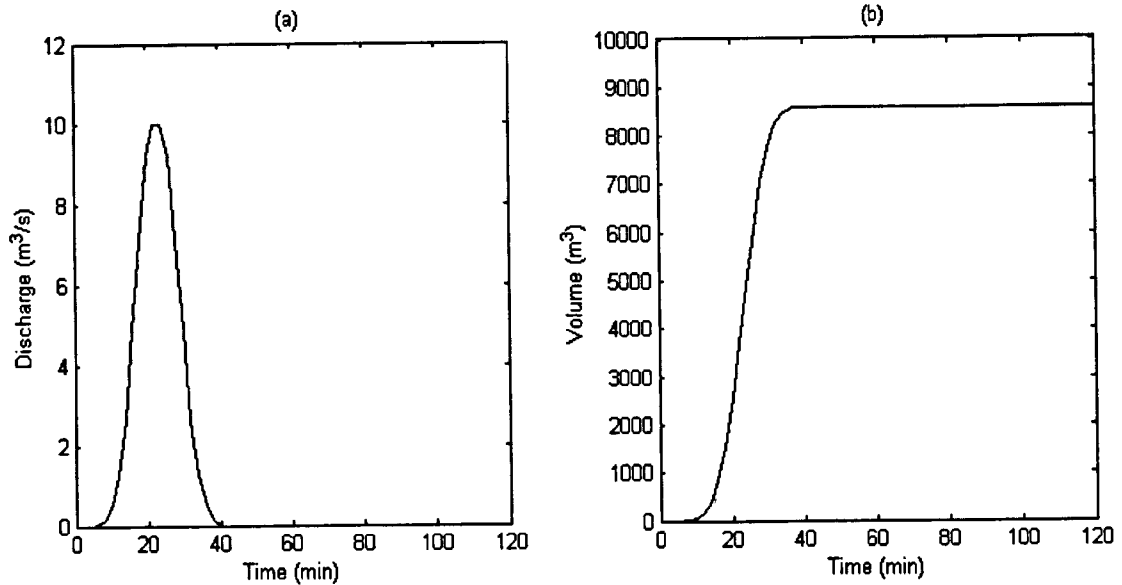


Figure 6.18 (a) Inflow hydrograph and (b) total mass volume introduced to the domain

6.3.3 Numerical Results

The water depth histories at the four gauge points G1-G4 predicted with Roe and TVD-LW schemes are shown in *Figure 6.19*. The water depth at G1 increases rapidly to the peak value after the arrival of the flood wave and then converges to a constant value. The depth history at G2 shows a typical shape of a flood hydrograph in an open channel because it represents the wave propagation over the road which can be considered as an open channel. The water depth at G3 rapidly increases after the arrival of the wave front and converges to a constant value without showing a peak value. (as seen at G1) The depth history at G4 represents flood wave propagates through the road network and then water ponds in the low ground near point G3. The Roe and TVD-LW schemes show similar results to each other at all the four points and there is no noticeable difference between them. The predicted depth histories look reasonable when they are compared with the results taken from other literature [89]. The numerical results of [89] were obtained with the six different numerical schemes: TUFLOW, DIVAST, DIVAST-TVD, TRENT, JFLOW and LISFLOOD-FP.

The inundation extents predicted at $t = 15\text{min}$, 30min , 45min and 60min with the Roe and TVD-LW schemes are presented in *Figure 6.20-23*. As shown in the figures, the Roe scheme based on the homogeneous form of the shallow water equations and the wetting/drying boundary solver reproduce the evolution of the urban flood very successfully.

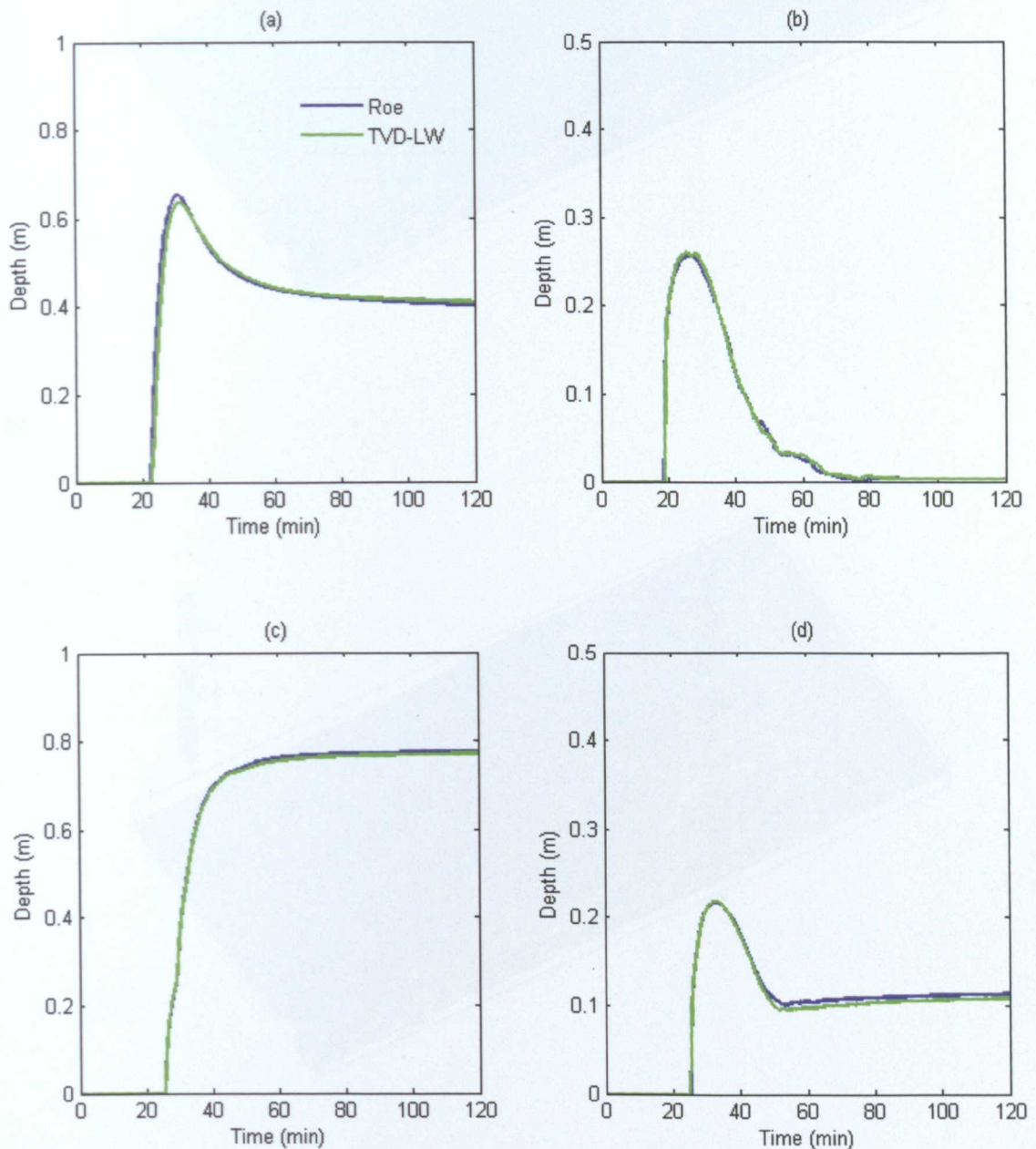


Figure 6.19 Water depth histories at the gauge points:

(a) G1, (b) G2, (c) G3 and (d) G4

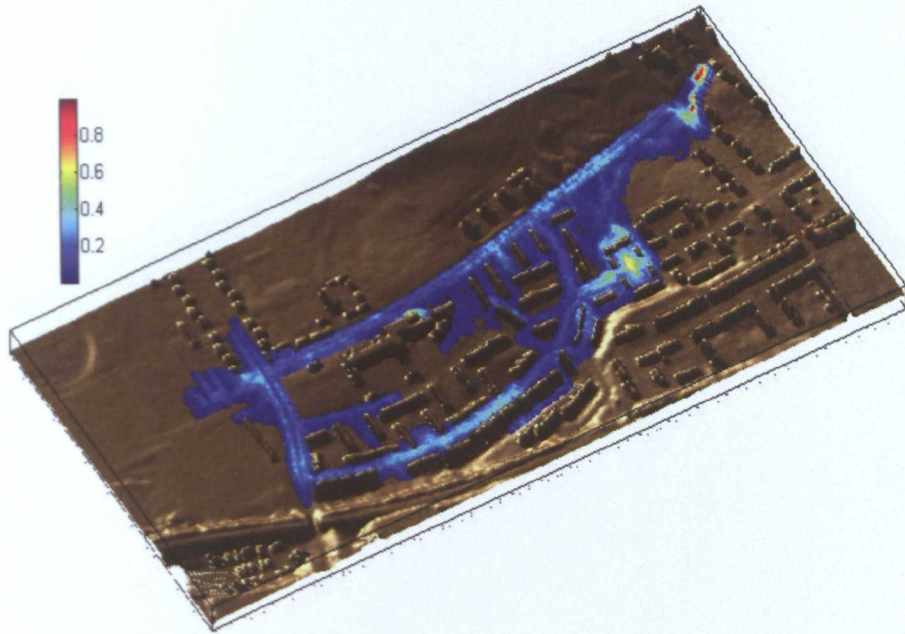


(a)



(b)

Figure 6.20 Predicted inundation extents at $t = 15$ min : (a) Roe and (b) TVD-LW

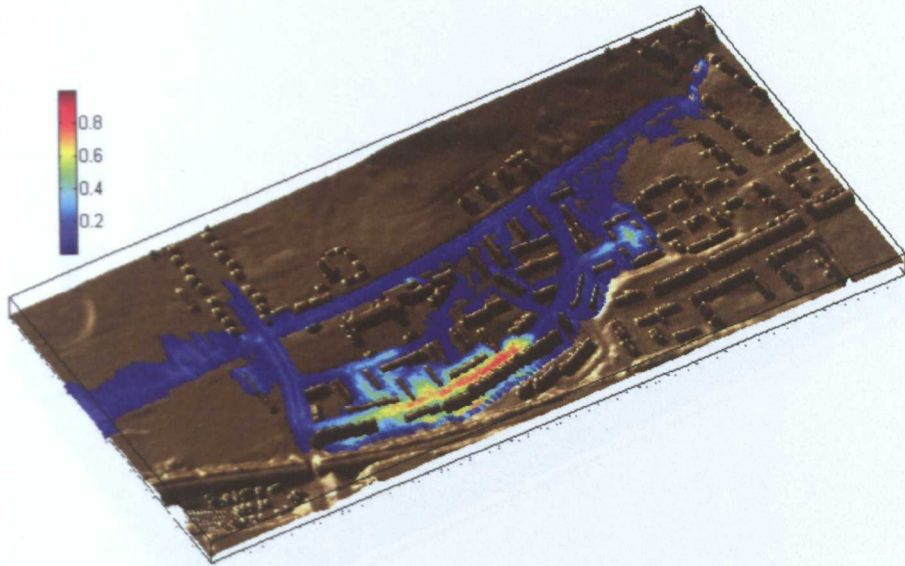


(a)

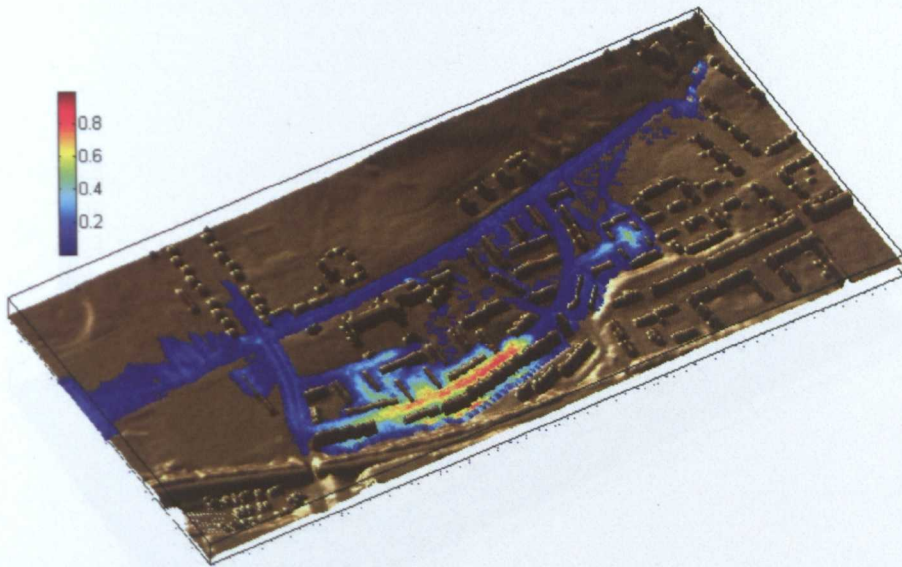


(b)

Figure 6.21 Predicted inundation extents at $t = 30$ min: (a) Roe and (b) TVD-LW



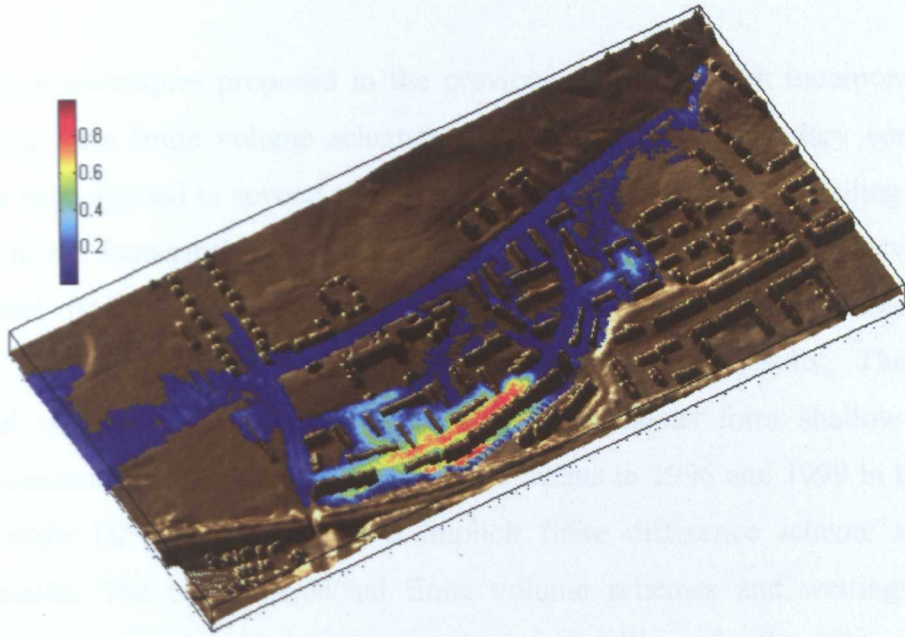
(a)



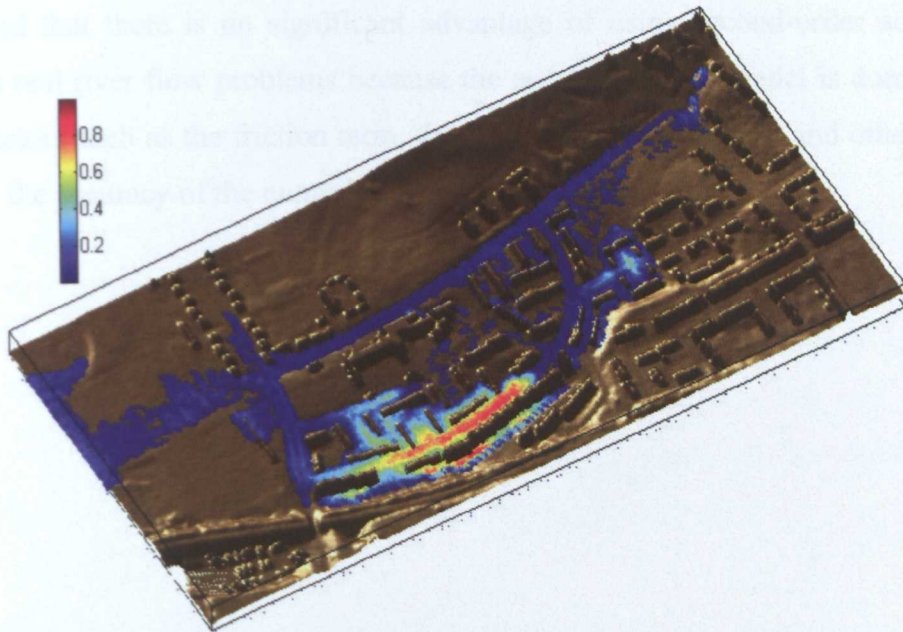
(b)

Figure 6.22 Predicted inundation extents at $t = 45$ min : (a) Roe and (b) TVD-LW

6.4 Summary



(a)



(b)

Figure 6.23 Predicted inundation extents at $t = 60$ min : (a) Roe and (b) TVD-LW

6.4 Summary

The numerical techniques proposed in the previous chapters which incorporate the homogeneous form finite volume schemes and wetting/drying boundary condition solver have been applied to several one- and two-dimensional flood modelling cases. According to the numerical results, all the proposed numerical schemes solved the open channel flow problems over complicated natural geometries without any noticeable numerical oscillations and produced reasonable results. The one-dimensional numerical schemes based on the homogeneous form shallow water equations successfully modelled the severe flood events in 1996 and 1999 in the Im-jin River while HEC-RAS which is a implicit finite difference scheme showed unstable results. The two-dimensional finite volume schemes and wetting/drying boundary conditions are applied to the inundation modelling of a floodplain and an urban area and produced well-balanced solutions. All the proposed finite volume schemes produced similar results for each case while the second-order accurate scheme needs much more run times than other first-order schemes. In other words, it is concluded that there is no significant advantage of using second-order accurate schemes in real river flow problems because the accuracy of the model is dominated by other factors such as the friction term, the uncertainty of hydraulic and other data. rather than the accuracy of the numerical schemes.

Chapter 7

Conclusions

7.1 Summary

The objective of this thesis was to investigate ways to solve highly unsteady shallow water flow problems such as flood wave propagation over highly irregular geometry both correctly and efficiently. To achieve this goal, Godunov-type finite volume schemes were chosen as basic tools to solve the one- and two-dimensional shallow water equations because of their accuracy and shock capturing ability. However, Godunov-type schemes cannot solve the shallow water equations correctly unless the source terms related to the bed slope and channel width variation are discretized properly. This is because the Godunov-type schemes were developed on the basis of homogeneous governing equations and cannot be compatible with an inhomogeneous system. To tackle this problem, a novel approach in which the inhomogeneous governing equation is modified into an homogeneous system was presented in this thesis. To eliminate the inhomogeneous terms, a new flux term which is compatible with the source terms is proposed. The elimination of the source terms enables one to apply the numerical methods developed for the homogeneous governing equation directly to the shallow water equations. The newly proposed source flux term can be combined with original flux term to form an integrated numerical flux term which represents the real flow condition through each cell interface.

Another point considered to achieve well-balanced numerical schemes is that the channel geometry should be reconstructed in order to be compatible with the numerical flux term which is computed with piecewise constant initial data. In this thesis, the channel geometry has been changed to have constant state inside each cell and, consequently, each cell interface is considered as a discontinuity. The definition of the new flux related to the source terms has been obtained on the basis of the

modified channel geometry. Then, the homogeneous form shallow water equations has been solved by using well-known conservative numerical schemes including approximate Riemann solvers. The numerical methods presented in this thesis have been applied to the one- and two-dimensional shallow water equations to solve open channel flows over highly irregular geometries.

A simple and accurate algorithm to solve the moving boundary problem in two-dimensional modelling case has also been presented in this thesis. To solve the moving boundary condition, the locations of all the cell interfaces between the wet and dry cells have been detected first and the integrated numerical fluxes through the interfaces have been controlled according to the water surface level of the wet cells. Moreover, the flux correction method has been proposed to reduce mass conservation errors which is caused by the negative water depth near moving boundaries.

The final part of the research is the application of the presented numerical methods to flood modelling over natural geometry. For one-dimensional modelling, the 1996 and 1999 flood events in the Im-jin River in Korea having highly irregular channel geometry have been simulated with the conservative schemes based on the homogeneous shallow water equations. In case of two-dimensional modelling, the inundation over a floodplain and an urban area are simulated. A floodplain area near the Nak-dong River in Korea has been considered and a hypothetical flood over the area caused by a sudden breach of the embankment has been simulated while a flood event occurring in 2002 over an urban catchment within the city of Glasgow, U.K. has been modelled with the proposed numerical methods. All the flood cases were modelled with the conservative numerical schemes proposed in this thesis and the results were compared each other to show the properties of the schemes.

7.2 Conclusions

The main conclusion of this thesis is that using the proposed homogeneous form of the shallow water equations and moving boundary solver is successful for both benchmark tests and flood events over natural geometries. Especially in case of benchmark tests, the proposed conservative numerical schemes produce accurate

solutions showing good agreement with analytical solutions, which shows the robustness and consistency of the proposed numerical methods. It is clear that the numerical schemes produce reasonable results without any noticeable errors in case of flood modelling over natural geometries.

The detailed findings and results can be summarised as follows:

The one-dimensional shallow water equations

The homogeneous form shallow water equations with the newly defined source flux term is considered as a good platform to solve open channel flow problems according to the numerical results of the benchmark tests. Various type of conservative numerical schemes including approximate Riemann solvers and TVD second-order accurate schemes have been applied to the homogeneous form equations and solved unsteady and steady flow problems in non-prismatic channels very accurately. The integrated numerical flux which is formed by combining the source flux with the original flux represents the real flow condition at each cell interface. For example, in the still water simulation problem, the integrated numerical flux at each interface is calculated as exactly zero which represents no movement of water and the numerical schemes maintain the quiescent state permanently. While all the presented conservative numerical schemes solve the steady and unsteady benchmark test cases correctly, some schemes show particular behaviour. For example, the Lax-Friedrichs scheme produces diffusive results when it is applied to transcritical flows with shocks. The TVD MacCormack scheme which is second-order accurate with a predictor-corrector step method converges to steady state faster than other schemes in case of steady state benchmark test cases.

The two-dimensional shallow water equations and wetting/drying boundary condition

The numerical method used for the one-dimensional equations is readily extended to the two-dimensional case. The definition of the source flux term in the homogeneous form two-dimensional shallow water equations has been obtained by using a similar approach to the one-dimensional case. The new source flux term in the two-

dimensional case has simpler form than the one-dimensional case because there is no term related to the variation of channel width in the two-dimensional equations.

Another important point considered in this thesis is the solution of wetting/drying boundary condition. A new moving boundary condition solver which uses the integrated numerical flux has been presented and applied to several benchmark test cases. The presented numerical results show that the wetting/drying boundary condition solver can solve the moving boundary problem accurately even though it has a very simple solution structure.

The flux correction method in which the integrated numerical fluxes of the cell having negative water depth are recalculated according to the ratio of the time that the cell stays wet has been proposed in this thesis and applied to the test cases together with the moving boundary condition solver. The main advantage of using the flux correction method is that it can reduce most of mass conservation error by removing negative water depth which cause the increase of the total mass volume. According to the numerical results of the test cases, the flux correction method reduced the mass error to almost zero.

Summing up all the results of two-dimensional study, it is concluded that the integrated numerical flux is a very useful concept in numerical modelling with the finite volume method because it represents the real state of the flow through each cell interface and, consequently, can be used for various boundary condition problems.

Application to the flows over natural geometry

The numerical methods proposed and validated in this thesis have been applied to flood modelling cases over natural geometries. In the case of one-dimensional modelling of the Im-jin River flood events, the proposed conservative numerical schemes produce almost identical results which are similar to the available observed water level data. The same flood events have been simulated with HEC-RAS which features an implicit finite difference scheme and HEC-RAS showed unstable results

for 1996 flood event while producing stable but slightly different results from the finite volume schemes for 1999 flood.

In two-dimensional modelling, the flood inundation simulation over an urban floodplain has been performed with the numerical schemes presented in this thesis. According to the numerical results, all the numerical schemes showed almost identical inundation extents with no significant numerical errors. There are no analytical solutions for the two-dimensional flood modelling case. However, the numerical results of the urban flooding case have been compared with those taken from other literature and show similarity.

The run times of each model were measured. The measured run times show that the second-order TVD Lax-Wendroff scheme needs much larger computing time than first-order schemes. From the comparison of the numerical results and run times, it can be concluded that there is no significant advantage of using higher-order schemes in open channel flows over natural geometry because the effect of source terms like friction force and bed slope is bigger than the improved accuracy of higher-order numerical schemes.

7.3 Recommended Future Work

The results and findings of the current research has convinced the author of the robustness and applicability of the proposed numerical techniques. It is straightforward to extend the numerical methods presented in this thesis to more complicated cases and to apply this to various situations. A number of possibilities for future work have been identified and are presented here.

- ***Application of the concept to other numerical schemes***

The homogeneous form shallow water equations can be solved with other conservative numerical schemes which are not presented in this thesis. The available numerical schemes are Osher's approximate Riemann solver, the Flux Vector Splitting method, ENO (essentially non-oscillatory) scheme and others.

▪ *Extension to MUSCL-type second-order accurate numerical schemes*

The source term treatment for MUSCL-type second-order accurate schemes is more complicated than flux limited schemes because the former consist of two evolution steps (predictor and corrector) and requires a data reconstruction process before the computation of flux terms. Especially, the reconstruction strategy for the data used for the calculation of the source terms should be considered carefully to secure numerical balance.

▪ *Application to the unstructured mesh grid*

All the two-dimensional modelling cases in the current research are performed on structured square grid cells. However, the numerical methods presented can also be used on unstructured grids and adaptive meshes. Especially, the total number of computational cells can be reduced by using an unstructured triangular grid and total computing time could be minimised by adopting an adaptive mesh refinement technique.

▪ *Sensitivity analysis*

The numerical results of the proposed methods can be changed by using different conditions like the calculation of the boundary conditions, the choice of friction coefficients, the shape of the mesh grid and so on. Especially, the evaluation of the effect of each term in the source flux, i.e. I_1 , bottom slope and friction term, is one of the important factor of the proposed methods. The boundary conditions used in this thesis is taken from [18] and a new approach to solve boundary conditions which is optimised for the solution of the shallow water equations with bottom slope and wall friction.

▪ *Extension to other hyperbolic conservation laws*

The ideas presented in this thesis can be applied to other conservation laws which describe the motion of fluids because they are hyperbolic systems of partial differential equations and have similar properties to the shallow water equations. Possible other hyperbolic conservation laws are the Euler equations and others.

References

- [1] Anastasiou K and Chan C : Solution of the 2D shallow water equations using the finite volume method on unstructured triangular meshes, *International Journal for Numerical Methods in Fluids*, **24**, 1225-1245, 1997
- [2] Alcrudo F and Garcia-Navarro P : A high resolution Gudunov-type scheme in finite volumes for the 2D shallow water equations, *International Journal for Numerical Methods in Fluids*, **16**, 489-505, 1993
- [3] Alcrudo F : A state of the art review on mathematical modelling of flood propagation, *1st IMPACT Project workshop*, Wallingford, UK, 2002
- [4] Bates P, Mason D, Neelz S, Pender G, Villanueva I, Wilson M and Wright N : A framework for modelling flood inundation, *Flood Risk Assessment*, Institute of Mathematics and its Applications, Southend-on-sea, UK, 2004
- [5] Bates P and De Roo A : A simple raster-based model for flood inundation simulation, *Journal of Hydrology*, **236**, 54-77, 2000
- [6] Beffa C and Connell R : Two-dimensional flood plain flow. I: Model description. *Journal of Hydrologic Engineering (ASCE)*, **6(5)** : 397-405, 2001
- [7] Beffa C and Connell R : Two-dimensional flood plain flow. II: Model validation. *Journal of Hydrologic Engineering (ASCE)*, **6(5)** : 406-415, 2001
- [8] Begnudelli L and Sanders F : Conservative wetting and drying methodology for quadrilateral grid finite-volume models. *Journal of Hydrologic Engineering (ASCE)*, **133(3)** : 312-322, 2007
- [9] Bermudez A and Vazquez M E : Upwind methods for hyperbolic conservation laws with source terms. *Computer & Fluids*, **23** : 1049-1071, 1994

- [10] Bradford S and Sanders B : Finite volume model for shallow-water flooding of arbitrary topography, *Journal of Hydraulic Engineering (ASCE)*, **128**, 289-298, 2002
- [11] Brufau P and Garcia-Navarro P : Two-dimensional dam break flow simulation, *International Journal for Numerical Methods in Fluids*, **33**, 35-57, 2000
- [12] Brufau P, Vazquez-Cendon M and Garcia-Navarro P : A numerical model for the flooding and drying of irregular domains, *International Journal for Numerical Methods in Fluids*, **39**, 247-275, 2002
- [13] Brufau P, Vazquez-Cendon M and Garcia-Navarro P : Zero mass error using unsteady wetting-drying conditions in shallow water flows over dry irregular topography, *International Journal for Numerical Methods in Fluids*, **45**, 1047-1082, 2004
- [14] Brunner : HEC-RAS River analysis system - Hydraulic reference manual, GUS Army Corps of Engineers, 1999
- [15] Burguete J and Garcia-Navarro P : Efficient construction of high-resolution TVD conservative schemes for equations with source terms: application to shallow water flows, *International Journal for Numerical Methods in Fluids*, **37**, 209-248, 2001
- [16] Burguete J and Garcia-Navarro P : Improving simple explicit methods for unsteady open channel and river flow, *International Journal for Numerical Methods in Fluids*, **45**, 125-156, 2004
- [17] Burguete J and Garcia-Navarro P : Implicit schemes with large time step for non-linear equations: application to river flow hydraulics, *International Journal for Numerical Methods in Fluids*, **46**, 607-636, 2004
- [18] Burguete J, Garcia-Navarro P and Murillo J : Numerical conditions for globally mass conservative methods to solve the shallow-water equations and applied to river flow, *International Journal for Numerical Methods in Fluids*, **51**, 2006

- [19] Caleffi V, Valiani A and Zanni A : Finite volume method for simulating extreme flood events in natural channel, *Journal of Hydraulic Research*, **41**, 167-177, 2003
- [20] Capart H, Eldho T and Huang S, Young D and Zech Y : Treatment of natural geometry in finite volume river flow computations, *Journal of Hydraulic Engineering*, **129(5)**, 385-393, 2003
- [21] Chadwick A, Morfett J and Borthwick M : Hydraulics in civil and environmental engineering, Spon, 2004
- [22] Chow V : Open channel hydraulics, Mcgraw-Hill, 1959
- [23] Crossley A : Accurate and efficient numerical solutions for the Saint Venant equations of open channel flow, *Ph.D. Thesis*, University of Nottingham, 2000
- [24] Crossley A and Wright N : Time accurate local time stepping for the unsteady shallow water equations, *International Journal for Numerical Methods in Fluids*, **48**, 775-799, 2005
- [25] Crowder R, Pepper A, Whitlow C, Sleight A, Wright N and Tomlin C : Benchmarking Hydraulic River Modelling Software Packages – Project Overview, *DEFRA & Environment Agency*, 2004
- [26] Crowder R, Pepper A, Whitlow C, Sleight A, Wright N and Tomlin C : Benchmarking Hydraulic River Modelling Software Packages – Results : Test B, *DEFRA & Environment Agency*, 2004
- [27] Crowder R, Pepper A, Whitlow C, Sleight A, Wright N and Tomlin C : Benchmarking Hydraulic River Modelling Software Packages – Test Specifications, *DEFRA & Environment Agency*, 2004
- [28] Cunge J, Holly F and Verwey A : Practical aspects of computational river hydraulics, Pitman publishing limited, 1980
- [29] Delis A and Skeels C : TVD schemes for open channel flow, *International Journal for Numerical Methods in Fluids*, **26**, 791-806, 1998

- [30] DHI Water & Environment : MIKE11 A modelling system for rivers and channels - User guide, DHI Software, 2003
- [31] Einfeldt B : On Godunov-type methods for gas dynamics. *SIAM Journal on Numerical Analysis*, **25**: 294-318, 1988
- [32] Engquist B and Osher S : One sided difference approximations for nonlinear conservation laws. *Mathematics of Computation*, **36(154)**: 321-351, 1981
- [33] Erduran K, Kutija V, and Hewett C : Performance of finite volume solutions to shallow water equations with shock-capturing schemes. *International Journal for Numerical Methods in Fluids*, **40** : 1237-1273, 2002
- [34] Erduran K, Kutija V, and Macalister C : Finite volume solution to integrated shallow surface-saturated groundwater flow. *International Journal for Numerical Methods in Fluids*, **49** : 763-783, 2005
- [35] Fennema R and Chaudhry M : Explicit methods for 2D transient free surface flows, *Journal of Hydraulic Engineering (ASCE)*, **116**, 1013-1034, 1990
- [36] Frazao S and Zech Y : Dam break in channels with 90° bend. *Journal of Hydraulic Engineering (ASCE)*, **128(11)** : 956-968, 2002
- [37] Garcia-Navarro P, Alcrudo F and Priesley A : An implicit method for water flow modelling in channels and pipes, *Journal of Hydraulic Research*, **32**, 721-742, 1994
- [38] Garcia-Navarro P, Fras A and Villanueva I : Dam break simulation: some results for one-dimensional models of real cases, *Journal of Hydrology*, **216**, 227-247, 1999
- [39] Garcia-Navarro P and Kahawitta R A : Numerical solution of the St. Venant equations with the Mac-Cormack finite difference scheme. *International Journal for Numerical Methods in Fluids*, **6**, 259-274, 1986

- [40] Garcia-Navarro P and Vazquez-Cendon M : On numerical treatment of the source terms in the shallow water equations, *Computers and fluids*, **29**, 951-979, 2000
- [41] Garcia-Navarro P and Saviron J M : McCormack's method for the numerical simulation of one-dimensional discontinuous unsteady open channel flow. *Journal of Hydraulic Research*, **30**, 95-105, 1992
- [42] Gascon L I and Corberan J M : Construction of second-order TVD schemes for nonhomogeneous hyperbolic conservation laws. *Journal of Computational Physics*, **172**, 261-297, 2001
- [43] Glaister P : Approximate Riemann solutions of the shallow water equations, *Journal of Hydraulic Research*, **26**, 293-306, 1988
- [44] Godunov S : A finite difference method for the computation of discontinuous solutions of the equations of fluid dynamics. *Matematicheskii Sbornik*, **47** : 271-306, 1959
- [45] Goutal N and Maurel F : Technical report HE-43/97/016/A, *Proceedings of the 2nd Workshop on Dam-break Wave Simulation*, Electricite de France, Department Laboratoire National d'Hydraulique, Groupe Hydraulique Fluviale, 1997
- [46] Goutal N and Maurel M : A finite volume solver for 1D shallow-water equations applied to an actual river. *International Journal for Numerical Methods in Fluids*, **38** : 1-19, 2002
- [47] Harten A and Hyman J : Self adjusting grid methods for one-dimensional hyperbolic conservation law, *Journal of Computational Physics*, **50**, 235-269, 1983
- [48] Harten A, Lax P, and van Leer B : On upstream differencing and Godunov-Type schemes for hyperbolic conservation laws. *SIAM Review*, **25** (1): 35-61, 1983

- [49] Heniche M, Secretan Y, Boudreau P and Leclerc M : A two-dimensional finite element drying-wetting shallow water model for rivers and estuaries. *International Journal for Numerical Methods in Fluids*, **6** : 365-386, 1986
- [50] Hervouet J, and Pertitjean A : Malpasset dam break revisited with two-dimensional computations. *Journal of Hydraulic Research*, **37(6)** : 777-788, 1999
- [51] Hubbard M and Garcia-Navarro P : Flux difference splitting and the balancing of source terms and flux gradients, *Journal of Computational Physics*, **165**, 89-125, 2000
- [52] Hubbard M and Dodd N : A 2D numerical model of wave run-up and overtopping, *Coastal Engineering*, **47**, 1-26, 2002
- [53] Jaffe D, and Sanders B : Engineered levee breaches for flood mitigation. *Journal of Hydraulic Engineering (ASCE)*, **127(6)** : 471-479, 1999
- [54] Jha A, Akiyama J, and Ura M : Flux difference splitting schemes for 2D flood flows. *Journal of Hydraulic Engineering (ASCE)*, **126(1)** : 33-42, 2000
- [55] Jha A, Akiyama J, and Ura M : High resolution flux-difference-splitting scheme on adaptive grid for open-channel flows. *International Journal for Numerical Methods in Fluids*, **36** : 35-52, 2001
- [56] Kawahara M and Umetsu T : Finite element method for moving boundary problems in river flow, *International Journal for Numerical Methods in Fluids*, **6**, 365-386, 1986
- [57] Lai C, Baltzer R and Schaffranek R : Conservation-form equations of unsteady open-channel flow, *Journal of Hydraulic Research*, **40**, 567-578, 2002
- [58] Lax P D : Hyperbolic systems of conservation laws II. *Communications on Pure and Applied Mathematics*, **10**, 537-566, 1957
- [59] Lax P D and Wendroff B: Systems of conservation laws. *Communications on Pure and Applied Mathematics*, **13**, 217-237, 1960

- [60] Leon A, Ghidaoui M, Schmidt A and Garcia M : Godunov-type solutions for transient flows in sewers. *Journal of Hydraulic Engineering (ASCE)*, **132(8)** : 800-813, 2006
- [61] LeVeque R : Numerical methods for conservation laws, Birkhauser Verlag, 1992
- [62] LeVeque R : Balancing source terms and flux gradients in high-resolution Godunov methods: the quasi-steady wave-propagation algorithm, *Journal of Computational Physics*, **146**, 346-365, 1998
- [63] LeVeque R : Finite volume methods for hyperbolic problems, Cambridge university press, 2002
- [64] MacCormack R W : Numerical solution of the interaction of a shock wave with a laminar boundary layer. Proceedings on 2nd International Conference on Numerical Methods in fluid Dynamics, Springer-Verlag, Berlin, Germany, 151-163, 1971
- [65] Macdonald I : Analysis and computation of steady open channel flow, *Ph.D. Thesis*. University of Reading, 1996
- [66] Mays L : Water resources engineering, John Wiley & Sons Inc., 2005
- [67] Nujic M : Efficient implementation of non-oscillatory schemes for the computation of free-surface flows, *Journal of Hydraulic Research*, **33**, 101-111, 1995
- [68] Roberson J, Cassidy J and Chaudly M : Hydraulic engineering, John Wiley & Sons Inc., 1997
- [69] Roe P : Approximate Riemann solvers, parameter vectors, and difference schemes, *Journal of Computational Physics*, **135**, 250-258, 1997
- [70] Rogers B, Borthwick A and Taylor P : Mathematical balancing of flux gradient and source terms prior to using Roe's approximate Riemann solver, *Journal of Computational Physics*, **192**, 422-451, 2003

- [71] Sanders B, Green C, Chu A, and Grant S : Case study: Modeling tidal transport of urban runoff in channels using the finite-volume methods. *Journal of Hydraulic Engineering (ASCE)*, **127(10)** : 795-804, 2001
- [72] Sanders B : High-resolution and non-oscillatory solution of the St. Venant equations in non-rectangular and non-prismatic channels. *Journal of Hydraulic Research*, **39** : 321-330, 2001
- [73] Spekreijse S : Multigrid solution of steady Euler equations, *CWI Tract 46*, Centre for Mathematics and Computer Science, Amsterdam, 1988
- [74] Thacker W C : Some exact solutions to the nonlinear shallow water wave equations. *Journal Fluid Mechanics*, **107** : 499-508, 1981
- [75] Thorndycraft V, Barriendos M and Llasat M : Palaeofloods, Historical data and climatic variability: Applications in flood risk assessment, *Proceedings of the PHEFRA Workshop, Barcelona, 2002*
- [76] Toro E , Spruce M, and Speares W : Restoration of the contact surface in the HLL-Riemann solver. *Shock waves*, **4:25-34**, 1994
- [77] Toro E : Riemann solvers and numerical methods for fluid dynamics – A practical introduction, Springer, 1999
- [78] Valiani A, Caleffi V, and Zanni A : Case study: Malpasset dam-break simulation using two-dimensional finite volume method. *Journal of Hydraulic Engineering (ASCE)*, **128(5)** : 460-472, 2002
- [79] Valiani A and Begnudelli L : Divergence form for bed slope source term in shallow water equations. *Journal of Hydraulic Engineering (ASCE)*, **132(7)** : 652-665, 2006
- [80] Villanueva I : Estudio de regimenes transtorios y permanentes en rios y canales, *Ph.D. Thesis*, University of Zaragoza
- [81] Villanueva I and Wright N : Linking Riemann and storage cell models for flood prediction. *Water Management (ICE)*, **159** : 27-33, 2006

- [82] Wan Q, Wan H, Zhou C and Wu Y : Simulating the hydraulic characteristic of the lower Yellow River by the finite-volume technique, *Hydrological Process*, **29**, 2767-2779, 2002
- [83] Wheater H : Progress in and prospects for fluvial flood modelling, *Phil. Trans. R. Soc. Lond*, **A360**, 1409-1431, 2002
- [84] Yoon T, and Kang S : Finite volume model for two-dimensional shallow water flows on unstructured grids. *Journal of Hydraulic Engineering (ASCE)*, **130(7)** : 678-688, 2004
- [85] Zhou J, Causon D, Mingham C, and Ingram D : The surface gradient method for the treatment of source terms in the shallow water equations. *Journal of Computational Physics*, **168** : 1-25, 2001
- [86] Zhao D, Shen H, Tabios Q, Lai J and Tan W : Finite-volume two-dimensional unsteady-flow model for river basins. *Journal of Hydraulic Engineering (ASCE)*, **120(7)** : 863-883, 1994
- [87] Zoppou C, and Roberts S : Catastrophic collapse of water supply reservoirs in urban areas. *Journal of Hydraulic Engineering (ASCE)*, **125(7)** : 686-695
- [88] Ministry of Construction and Transportation : Comprehensive River Management Plan for the Im-jin River, Ministry of Construction and Transportation, 2001
- [89] Hunter N M, Bates P D, Neelz S, Pender G, Villanueva I, Wright N G, Liang D, Falconer R A, Lin B, Waller S, Crossley A J, and Mason D C : Benchmarking 2D hydraulic models for urban flooding. *Water Management (ICE)*, **161** : 13-30
- [90] Liang D, Falconer R A, and Lin B : Coupling surface and subsurface flows in a depth averaged flood wave model. *Journal of Hydrology*, **337** : 147-158
- [91] Yee HC : A class of high-resolution explicit and implicit shock-capturing methods, **NASA-TM 101080**, 1989